Multimodal Signal Processing for the Diagnosis of Cardiorespiratory Disorders

Nadi Sadr Lahijany

A thesis submitted in fulfilment of the requirements for the degree of

Doctor of Philosophy

FACULTY OF ENGINEERING AND INFORMATION TECHNOLOGIES

THE UNIVERSITY OF SYDNEY

2017

Statement of originality

This thesis is submitted to the University of Sydney in fulfilment of the requirement for the degree of Doctor of Philosophy. This thesis has not been submitted for any degree at this or any other institution. This is to certify that to the best of my knowledge, the intellectual content of this thesis is the product of my own work and that all the assistance received in preparing this thesis and sources have been acknowledged, specifically:

- The research original subject, title and outline were progressed in discussion with Prof Philip de Chazal, Prof Alistair McEwan, Prof André van Schaik and Dr Paul Breen.
- Section 4.1, the false arrhythmia alarm detection in the ICU, was performed as a submission to the *Computing in Cardiology Challenge 2015* and I was the lead member of a team including Jacqueline Huvanandana, Dr Doan Trang Nguyen and Dr Chandan Kalra, under the supervision of Prof Philip de Chazal and Prof Alistair McEwan.
- Advice and editing assistance for the preparation of this thesis were provided by Prof Philip de Chazal, Prof Alistair McEwan, Benjamin Johnston and Dr Madhuka Jayawardhana.

Nadi Sadr

Acknowledgment

I would like to gratefully acknowledge a number of people who have been on this journey with me over the past few years as I was working on my PhD program in Sydney. I am deeply thankful for the enormous support of my supervisor, Prof Philip de Chazal; for his quick responses and accepting unplanned meetings with a kind smile whenever I showed up at his office. Every time I entered his office with problems about my research program, he made it seems easy to solve, and I left with positivity. It was such a privilege to work under his supervision and I learned not only how to become a good researcher, but also how to be a good person. I would also like to thank Prof. Alistair McEwan, Prof. André van Schaik and Dr. Paul Breen for their help in developing the ideas and reviewing the papers and thesis chapters. I have learned a lot from them.

I would like to thank all of my friends at the University of Sydney, Western Sydney University and the Biomedical Engineering and Neuroscience (BENS) group. This journey would never have been this rewarding without the support of such friendly, intelligent and helpful people. To my friends at the Sleep Research team of the University of Sydney, Dr. Madhuka Jayawardhana, Benjamin Johnston and Dr. Hadis Nosrati for their on-going support and encouragement that made the hard days and deadlines less stressful.

To my father from whom I am still learning how to be strong, hardworking, open to new ideas and positive even under stressful situations. To my mother, my first teacher who I have always felt that her presence makes everything goes smoothly in my life. Thanks to my brother and sister-in-law, Reza and Salma, who were the first ones that confidently supported my decision to start my PhD program in Sydney. Thanks to my adorable sisters, Ati and Hedi, who are the precious gifts of my life and after our mum's passing, filled my life with love and care every step of the way. A big loving thank you to Ati for being the reason of starting this journey, for all her constant care, filling up my fridge with healthy yummy foods, surprising me by showing up at the door, bringing life to my place, listening to my nags, calming me down when I was under stress and always having a place for me to unwind. Finally, this thesis is dedicated to the love of my life, Bobak, for his encouragement and believing in me. This would have never happened without his constant support and confidence in me.

Abstract

This thesis addresses the use of multimodal signal processing to develop accurate and robust algorithms for the automated processing of two cardiorespiratory disorders.

False alarms in the intensive care unit (ICU) impact the patients and the clinical staff due to noise disturbance, desensitisation to warnings and slowing of response times, which can lead to disruption of care. These extra alarms also result in physiological and psychological distress for patients and the attending staff. Thus, the reduction of the number of false alarms could lead to better health outcomes in the ICU. The first application of this thesis was aimed at reducing the false arrhythmia alarms in the ICU by processing multimodal signals including photoplethysmography, arterial blood pressure, Lead II and augmented right arm ECG. The goal was to detect five critical arrhythmias comprising asystole, extreme bradycardia, extreme tachycardia, ventricular tachycardia and ventricular flutter or fibrillation.

We developed a hierarchical approach to process the four signals as well as a custom signal processing techniques for each arrhythmia type. We submitted our algorithm to the *PhysioNet/Computing in Cardiology (CinC) Challenge 2015* which achieved an overall test set score of 74.03% with 98% true positive rate (TPR) and 66% true negative rate (TNR) for retrospective analysis and a score of 69.92% with 95% TPR and 65% TNR for real-time analysis. Our result placed us among the top ten scores of the *PhysioNet/CinC Challenge 2015*. Our proposed system also achieved the highest score among the challenge entries in detecting tachycardia false alarms with a score of 99.1%, TPR of 100% and TNR of 80%.

Sleep disorders are a prevalent health issue, which are currently costly and inconvenient to diagnose as they normally require an overnight hospital stay by the patient and the use of specialised, expensive equipment. In the second application of this project, we designed automated signal processing algorithms for the diagnosis of sleep apnoea with a main focus on the electrocardiogram (ECG) signal processing.

We extracted respiratory information from the ECG signal (ECG derived respiration; EDR signals) using different methods: QRS-complex area, principal component analysis (PCA) and kernel PCA. We proposed two algorithms (segmented PCA and approximated PCA) for EDR estimation to enable applying the PCA method to overnight ECG recordings. Previous published methods were limited to processing approximately one hour of ECG signals. We rectified the computational issues and memory requirement of PCA application for lengthy recordings. We compared the ECG derived

respiratory information against the chest respiratory effort signals for signal shape similarity and apnoea detection capability.

The performance of the apnoea detection was evaluated using the three automated machine learning algorithms of linear discriminant analysis (LDA), extreme learning machine (ELM) and support vector machine (SVM). We evaluated the performance of the algorithms on two databases: the *MIT PhysioNet* database and the *St. Vincent's* database. The results showed that the QRS area method for EDR estimation combined with the LDA classifier was the highest performing method. Although the sample-by-sample comparison of the EDR signals against the chest respiratory signal showed low correlation, the apnoea detection results demonstrated that EDR signals contain respiratory information useful for discriminating sleep apnoea.

As a final step, heart rate variability (HRV) and cardiopulmonary coupling (CPC) features were extracted and combined with the QRS area EDR features. These features were processed with the LDA classifier and temporal optimisation techniques were applied. The cross validation results of the minute-by-minute apnoea classification achieved an accuracy of 89%, a sensitivity of 90%, a specificity of 88%, and an AUC of 0.95 which is comparable to the best results reported in the literature. We also estimated the apnoea hypopnoea index (AHI) of the recordings from the minute-by-minute apnoea annotations. Based on thresholding the estimated AHI, our system obtained an accuracy of 100% for the *MIT PhysioNet* database and 84% for the *St. Vincent's* database for separating normal patients from apnoeic patients.

Contents

Glossary

AASM: American Academy of Sleep Medicine

Apnoea: Restriction (90% or more) of airflow for at least 10 seconds in adults or two breaths in children and a blood oxygen saturation drop of greater than 4% [1] [2].

Apnoea-hypopnoea index (*AHI*): The most common measure of sleep apnoea which is the average number of apnoea and hypopnoea events per hour computed over total sleep time (TST) [2].

Arousals: An EEG event when there is an abrupt shift in EEG frequency, which may include theta, alpha activity and/or frequencies greater than 16 Hz (but not sleep spindles) [3].

Arousal index (*ARI*): Total number of arousal events divided by total number of hours of sleep [1].

Arterial blood pressure (*ABP*): A hemodynamic pressure imparted to the blood by contraction of left ventricular and preserved by the elasticity of the arterial system and can be monitored using different methods (manometry, oscillometry, plethysmography and ultrasound) [4], [5].

Respiratory disturbance index (*RDI*): Average number of respiratory disturbances (obstructive apnoeas, hypopnoeas and respiratory event–related arousals or RERAs) per hour [2].

Asystole: A cessation of cardiac rhythm for more than 3 seconds [1].

Arterial fibrillation: An abnormal ventricular rhythm accompanied by substitution of P waves by rapid electrical fluctuations [1].

Autonomic nervous system: A part of nervous system which operates automatically to regulate physiological activities in the body [6].

Baroreceptors: Sensors in blood vessels which are excited by expansion of blood vessels to recognise blood pressure elevation [3].

Baroreflex: A negative feedback system to sustain blood pressure. Slow rate breathing intensifies Baroreflex sensitivity and diminishes sympathetic activity and chemoreflex operation [3].

Bradycardia: An abnormal heart rate of less than 60 beats per minute [1].

Cheyne stokes breathing: An abnormal breathing pattern with a crescendo and decrescendo alteration in breathing amplitude, usually detected as deep and sometimes fast breathing [1].

Chemoreceptors: Carotid chemoreceptors stimulate breathing during hypoxia and are located near the bifurcation of the carotid artery in the throat to warn that there is a drop in the brain's oxygen or a rise in carbon dioxide levels [7].

Continuous positive airway pressure (*CPAP*): Standard treatment for sleep apnoea by inducing positive pressure airflow through the mouth [8].

Delta-sleep efficiency index (*DSE*): The percentage of delta-sleep relative to total time in bed; normally is about 20% of the night [9].

ECG or EKG: Electrocardiogram test which records the electrical activity of the heart measured on the skin surface [1].

Extreme bradycardia: A drop of heart rate define as three or more consecutive impulses at a rate of less than 60 beats per minute (bpm) [10].

Extreme tachycardia: An increase of heart rate defined as three or more consecutive impulses at a rate of over 100 bpm [11].

Heart rate (*HR*): The measure of heart beats derived from the number of heart contractions per minute [12].

Heart rate variability (*HRV*): The time variations of the intervals between two heart beats (R-R) [12].

Hypercapnia: Abnormal rise of carbon dioxide level in blood [13].

Hypopnoea: A particular decrease of airflow for at least 10 seconds in adults or two breaths in children accompanied by drop in blood oxygen saturation of at least 3% [1].

Hypopnoea index (*HI):* Number of hypopnoea events per hour divided by TST [1].

Hypoxia: Deficiency in oxygen reaching the tissue [13].

Non-rapid eye movement (*NREM*): Mostly the initial state of sleep in adults consisting of 3 stages representing the depth of sleep which is detected by synchronisation of EEG activity. The 90-min NREM-REM cycle occurs three to six times during overnight sleep [14].

Obstructive sleep apnoea in children: A sleep breathing disorder characterised by interruptions of 10 s to 1 min in respiratory gas exchange which leads to sleep fragmentations; mostly happens due to obesity, enlarged tonsils or adenoids [15] [16].

Oxygen desaturation index (*ODI*): The number of oxygen desaturation periods per hour of sleep [17].

Parasympathetic nervous system: Physiologically functions opposite to sympathetic system and acts as *"rest and digest".* It slows down the heart rate in bradycardia [6].

Photoplethysmography (*PPG*): The optical plethysmography using the intensity of the absorbed light in the tissue through the skin providing clinical information such as the cardiac pulse pressure and respiration [18].

Polysomnogram (*PSG*): A sleep study for diagnosis of sleep disordered breathing using multichannel recordings to determine the respiratory and sleep measures [19], [20].

Pulse transit time (*PTT*): The delay between detected onset beats of the blood pressure waveform and R peaks of the ECG signals [21].

QRS complex: The typical feature in ECG signal which consists of a typical R peak and a series of deflections in ECG representing electrical activity produced by ventricular depolarization and contraction of the ventricles [1].

Rapid eye movements (*REM*): EOG events comprises of series of conjugate eye movements which includes a slow rate preceding a rapid rhythm in the opposite orientation as the subject reads [1].

Respiratory effort related arousals (*RERA*): A reduction in airflow resulting in arousals but the oxygen desaturation is lower than the hypopnoea criteria [19].

Respiratory inductance plethysmography (*RIP*): Capturing the respiratory effort signals by estimating the chest and abdominal movements using belts with installed sinusoid wire coils to measure the self-inductance changes due to the volume change [22].

RR interval: The interval between two adjacent R peaks of consecutive QRS complexes in ECG signal [23].

Respiratory sinus arrhythmia (*RSA*): It is the cyclical changes of heart rate associated with respiration which causes a faster heart rate during inspiration and slower during expiration [24].

Signal quality index (*SQI*): A measure of assessing the quality of signals and the rate of the distortions generated by noise and artefact [25].

Sleep apnoea (*SA*): A pause of airflow for more than 10 seconds in adults [26].

Sleep apnoea syndrome (*SAS*): At least 30 apneic episodes observed in both REM and NREM sleep over 7 hours period [2].

Sleep efficiency (*SE*): The ratio of total sleep time to the total time in bed ready to go to sleep [27]. For a normal sleep, SE is about 85% [9].

Sleep latency (*SL*): Lights out to first epoch of any sleep in minutes [1].

Sleep onset latency (*SOL*): The time duration from "lights out" or bedtime, to onset of sleep; normally about 15 minutes [9].

Slow wave sleep (*SWS*): It is Stage 3 NREM sleep state and is a deep sleep stage. It is characterised by slow wave with high voltage activity in the EEG. It is also called N3 stage, delta sleep or deep sleep [28].

SaO_2: Arterial oxygen saturation representing the ratio of oxygenated (saturated with oxygen) haemoglobin in the arterial blood [29].

SpO_2: Peripheral capillary oxygen saturation representing the ratio of the oxygenated haemoglobin in to the total haemoglobin in the blood, measured by pulse oximetry [30].

Stage R (*REM*) latency: sleep onset to first epoch of Stage R in minutes [1].

Sympathetic nervous system: It operates to set and organise the body to confront a potential threat namely *"fight or flight".* It increases heart rate in tachycardia [6].

Tachycardia: An abnormal cardiac rate of greater than 100 per minute for at least 3 beats with QRS duration of 120msec [1].

Total in bed (*TIB*): The total time spend in bed from the "lights off" (i.e. sleep study starts) ready to go to sleep to the "light on" (i.e. sleep study ends) [31].

Total sleep time (*TST*): The total time spent in REM and NREM sleep (during the PSG) [31].

True positive rate (*TPR*): The ratio of the number of positives classified correctly to the total number of positives [32], [33].

True negative rate (*TNR*): The ratio of the number of negatives classified correctly to the total number of negatives [32], [33].

Ventricular tachycardia (*VT* or *Vtach*): A common arrhythmia with high rate of heart rate produced by abnormal electrical impulses spreading through the myocardium of ventricles [34].

Ventricular flutter or fibrillation (*VF* or *VTF*): An arrhythmia produced by uncoordinated cardiac contractions causing ventricular myocardium nor responding to the sinus node stimuli [34]. The ventricular flutter causes the heart rate increases over 250-350 bpm [34].

Sinoatrial (*SA*) node: The generator of heart rhythm in the right atrium wall which produces a heart rate of approximately 60-100 bpm in a healthy adult [11].

Atrioventricular (*AV*) node: A major element of the normal impulse conduction path in the interatrial septum which receives the electrical impulse dispersing from the SA node [11].

Vagal tone: The biological activity of the vagus nerve (tenth cranial nerve) which is the key element of the autonomic nervous system for parasympathetic activity and controls the SA node stimulation and heart rate [35].

List of figures

List of tables

CHAPTER 1

INTRODUCTION

1. Introduction

This thesis focuses on the automated diagnosis of cardiorespiratory disorders using multimodal signal processing methods. The two applications of cardiorespiratory disorders addressed in this thesis are life-threatening heart arrhythmias and sleep disordered breathing (SDB). This chapter discuss the introduction to the research and outlines the motivation behind the topic, objectives and aims of the thesis. Then, the contributions of the work carried out, the significance and outcome of the research are explained. Ultimately, the structure of the thesis and the publications resulted from this work are listed.

1.1. Motivation

Cardiorespiratory disorders are prevalent health issues and their current diagnosis tools present major issues, such as cost, disturbance of sleep and breathing, and high rate of false alarms.

In the first application of this thesis, we detected the heart arrhythmias in order to reduce the false alarms in the intensity care unit (ICU). In general, cardiac rhythm variation from normal rhythm is known as arrhythmia which might become life-threatening due to drops in cardiac output or the triggering of further severe arrhythmias [11]. Thus, the diagnosis of cardiac dysfunctions plays a significant role in health care, particularly in the ICU. An ICU monitors the biological signals of patients in critical conditions that need persistent monitoring for treatment management [36]. Cardiorespiratory monitoring is a crucial matter, as arrhythmias such as ventricular tachycardia, ventricular flutter or fibrillation can generate fluctuations in blood pressure, increase mortality rate and may eventually lead to stroke and unexpected sudden death [37]. Many of these monitoring systems incorporate alarms designed to warn of life-threatening clinical conditions or functional failures of the equipment [38], [39]. The number of the alarms in the ICU has increased in recent years due to technological advancement of the medical instrumentation [40]. The alarms emitted from the life-support devices or physiological monitors can be classified into two groups: technically correct alarms or false alarms [41]. False alarms are alerting signals arising from monitoring equipment with no linked clinical cause or life-threatening conditions in the patient [38], [42]. Studies show that over 85% of the ICU alarms are false [40]–[43] with the resulting sound noise level in the ICU associated with alarms announced up to 90 dB [44]–[46]. Indeed, this noise can be distressing for the patients and medical staff [40] and can lead to physiological and psychological issues [44], [47]. For example, given the importance of sleep in many treatments, sleep deprivation is a major consequence of noise in the ICU [47], [48]. It is reported that weakened immune function and elevated negative nitrogen balance can be a result of sleep deprivation, which may lead to slower

treatment progress and worsened disorders [49]. Hence, noise control by reducing false alarms helps the patients sleep, which diminishes the stressors in the ICU for more effective treatment [28],[30]. Moreover, a resulting critical health issue in the ICU is medical staff losing sensitivity to frequent false alarms, referred to as alarm fatigue, which in turn increases the likelihood of missing true alarms [43], [51]. The disruptive consequences of false alarms can be alleviated by developing automatic systems for life-threatening arrhythmia detection and reduction of the false alarms which was the motivation of the first application of this thesis toward advancement of the monitoring systems.

The second part of the thesis investigated automatic detection of SDB which is a substantial burden on the healthcare system. SDB is characterised by a reduction or total pause of airflow for at least 10 seconds during sleep [52], [53]. Epidemiologic studies have shown that sleep apnoea (SA) is a widespread medical condition and have revealed a high rate of undiagnosed SA in adults [54]. It was indicated that on average, mild SA occurs in about 1 in every 5 adults and moderate SA exists in more than 1 in every 15 adults among caucasian men and women [54]. Generally, about 24% of men and nine percent of women suffer from the breathing effects of obstructive SA (OSA); and approximately 85% of adults with OSA are undiagnosed [2]. Investigators have also demonstrated that even mild OSA can cause serious detrimental health effects and that untreated OSA may lead to severe health issues such as cardiovascular disease, hypertension and stroke [54]. Furthermore, the resulting daytime tiredness and sleepiness may lead to workplace and road accidents [55]. As a result, diagnosis and treatment of OSA is important for both patients and society to reduce the associated health costs [20]. Current methods of identifying SA are complex, cumbersome and expensive to implement [38],[39]. Polysomnography (PSG) is the standard testing procedure for apnoea diagnosis which records a number of physiological signals during an overnight stay in a hospital [38],[39]. Sleep studies are expensive and patients may not sleep well due to the attachment of wires and sensors to the head, torso and limbs which can cause discomfort [20], [56]–[58]. As such, there is no doubt about the necessity of developing simpler diagnosis tools for SA. However, reliable methods of SA diagnosis with the ability to replace PSG are still unproven [54]. Sleep tests utilise different sensors which may measure redundant physiologic parameters and the number of sensors can be decreased without losing the information or reducing the accuracy of diagnosis [59]. These factors motivated the second application of multimodal signal processing, which was to reliably detect SA with minimal number of sensors in order to reduce cost, complexity and invasiveness of sleep tests [23].

1.2. Objectives

The objective of this thesis was to propose multimodal signal processing algorithms for identifying cardiorespiratory disorders. The two categories of disorders considered in this thesis were

interconnected, in that an undiagnosed or untreated disorder from each category might generate, exacerbate or aggravate the other.

The first objective of the study was real-time and retrospective identification of life-threatening arrhythmias, comprised of extreme bradycardia, extreme tachycardia, ventricular tachycardia, ventricular flutter and fibrillation, with supporting information about presenting an index for ECG signal quality evaluation [60], [61]. The first application of the thesis aims to present an algorithm which uses the multimodal signals from ECG leads II and V and the pulsatile signals; photoplethysmography (PPG) and arterial blood pressure (ABP).

In the second application of the thesis, the main objective was the diagnosis of SA using ECG signals. This study extracted respiration from ECG signals through three different methods including the principal component analysis (PCA) approach. Following initial PCA analysis on short excerpts of the ECG recordings, the objective was to extend the application of PCA and propose algorithms to enable a feasible implementation of PCA on overnight ECG signals. Through this objective, the aim was to reduce processing time and memory requirement of estimating ECG derived respiratory (EDR) signal using the PCA method. Furthermore, this thesis was a study of how to use the chest respiratory effort signal from the inductance plethysmography to evaluate the respiratory information derived from ECG signal for SA detection. Ultimately, it was how to process features extracted from the signals with automated classifiers developed by different machine learning algorithms as well as how to optimise their performance.

1.3. Thesis contributions

The fundamental contribution of this thesis is providing efficient and systematic signal processing algorithms for the diagnosis of cardiorespiratory disorders. The contributions are listed for two categories of the disorders studied in this thesis and the results of different phases were partly published in [60]–[69].

In more detail, the contributions are the following:

1) The proposed algorithm for the first application of this thesis accomplished the top ten highest scores at the International *Computing in Cardiology Challenge 2015* [33]. In particular, the proposed method for detecting extreme tachycardia attained the highest rank and an outstanding score for the true negative rate (TNR) and true positive rate (TPR). Consequently, in addition to submitting a paper to the *Computing in Cardiology* conference published in the *IEEE Xplore*, we were invited for a submission to the focus edition of the journal of *Physiological Measurement* which was published in August 2016. The novelties leading to these outstanding results were as follows.

i. I implemented a robust heart beat recognition based on Hilbert QRS detection to extract QRS complexes and optimised the outputs of QRS detection beats using a correction algorithm.

ii. I presented a signal quality index (SQI) for ECG signal evaluation using four tests which evaluate different features, such as minimum and maximum of heart rate, RR-interval and standard deviation of the ECG signal in the segment containing the alarm.

iii. My developed algorithm for extreme tachycardia alarm detection utilised the largest variety of features compared to my detection algorithm for other alarm types, and included time-domain statistical features extracted from all of the available four signals. I also modified the SQI measure and optimised the threshold of the features. The combination of these strategies resulted in 19% increase in TPR, 20% increase in TNR and 42% enhancement in the score of tachycardia compared to the initial sample entry of the *CinC Challenge*.

iv. To sum up, modification of the SQI measure for different arrhythmias rather than using a fixed SQI for every arrhythmia by setting the threshold in an iterative performance evaluation, and considering various possible effects of each arrhythmia on the features of the signals contributed to enhanced performance of arrhythmia identification and false alarm reduction.

2) In the second application of the thesis, novel methods of estimating the respiration from the overnight ECG signal were proposed and the SA detection using these EDR signals was compared with using the chest respiratory effort signal for the same purpose. The novelties can be summarised as follows.

i. I developed two algorithms to estimate EDR of the full overnight ECG signals using principal component analysis (PCA). The first approach incorporated segmented PCA method executed on segments of 30 minutes over the overnight ECG recordings. The second solution was an approximation technique adapted from a speech recognition study. Both approaches solved the computational problems and limitations of PCA application on the lengthy recordings and caused enormous drop in the required processing time and memory storage while running on a standard PC. Moreover, this is the first study using PCA to estimate EDR of the full overnight ECG signals without the requirement of eliminating artefacts or ectopic beats.

ii. This thesis also answered a question that appears to be unanswered in the literature that "in comparison to the respiratory effort signals, how well does the EDR capture relevant breathing information for SA detection". The answer was obtained by performing a side-by-side comparison of the information for identifying SA contained in the chest respiratory effort signal and the EDR signals. The results suggest that the important SA

discrimination information is not lost during the heartbeat based sampling process of the EDR signal.

iii. I evaluated three different EDR estimation techniques and obtained the highest performing EDR signal for apnoea detection. I also performed three automated machine learning algorithms and selected the highest performing approach for SDB detection.

iv. Finally, by combining the highest performing EDR signal with HRV and CPC features and applying temporal optimisation techniques, I enhanced the apnoea classification performance using the highest performing machine learning technique.

1.4. Significance of research

This thesis aimed to enhance the diagnosis of cardiorespiratory disorders by deriving more clinical information beneficial to the diagnosis of the disorders from individual signals. Moreover, the goal was to combine the derived information from multimodal signals while the intention was to reduce the number of diagnostic signals, the corresponding costs, complexity and invasiveness of existing methods.

In the first application, due to the fact that major characteristics of arrhythmias are associated with heart rate, using a reliable QRS detection method was a highly significant component in developing an automated arrhythmia diagnosis system. Accordingly, a robust heart beat detector based on Hilbert algorithm was selected and applied in order to initiate a reliable feature extraction stage. Moreover, since the noisy characteristics of ECG signals trigger false alarms, multiple steps were taken to minimise the negative effect of artefacts including, interference removal of ECG signals, SQI, and the use of information from multimodal signals. On the other hand, in some arrhythmias, interference removal and examining the SQI failed to help in false alarm reduction and a fixed method of SQI evaluation was not suitable for analysis of a variety of arrhythmias with different properties. Thus, the various characteristics of the arrhythmias led to different implementation processes for individual arrhythmia alarm detection. In fact, we found that the best arrhythmia detection performance was achieved by adapting the SQI measures to each arrhythmia, setting the threshold in an iterative process, and considering a variety of features for each arrhythmia. Our best performing algorithm used all available multimodal signals, extracted a number of statistical features from each signal and combined the processed information. Our proposed algorithm reduced the rate of false alarms in the ICU, achieved outstanding performance in detection of extreme tachycardia and accomplished an overall high score among the top ten highest scores of the challenge.

The second application was targeted at minimising the number of required diagnostic signals, complexity and invasiveness of sleep tests [23]. To achieve the said objectives, this thesis demonstrated the SA detection capabilities of multimodal signals and different machine learning

techniques as well as extracting respiratory signals from the ECG signal. This ECG-derived respiratory signal (EDR) was estimated using a standard method based on the QRS area as well as a novel method of principal component analysis (PCA) [70], [71]. The limitations of the PCA method have restricted implementations to use a segment of the data rather than the entire recordings [70], [72], [73]. In the early stages of the thesis, we published a paper [63] in which PCA was applied to 60 minutes of ECG signals to extract ECG-derived respiratory signals. Subsequently, two refined PCA algorithms were developed - "segmented PCA", applying PCA to 30 min segments of ECG recording, and "approximated PCA", using an approximation technique for PCA- which permitted the PCA method to be applied to a full overnight ECG recordings. Our algorithm refinement solved the memory and processing time limitations of the PCA method. These solutions are discussed in more detail in section 0.

We also used the chest respiratory effort signal as a reference measure to evaluate the performance of EDR signals in SA detection. To compare the information for identifying SA incorporated in the chest respiratory effort signal and the EDR signals, different resampling techniques were applied on respiratory effort signal, including heart-rate based sampling through which inclusion of heart rate information in unison with respiratory effort signal was inspected. The results suggest that the important SA discrimination information is preserved during the heartbeat based sampling process inherent in the EDR signal. Also a variety of features were extracted from the ECG and respiratory signals and their performance in SA detection examined. We combined best performing features and applied different machine learning techniques including, linear discriminant analysis (LDA), extreme learning machine (ELM) and the support vector machine (SVM). Ultimately, the results were optimised by merging the information of power spectral densities of heart rate variability and EDR signals to extract cardiopulmonary coupling features which further boosted the accuracy of apnoea recognition. The proposed algorithm has a potential application in a home-based diagnosis tool.

1.5. Thesis structure

The remainder of this thesis is outlined as follows:

Chapter 2 presents a background of the physiology of the cardiorespiratory disorders discussing both arrhythmias and sleep disordered breathing. The discussion of arrhythmias defines the nature and characteristics of asystole, extreme bradycardia, extreme tachycardia, ventricular tachycardia and ventricular flutter and fibrillation as well as the background of false alarms in the ICU. In the second section, types of SA, epidemiology, anatomy, aetiology, pathophysiology, neurology and treatment of SA are described. The sensors used in this study are then outlined including ECG, respiration monitoring, photoplethysmography (PPG) and arterial blood pressure (ABP). Next, the background of

the existing diagnosis and monitoring systems and the involved issues are surveyed for both false arrhythmia alarms in the ICU and sleep tests.

Chapter 3 describes the current state of the art for diagnosis and monitoring systems and discusses the methodology issues regarding false arrhythmia alarms in the ICU and sleep tests. This chapter also surveys the widely used signal processing techniques in the literature for diagnosis of the cardiorespiratory disorders. We investigated features such as heart rate variability (HRV) and ECG derived respiration (EDR) and machine learning techniques, such as linear discriminant analysis (LDA), extreme learning machine (ELM) and the support vector machine (SVM).

Chapter 4 describes the algorithms and methods developed during this project for reducing false arrhythmia alarms in the ICU. The chapter covers the presented signal processing algorithms of the first application of this thesis; commencing with the used databases, extracted features, and the details of our novel multimodal signal processing techniques. It is then followed by reporting the results of our proposed algorithm and discussing the outcomes. This chapter emphasises the impact of the first application of this project in resolving the issues of the current systems.

Chapter 5 explains the algorithms developed during this project for detection of sleep disordered breathing (SDB) using multimodal signals. The developed signal processing algorithms of the second application of this thesis is described, including the used databases, the chest respiratory effort signal, the extracted features, and the details of our novel ECG derived respiration approaches. Then, the results of our proposed algorithms are reported in three phases in separate sections. The final section discusses the results and evaluates the outcomes of the proposed methods in different phases of the study. This chapter highlights the contributions of the thesis and the novelty of the developed algorithms for the second application of the thesis in detail.

Chapter 6 concludes the thesis and discusses the outcome of both applications and the significant areas for future work.

1.6. List of publications

1. N. Sadr, P. de Chazal, "Respiratory Information Evaluation of the ECG Derived Respiration Methods for the Diagnosis of Sleep Disordered Breathing," *IEEE Trans. Biomed. Eng.*, (to be submitted), 2017
2. N. Sadr, M. Jayawardhana, P. de Chazal, "Sleep Apnoea Diagnosis Using Respiratory Effort-Based Signals – a Comparative Study," *39th Annu. Int. Conf. IEEE Eng. Med. Biol. Soc.*, (in press), 2017

3. N. Sadr, J. Huvanandana, D. T. Nguyen, C. Kalra, A. McEwan and P. de Chazal, "Reducing false arrhythmia alarms in the ICU using multimodal signals and robust QRS detection," *Physiol. Meas.*, vol. 37, no. 8, pp. 1340–1354, 2016
4. N. Sadr and P. de Chazal, "Comparing ECG Derived Respiratory Signals and Chest Respiratory Signal for the Detection of Obstructive Sleep Apnoea," *Comput. Cardiol.*, vol. 43, pp. 1029–32, 2016
5. N. Sadr and P. de Chazal, "A Comparison of Obstructive Sleep Apnoea Detection using Three Different ECG Derived Respiration Algorithms," *Comput. Cardiol.*, vol. 42, pp. 301–304, 2015
6. N. Sadr, J. Huvanandana, D. T. Nguyen, C. Kalra, A. McEwan and P. de Chazal, "Reducing False Arrhythmia Alarms in the ICU by Hilbert QRS Detection," *Comput. Cardiol.*, vol. 42, pp. 1173–76, 2015
7. N. Sadr and P. de Chazal, "Automated Detection of Obstructive Sleep Apnoea by Single-lead ECG through ELM Classification," *Comput. Cardiol.*, vol. 41, pp. 909–912, 2014
8. N. Sadr and P. de Chazal, "A Fast Approximation Method for Principal Component Analysis Applied to ECG Derived Respiration for OSA detection," *38th Annu. Int. Conf. IEEE Eng. Med. Biol. Soc.*, pp. 6198–6201, 2016
9. N. Sadr, P. de Chazal, A. Van Schaik and P. Breen, "Sleep apnoea episodes recognition by a committee of ELM classifiers from ECG signal," *37th Ann. Int. Conf. IEEE Eng. Med. Biol. Soc., EMBS*, vol. 2015-Novem, pp. 7675–7678, 2015
10. N. Sadr, P. de Chazal, " Detection of epochs of sleep apnoea from the ECG using a committee of ELM classifiers and heart rate variability parameters", *36th Ann. Int. Conf. IEEE Eng. Med. Biol. Soc. (EMBS)*, 2014
11. P. de Chazal and N. Sadr, "Sleep apnoea classification using heartrate variability, ECG derived respiration and cardiopulmonary coupling parameters," *38th Annu. Int. Conf. IEEE Eng. Med. Biol. Soc.*, pp. 3203–3206, 2016
12. H. Nosrati, N. Sadr and P. de Chazal, "Apnoea-hypopnoea index estimation using craniofacial photographic measurements," *Comput. Cardiol.*, vol. 43, pp. 1033-1036, 2016
13. P. de Chazal, N. Sadr and M. Jayawardhana, "An ECG oximetry system for identifying obstructive and central apnoea events," *37th Annu. Int. Conf. IEEE Eng. Med. Biol. Soc. EMBS*, vol. 2015-November, pp. 7671–7674, 2015
14. P. de Chazal, N. Sadr, M. Jayawardhana, H. Nosrati, "Automated detection of sleep apnoea with minimally invasive sensors", *38th Ann. Int. Conf. of the IEEE Eng. in Med. and Biol. Soc.*, 1 page, 2016

Chapter 2

Clinical background

2. Clinical background

In this chapter, principal clinical information, upon which the thesis was built, is provided, outlining the physiological basis of two categories of cardiorespiratory disorders, including arrhythmias and sleep disordered breathing (SDB), the effect of these conditions on the patients as well as the sensors for multimodal recordings and current state of diagnosis and monitoring techniques. This information is intended to provide the reader with a greater understanding of the clinical context of this research, such that later discussion of potential applications can be well understood. The chapter will be concluded by explaining the issues involved with current diagnosis and monitoring systems for the two conditions, which led to proposing this project.

2.1. Cardiorespiratory disorders

Cardiorespiratory disorders incorporate a widespread range of cardiac dysfunction and respiratory disorders. The cardiovascular system may face destructive alterations due to different factors; a simple example of an inevitable factor affecting the cardiovascular system is aging. This generates impairments in blood vessels leading to condensed or thickened arteries, reduced compliance of blood vessels and a stiffened left ventricle. These changes might cause conduction disorders or different cardiac arrhythmias such as bradyarrhythmia and tachyarrhythmias [74]. Arrhythmias are associated with a number of pathophysiology sources including disorders linked with impulse production, impulse conduction or a combination of both [11]. There are a number of risk factors linked with arrhythmias, such as hypertension, valvular heart disease, obesity, respiratory disorders and obstructive sleep apnoea (OSA) [75]. That is, arrhythmias and OSA are interrelated and their occurrence exacerbates one another. Thus, diagnosis of these two types of disorders will be investigated in this thesis and I first discuss the diagnosis of arrhythmias as an important focus in a healthcare system. Among cardiac disorders, the life-threatening arrhythmias including asystole, extreme tachycardia, extreme bradycardia, ventricular tachycardia, ventricular flutter and fibrillation were studied in this thesis.

2.1.1. Arrhythmia diagnosis

In order to study the diagnosis of cardiac malfunction, the normal cardiac mechanism and heart rate is first surveyed. The function of two different types of cardiac cells provide a normal heart beat, with the myocardial contractile cells empowering the contractions for blood pumping and the specific conduction system (SCS) cells responsible for the generation (automatism capacity), transmission (conduction capacity) and order of the contractions [76]. The cooperation of the two types of cardiac

cells generates the normal rate and passage of blood pumping through the correct route at the correct timing, controlled by the autonomic nervous system (*ANS*) [76]. The major components of the conducting system, SCS, are sinoatrial node (*SA node*), atrioventricular node (*AV node*), His bundle, bundle branches and Purkinje fibres, as demonstrated in Figure 2.1 [76].

The SA node is the generator of heart rhythm and in a healthy adult at rest produces a heart rate of approximately 60-100 beats per minute (*bpm*) [11]. As sinus node cells provide quicker diastolic depolarisation (see Figure 2.1), these cells provide the highest automatism [76]. The normal impulse conduction path commences at the SA node, then disperse through specialised atrial transmitting traces to the AV node and then to the ventricular myocardium which initiates the contraction of the ventricles [11].

During the cells' resting phase, the contractile cells polarise due to the balance between outside positive charges and inside negative charges, causing a stable potential difference on the cell membrane and consequently, the diastolic transmembrane potential (*DTP*) [76]. During the heart stimulation, when the DTP passes the threshold, depolarisation and repolarisation of the cardiac cells create a transmembrane action potential (*TAP*) [76]. The depolarisation, repolarisation and rest phases of two samples of a cardiac cell are exhibited in Figure 2.2.

When the stimulus spreads to the atrial and ventricular muscle cells, a TAP is generated, as displayed in Figure 2.1 [76]. The union of all of the depolarisation and repolarisation curves and vectors through the pathway of the cardiac electric stimulus can be measured as a potential difference on the skin surface. During every recorded cardiac cycle, an atrial depolarisation causes a P wave, a ventricular depolarisation generates a QRS complex and a ventricular repolarisation generates a T wave,

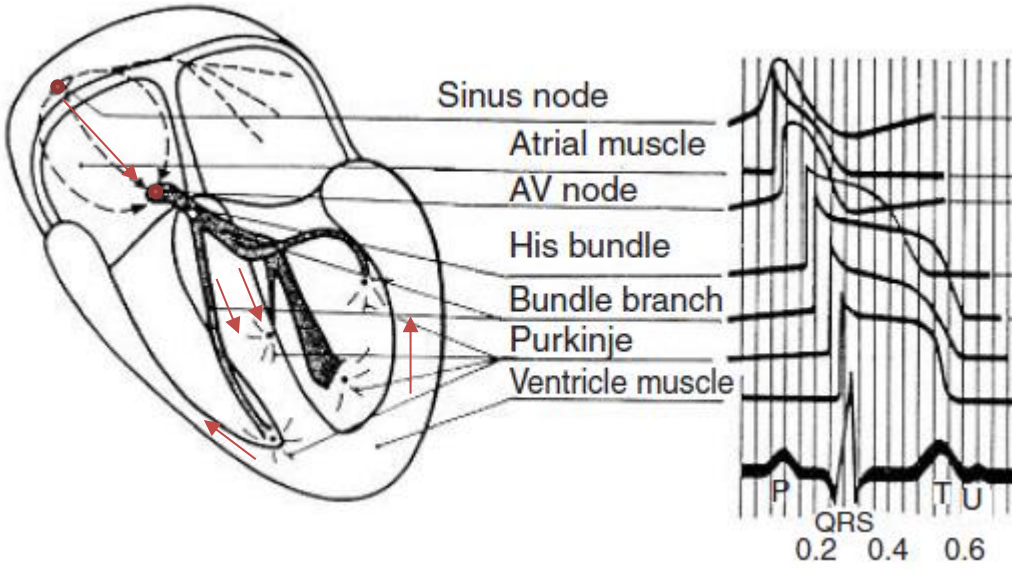

Figure 2.1. The components of conducting system and atrial and ventricular muscles as well as transmembrane action potential (TAP) morphologies of these different components forming the cardiac waves. (Figure adapted from Figure 5 [76]). The arrows show the generation and traveling of a normal impulse through the conduction path.

producing P-QRS-T sequence through the union of them [76], [77]. Thus, the occurrence of a normal QRS complex is an evidence of a normal electrical impulse travelling from His bundle through the left and right bundle branches to the Purkinje network as well as a normal depolarisation taking place in the right and left ventricles. In this thesis, different features were measured using the QRS complexes for diagnosis of arrhythmias as well as SDB, and are described in sections 3.5 and 0.

The intervals between the waves change according to the heart rate [76]. During sleep, the heart rate drops to 30-50 bpm and a number of variations normally occur including, sinus pauses for three seconds and junctional rhythms [78], [79]. Respiratory sinus arrhythmia (RSA) is a normal sinus arrhythmia initiated by cyclical changes of vagal tone which is a parasympathetic activity from ANS for regulating the resting state of heart [24]. It is typically associated with respiration, with a faster heart rate during inspiration and slower during expiration [24]. It exists in healthy subjects and is not considered as a cardiovascular disorder. As RSA is easily measured, it is a convenient measure of parasympathetic nervous system function. It will be described in more details in section 2.1.2.

Any variation from normal impulse conduction, the sources of impulse or ventricular rate can cause arrhythmia; that is the deviation of cardiac rhythm from the regular sinus rhythm [11], [80]. Arrhythmias may become life-threatening as a result of drop in cardiac output, myocardial blood flow

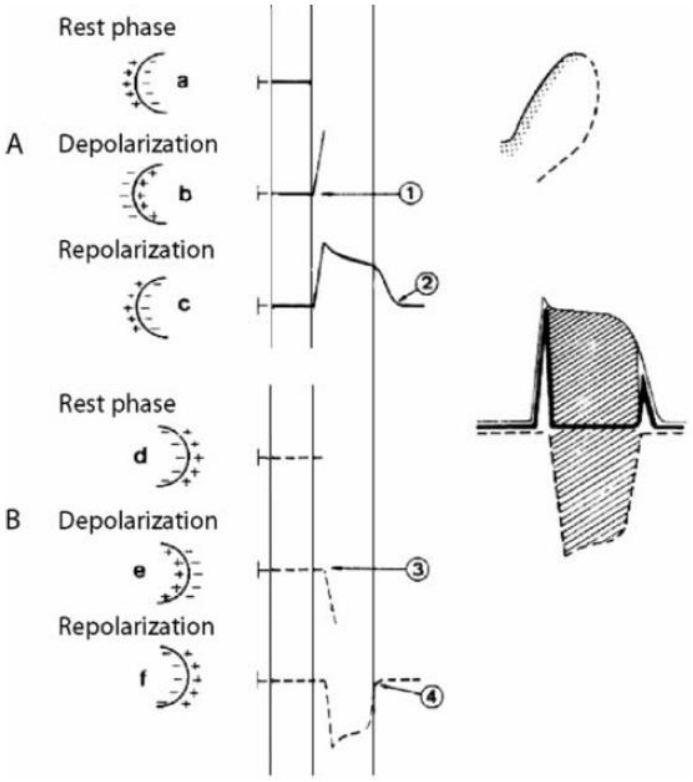

Figure 2.2. Demonstrating the depolarisation, repolarisation and rest phase of two sample cardiac cells. The correlation between TAP of, (A) the furthest subendocardium, and (B) the nearest subendocardium section of the left ventricle and the resulting ECG wave are displayed. As shown in (A), in the farthest part, the depolarisation commences at 1 and the repolarisation finishes at 2. While it can be observed in (B) that in the nearest part; the depolarisation commences at 3 and repolarisation ends at 4. (figure adapted from Figure 10 [76]).

or a sudden trigger of another severe arrhythmia [11].

The diagnosis of arrhythmias involves discovering the location of the conduction disturbance, determining the existing atrial and ventricular rhythms and determining the links between the atrial and ventricular impulses [24]. ECG recordings are routinely used to confirm the presence of arrhythmias as well as evaluating the cardiac condition [79]. Among the standard ECG leads used for arrhythmia diagnosis, leads II or V_1 are the most favourable in detection of cardiac rhythms as they present the maximal P and QRS wave amplitudes [81]. The ECG electrodes and leads are discussed in section 2.2.1. The developed algorithm of this thesis using ECG signals for automated diagnosis of arrhythmias is described in section 4.1.2.

The characteristics of five arrhythmias will be described in the remainder of this section. Our definitions of these arrhythmias are based on the definitions provided by the *Computing in Cardiology (CinC) Challenge 2015* [33].

Extreme bradycardia is an arrhythmia characterised by heart rate, defined as five beat intervals in succession being greater than 1.5 seconds [33]. It is one of the classes included among sustained arrhythmias and may be generated by a diminished impulse genesis or conduction [11]. A common cause of bradycardia is a dysfunction of SA node, which can be generated by a number pathologic causes, categorised in two groups: intrinsic and extrinsic causes [10]. Intrinsic causes occur when nodal tissue is substituted, i.e. cardiac muscle fibres in the right atrium wall pass SA node pulses through to the conduction system of the ventricles, by fibrous tissue [79], [10]. The intrinsic causes can be produced by aging, infiltrative diseases, surgical trauma, familial diseases and infectious diseases [79], [10]. Extrinsic causes may be produced by pharmacological agents, prescribed drug use, hypothermia, electrolyte imbalance, neurologic imbalances and situational disturbances such as coughing, vomiting or defecation [79], [10]. Non-extreme bradycardia may occur in both healthy and ill patients, generated by intrinsic dysfunction, impairment of conduction mechanism or by the normal reaction to extrinsic causes [79]. For example, during inspiration, the heart rate elevates and bradycardia is observed during expiration phase [24]. Mangrum and DiMarco pointed out that extreme bradycardia might be linked with no symptoms or long-term clinical significance [79]. Asymptomatic bradycardia is commonly observed during sleep [79], [82]; however, if a patient reveals severe nocturnal bradycardia, there is a high likelihood of the presence of OSA [79]. Pacemakers are an effective therapy for bradycardia [79].

Extreme tachycardia is defined as a heart rate elevation of more than 140 bpm for 17 consecutive beats [33]. It can be a sustained arrhythmia and may be produced by disorders involving impulse conduction or impulse generation, such as enhanced automaticity or triggered activity [11]. Left uncontrolled, extreme tachycardia may develop into cardiac failure, cardiac ischemia or ventricular fibrillation [11].

Ventricular tachycardia (VT) is defined as five or more ventricular beats with heart rate higher than 100 bpm [33]. The contours of the consecutive ectopic ventricular impulses mostly are similar with fixed intervals in between [11]. VT has different clinical features including:

(1) Hypotension is not commonly associated with VT [11]. If the heart rate is above 180 bpm, it is generally considered as *ventricular flutter* [11].

(2) The beat-to-beat change in blood pressure and an increased right atrial pressure are commonly seen with VT [11]. Among the ECG features of VT; RR intervals may be moderately irregular with a change of 0.01-0.02 seconds per beat. Variations in the preceding P wave, fusion beats, or narrowed QRS complex rarely occur [11].

(3) An inverted P may be present in ECG lead II and an upright P generally exists in ECG lead aVR [11].

(4) The QRS complex is often homogenous and mono-morphic, i.e. having a uniform and consistent morphology [11].

(5) Other conditions may precede the onset of VT such as ischaemic heart disease, ventricular aneurysm, cardiomyopathy, drug toxicity, hypokalaemia and hypomagnesaemia [11].

These clinical features can be detected using ECG signals, lead II and aVr, and blood pressure signal which were utilised in this thesis and the developed algorithms are described in section 4.1.8.

Ventricular flutter or fibrillation (VF) is defined as a fibrillatory or flutter waveform for at least four seconds [33]. VF is characterised by an absence of a well ordered ventricular myocardial contraction sequence, and instead is produced by a disorganised and random transmission of electrical signals throughout the cardiac muscles [11],[83]. In terms of the ECG signal characteristics, an abnormal, disorderly and distorted deflections of changing height, width and form in the waves can be observed in a recording with VF [83]. A number of elements and diseases are linked with VF, such as cardiomyopathies and electrocution [11]. Most importantly, loss of cardiac output and cerebral perfusion may lead to death as a result of VF. This can be prevented by restoring sinus rhythm through immediate external cardiac massage and direct current defibrillation [11]. *Flutter* is the quick and regular electrical activity of atria or ventricles, detected in a minimum of one ECG lead [84]. It can be detected by identifying the absence of an isoelectric line between consecutive ECG waveforms of the fluttering chamber [84]. Ventricular rhythm is regular during ventricular flutter and the rate generally surpasses 250 bpm. A consequence of the high heart rate is that the identification of the QRS complexes and T waves in the ECG is impossible [84].

Asystole (ASY) is an absence of a heart beat for more than four seconds [33]. The periods of asystole linked with the SA node have a minimum of two potential sources comprised of sinus arrest or sinoatrial blockage [85]. It can also be observed in healthy subjects during sleep, as sleep can elevate second-degree atrioventricular blockage and cause short cardiac asystole [86]. Moreover, OSA creates

cyclic cardiac fluctuation and raises the likelihood of developing asystole, tachydysrhythmias and ectopic ventricular and atrial function [86], [87].

2.1.2. Sleep disordered breathing detection

In 2005 the international classification of sleep disorders (*ICSD*) defined several sleep related disorders, such as insomnia (difficulty initiating or maintaining sleep), SDB, hypersomnia (excessive sleepiness), parasomnia (abnormal events during sleep), sleep-related movement disorders and circadian rhythm sleep disorder (disruption of circadian time keeping system) [88].

SDB is associated with transient upper airway resistance, consecutive decrease or pause of airflow produced by partial or total obstruction of upper airway during sleep (see Figure 2.3) which involve sleep fragmentation, arousals, bradytachycardia and oxygen desaturation [26]. SDB contains a broad range of disorders from mild to severe OSA to upper airway resistance syndrome. Sleep apnoea (*SA*) is a common SDB accompanied by interruptions in breath during sleep [89]. SA patients undergo intermittent episodes of hypoxia and reoxygenation during transient blockage of airflow. The chronic repeated hypoxia effect of sleep apnoea syndrome may lead to serious systematic impairments such as chronic rise of daytime blood pressure, high risk of stroke, cardiovascular disease, damage of glucose control and insulin resistance, metabolic disorders and oxidative stress. Different conditions relate SA with cardiovascular disease, such as sleep fragmentation, oxidative stress, systematic inflammation, hypercoagulability, endothelial dysfunction and variation from snoring (see Figure 2.4) [2], [52], [90].

Guilleminault initially defined a SA event as involving at least a 10-second pause in breathing [91]. Currently, apnoea severity is measured with the apnoea-hypopnea index (*AHI*) which is the average number of apnoea and hypopnea events per hour of sleep. An AHI of greater than 5 is defined as SA [53]. An AHI of 5 or less is not clinically important and assumed normal.

In 1980 Block *et al*. first defined hypopnoeas as the shallow breathing events which produce oxygen desaturation and reduction of airflow, rather than complete blockage or absence of airflow [92], [93]. There are a number of criteria to describe hypopnoea events. They can be explained according to different characteristics such as the reduction in amplitude of breathing from baseline, rate of oxygen desaturation, or arousal and event duration [53], [94].

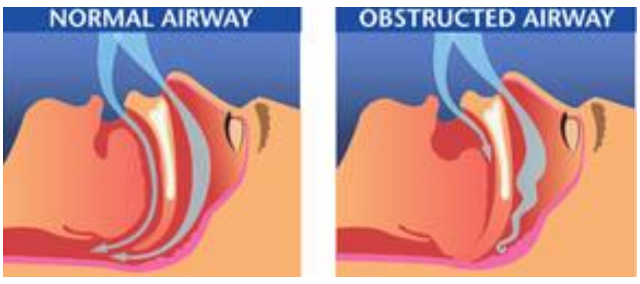

Figure 2.3. Blockage of airway in obstructive sleep apnoea. (figure adapted from [333].)

American Academy of Sleep Medicine (*AASM*) intended to standardise the clinical guidelines for the SDB events. The definitions of OSA and hypopnoea provided by AASM for different years are demonstrated in Table 2.1. The first publication by AASM for a standard SDB definition in 1999 indicated that obstructive apnoea or hypopnoea events are associated with partial or total block of air flow in upper airway leading to an interruption of regular breathing (see Figure 2.3) [53], [95]. AASM report in 1999 stated that due to the identical pathology of obstructive apnoea and hypopnoea events, identification is not required in regular clinical practice [53]. Thus, similar criteria were defined for both events, with criterion 3 required to be fulfilled in addition to either criteria 1 or 2 (see Table 2.1) [53]. The manual for respiratory scoring published by AASM in 2007 included two definitions of "Recommended" and "Alternative" for hypopnoea, as explained in Table 2.1 [96]. AASM published an update on the 2007 respiratory scoring manual in 2012 and recommended changes to the previous guideline (see Table 2.1) [92].

The symptoms of apnoea consist of snoring, choking, gasping, daytime sleepiness, morning headaches, sexual disability, depression, poor memory, concentration or cognitive potentials [97]. If SA remains untreated, it may have severe health consequences such as metabolic syndrome, obesity, cardiovascular disorders, arrhythmias, hypertension and stroke (see Figure 2.4) [54]. Furthermore, the resulting daytime sleepiness may lead to occupational and motor vehicle accidents [55]. As a result, diagnosis and treatment of SA is important for both patients and society to reduce the associated health costs [20]. Polysomnography (PSG) is the standard sleep test for apnoea diagnosis which records many signals during an overnight stay in a hospital. Sleep studies are expensive and patients may not sleep well due the attachment of wires and electrodes to the head, torso and limbs which can cause discomfort. Thus, an ongoing research goal is to develop simpler diagnosis for SA, reduce the

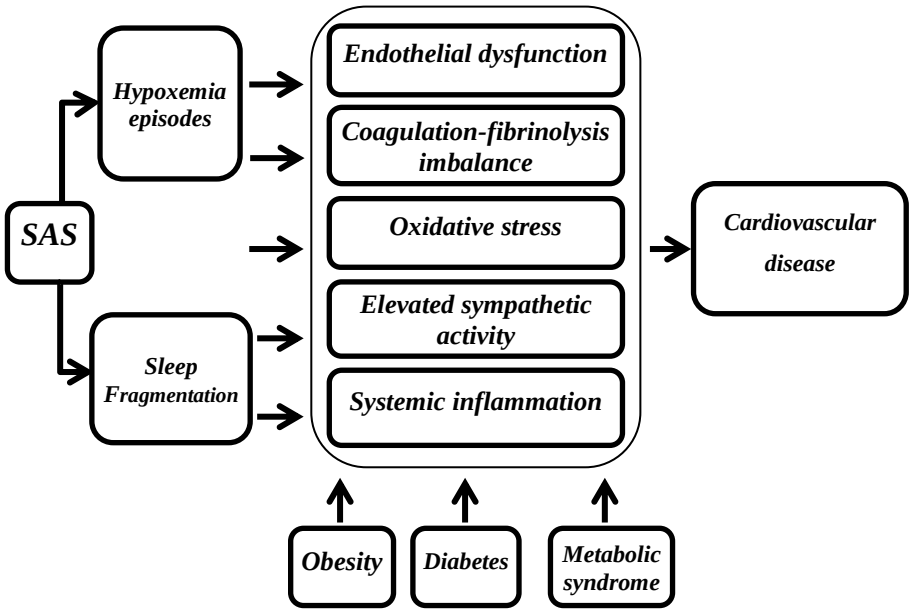

Figure 2.4. Schematic representation of the events occurring in sleep apnoea syndrome (SAS) commencing by sleep fragmentation and hypoxia as well as the associated disorders (figure reproduced from Figure 1 [90]).

number of diagnostic signals and diminish the cost and invasiveness of sleep tests, but proposing reliable methods of alternative SA diagnosis methods to the PSG is still contentious [23], [54].

A. Types of sleep apnoea

There are three major types of apnoea and hypopnoea:

(1) **Obstructive Sleep Apnoea (*OSA*)**: The physiological blockage of upper airway partially or totally with accompanying respiratory effort [97], [98]. In general, the initial illustration of an OSA patient is attributed to a character in the novel of "*The Posthumous Papers of the Pickwick Club*" by *Charles Dickens* in 1836. He was an extremely obese, sleepy boy who snored loudly [99], [26], [100]. This condition and the associated clinical characteristics were first noted by the physician Broadbent in 1877 [101], [26]. OSA is a common type of apnoea and can be categorised by the AHI or the respiratory disturbance index (RDI). RDI is defined as the AHI plus respiratory event-related arousals per hour of sleep [26]. OSA is divided into three classes:

Mild OSA: An *AHI* or RDI between 5 to 15 events per hour [26], [53]. Sleepiness might be observed during tasks needing trivial attention, such as watching TV or reading [2].

Moderate OSA: An AHI or RDI of 15 to 30 events per hour and sleepiness may occurs in activities requiring some attention, such as meetings or presentations [2], [26].

Table 2.1. The criteria and updates provided by AASM for apnoea and hypopnoea during 1999 to 2012.

Year	**Apnoea**	**Hypopnoea**
1999 [53] **Chicago Criteria**	1) Drop in airflow > 50% from baseline[1], or 2) Arterial oxygen desaturation ≥ 3% or an arousal, and 3) The event duration ≥ 10 seconds	1) Drop in airflow > 50% from baseline[1], or 2) Arterial oxygen desaturation ≥ 3% or an arousal, and 3) The event duration ≥ 10 seconds
2007$_{Rec}$[2] [96]	1) Peak signal excursion* ≥ 90% of pre-event baseline, and 2) The event duration ≥ 10 seconds, and 3) Event's duration meeting amplitude reduction criteria ≥ 90%	1) Nasal pressure peak signal excursions drop ≥ 30% of pre-event baseline, and 2) Duration of this drop ≥ 10 seconds, and 3) Arterial oxygen desaturation from pre-event baseline ≥ 4% 4) Event duration meeting amplitude reduction criteria for hypopnoea ≥ 90%
2007$_{Alt}$[3] [96]	* using oronasal thermal sensor, PAP (positive airway pressure) titration device or alternative apnoea sensors	1) Nasal pressure signal drops ≥ 50% of baseline 2) Duration of this drop ≥ 10 seconds, and 3) Arterial oxygen desaturation from pre-event baseline or an event associated with arousal ≥ 3% , and 4)Event duration meeting amplitude reduction criteria for hypopnoea ≥ 90%
2012 [92]	1) Drop in peak thermal sensor excursion ≥ 90% of pre-event baseline 2) The event duration ≥ 10 seconds 3) If a portion of hypopnoea event, meets criteria for apnoea, the entire event scored as apnoea	1) Nasal pressure signal excursion drop ≥ 30% of pre-event baseline, and 2) Duration of this drop ≥ 10 seconds, and 3) Arterial oxygen desaturation or event with arousal ≥ 3%

[1] Baseline is the mean amplitude of stable breathing or three largest breaths in the two minutes preceding the event onset for patients without stable breathing.
[2] Recommended

Table 2.2. Comparison of obstructive sleep apnoea and central sleep apnoea (table reproduced from [102]).

Obstructive apnoea or hypopnoea	Central apnoea or hypopnoea
Signs of efforts during apnoeas: chest wall movement, oesophageal pressure, pulse transit time	No sign of effort during apnoeas
Flow or nasal pressure tracing has flat tops in inspiration	Flow or nasal pressure has round tops in inspiration
Oxygen saturation curve is asymmetrical with slow decrease and quick recovery	Oxygen saturation curve is sinusoidal
Period of apnoea cycle is variable	Period of the cycle is constant
Snoring is usually present	Snoring is often absent

Severe OSA: An AHI of more than 30. It can be accompanied by sleepiness in more active tasks, such as talking or driving [2], [26].

(2) **Central Sleep Apnoea (*CSA*):** Central sleep apnoea does not originate from obstruction in airway; it is associated with periodic apnoeic and hypopneic events generated by reduced neural stimulation for breathing cycles [54]. The cessation of airflow is the consequence of lack of neurological drive for respiratory effort while the upper airway is open [2].

(3) **Mixed Sleep Apnoea:** It is accompanied by both obstructive and central symptoms. An initial failure in breathing efforts allows upper airway to obstruct. Usually, it comes with a period of central apnoea for several seconds before the obstruction followed by a rise of respiratory effort during blockage of airway [23].

The comparison of two main types of sleep apnoea is shown in Table 2.2. Firstly, indications of breathing efforts such as chest wall movements can be observed in OSA events, but there is no manifestation of breathing efforts in CSA events [102]. Second, the flow limitation in an OSA episode generates flat tops in the nasal pressure signal during inspiration, while this flat top is absent in CSA episodes and their flow signal exhibits round peaks during inspiration [102]. Third, assessing the oxygen saturation trace, OSA creates an asymmetrical trace with slow deceleration and sharp recovery, whereas CSA has a sinusoidal trace [102]. Fourth, in contrast to OSA which provides a variable period of cycles, CSA reveals a constant period of the cycles. Finally, snoring exists in OSA but is absent during CSA [102].

B. Epidemiology

Epidemiologic studies have shown that about 24% of men and nine percent of women suffer from the breathing effects of OSA and over four percent of men and two percent of women suffer from daytime sleepiness caused by OSA [2], [54]. On the other hand, approximately 85% of adults with SA are undiagnosed [2], [54]. Age is one of the affecting factors and the studies of over 65 years old subjects demonstrated higher rates of disordered population. For example, Ancoli-Israel *et. al* estimated OSA (defined as AHI of over 10) occurring in 70% of the men and 56% of women subjects

Table 2.3. Prevalence of OSA around the world, m = male, f = female, N/A= not applicable (table reproduced from Table 2 [104])

Study	Location	Ethnicity	Gender	Age (years)	OSA rate (%)
Bearpark *et al.* [105]	Australia	Caucasian	m	40-65	3
Bixler *et al.* [334]	USA	Caucasian	m, f	20-100	3.9(m), 1.2(f)
Ip *et al.* [154]	Hong Kong	Chinese	m	30-60	4.1
Ip *et al.* [335]	Hong Kong	Chinese	f	30-60	2.1
Kim *et al.* [336]	Korea	Korean	m, f	40-69	4.5(m), 3.2(f)
Lam *et al.* [337]	Asia	Asian	m, f	Middle aged	4.1-7.5(m) 2.1-3.2(f)
Udwadia *et al.* [106]	India	Indian	m	25-65	7.5
Young *et al.* [338]	USA	Caucasian	m, f	30-60	4 (m), 2(f)

with age ranged between 65 and 95 years old [103]. It should be noted that different studies use different thresholds for the AHI of OSA, but it is often defined between 5 and 10.

Around 1 in 20 adults suffer from OSA syndrome, which is OSA with daytime effects such as excessive sleepiness. In addition, population-based epidemiologic studies estimated that one in five adults endure minimally-symptomatic or asymptomatic OSA which is scarcely diagnosed [54]. Individuals with large neck sizes, smokers, alcohol consumers, overweight and obese people, middle-aged or older men, post-menopausal women, those with Down syndrome, and those with a family history of SA are among the groups with higher risk [2], [53], [102]. Also, it is reported that pregnancy may cause OSA [54]. Other risk factors include abnormalities in the bony or soft tissue in head or neck or abnormal nasal morphology [2]. Epidemiological studies show that SA mostly coincides with obesity [52], [90], [98]. SA occurs in 40% of obese persons and approximately 70% of SA patients are obese [90]. A study reported that 58% of severe OSA syndrome cases were a result of obesity [52], [90], [98]. Obesity is a critical cardiovascular risk factor related to OSA syndrome and when obesity is accompanied by OSA, it can result in other disorders including cardiovascular diseases or diabetes [98], [90]. Roebuck *et al.* investigated the prevalence of OSA worldwide and summarised the studies of different locations and ethnicities, as illustrated in Table 2.3, indicating the age ranges and genders under inspection and provided the OSA rate [104]. For example, Bearpark *et al.* reported 3% OSA rate among Caucasian men in Australia with age ranged between 40 and 65 [105]. Udwadia *et al.* studied Indian men population in India and announced 7.5% OSA rate among age of 25 to 65 [106]. The prevalence of SA and undiagnosed cases as well as the associated critical health issues show the importance of conducting research for developing simpler diagnosis and treatment tools for SA [54].

C. Aetiology

When the airway is blocked and breathing is obstructed, the rhythmic breathing effort continues until the effort or the drop of oxygen level in blood or hypoxia or hypercapnia force an arousal. Following an arousal, breathing recommences with blood oxygen and carbon dioxide levels restoring to normal

Table 2.4. Pathophysiology causes of obstructive sleep apnoea (table adapted from [89] , [97])

Risk category	***Factors***	***Comment***
General factors	Age	Male sex, hormone
	Gender	Central and neck size
	Obesity	
	Drugs	Ethanol, hypnotics
	Genetics	Multifactorial, higher risk in first-degree relatives
Reduced upper airway calibre	Anatomical injuries Neck flexion Nasal Obstruction	Macroglossia, small mandible, jaw placement, tonsils or adenoid hypertrophy, enlarged uvula, soft or hard palate or lateral wall tissue
Mechanical factors	Supine posture Upper airway resistance elevation Upper airway compliance elevation	
Upper airway muscle operation	Upper airway dilator muscle dysfunction Upper airway muscle and diaphragmatic contraction damage	
Upper airway reflex	Negative pressure feedback response injury from the lungs	
Neuromuscular	Myopathies, muscular dystrophies, neuromuscular disorders	
Central factors	Decreased chemical transfer Rhythmic elevation of central drive Deficient response to breath load	
Arousal	Arousal response damage Postapnoeic hyperventilation	
Diseases	Endocrine	Hypothyroidism, acromegaly, diabetes
	COPD, asthma, renal failure	
Extrinsic	Alcohol, CNS depressants	Hypnotics, narcotics

and the patient goes back to sleep [102]. Patients with the anatomic enlargements or obstacles in the airway are prone to pharyngeal obstruction during sleep [102]. As highlighted in the literature, upper airway blockage during OSA originates from a combination of anatomic components inclining the airway to block during inspiration, together with neuromuscular compensatory components which reduce during sleep resulting in incapability to preserve the airway open [54]. A combination of physiologic, anatomic, mechanical and clinical interactions contribute to SA syndrome [89], [97]**,** [107]. The aetiology or the causes of the SA disorder were summarised into three major groups of factors; the first group is anatomical factors, the second group is physiologic effects and the third group is neurologic factors [89], [97], [107]–[110]. Most of the aetiology elements of SDB are listed in Table 2.4 and are explained in the following sections.

D. Anatomical factors

The upper airway consists of four anatomical parts: 1) Nasopharynx which is from the nares to the hard palate; 2) Velopharynx or retropalatal oropharynx goes from the hard palate to the soft palate; 3) Oropharynx starts from soft palate to the epiglottis; 4) Hypopharynx which is considered from the base of tongue to the larynx, shown in Figure 2.5(a) [108]. The upper airway consists of about 20 muscles in four groups: 1) muscles regulating the position of the soft palate, 2) tongue muscles

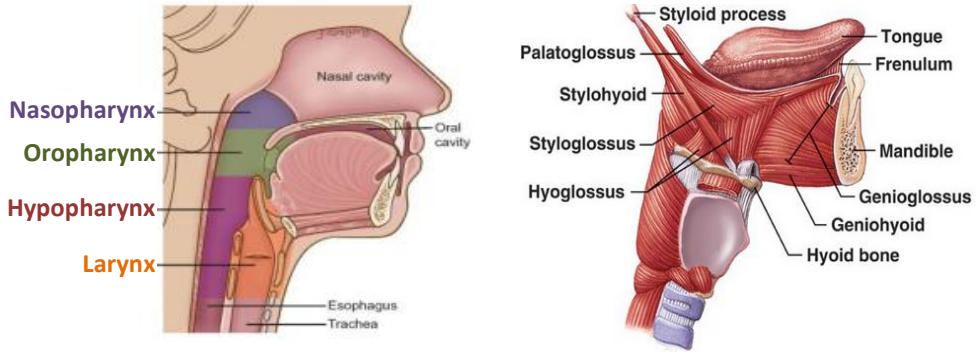

(a) (b)

Figure 2.5. Anatomy of the (a) main segments of the upper airway and (b) the main muscles of the upper airway (source: /headandneckcancerguide.org/ and /juniordentists/)

(genioglossus, geniohyoid, hyoglossus, styloglossus), 3) the hyoid apparatus and 4) the posterolateral pharyngeal walls (palatoglossus, pharyngeal constrictors) [108]. The main muscles are shown in Figure 2.5(b). These groups of muscles work together to maintain the airway open. Soft tissue components of the walls of upper airway comprise of tonsils, soft palate, uvula, tongue and lateral pharyngeal walls [108]. There are two craniofacial bony structures contributing to the airway size including mandible and the hyoid bone [108]. A firm or bony structure is absent in the airway to support the cross sectional area of the upper airway. The majority of OSA patients have a narrower upper airway in terms of anatomical characteristics [111]. It might be caused by obesity generating a load of body mass around the upper airway, or the small mandible, jaw placement, enlarged tonsils, enlarged tonsil soft palate, or tongue hypertrophy meaning thickening or increase in bulk of the tongue [112], [113]. An essential system in pathogenesis of OSA is the interaction of pharyngeal anatomy and reduction of upper airway dilator muscle activity for preserving airway open during sleep, as listed in Table 2.4 [114]. The largest upper airway dilator muscle is genioglossus which is the fan-shaped muscle between mandible and tongue and involves in other aetiology factors as will be described in the following sections (see Figure 2.5(b)). The anatomic enlargements, density increase and obstacles form an important category of SDB causes affecting the breathing procedure [115]. These anatomical factors, especially the upper airway dilator muscle activity, also contribute to the physiological factors and are described in the following section.

E. Physiological factors

The normal physiologic procedure of sleep in healthy control subjects involves the following series of actions: during NREM slow wave sleep, the mean blood pressure drops, heart rate decreases, sympathetic burst frequency reduces [109]. Sympathetic bursts are the synchronous discharges produced by the nerve activity controlled by autonomic nervous system [109]; the frequency and duration of these bursts estimates sympathetic activity [116].

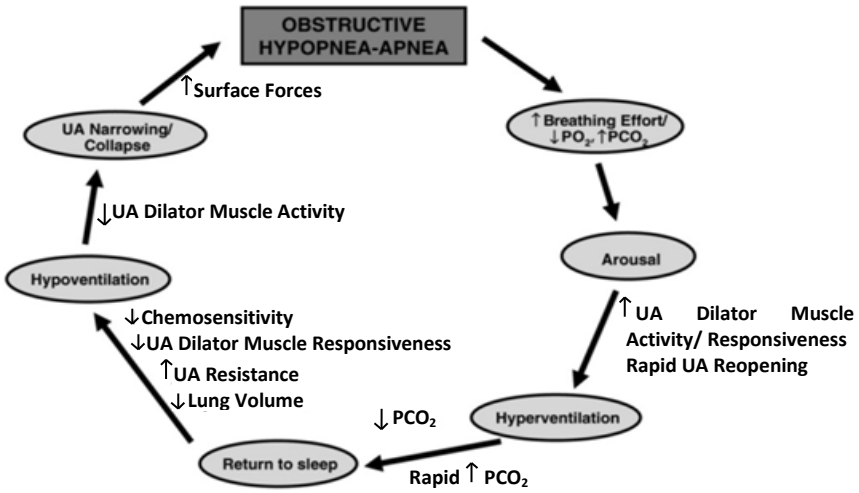

Figure 2.6. Schematic representation of pathophysiological sequence of OSA. The factors which are mentioned outside the circle are either protective or restorative and those inside the circle are preservative. UA stands for upper airway. Some of the factors are not proven or tested in a large scale yet, while others are certified therapies, such as continuous positive airway pressure (figure adapted from Figure 2 from [98]).

In this section, I explain the physiological factors contributing to SA. These factors include the upper airway muscle tone, pharyngeal sensitivity and the heart rate variability (HRV), which is one of the main features used in the developed algorithm of this thesis for SA detection [116]. A schematic representation of the simplified physiological process of an SA episode is demonstrated in Figure 2.6 [98], [117]. The elements displayed outside the circles are either protective or restorative while the factors indicated inside the circle are preservative. This circular flowchart displays the loop of mechanisms caused by OSA or hypopnoea commencing by drop of oxygen level, elevated CO_2 and augmented breathing effort, followed by arousals. As shown on the right of Figure 2.6, an arousal rectifies the negative consequences through upper airway dilator muscle activity and hyperventilation which amplify the oxygen level and reduce the CO_2 level; ultimately, leads to return to sleep. Then, in the event of an apnoeic episode, represented on the left of Figure 2.6, lung volume decreases, upper airway resistance elevates and muscle activity and chemosensitivity drop; generating hypoventilation. Eventually, the series of mechanisms produce narrowing or blockage of upper airway leading to SA event.

Typically, there is a phasic rhythm of breathing which commences by contraction of the diaphragm during inspiration. Following the inspiration, a negative pressure remains within pharyngeal area [110]. Consequently, these rhythmic breathing events create an intrapharyngeal prediction of negative pressure after each inspiration [118]. Overall, the procedure generates a rhythmic muscle activity [115]. That is, the dilator muscles contract at the onset of inspiration to open the airway. However, the activity of these muscles reduces during sleep; thus, no further neuromuscular compensation remains to keep the airway open [114], [119]. An important pathophysiological origin of OSA is the significant drop of upper airway muscle tone and dysfunction of the neuromuscular reflex of the

pharyngeal dilator muscle which will be explained in the following section (neurological factors) [114], [119].

The HRV or RR intervals, defined as the intervals between two adjacent peaks of heart rate, is affected by respiration through two mechanisms; 1) a direct autonomic respiratory-cardiac link through cardiovagal motor neurons, 2) an indirect effect of respiration through changes in blood pressure which affects baroreceptors [120]. It was shown that the RR interval decreases between the end of one expiration and the beginning of the next inspiration [120]. It is a beneficial feature in diagnosis of SA by ECG recordings.

HRV is often quantified by examining the power spectrum of the RR intervals. The spectrum of HRV consists of three elements: 1) a high-frequency (HF) component of heart rate around 0.15 to 0.4 Hz, mostly due to respiratory sinus arrhythmia (RSA), 2) a low-frequency (LF) or mid-frequency element around 0.4 to 0.15 Hz supposedly related to baroreflex functions in blood pressure control and 3) a very low-frequency (VLF) component around 0.01 to 0.04 Hz, which is most likely linked with low

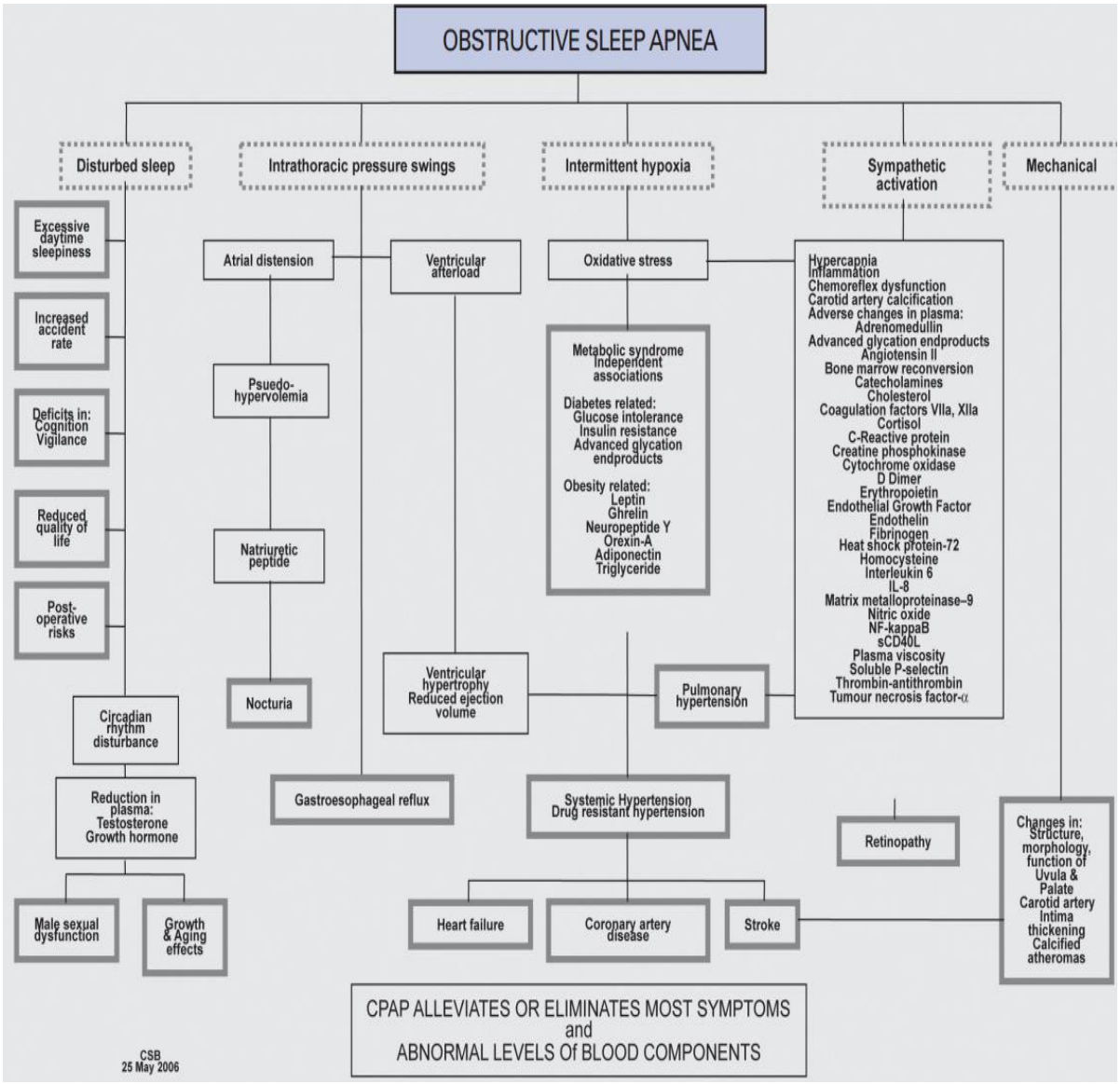

Figure 2.7. OSA physiological effects (figure adapted from Figure 1 of [107]).

frequency periodicities in respiration [121], [122], [110]. Spectral measures, such as ratio of LF to HF power and normalised HF power are used as a discriminating feature for detection of OSA since abnormal breathing patterns distort these measures [120]. Khoo *et al.* (2003) used a mathematical model to separate the origin of HRV into two parts: 1) The part generated by respiratory-cardiac coupling and, 2) the part originating from the baroreflexes [120]. Both of the mechanisms decrease in OSA patients compared to normal subjects. In addition, baroreflex gain elevates in normal subjects during sleep but does not change in OSA patients [120]. The results of spectral analysis of cardiovascular alteration agreed with other studies indicating that parasympathetic activity decreases and sympathetic activity increases in OSA syndrome [120]. The authors proposed a model-based technique including HRV and stated that spectral analysis provides a non-invasive recognition of OSA syndrome [120]. Spectral analysis of HRV was used in this thesis for OSA detection and will be described in section 0.

There are other physiological factors affecting OSA which are demonstrated in Figure 2.6. Apnoea events occur during REM (rapid eye movement) sleep in some OSA patients and prolonged hypopnoea and apnoea events and profound hypoxemia occur during REM in comparison with NREM sleep [123], [124]. REM sleep is accompanied by several physiological events, such as diminished upper airway muscle tone, damaged genioglossus reflex responses to negative pressure and decreased chemosensitivity [123], [124]–[129]. On the other hand, the arousal threshold seems to increase during REM which is prone to diminish the event duration, rather than extending it [124], [126].

SA has physiologic consequences, as shown in Figure 2.7, which may aggravate SDB conditions leading to establishment of a damaging loop. OSA has direct physiologic effects including, disturbed sleep, intrathoracic pressure oscillations, hypoxia, sympathetic activation and mechanical effects [107]. These direct alterations lead to a number of physiological consequences including excessive tiredness and sleepiness, gastroesophageal refluxes, oxidative distress, growth and aging effects, pulmonary hypertension, and cardiovascular disorders [107].

F. Neurological factors

SA patients often have high levels of nerve activity or sympathetic burst frequency occurring during wakefulness with further elevations in blood pressure and sympathetic activity occurring during sleep [109], [110]. In fact, sympathetic activity elevates mainly within stage II and REM sleep in case of SA [109]. During an apnoea event, blood pressure slowly elevates until cessation of apnoea [109]. Upper airway receptors operate as afferent of the reflex of the pharyngeal dilator muscle. They promote an increase in the genioglossus muscle activity due to negative pressure during inspiration on wakefulness. Knowing these mechanisms, it has been proposed that SA may originate from; 1) the impaired afferent affecting pharyngeal sensitivity of receptors and sensory nerves causing the reflexes

and rhythm not correctly conducted and 2) the injured efferent of motor nerves and muscles leading to misoperation of the muscles in maintaining the airway open [115]. Somers et. al, in 1995, studied the sympathetic neural mechanisms of patients with SA [109]. They found that in SA patients during sleep, sympathetic activity and blood pressure increase significantly, to a high level of 240/130 mmHg in some cases, while the same measures decreased in healthy subjects [109].

Affective, cognitive and autonomic nervous system are affected in OSA patients. This implies cerebral damages and central nervous system dysfunction due to OSA [130]–[132]. EEG recordings, magnetic resonance spectroscopy or other functional images revealed symptoms of declined neuronal density, functional asymmetry of the brain, brain dysfunction and anatomic damage among OSA patients [133], [31], [153]. Periodic hypoxemia, hypercapnia, sleep segmentation and arousals in severe OSA lead to neuropsychologic deficits [131], [132], [134], [135].

G. Treatment

There are a number of treatment plans for SA and the major groups are described in this section [26].

Assistive devices: The standard method for treating OSA is continuous positive airway pressure (CPAP), a prevalent choice for treating severe OSA and a reasonable option for moderate and mild OSA, when used correctly, it is an effective OSA treatment [38], [20], [104], [136], [137], [162]. It was first proposed as a treatment, in 1980 by Dr Colin Sullivan at the University of Sydney [138], [107]. Prior to this, the frontline treatment was a tracheotomy which was a highly invasive procedure with severe repercussions [107]. Dr Sullivan developed a non-invasive ventilation system to compensate the respiratory drop during sleep by pressurised airflow running through a mask [8], [107], [138]. The treatment keeps the airway open and helps the patients maintain normal oxygen levels [164], [165]. The schematic of the first proposed apparatus by Sullivan is shown in Figure 2.8. CPAP treatment of SA manifested alleviation of all of the symptoms and limits oxygen desaturation and reduces sympathetic activity and blood pressure during sleep [109]. Haba-Rubio *et al.* investigated the impact of CPAP treatment on arousal threshold of OSA patients and validated that the treatment reduces the inspiratory-effort-related arousal threshold as well as reduced the ventilatory drive in response to upper airway collapse [137]. Canessa *et al.* stated that CPAP treatment can restore both clinical and cerebral damages of OSA and that it enhanced recognition skills, action performance and memory of the patients and increased grey-matter volume [134]. It is an effective

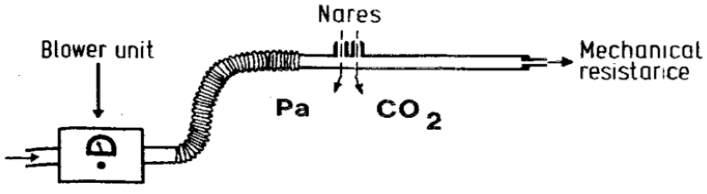

Figure 2.8. The first CPAP apparatus described by Colin Sullivan (figure adapted from Figure 2 [8]).

therapy when used properly; nevertheless, about 30-35% of patients are non-compliant or intolerant resulting from negative side effects, such as skin abrasions, bruising, dryness, or abdominal cramps [26], [139],[139], [140]. Esquinas and Cistulli suggested that the adherence can be investigated based on the OSA severity within the two categories of moderate and severe OSA [141]. This division explains that there is larger CPAP adherence observed in patients with more severe OSA in comparison with milder severity [141], [142].

Technological improvements were introduced to the CPAP device attempting to increase patient adherence, including BiPAP and APAP [38], [82], [104], [162]. Autotitrating PAP (APAP) is a method which detects the required level of pressure based on the sleep stage and body position and varies the airflow accordingly and supplies the optimum pressure [139], [143]. However, despite studies showing that patients preferred APAP over CPAP, the studies did not validate higher adherence to APAP than CPAP [143]. The Bi-level PAP (BiPAP) provides two levels of airflow pressure with lower expiratory positive airway pressure [139]. BiPAP provides OSA treatment with lower mean pressure compared to CPAP and is capable of elevating ventilation by pressure support [144]. A large number of studies have shown that BiPAP also does not improve adherence [145].

Diet and lifestyle: Behavioural alterations including losing weight, avoiding sleeping medicines, alcohol and tobacco, or body position therapy, such as changing sleeping position from supine to side or raising the head from the bed, can help OSA patients and reduce apnoea and hypopnoea events [2], [88], [26], [102].

Therapeutic devices: Oral appliances are similar to a sports mouth guards and keep the airway open by maintaining lower jaw, tongue, soft palate and uvula at their normal stable position [2], [104]. These can be useful for mild to moderate OSA patients and are an alternative for patients who are unable to tolerate CPAP properly [104]. There are also a number of over-the-counter remedies, such as nasal dilator strips, internal dilators and lubricant sprays, to alleviate snoring but their effectiveness remains unproven [2].

Electrical stimulation: Electrical stimulation of the lingual muscles by fine electrodes implanted into the genioglossus or the hypoglossal nerve have demonstrated that this treatment can enhance upper airway patency and preserve airflow without arousals [146], [147].

Surgery: Surgery can also be performed in cases where alternative treatments have failed [52], [104]. The eligible patients for surgery are those with apparent anatomic deformations [52]. Through surgery, ablation of tissue in the soft palate, uvula, tonsils, adenoids, tongue or rectification of the craniofacial bone structure can be performed [52].

H. Diagnosis

The polysomnogram (*PSG*) is the standard SA diagnosis device. It is a multi-channel recording of electrocardiography (*ECG*), electrooculography (*EOG*), chin electromyography (*EMG*), leg EMG

derivations, oxygen saturation, electroencephalography (*EEG*), oronasal airflow, respiratory measurement, effort parameters and body position [1], [53], [20], [71], [148]. PSG, generally, requires an overnight stay in the unfamiliar environment of a hospital or sleep clinic with a number of sensors and wires attached to the face, skull, chest and limbs. An example of a simplified set up is shown in Figure 2.9 [53], [20], [148].

The AASM has published a guideline for PSG and manual for scoring sleep and related events [1]. It includes recommended measures for the routine PSG scoring as well as optional rules and measures

Table 2.5. Examples of measurements proposed by AASM for PSG test in two categories of optional and recommended [1].

	Recommended	**Optional**
Sensors and measures	**sleep scoring data** light out and on time total sleep time total recording time sleep latency stage R (*REM*) latency percentage of sleep efficiency *(TST[1]/TIB[2])* **arousal events** number of arousals arousal index **respiratory events** number of obstructive apnoeas number of mixed apnoeas number of central apnoeas number of hypopnoeas apnoea index hypopnoea index minimum oxygen saturation during sleep respiratory efforts related to arousals occurrence of Cheyne Stokes breathing (yes/no) **cardiac events** average and highest heart rate during sleep highest heart rate during recording **movement events** number of periodic limb movements of sleep (*PLMS*) number of movements per hour divided by TST (PLMS with arousals and PLMS index) **in case of arrhythmias (yes/no)** heart rate arrhythmia and duration of pause the lowest heart rate (bradycardia) the longest pause (asystole) highest heart rate (sinus tachycardia during sleep) arterial defibrillation **summary statements** findings related to sleep diagnosis EEG abnormalities ECG abnormalities	**respiratory events** respiratory effort related arousals respiratory effort related arousal index oxygen desaturations (total number) ≥3% or 4% oxygen desaturation index ≥3% or 4% occurrence of hypoventilation (yes/no) **summary statement** sleep hypnogram **alternating leg muscle activation** minimum bursts of leg muscle activity maximum frequency of alternating EMG bursts in 0.5 Hz maximum frequency of alternating EMG bursts in 3 Hz **respiratory effort related arousal events** respiratory effort related arousals

[1] Total sleep time
[2] Time in bed ready to go to sleep

suggested for uncommon events or the events which are not known as physiologically important events [1]. Some of the measures are listed in Table 2.5.

The PSG test has disadvantages: it is expensive, requires overnight specialised staff and facilities, in many sleep test centres there are long waiting times, and the attachment of electrodes disturbs the patient's sleep [20]. Quantifying and detecting sleep issues using simpler sensors and signals to minimise the disturbance is an appealing and challenging topic [148]. The aim of this thesis is to reduce the number of sensors, cost and disturbance on sleep and breathing and develop algorithms to extract useful information for SDB detection from fewer signals.

2.2. Sensors

In the published literature, a number of sensors have been used for automated diagnosis of cardiorespiratory disorders, among which this thesis focused on the minimally invasive types; with the term "minimally invasive" meaning to target minimising the disturbance on the patients and their normal activities. Previous sections of chapter 2 described different physiological features contributing to cardiorespiratory disorders which can be used for monitoring the disorders. For the first application (arrhythmia diagnosis in the ICU), we used sensors which capture the heart rate and cardiac information: electrocardiogram (ECG), arterial blood pressure (ABP) and photoplethysmogram (PPG). The use of multimodal signals is beneficial in enhancing the performance of automated diagnostic algorithm by combining the information through signal fusion in order to compensate the missed information or artefacts of an individual signal by considering the information of other simultaneous recordings [55], [185].

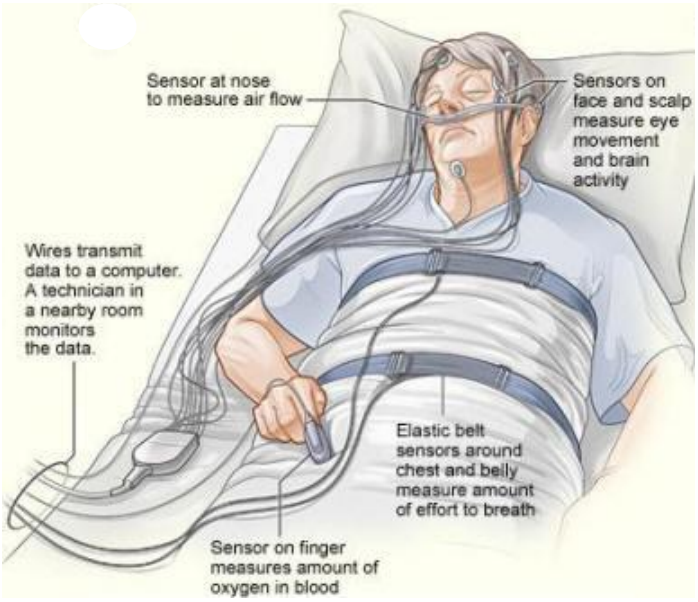

Figure 2.9. An example of polysomnography set-up and simplified attachment of sensors of PSG (source: /qa.virinchihospitals.com/).

The second application of this thesis (automatic diagnosis of SDB) incorporates evaluation of clinical features and objective sleep study [151]. The typical clinical features collected for SDB diagnosis include age, sex, body mass index (BMI), pharyngeal characteristics and bed partner observation of apnoea events [151], [152]. The information acquired from physical tests, questionnaire and patient history can estimate the state of SA to some extent and are the first stage of monitoring SA [151], [153]–[156]. In fact, SA diagnosis is not possible by only considering clinical features and requires identification of abnormal respiratory events as well [151]. There are three main categories of breathing monitoring methods for SDB detection; a group of instruments that evaluate blood gas variations such as oximetry, or end-tidal O_2 measurements [157]. Another group of instruments quantify oronasal airflow directly, such as thermistors. The third group estimates motion of an object, volume, or tissue changes, such as trans-thoracic impedance methods or inductance plethysmography [157]. The respiratory monitoring sensors which directly measure the air flow provide accurate measurement of apnoeas. However, they mostly disturb sleep and interfere with normal breathing [158].

As shown in Figure 2.10 [159], SA episodes can be readily distinguished by observing the airflow signal and the influence of airflow reduction on other signals, such as the respiratory effort signals, ECG signal and oxygen saturation. The drop of airflow during apnoeic event results in a decrease of amplitude in the respiratory effort signals as well as a reduction of the oxygen saturation level with a delay [159]. In fact, the level of oxygen saturation drop and the recovering process depend on the level of reduction of airflow [160], [208]. Observing the signals of Figure 2.10 reveals the high potential of flow signals, respiratory signals and SaO_2 in detecting apnoea events. Referring to the sleep disturbance of the sensors, the flow signal is associated with a high level of interference with sleep and natural breathing procedure due to the placement near the nares. Then, in terms of level of disturbance, it is followed by the respiratory inductance plethysmography (RIP) sensors with respiratory bands placed on the chest and abdominal area which also slightly restrict the movements generated by normal [1], [96], [104], [161]. On the other hand, the ECG recording provides a much lower level of interference with the sleep and breathing cycles. Thus, this thesis aimed for indirect respiration monitoring methods from movement in thorax or abdomen, such as deriving the respiratory effort from ECG signal which involves simple recording and minimal disturbance on sleep and breathing. Also this thesis utilised chest respiratory effort signals measured by plethysmography to evaluate the performance of the ECG-derived respiratory signals for SA detection.

There are a large number of commercial and consumer products for minimally invasive sleep analysis available in the market capable of detecting apnoea events. For instance, actigraphy is a technology to measure movements and activity patterns by sensitive accelerometers [13]. There are different types of actigraphy systems; an example is wrist or ankle watches such as the commercial model of Actiwatch [162]. AASM has stated that actigraphy can be used for estimating the sleep time and

evaluation of circadian rhythm disorders [163]. The results of the studies on evaluating Actiwatch for extracting sleep patterns reported a wide range of accuracies. Also the dependency of the performance on the population under study and sleep characteristics of the subjects reduces the liability of the sensor and its potential for diagnostic use [164]–[166]. The other example is the bio-motion sensor which uses radiofrequency wave reflection to determine the location, position and velocity of movements of objects and evaluating sleep/wake status in some studies [17], [167], [168]. The mechanism of this non-invasive sensor is to compare the phase difference of the reflected wave and transmitted wave to estimate chest movement [27], [167], [169]–[171]. In studies, this technology was used to detect breathing rate and compare with actigraphy in identifying sleep/wake patterns and estimating sleep quality in OSA patients [27], [167], [169]–[172]. O'Hare *et al.* in 2014 compared sleep parameters estimated by non-contact sensors and actigraphy with the results of PSG [172]. The study utilised different sensors including two non-contact radiofrequency biomotion sensors of SleepMinder and SleepDesign (*HSL-101*) and an actigraphy-based system of Actiwatch [172]. They discovered that the performance of the biomotion radiofrequency sensors is comparable with

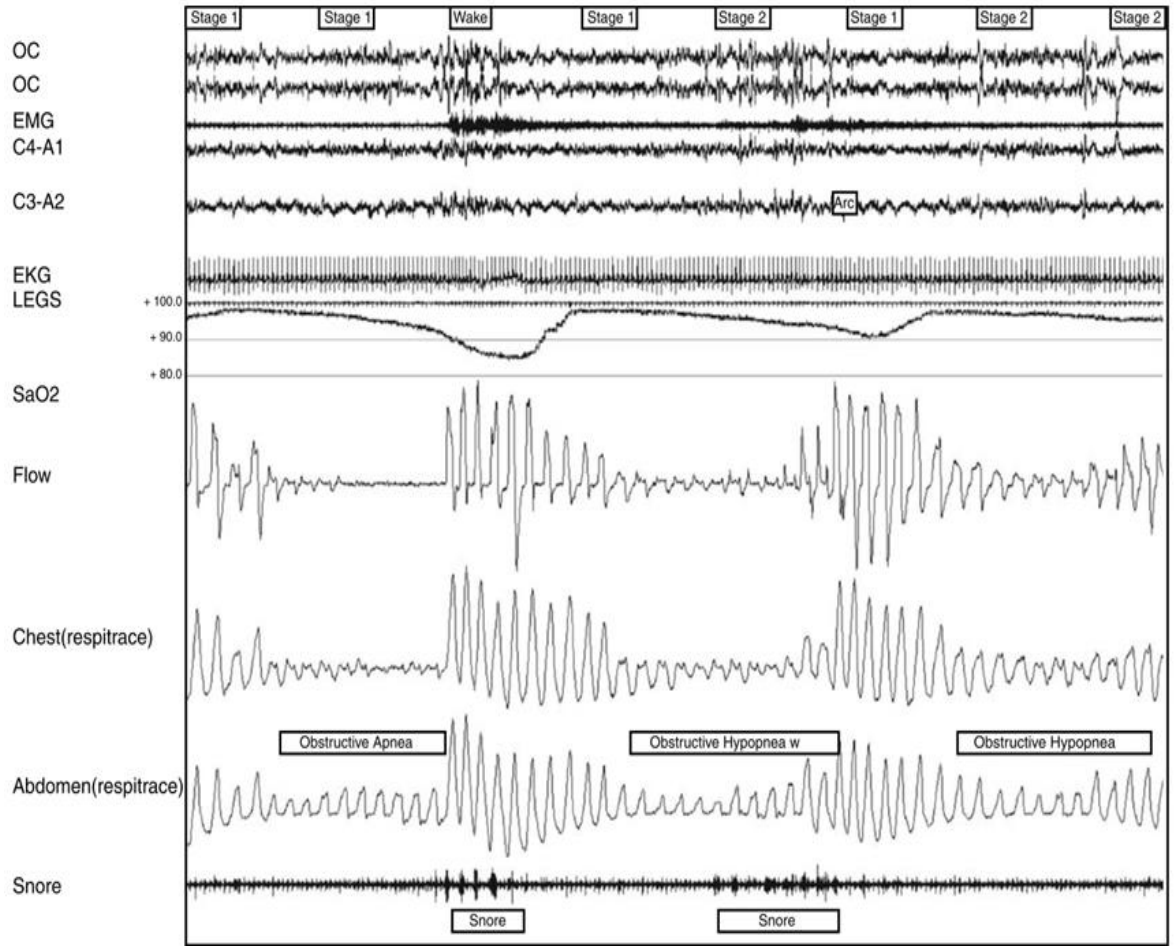

Figure 2.10. A sample PSG recording of an OSA patient with three consecutive obstructive events, one apnoea and two hypopnoeas. It can be seen that event-associated oxygen desaturation depends on the range of decreased flow during the events. The flow is a nasal pressure recording, with inspiration in the upward trend and restriction of upper airway flow occurs when remaining plateau during hypopnoea (figure adapted from Figure 50-5 [159]).

actigraphy in estimating sleep/wake measures, but compared to PSG, all three devices overestimated sleep time and underestimated sleep-onset latency and wake-after-sleep onset [172]. Another study by de Chazal *et al.* in 2011 evaluated the performance of the biomotion sensor on 113 subjects against gold-standard PSG [167]. They reported that the sensor is capable of detecting sleep-wake patterns but lower accuracy is achieved in subjects with higher AHI than in subjects with lower AHI. Also, they stated that their algorithm slightly overestimated sleep efficiency and TST [167]. Although these sensors provide sleep measures in a minimally invasive fashion, the detected information is not adequate for diagnosis of SA and PSG is still known as the standard sleep test for SDB recognition. The focus of the second application of this thesis was using ECG recording, aiming to extract reliable respiratory information and features linked with SDB (while reducing the disturbance on sleep and breathing procedure of respiratory inductance bands). The methodology of this application using the information of the sensors to detect cardiorespiratory disorders will be described in the following chapters 3, 4 and 5. In this section, I will present some details regarding the utilised sensors in both applications of the thesis, starting with ECG recordings, followed by PPG, oximetry, RIP and ABP.

2.2.1. ECG

Einthoven presented the ECG over a century ago to record the electrical activity of heart [76]. The ECG signal is recorded via a number of electrodes and leads in different locations on the body surface which record the heart's electrical activity from different sites of the cardiac muscles. This results in different ECG morphologies, as exhibited in Figure 2.11 (A-C) [76]. The limb leads are shown in Figure 2.11 (A-C), with individual lead measuring the impedance difference and consisting of two electrodes of opposite polarities (bipolar) or a positive pole and a reference (unipolar) [76], [84], [77]. Limb leads include leads I, II, III which are bipolar in the frontal plane placed between right arm, left arm or left leg, satisfying Einthoven's law of $V_I + V_{III} = V_{II}$ [75], [77].

The cardiac and physiologic mechanisms of cardiorespiratory disorders were described in sections 2.1.1 and 2.1.2. The first application of the thesis (arrhythmias diagnosis), generally, involves discovering cardiac rhythm variation and the location of the conduction disturbance [11], [24]. ECG recordings are the preferred sensor in detection of cardiac rhythms and, thus, arrhythmias [81]. Mäkivirta *et al*. used ECG signals to reduce false arrhythmia and in comparison to the results of popularly-used patient monitoring system, they were able to reduce false alarm frequency from 88% to 51% [173]. Studies stated that artefacts are inevitable in ECG recordings and may lead to misdiagnosis of arrhythmias and can be the source of false alarms [173], [174] and that multimodal signal processing helps with noisy signals or missing values and enhances the results for this application [51], [175]–[181]. Our solutions to these issues using simultaneous information of further sensors and multimodal methods for this application will be discussed in sections 3.1 and 3.3.

Guilleminault *et al.* originally suggested that SA is accompanied by a cardiac pattern which can be recognised by HRV analysis using the ECG signal for the second application of the thesis [148], [182]. Figure 2.12 demonstrates a sample ECG, HR, oxygen saturation signal and PPG during an apnoeic event [104]. Distinctive patterns of ECG signal generated by the apnoea event are apparent. It can be seen that about 10 s after an apnoea event commences, the heart rate decreases followed by an elevation, which matches to the original definition of apnoea event by Guilleminault *et al*. [182], [104]. Also the increase in R-R intervals can be easily identified in the ECG signal.

In a study by Gubbi *et al.* in 2009, eight level wavelet packet analysis was implemented in order to non-invasively classify OSA from CSA by ECG signal [183]. Their best tree analysis indicated that OSA is mainly in the low frequency band of R-R intervals and CSA is on both low and high frequency, significantly between 64 to 96 Hz [183]. It was the most discriminating feature for classification of these two types of apnoea. Their combined outcome was presented about 85% accuracy with 88% sensitivity and 84% specificity. They reported that the accuracy of best tree entropy was 91% with sensitivity of 92% and specificity of 91% [183]. In 2007, O'Brien and Heneghan distinguished OSA from CSA and hypopnoea by a single lead ECG and compared with plethysmography [157]. Their results of single lead ECG showed 82% accuracy in apnoea classification [157]. Penzel *et al*. in 2002 compared thirteen studies of apnoea detection using ECG recordings [148]. Different methods and transformations were used and a number of features, besides HRV, were extracted with some of the algorithms involving fully automatic analysis and the others requiring visual and auditory classification [148], [184]–[192]. The highest obtained score for identifying each one minute of apnoea and hypopnoea was about 92% by two teams using manual verification of apnoeic events and the highest score among the automatic algorithms was achieved by de Chazal *et al*. algorithm which was 89.4% [148], [184]. The best performing approaches and features will be explained in section 3.2. In the developed algorithm of this thesis, a number of features were extracted from ECG signal containing information regarding apnoea events which will

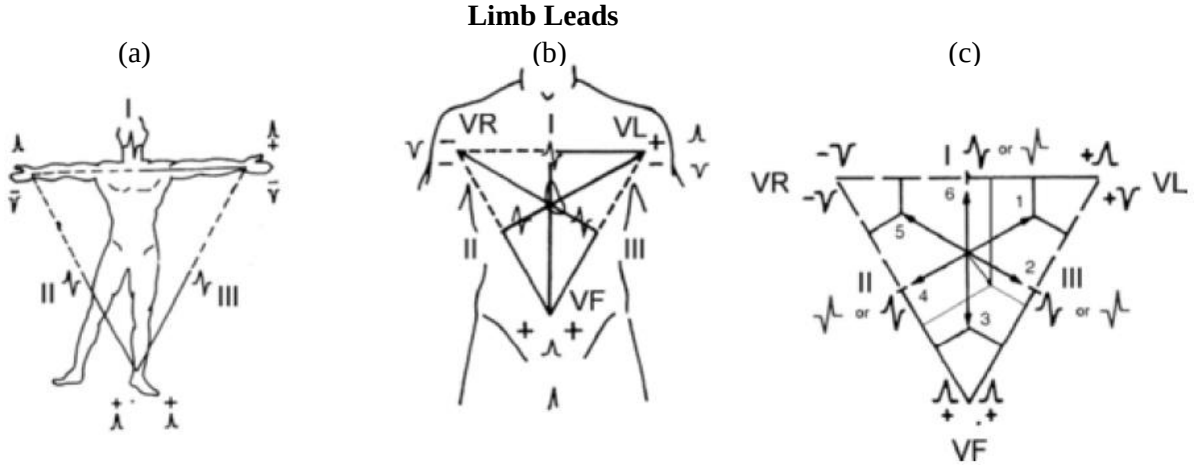

Figure 2.11. (a) Einthoven's triangle, (b) Einthoven's triangle located on the chest, with the positive polarity electrode of the leads shown in solid lines and negative electrode shown in dotted line, (c) vectors 1 to 6 generate different projections due to their site (figure adapted from Figure 11 [76]).

Table 2.6. Frequency ranges of the PPG signal and the usage (table adapted from Table 1 [18])

Frequency	Range (Hz)	Explanation
Very low	0.001-0.03	Myogenic response to pressure changes, energy saving and thermoregulation mechanisms
Low	0.04-0.11	Reflect changes in sympathetic tone
Intermediate	0.12-0.18	Reflect efferent vagal activity
Respiratory	0.19-0.30	Respiratory-induced oscillations
Cardiac	0.75-2.50	Arterial pulse-induced oscillations

be described in more details in section 3.5. Extracting the respiratory information from ECG signal through a reliable and computationally efficient approach and evaluating the results compared to a reference respiratory signal is challenging. It was carried out in this thesis with the background methodology discussed in section 3.5.2 and our developed algorithms described in section 5.1.3.

2.2.2. PPG

PPG technique is composed of two elements, each containing useful clinical information: the AC element which is the pulsatile physiological waveform (mostly referred to as PPG signal) and the DC element linked with the average blood volume which varies by respiration and other activities [104], [18]. The AC element reveals alterations in the cardiac patterns and blood volume [104]. The PPG system involves transmitting light into the tissue where it is partly absorbed and scattered and then detected by photodetector [18]. Due to the higher absorption coefficient of tissue blood component compared to other parts, PPG easily detects the variations in the blood volume [18]. Hertzman and Spealman, in 1937, noted the potential of the PPG in estimating blood volume changes in the finger [193]. The PPG signal contains a wide range of information including cardiovascular, respiratory and neural fluctuations as showed in Table 2.6. It should be noted that the frequency ranges displayed in Table 2.6 are approximate [18]. Different frequencies of PPG signal contain different information. Thus, extracting the frequency components of PPG signal can be used for recognition of cardiorespiratory disorders [18]. On the other hand, PPG waveform is prone to significant distortion by missing values and different types of noises and artefacts, such as motion artefact which can result in false detection of the cardiorespiratory disorders [104]. In 2014, Roebuck *et al.* reviewed the recently developed signal processing methods using PPG, including: 1) decreasing the impact of motion artefact and false desaturation alarms of the device, 2) invention of new measuring indices to enhance the diagnosis of respiratory disorders, 3) computing indirect measures of heart rate and respiration from PPG waveform which makes it more probable to replace hospital-based PSG systems [104]. Aboukhalil *et al.* reported that use of pulsatile signals, such as PPG signal, which incorporate cardiac cycles improves the diagnosis of false arrhythmia alarms when combined with cardiac cycle information from ECG signals [175]. The developed algorithm for arrhythmia detection utilising the pulsatile signals including PPG signal will be illustrated in sections 4.1.6 and 4.1.8.

2.2.3. Oximetry

Oximetry is derived from PPG technique which performs by emitting light of two wavelengths passing through the tissue, for instance, fingertip to a photodetector [151], [18]. Squire, in 1940, reported that oxygen saturation changes cause alterations in red and infrared light emission through tissue [194]. Among the applications of PPG, it is the most extensively used method, which was introduced to the global market in the 1980s [18].

By this system, the changing absorbance of each of the wavelengths caused by the pulsing arterial blood is measured [151]. In fact, the ratio of oxygenated and deoxygenated haemoglobin at two wavelengths of red (660 nm) and infrared (940 nm) generates the respiratory information using pulse oximetry [18]. It is a reliable method for diagnosis of sever OSA which involves a repetitive pattern of oxygen desaturation [151]. The results of an experiment by Sériès *et al*. in 1989 showed that lung volumes have a wide impact on the amount of O_2 desaturations of more than 90% after OSA, and O_2 desaturation increases exponentially with apnoea length [195]. In 1991, Pépin *et al*. proposed that

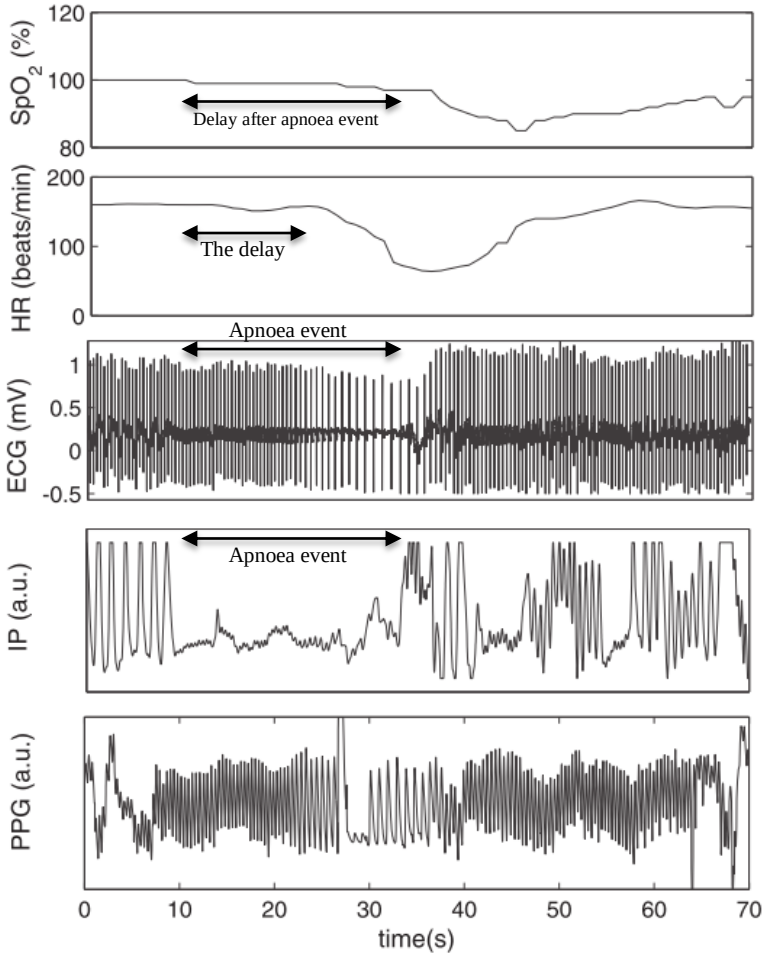

Figure 2.12. A sample of oxygen saturation signal, heart rate (HR), ECG, PPG and IP (impedance pneumography) during an apnoeic event (figure adapted from Figure 1 [104]). Distinctive patterns of HR and oxygen level is apparent in the signals in about 10 s after commencing apnoea event, HR drops followed by an elevation, and oxygen level drops with a delay of about 20 s after the apnoea event and then slowly increases.

home oximetry is a simple technique for apnoea diagnosis [160]. They indicated that an apnoea and hypopnea event lasting for less than 10 s may not be detected by respiratory disturbance index (RDI), but can be detected using oximetry outputs [160]. A sample of oxygen saturation signal during an apnoeic event is displayed in Figure 2.12 [104]. It shows that the oxygen level drops with a delay of approximately 20 s after the beginning of apnoea event, then slowly increases to its pre-apnoea value, confirming the findings of Sériès *et al*. in 1989 [104], [195].

Oximetry is able to detect severe cases of OSA that need urgent treatment [196]. A work by Sériès *et al*. in 1993 implemented oximetry to detect sleep apnoea/hypopnoea syndrome using unfixed oxygen desaturation criteria and a high sampling frequency to obtain more precise SaO_2 tracing [197]. They concluded that the method can be used as the first evaluation of the patient to confirm the requirement of the overnight PSG [197]. They added that due to the low specificity of 47.7% and low positive predictivity of 61.4%, a validation by PSG test is essential for final diagnosis [197]. They stated that due to several factors affecting desaturation baseline levels (expiratory reserve volume, total apnoea time and different types of apnoea), implementing a fixed threshold for drop of SaO_2 levels fails to lead to a reliable diagnosis [197]. A study of home oximetry by Golpe *et al*., in 1999, stated that while oximetry results have some correlations with PSG, it is not completely reliable and 15% of the OSA patients were not diagnosed by only oximetry recording [196]. Moreover, oxygen desaturation may not be present during hypopnoea or events of increased upper airway resistance [151]. The sensitivity of OSA diagnosis by oximetry in the literature was reported in a range of 31 to 98% with specificity of 41 to 100% [151], [196]–[198]. The wide range is due to different patient population and more importantly different devices with different protocols, such as averaging in some studies [151], [196]–[198]. Furthermore, oximetry as the single recording is unlikely to be successful in recognising milder apnoea [151], [196]–[198].

Heneghan *et al.* in 2008 performed synchronous recording of ECG and pulse oximetry by utilising a combined Holter-oximeter method and reported that a downside of oximetry signal was inability in analysis of epochs damaged by artefact [199]. Thus, multimodal signals can be beneficial to enhance the diagnosis as will be described in detail in the following chapters.

2.2.4. Respiratory inductance plethysmography

There are a number of methods for monitoring respiratory measures including, electric impedance plethysmography (EIP), respiratory inductance plethysmography (RIP) and piezoelectric inductive displacement sensors, with RIP reported with higher accuracy, sensitivity and patient safety for detecting OSA and estimating the respiratory characteristics such as tidal volume, mean inspiratory flow and inspiratory and expiratory times [22], [161], [200]–[204] . The AASM also recommends RIP as a more reliable technique for respiratory effort measurement than other wearable respiratory monitoring techniques such as EIP, strain gauge sensors and piezoelectric displacement sensors [205].

Cohn in 1977 initially utilised RIP for non-invasive respiratory monitoring, comprised of two bands containing winding coils around the rib cage and abdomen [206]. In the RIP technique, the respiration is detected based on the cross-sectional area which is identified by the inductance of the conductive loop and the alteration of self-inductance [200]. Volume of the chest and abdomen and the rib-cage activity can be obtained by computing the cross-sectional area of the chest and the band loop through an impedance plethysmography or an elasticated band worn around the torso [200], [202]. This method can include some artefacts, such as alterations due to the cardiac activity recognised as breathing, or muscle movements during apnoea events mistakenly detected as breathing, or sigh acts saturating the impedance signal leading to errors in breathing detection [202]. Bradley *et al*. studied the cardiorespiratory measurements estimated by RIP [204]. They used LifeShirt® incorporating a vest with the embedded core technology of RIP to capture respiratory pattern non-invasively, with the term non-invasive meaning that it is unobtrusive [204]. They indicated that the device had the ability to detect cardiorespiratory measures, such as ventilation, respiratory rate and heart rate [207], [208]. A sample PSG recording of an OSA patient containing chest and abdominal respiratory effort signals is shown in Figure 2.10 [159]. The excerpt of the demonstrated recordings incorporate three consecutive obstructive events; one apnoea and two hypopnoeas [159]. A significant decrease in amplitude can be observed in both chest and abdominal respiratory effort recordings during the events, with the reduced amplitude depending on the range of decreased flow. It can also be noticed that the range of amplitude reduction is more apparent in the chest respiratory signal compared to the abdominal signal. Therefore, it was one of the reasons that we utilised the chest respiratory effort signal for SDB detection; comparing the results with ECG-derived respiration, as will be outlined in section 5.1.3. O'Brien *et al.*, in 2007, studied the comparison of a single lead ECG (Holter monitor) with inductance plethysmography of the rib-cage and abdomen to detect OSA as well as CSA and hypopnoea [157]. They stated that tidal volume can be accurately measured through calibration against a spirometer. The results of a single-lead ECG were correlated with the detection outcome by inductance plethysmography with 82% accuracy in apnoea classification [157]. Therefore, it was used in this thesis as a suitable sensor to classify SDB and to be used for evaluating the respiratory information extracted from ECG, as will be described in chapters 3 and 5.

2.2.5. ABP

Arterial blood pressure (ABP) is a biomarker of the haemodynamic state of the patient, representing the tissue and organ perfusion [4]. Systematic blood pressure is generated by the blood forcing the arterial wall, originating from the cardiac output and systematic vascular resistance [4]. The physiologic effects of cardiorespiratory disorders on ABP were described in chapter 2. Aboukhalil *et al.* in 2008 reported that implementing pulsatile signals, such as ABP, which contain cardiac cycles, improves the diagnosis of false arrhythmia alarms by ECG signals [175]. They used ABP as one of

Table 2.7. Comparison of candidate sensors for diagnosis of cardiorespiratory disorders.

	Diagnosis Characteristics				
Sensors	**Low disturbance**	**Low cost**	**Accuracy**	**Arrhythmias**	**SDB**
ECG [71], [104], [157], [179], [339]	Good	Good	Good	Yes	Yes
Oximetry [29], [104], [199], [340]–[343]	Good	Good	Good	Yes	Yes
PPG [18], [104], [175], [344]–[346]	Medium	Medium	Good	Yes	Yes
RIP [22], [104], [157], [161], [200]–[205]	Medium	Good	High	Yes	Yes
ABP [51], [104], [212], [347]–[349]	Good	Good	Medium	Yes	No
Holter-Oximetry [104], [199], [269], [343], [350], [351]	Good	Good	High	Yes	Yes
Radio-freq biomotion sensor [27], [104], [162], [167], [169]–[172]	Good	Good	Good	No	Yes
EEG [104], [352]–[355]	Bad	Good	High (sleep quality)	No	No
Nasal transducers [104], [151], [356]	Bad	Good	Good	No	No

the pulsatile signals to verify the false arrhythmia alarms. As it is recorded from a separate sensor than the ECG leads, it rarely contains identical interference to the ECG signal [175]. Also, ABP is regarded as the pressure signal with the least noise and artefact [51]. In fact, for our application, the ABP signal was recorded using a separate sensor placed at a distance from the torso where different noise features from ECG characteristics present [4], [175], [209], [210]. Therefore, excluding the large body movements which alters the signals of both sensors, the existence of ECG-affiliated artefacts on the ABP signal appears improbable [175]. Thus, utilising ABP in conjunction with ECG signal helps reduce false detections and benefits the diagnosis of cardiorespiratory disorders [51], [175], [211], [212]. Through ABP analysis, the morphology and timing of the ABP signal can be compared to the ECG characteristics and reduce the false positive and negative detections [175].

The major characteristics of nine sensors for cardiorespiratory diagnosis are compared in Table 2.7, including the disturbance to the patient, cost and accuracy. For instance, the ECG signal is marked as a suitable sensor for diagnosis of both arrhythmias and SDB and provides a good accuracy with low disturbance and cost. Lawless *et al*., in 1994, stated that 44% of the ICU alarms were generated by pulse oximeter, while 31% of the alarms were generated from ventilator and 24% from the ECG recording [41]. Thus, we focused on using ECG, PPG and ABP for arrhythmia diagnosis in the first application and using ECG and RIP for SDB diagnosis in the second application, which are explained in chapters 3, 4 and 5.

2.3. Issues with the existing systems

2.3.1. False arrhythmia alarms

As false alarms of the monitoring systems in the ICU are preferred to missing a true alarm, the ideal sensitivity is 100% to distinguish every clinically significant incident [39], [43], [213]. Over 85% false alarms were reported in the ICU and the resulting noise causes disturbance for the patients and medical staff as well as alarm fatigue, and influences sleep of the patients and thus the recovery process [40]–[43], [47], [49], [51]. The negative consequences of false alarms can be alleviated by automatic detection of false alarms and the source of the alarm using multimodal signals to enhance the diagnosis [214]. Studies have proposed different approaches for signal quality index evaluation [215]–[218]. We assessed different tests and features for the signal quality index of each signal before further processing. Also in order to reduce the effects of noisy or low quality excerpts of signals with missing values, we evaluated signal fusion. The proposed algorithms of this thesis are described in the following chapters 3 and 4.

2.3.2. Sleep tests

The standard sleep studies are associated with several major problems [53], [71], [148]. First, they are costly due to the required specialised staff and facilities overnight. Second, limited resources cause long waiting times for the test [20]. Above all, as the standard sleep test involves the recording of a large number of signals and measures, a crucial drawback is the disturbance on sleep caused by the attached wires and electrodes [53], [20]. The patients also may have issues with falling asleep in the unknown environment with the attached set up. Furthermore, studies have concluded that the results of the sleep tests vary from night to night depending on the study environment and the technology used for the test [102]. In fact, the unknown environment of the sleep laboratory affects the quality of sleep and generate unusual patterns of sleep which are different from the typical sleep patterns at home [102]. As a result, many patients prefer to go through a simpler sleep test with the intention to reduce the financial cost and waiting time [20]. Therefore, an ongoing research goal is to reduce the number of diagnostic signals, the invasiveness and cost of sleep tests [23]. In that case, the test can be simply performed for a couple of nights aiming to collect more information and eliminate the variations resulting from environmental factors, sleeping position, or other variable factors [20].

The available portable devices for non-laboratory sleep tests were comprehensively studied [58], [59], [219]. The AASM recommends that the use of current portable monitors is acceptable for a limited category of subjects with a high likelihood of moderate to severe OSA, with a manual evaluation of the test data by a sleep specialist [220]. The major problem of the existing portable monitors is the

low sensitivity and specificity in diagnosis, so enhancing the performance plays the key role toward delivering reliable simpler tests [219]. One solution is to utilise fewer non-invasive sensors and better signal processing techniques to obtain higher performance for SA diagnosis.

2.4. Summary

This chapter surveyed the literature relating to the physiology of cardiorespiratory disorders (life-threatening arrhythmias and SDB). I began with discussing the types of the disorders, the epidemiology and aetiology of the disorders as well as the treatment and diagnosis tools. The anatomical, physiological and neurological mechanisms and the resulting alterations in the corresponding features such as HRV or RR intervals and the frequency components of HRV associated with the disorders were described.

Also the sensors for diagnosis of the cardiorespiratory disorders were discussed. According to the sections which described the aetiology of the disorders, there are features associated with the disorders which can be identified by the ECG signals. Also evaluating the diagnostic characteristics of the candidate sensors showed that the ECG signal provides a low disturbance and low cost tool which is suitable for both arrhythmia and SDB diagnosis with a good accuracy. Thus, the ECG signal was chosen as the main focus of this thesis for detecting the cardiorespiratory disorders. The features that were used to develop the algorithms of this thesis such as the further respiratory features that can be extracted from ECG signals are described in the next chapter.

For false arrhythmia alarm detection, further signals such as PPG and ABP were also utilised to enhance the performance by multimodal signal processing. The pulsatile signals provide further information beneficial for arrhythmia detection which can help improve the performance results. The RIP provides useful information for SDB detection with minimal disturbance. Also, as it is placed on the chest similar to the ECG sensors, the signal can be used to assess the respiration derived from one ECG signal. Thus, it was used for SDB detection and the performance results were used to evaluate and compare with the results of respiratory information derived from the ECG signal.

Lastly, I presented the issues associated with the current diagnosis of cardiorespiratory disorders and elucidated the issues which encouraged the two applications of this thesis. In chapter 3, I will review the methodology of the two applications. The background literature for the major components of my system includes: interference removal, QRS detection, feature extraction and machine learning techniques.

Then, the developed algorithms of this thesis and the results will be described in chapters 4 and 5.

Chapter 3

Methodology

Background

3. Methodology background

In chapter 2, the clinical background of both applications of the thesis was presented. The sensors, which were used in the literature for general diagnosis, and the issues of the current tools for the diagnosis of arrhythmias and SDB were listed.

In this chapter, I aim to describe the methodology background to the signal processing and machine learning required to develop the applications for automatic detection of the cardiorespiratory disorders. I begin by presenting an overview of the two applications, in sections 3.1 and 3.2, followed by the signal processing techniques including preprocessing and noise removal (section 3.3), QRS detection methods (section 3.4) and RR correction methods. Then, I explain the two biosignals captured from the ECG signal including HRV (or RR intervals) and ECG derived respiration (EDR) in section 3.5. It is followed by introducing the feature extraction process from the utilised sensors including the two main categories: cardiopulmonary coupling features and power spectral density features in section 3.6. Finally, in section 3.7, the details of the machine learning techniques including LDA, SVM and ELM are illustrated (see section 3.7).

A number of sections of this chapter survey the signal processing methods applied to the ECG signals in the literature. It is due to the fact that the ECG signals are the main focus of this project and they are also widely studied in the literature for the diagnosis of cardiorespiratory disorders, providing beneficial information. In the following chapter, the developed algorithms for both applications using multimodal signal processing techniques are explained in more detail.

3.1. False arrhythmia alarm reduction

The methodology background of the first application of this thesis will be explained in this section. First, the methods of arrhythmia detection which help to identify true alarms were surveyed. Thus, the main blocks of an automated system for arrhythmia diagnosis will be first listed in this section. Then, the proposed approaches for reducing the false arrhythmia alarms will be surveyed. Researchers have found out that false arrhythmia alarms often originate from single-channel ECG artefact and low voltage signals [175]. Therefore, the studies of reducing the false arrhythmia alarms can be categorised into two main groups. The first category of studies investigated the use of different filters to eliminate the effect of artefacts on the signals which were reported as a major source of generating false arrhythmia alarms. The second category of studies investigated the use of multimodal signals to decrease the effects of artefacts.

The block diagram of a typical arrhythmia diagnosis system is displayed in Figure 3.1, as first proposed by Englese and Zeelenberg in 1979 [221]. They presented the principal modules of an ideal

automated arrhythmia detection system in this block diagram, while some systems may not include all of the modules and some others might contain additional blocks [221]. As shown in Figure 3.1, the effect of the undetermined noise has been emphasised as a superimposed element on the original undistorted ECG signal during arrhythmia detection [221]. An important block is beat detection to recognise the heart beats as an essential feature for arrhythmia detection. Then, beat delineation and characterisation is implemented on the detected beats which is followed by beat classification and rhythm classification to investigate the presence of arrhythmias as well as the identification of false and true alarms. Different phases of the system including noise removal, beat detection and rhythm classification will be described in the following sections 3.3, 3.4, 3.7 and our developed algorithms for classifying the arrhythmias and alarms will be explained in the following chapter in section 4.1.

In earlier studies, the usage of different filters, such as Kalman filter and median filter, in order to decrease the artefacts of the ECG signals as well as the transients with sources other than arrhythmias were examined [173], [174]. In a study using filters for reducing false alarms, Sittig and Factor implemented a multi-state Kalman filter to remove artefacts and sudden changes of the signal. They used two sets of data, with an actual dataset and a simulated data stream; while their developed system was tested on the simulated data [174]. They indicated that quick adaptation of the Kalman filters to variations of the baseline of the signals occurs in both data sets [174]. Further investigation on their proposed system is required to test the performance on the real data. It should be noted that the number of previous studies on reducing false alarms of severely ill patients is limited and only applied on small datasets [175], [173]. In this project, we applied the developed algorithms on large bedside monitor dataset of 1250 life-threatening arrhythmia alarms sourced from four hospitals in the

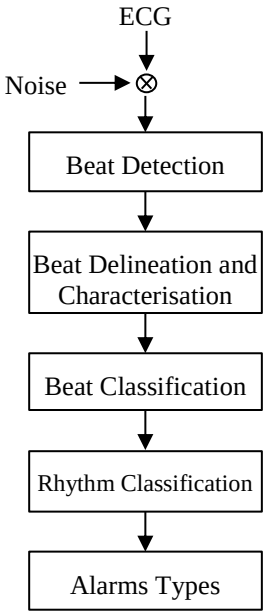

Figure 3.1. The block diagram of the principal modules of an ideal automated arrhythmia detector using ECG signal (figure adapted from Figure 1 [221]).

USA and Europe to provide a reliable and practical system for real data.

In another research on postoperative monitoring in cardiac patients in ICU, Mäkivirta *et al*. applied a dual limit system with a two-stage median filter on heart rate to eliminate variations [173]. The first median filter had a delay of 15 s which eliminated short transients; thus, the significant clinical cardiac dysfunctions remained in the output of the filter. The second median filter had longer delays of 1 and 2.5 min, discarding more artefacts [173]. The method resulted in decreased false alarm frequency. By comparing the results to the popularly-used patient monitoring system, they stated that their proposed system detected every correct alarm and demonstrated increased true alarms from 12% to 49% as well as reduced false alarm frequency from 88% to 51% [173]. A two stage median filter was also utilised in this thesis for noise removal as the first stage of the developed algorithm for the first application which will be explained in section 4.1 in detail.

Mäkivirta *et al*. compared their results to a common patient monitoring system, and found that their proposed system detected every correct alarm and demonstrated increased true alarms from 12% to 49% as well as reduced false alarm frequency from 88% to 51% [173]. As an example of using multimodal signals for this application, Clifford *et al.* in 2006 analysed an open access MIMIC dataset containing five life-threatening arrhythmia alarms including, asystole, extreme bradycardia, extreme tachycardia, ventricular tachycardia (VT), ventricular fibrillation (VF)/tachycardia in the ICU [51]. They utilised arterial blood pressure (ABP) and ECG signals for alarm identification [51]. They detected 25% false alarms from 89 arrhythmia alarms, mostly arising from heart rate transients (asystole, tachycardia and bradycardia), which reduced the number of false alarms by about one third compared to the false alarms detected by the existing cardiac monitors [51]. They emphasised that their morphology-based algorithm applied on the ABP signal performed successfully in dismissing every false alarm without removing any true alarm [51]. They reported low results for VT and VF false alarm detection and recognised a single VT false alarm (6.25% false alarm rate) and no VF/VT false alarm detection [51]. In another study, Aboukhalil *et al.* used a single-lead ECG signal simultaneously with arterial blood pressure (ABP) signals aiming to combine the information and improve the diagnosis [175]. They confirmed that exploiting information from multimodal signals enhances the arrhythmia detection. Thus, we utilised four signals (ABP, PPG, ECG lead II and aVr) to improve the false alarm detection rate for the first application of this thesis.

Researchers have found that false arrhythmia alarms can be better recognised by signal quality evaluation and multimodal signal fusion [150]. Also reliable detection of the heart beats, which is a major component of arrhythmia detection, has a direct effect on the features beneficial for this application. It can be achieved using concurrent signals and signal integration [32], [51], [60], [149], [222]. Johnson *et al*. in 2014 proposed a multimodal heart beat detection algorithm which was based on signal quality indices (SQI) using ECG signal and ABP signal [223]. It should be noted that the onset of the ABP pulses appear with a delay after the left ventricle contracts [21]. The multimodal

signal fusion algorithm proposed by Johnson *et al*. collected R peaks of the ECG signals and the pulse transit time (PTT), defined as the delay between detected onset beats of the blood pressure waveform and R peaks of the ECG signal. Then, the R peaks were matched according to the delay and extracted features for computing the SQI [21], [149]. They used the SQI measures of the signals to identify the high quality signal (ECG or ABP) which was selected for robust heart beat detection [149]. A number of studies utilised different peak detectors for blood pressure and ECG signal to compare and evaluate the resulted detection beats and select the method with better performing QRS detections [51], [149], [150], [223]. In this thesis, a robust QRS detection method based on Hilbert-transform-based algorithm is used and is explained in section 3.4. Also the above multimodal signal fusion was implemented to examine whether this method can enhance the heart beat detection of the utilised dataset by integrating ECG and ABP signal, which will be described in section 4.1.

False alarm analysis can be categorised into two types: real-time and retrospective analysis. The real-time analysis is associated with data segments ending at the time of the alarm occurrence without additional information after the alarm. While, the retrospective analysis involves segments with data after the alarm to provide more information [33]. In this thesis, we examined our developed algorithms for both categories.

Studies show that better VT and VF alarm detection can be achieved through algorithms that included statistical analysis and morphological methods. For example, Plesinger *et al*. applied QRS detection based on amplitude envelopes using the Fourier and Hilbert transform, and used descriptive statistical analysis of the QRS temporal distribution, evaluating the heart rate (HR) and observing low-frequency ECG activities [176]. They achieved true positive rate (TPR) of 92% and true negative rate (TNR) of 88% for false alarm reduction of five life-threatening arrhythmias (see section 3.8 for definitions of the performance measures) [33], [176]. Ansari *et al.* presented a multimodal peak detection algorithm using ECG leads II and V, PPG and ABP and combined the outcome of several peak detection methods through a polling scheme to obtain a robust peak detection algorithm [177]. Then, they applied phase wrapping via a simple decision criteria and a machine learning technique [177]. They obtained TPR of 89% and TNR of 79% in real-time approach [33], [177]. In another study, Fallet *et al.* measured HR based on the quality of the signals: HR was either calculated from the pulsatile signals, PPG or ABP, using an adaptive frequency tracking for the cases which pulsatile signals have suitable quality, or measured based on ECG signal using adaptive mathematical morphology approach, if the ECG signal provided high quality [222]. Their algorithm resulted a 94% TPR and 77% TNR in real-time [222], [33]. Among the five arrhythmias, ventricular fibrillation or flutter is recognised as the most difficult condition to detect using the ECG signal [178]–[180]. Different methods were applied in the studies such as threshold crossing intervals (TCIs) [224], autocorrelation function (ACF) [181] and complexity measure [178] which the results were compared in the studies [179], [180]. The comparisons showed the importance of tuning the threshold and

choosing the appropriate criteria, which were noted in this thesis. The details of our developed algorithm for reducing false arrhythmia alarms, the feature extraction, setting the thresholds, measuring the SQI of every multimodal signals, signal fusion, classification and alarm detection will be described in the following section 3.5 and section 4.1.

3.2. Sleep disordered breathing recognition

A large number of studies have investigated the diagnosis of SDB with different sensors and methods intending to reduce the number of sensors and invasiveness while optimising the performance [29], [140], [202], [220], [225]–[228]. The block diagram of an example of an automated SDB diagnosis system is shown in Figure 3.2. In this example, ECG recordings were used and different blocks were applied including, preprocessing, beat detection and feature extraction with a final phase of machine learning, which will be described in detail in the following sections 3.3 to 3.7. The main focus of this project and the developed algorithm was to use the ECG signal for SDB detection, which will be explained in chapter 5.

As explained in section 2.2.1, apnoea events are often associated with a cyclic variation of the heart rate, characterised by bradycardia followed by sudden tachycardia; this fact has been widely used as a characteristic for SA detection [182]. D'Addio *et al*. referred to the fact that spectral analysis of the heart rate variability (HRV) during SDB reveals cardiac arrhythmias of tachycardia-bradycardia sequences and dynamic respiratory patterns which leads to nonlinear heart period modulation and is widely used for evaluating the autonomic nervous system function [229]. The bradycardia-tachycardia cycle which is associated with SA originates from autonomic nerve activity. It has two apparent effects: 1) the RR-interval information changes and 2) the respiration changes which alters the

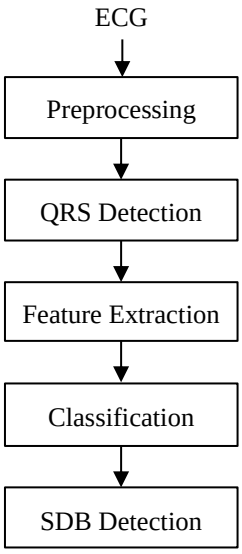

Figure 3.2. Block diagram of an example of automated SDB diagnosis system using ECG signals as inputs.

modulation of the ECG signal amplitude [230]–[232]. Thus, the ECG signal provides an indirect measurement tool for estimating respiration, beneficial for automatic SDB diagnosis.

Accordingly, the biosignals such as RR-intervals and ECG derived respiration as well as features such as power spectral density and cardiopulmonary coupling are used in this thesis, with the methodology explained in sections 3.5 and 3.6.

Respiration physically displaces the ECG sensors which results in a rotation of the cardiac vector and a change in the electrical impedance [230], [231], [232]. The respiratory patterns acquired from an ECG signal are commonly referred to as the ECG-derived respiratory signal (EDR) [233]. There are a number of methods of EDR extraction. Some of the early methods used the R wave amplitude, RS amplitude, QRS complex area and R wave area [234][235]. There are also novel techniques such as empirical mode decomposition (EMD) [236], [237], discrete wavelet transform (DWT) [236], [238] and principal component analysis (PCA) [70], [239]. PCA methods will be described in more detail in section 0. In this thesis, two novel algorithms were proposed for estimating the EDR using the PCA method for an overnight ECG recording and were compared to the QRS complex area method. The developed algorithms for EDR estimation in this project will be explained in section 5.1.3.

A study by Mendez *et al.* in 2007 presented a bivariate autoregressive model using the *PhysioNet and Computers in Cardiology (CinC) Challenge 2000* database [240]. They derived beat-by-beat power spectral density (PSD) of HRV and R peak area as the features of the algorithm and applied the k-nearest neighbour (KNN) algorithm as the supervised learning classifier to obtain minute-based classification, and achieved an accuracy of approximately 86% on both training and test sets [240]. In this thesis, we utilised PSD features of HRV for sleep apnoea detection, as described in sections 0 and 5.2.3. Another study of apnoea detection by Xie and Minn in 2012 used a combination of classifiers; AdaBoost, Decision Stump, Bagging and SVM [241]. They also applied feature selection on ECG features and SpO_2 features and compared the performance results of different combinations of classifiers and feature sets [241]. They reported the highest accuracy of a combination of classifiers on the combined feature set to be 84.4%, with the highest specificity of 85.9% [241]. Penzel *et al*. in 2002 compared thirteen studies of automatic algorithms and methods which required visual inspection for apnoea detection using different frequency and time domain features and transformations [148]. The methods, features and transformations which were utilised by the proposed algorithms are comprised of spectral analysis of HRV [184]–[189], Hilbert transform to capture frequency information of the HR [188], [190], time-frequency maps for presenting HRV [185], [186], [188] and thresholding for the ratio of the spectral power if the heart rate is in two frequency bands (0.01-0.05 and 0.005-0.01 cycles per beat) [189]. Besides HRV, the proposed algorithms used several other ECG derived features, including ECG pulse energy [186], R-wave duration [187], amplitude of the S components of every QRS complex [186], [191] and PSD of the R-wave amplitude [184]. An algorithm used T-wave amplitude utilising the discrete harmonic wavelet transform as well as time-

domain methods to detect variation in HR consistent with transition to arousal from sleep by the end of the respiratory events [148], [192]. Penzel *et al*. stated that some of the algorithms provided fully automatic analysis and the others required visual and auditory classification, with the highest obtained scores being about 92%, by two teams using manually verification of apnoeic events [148]. As a result, the highest score among the automatic algorithms was achieved by de Chazal *et al*. algorithm, which was 89.4% for identifying each one minute of apnoea and hypopnoea [184] and later improved to 90.5% [71]. The results revealed that the algorithms which used frequency-domain features of HRV and/or EDR signal with R-wave morphology were the best performing approaches [148], [184], [186], [187], [192]. In this thesis, both time-domain and frequency domain features including PSD features were extracted from both HRV and EDR signals. The features extracted from HRV and EDR will be explained in sections 5.1.4 and 5.2.

In the following sections of this chapter, we illustrate the major components of automated systems for diagnosis of cardiorespiratory disorders and the signal processing approaches presented in the literature addressing both applications of this thesis.

3.3. Preprocessing and interference removal

Presence of noise and interference during ECG recordings is commonplace [242]–[244]. The ECG signals are mostly distorted by different interference, such as motion artefact, power-line interference, and baseline drift [33], [221], [245], [246]. These artefacts may lead to false diagnosis of arrhythmias and therefore false alarms in monitoring equipment [247].

A study by Englese and Zeelenberg in 1979 highlighted that the major issue in malfunction of the arrhythmia diagnosis systems is the QRS detection failure which itself is mainly caused by the input artefacts [221]. Thus, a crucial stage prior to feature extraction and QRS detection is to monitor the artefacts and reduce the noise to provide a reliable cardiorespiratory diagnosis [221], [246].

Englese and Zeelenberg defined the noise, particularly in the arrhythmia diagnosis studies, as any distortion of the signal or any kind of concealment of the original data of ECG signal [221]. They have categorised the effects of noise on the arrhythmia diagnosis performance into two groups of direct and indirect effects on different blocks of arrhythmia detection system shown in Figure 3.1. The direct effects distort the system in two ways: 1) affecting the beat detection and resulting in false positive and false negative detections, 2) affecting beat delineation and characterisation. The second effect distorts the characteristics of the signal and the measurements such as errors in height, duration and area [221]. The indirect effects also distort the system in two ways: 1) beat classification errors caused by timing and measurements inaccuracies, 2) rhythm classification errors resulting from incorrect beat classification [221]. Englese and Zeelenberg listed two primary methods for managing the noise of ECG signal; 1) noise elimination at the source through ensuring the accurate placement

and contacts of the electrodes to obtain the optimum signal quality, 2) detecting and reducing the noise using different signal processing techniques [221], [246]. In this thesis, the ECG signals were preprocessed by first reducing the noise in individual channels by using filters and then using the signal quality index to select and weight the signals.

A common source of noise on an ECG signal is baseline drift. It is a result of interferences, such as motion artefact and can lead to deformation of the ST segment. It plays an important role in interfering with arrhythmia detection [246], [248], [249]. Also the baseline wander noise can distort the low frequency component of the ECG recordings and can alter the features of ECG signal useful for SDB recognition [246]. For instance, the sudden shifts in the ECG baseline can have a large effect on the EDR signal [291]–[293], [295]. Thus, elimination of baseline wander should be performed before any further processing to avoid these artefacts. Different filters and methods have been used for removing the baseline wander [242]–[244], [246], [250]–[252]. In this thesis, a two stage median filter was used for baseline elimination which is explained in sections 4.1.3 and 5.2.

3.4. QRS detection

The first step toward ECG feature extraction after preprocessing is QRS detection. Most of the studies of the automated detection of cardiorespiratory disorders using ECG signals addressed the QRS detection for R-R interval analysis [37], [253]–[257]. Different QRS detection algorithms applied to ECG signals but selecting a reliable method is highly significant [258]–[261]. It should be noted that a useful ECG signal processing step is artefact detection, which was not addressed in this thesis and is suggested as an area of further work.

A well-known QRS detection algorithm is the Pan Tompkins, which identifies the QRS complexes using different ECG features, such as slope, amplitude and width [262]. It involves several signal processing steps [262]. First, the noise in the ECG was reduced using a band-pass filter [262]. Then, the filtered signal was differentiated and squared to obtain the information of the slope of the QRS complex and intensify the slope in order to distinguish the QRS complexes from the T-waves [262]. Next, a moving window integration was applied to extract the information about the slope and width of the QRS complex [262]. The algorithm involves three phases with the first two phases of initialising and adjusting the thresholds for QRS detection and the final phase of the detection [262]. There are two sets of thresholds in this algorithm, including the filtering thresholds and the moving window integration threshold. They improve the reliability of the QRS detections by updating and adjusting the thresholds throughout the phases [262]. Finally, the output of the algorithm is a series of pulses at the location of the QRS complexes [262]. The algorithm was applied to the MIT-BIH arrhythmia database and achieved an accuracy of 99.3% for the QRS detection [262].

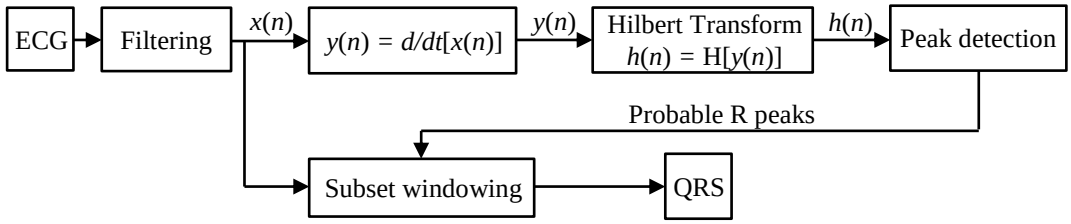

Figure 3.3. The block diagram of the Hilbert QRS detector algorithm (reproduced from Fig. 3 from [263]).

Another widely used QRS detection algorithm was developed by Englese and Zeelenberg in 1979 [221]. They aimed to detect arrhythmias and proposed a QRS detection method as an important subsystem of arrhythmia detection [221]. The proposed QRS-complex detection technique by Englese and Zeelenberg used a single data scan with a simple high-pass filter to detect the R peaks [221]. They stated that the presented algorithm determines QRS onset point, end point, baseline and R peaks [221]. They noted that the proposed method is sensitive to wide-band noise, such as EMG and motion artefacts. Since, it provides a simple and efficient method; it is extensively used with an additional noise removal phase prior to the QRS detection. They reported an accuracy of 98.6% for QRS detection by the algorithm [221]. This algorithm was used for the *MIT PhysioNet Apnea-ECG* database to detect the onset beats of the QRS complexes which were provided with the dataset and utilised for the second application of this the sis (see section 5.1.1).

Another method of identifying the QRS complexes was introduced by Benitez *et al*. in 2001 using the Hilbert transform [263]. The zero crossings on the x-axis of the Hilbert transform of the signal represent the inflection points of the original signal [263]. Also the peaks of the Hilbert transformed conjugates of the signal correspond to the zero crossings between positive and negative inflection points of the original signal [263]. Benitez *et al*. used this characteristic to detect the zero crossings of the first differential of the ECG signal (d/dt(ECG)) to develop a novel robust approach to identify the R peaks from large T and P waves [263]. The block diagram of their proposed algorithm is shown in Figure 3.3. First, they used a band pass FIR filter using a Kaiser-Bessel window with the band stop frequencies at 8 and 20 Hz to eliminate muscular noise and emphasise the QRS complexes [263]. Then, they eliminated the motion artefacts and baseline wander noise using the first differential of the filtered signal [263]. The rising and falling of the R peaks of the original signal correspond to the maximum and minimum points of the first differential, which can be detected using the zero crossing [263]. The Hilbert transform was applied to the first differential of the ECG signal implementing the following steps. First, the Fourier transform was applied and the DC component was removed. Then, multiplied the positive and negative harmonics by $-j$ and j and obtained the inverse Fourier transform [263]. They applied a moving window of 1024 samples to $y(n)$ prior to applying the Hilbert transform, as the Hilbert transform performs well on short length of the signals [263]. Benitez *et al*. state that the peaks which are detected from the Hilbert transform ($h(n)$) indicate the peaks of the QRS complexes with an accuracy of a few milliseconds. Thus, in order to develop a robust and accurate QRS peak

detector, they applied a second step detector. By applying the Hilbert transform, the P-waves and T-waves are minimised in comparison to the QRS peaks. Thus, they applied an adaptive threshold detector by setting the threshold according to the noise level of the segment, the maximum amplitude of the peaks in an iterative procedure and the average RR intervals. In order to guarantee the accuracy and robustness of the QRS detector, a second step was performed by applying a simple peak detector again on windows of ±10 samples around the peaks detected from the previous step [263].

This algorithm was tested on a number of datasets of different ECG leads and the performance was compared to the performance of other QRS detection algorithms [264], [265]. Benitez *et al*. tested the developed algorithm on *MIT-BIH arrhythmia* database and obtained an average detection rate of 99.87% with a sensitivity of 99.94% and a positive prediction of 99.93%. They concluded that the method is robust and can minimise the disruptive effect of motion artefact, baseline wander and muscular noise [263]. Thus, we applied this algorithm to the *PhysioNet/Computing in Cardiology (CinC) Challenge 2015* database for the first application of this thesis as well as the *St. Vincent's University Hospital, University College Dublin Sleep Apnea* database for the second application as will be explained in sections 4.1.1 and 5.1.1.

A. RR correction

The findings of the studies on a variety of QRS detection algorithms have indicated that even after applying noise removal and optimising the performance of QRS detection methods, errors still present in the output of the QRS detection algorithms, with missed and/or spurious QRS detections [148], [266], [267]. Thus, RR correction is an essential part of the ECG signal processing since noise is unavoidable during recording and affects the following steps such as feature extraction [265], [268].

The simplified context behind the correction algorithms mostly involves; first, the elimination of RR intervals which are physiologically implausible, and second, the interpolation of RR intervals with missed or undetected QRS complexes [265]. First, following the application of QRS detection algorithm, the RR intervals are derived from the QRS detections [265]. Shouldice *et al*. in 2004 used a correction algorithm as a post-processing step to ensure presence of physiologically reasonable QRS onset detections [265]. Through the proposed algorithm, if an RR interval is smaller than 150 ms, the second R-wave is marked as spurious and eliminated [265]. On the other hand, if an RR interval is greater than double of the trimmed mean at 10%, i.e. the largest 5% and smallest 5% of intervals eliminated, of the entire RR intervals, it is labelled as a missed R-wave [265]. Then, the missed RR intervals were estimated and inserted [265]. An estimation of the missed RR interval was measured using the mean of the preceding 5 intervals [265]. If the original incorrect RR interval is greater than 2.2 times this estimation, then an integer number of the revised RR intervals is produced to be inserted into the RR-intervals using a sliding window based on the preceding 5 intervals [265].

Similar QRS correction algorithm, proposed by de Chazal *et al*., is implemented in this thesis to remove incorrect QRS detection beats as well as interpolate missing QRS detection points [71], [269]. Through this automated algorithm, every individual R-R interval is compared to a robust RR-interval (*Rob*[n]); i.e., the result of a five sample interval width median filtered R-R intervals. The automatic algorithm interpolates missed QRS detections and removes false detections. To detect incorrect QRS detections, the sum of two adjacent RR intervals is computed, $Sum[n]=RR[n]+RR[n+1]$. Then, the corresponding robust RR-interval, $Rob[n]$, is subtracted from the sum of RR-intervals and the absolute value of the result taken. If this output is less than the absolute value of the subtraction of the robust interval from both of the two RR-intervals individually, then it is labeled as an incorrect QRS complex and the corresponding QRS detection is removed [71].

$$If\ |Sum[n] - Rob[n]| < |RR[n] - Rob[n]|\ \&\ |Sum[n] - Rob[n]| < |RR[n+1] - Rob[n]|$$

$$Then\ QRS[n]\ is\ incorrect.$$

Also each RR-interval is compared to the robust RR interval. If it is about twice the robust interval, it is labeled as a misplaced QRS and interpolation is applied until it is reduced to about 80% of the robust interval. Finally, the RR-intervals are computed as the intervals between two adjacent QRS detections. The details of the implemented algorithm of this thesis are described in section 5.2.3.

3.5. Biosignals

The effects of arrhythmias and SDB on the heart rate and cardiac characteristics of the ECG signals have been described in a previous chapter. The corresponding biosignals can be captured from the ECG recordings and used to detect cardiorespiratory disorders.

Table 3.1. A list of statistical features of HRV [71], [110], [148], [267], [271].

Features	Description
SDNN	The standard deviation of the NN interval by measuring the square root of variance
SDANN	The standard deviation of the average NN interval in every 5-minute segment of the recording
SDNN index	The mean of the standard deviation of NN-intervals for all consecutive 5-minute segments calculated during 24h
RMSSD	The square root of the summed squares of differences of successive NN intervals
MeanNN	The mean NN interval or heart rate
DiffNN	The difference between the longest and shortest NN interval
DiffHR	The difference between night and day heart rate
NN50	The absolute value of 50 NN counts by calculating the number of interval differences of successive NN intervals greater than 50 ms
pNN50	The relative number of successive pairs of NN-intervals that differ more than 50ms by measuring the proportion of NN50 over the total number of NN intervals
Allan factor	RR intervals which is the fractal rate measured over time-segments

It was explained in the previous chapter that during inspiration, the thorax pressure reduces and venous return increases, causing the expansion of the right atrium. It leads to a reflex which increases the instantaneous heart rate or reduces the RR-intervals [104]. The entire process is reversed during expiration and produces reduction in heart rate [104]. Thus, some of the main features extracted from resampled RR-interval time series include respiratory information. The breathing modulation signal can only be recovered when the average Nyquist frequency condition is fulfilled; i.e., the heart rate is greater than twice the breathing rate [104]. As noted in a study in 2006, Clifford *et al*. found that the average Nyquist criteria is not satisfied in patients with rapid breathing cycles [270]. In this thesis, this information was captured using the interval based power spectral density features (see section 5.1.4). Two biosignals are estimated from ECG recordings in this thesis including RR-intervals or HRV and EDR signals. This section commences with explaining the RR-intervals in section 3.5.1.

3.5.1. RR interval (HRV)

A widely used biosignal for detecting cardiorespiratory disorders is heart rate variability (HRV). Using the QRS detection beats, the RR-intervals were computed as the intervals between every pair of adjacent QRS detections, providing a measure of HRV. A number of features are extracted from this biosignal for cardiorespiratory diagnosis in the published studies. Variations in heart rate can be evaluated using a number of strategies, with the simplest approach perhaps being the time-domain measures. The time-domain features consider heart rates by their time samples or the intervals between successive heart beats, as shown in Figure 3.4 [71], [110], [148].

In order to extract the time-domain features from ECG recordings, the QRS complexes are first detected and normal-to-normal (NN) intervals are determined as the intervals between adjacent QRS complexes [110]. A major category of features is comprised of statistical variables measured using

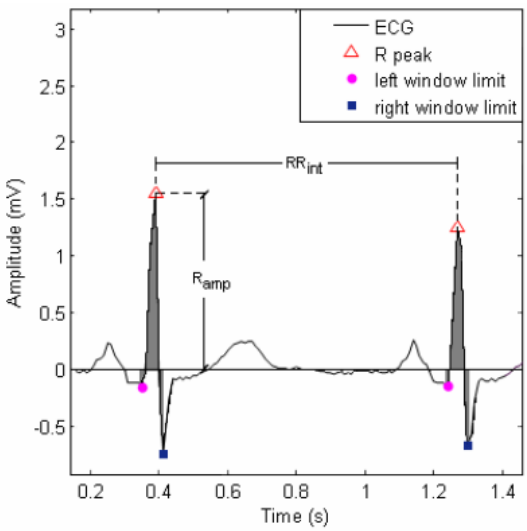

Figure 3.4. Demonstration of some characteristics of ECG signals used in the studies for RR-interval (HRV) and EDR estimation: R peak amplitude (R_{ampl}), RR interval (R_{int}) and R wave area as the shaded area (figure adapted from Fig. 1 [235]).

two methods; direct calculations from the NN intervals, or derivation from the differences between NN intervals [110]. The most commonly used statistical features of HRV are listed in Table 3.1. A simple statistical feature is *SDNN* which represents all the cyclic variations of the recording [110]. The *SDANN* is a measure of heart rate variations of cycles longer than 5 min, and the SDNN index indicates the variations caused by cycles of shorter than 5 min [110]. [71], [148], [267], [271]. Time domain features can be computed using the entire ECG recording or computed using short segments of the recordings which provides information to evaluate varying activities, such as rest or sleep [110]. The time domain and frequency domain features which were extracted for the two applications of this thesis are described in sections 4.1.7, 4.1.9, 5.1.3 and 5.1.4.

3.5.2. ECG derived respiration (EDR)

The other biosignal measured in the second application of this thesis using the ECG recording was EDR signal. It was explained in previous sections that sleep apnoea is often associated with a cardiac rhythm pattern resulting from autonomic nerve activity which can be derived from ECG recordings [182]. In addition to the information derived from HRV, respiration is another effect apparent on the ECG and it manifests as a modulation of the ECG signal amplitude [157], [230]–[234]. A sample ECG signal and the corresponding respiratory signal are shown in Figure 3.5. The respiratory patterns acquired from an ECG signal are commonly referred to as the ECG-derived respiratory signal (EDR) [233]. The ECG signals are modulated by respiratory cycle through different mechanisms [158]. The EDR signal is generated due to three major physiological mechanisms:

(1) Changes in the cardiac electrical axis caused by the air flow through to the lungs, generating respiratory information on the ECG signal [146], [230], [231], [260].

(2) The second observable and largely used effect is the periodic change and attenuations of the ECG amplitude, mostly apparent on the R peaks, due to the physical effect of respiration causing displacement of the ECG electrodes on the chest relative to the heart [104], [230].

(3) The other effect is generated by respiratory sinus arrhythmia (RSA) with physiological modulation of the heart rate or RR interval which reduces during inspiration and increased during expiration and mostly lags the respiratory effort with a changing phase [104], [232].

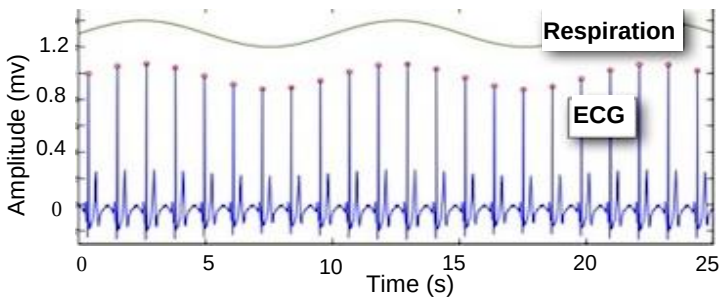

Figure 3.5. A sample ECG signal and the corresponding respiratory signal as a modulatory signal on the ECG (Figure adapted from (source: /ibt.kit.edu/).

Thus, via ECG signal processing, the respiratory patterns or EDR can be acquired simultaneously with HRV information [233], [234]. It should be noted that the ECG movement artefact and the changing electrode impedance, which affects the ECG amplitude, can have adverse effects on the overnight EDR signal estimation. The distinct advantage of using the ECG system to derive respiratory information over direct measurement of respiration by nasal sensors is its low cost, efficiency, simple recording and ability to monitor continuously with minimal disturbance on sleep and breathing [236]. A number of strategies for acquiring the EDR signal are explained in section 5.1.3 and we have published the novel approaches in [63], [65], [66].

3.6. Features

Several features and methods were used in the studies for SDB and arrhythmia diagnosis, such as non-linear statistics, time domain and frequency domain features [110], [148]. Some examples of the features and methods used in the literature for the two applications of this thesis are shown in Table 3.2. As displayed in the table, different QRS detection approaches have been first applied in the

Table 3.2. Examples of features and methods used for diagnosis of cardiorespiratory disorders; sleep apnoea and life-threatening arrhythmias. Some features extracted from ECG sensor and either oximetry sensor for SA detection or PPG sensor for arrhythmia detection are listed below from the literature.

Features and Methods		
Sensors	**SDB**	**Arrhythmias**
ECG	RR-based and EDR based features in time and frequency domain by a wide range of classifiers [71], [110], [148]	Position of P wave, QRS complex, R peak, T wave and intervals between them; 97.3% of arrhythmias detected [37]
	PSD, wavelet transform, Bayesian hierarchical model, Hilbert amplitude and frequencies, [148]	Descriptive statistical features and QRS detection by amplitude envelopes, Fourier transform; 92% TPR [176]
	Non-linear statistics, moving average, low-pass filter, U shape patter detection, cyclical variation in heart rate, R or S amplitude, R duration [148]	Multimodal peak detection, phase wrapping via a simple decision criteria or machine learning technique; TPR of 89% [177]
	RR interval and EDR features by an autoregressive model and KNN, Acc over 85% by SVM [240], [280]	HR based on high quality ECG using adaptive mathematical morphology approach; with 94% of TPR [222]
	RR Interval and EDR features (mean, STD, NN50, PNN50, RMSSD, SDSD, Allan factor, PSD), entropy, by LD and QD over 85% Acc [71], [267]	Threshold crossing intervals (TCIs) [224], autocorrelation function (ACF) [181] and complexity measure [178]
Oximetry (for apnoea) **PPG (for arrhythmias)**	Mean and min of Sp_{o_2}, number of Sp_{o_2} less than 92% saturation, square root of the 5% to 95% in sorted Sp_{o_2}, mean of absolute differences in successive Sp_{o_2}, number of time Sp_{o_2} greater than 2.9% or less, the same for less than 2.9% [23]	Multimodal peak detection algorithm using high quality PPG and combine the outcome of several peak detection methods through a polling scheme to obtain a robust peak detection algorithm for arrhythmia detection [177]
	Linear discriminants (LD), Quadratic discriminants (QD) and combination of classifiers, 94% Sen, 93% Sp [23]	HR extracted from good quality PPG using adaptive frequency tracking [222]

studies of ECG signals as an essential phase prior to feature extraction [148], [176], [177]. Accordingly, HRV or RR-interval based features were extracted and/or a variety of transformations were performed, such as Fourier transform and wavelet transform [148], [176], [177]. The features extracted from ECG signal can be divided into two major groups of time domain and frequency domain features. Some of the time domain features of ECG recordings are RR variability, R or S amplitude and R duration and frequency domain features such as LP/HP ratio and PSD features [148].

As shown in Table 3.2, studies use other signals such as PPG signal for arrhythmia detection and involve application of different classifiers [23], [222], [177]. The developed algorithms of this thesis for arrhythmia detection using PPG signal and ECG signal are described in section 4.1.

3.6.1. Cardiopulmonary coupling (CPC)

Cardiopulmonary coupling (CPC) measures the interrelationship of the respiration and heart rate [69]. As stated in the former chapter, neurological modulation of sino-atrial node during RSA causes variations in the RR-interval series due to respiration [104]. Although the shifts in the QRS morphology caused by respiration have mostly mechanical origins, they result in variations in the phase difference between the two signals (HR and respiration) [104]. Clifford *et al*. in 2005 highlighted that respiration is directly linked with the strongest coupling frequency, which can be a suitable indicator of activity [273]. CPC captures the combined information of respiration and HR and identifies the variations in activity [104], [273]. Since SDB is associated with cyclic variation in the breathing pattern, which is associated with the most dominant coupling frequency during sleep, it can be simply distinguished by CPC features. Due to the fact that the ECG noise largely corresponds to movements and activity alterations, CPC was reported to be less effected by noise [273]. Different coupling frequencies are linked with each sleep stage and the disturbed sleep pattern is linked with coupling at about 0.1 Hz [69].

Thomas *et al*. in 2005 utilised Fourier-based methods to analyse the RR interval time series and EDR signal to derive CPC between HR and respiration [274]. First, applying the Fourier transform to the RR interval time series and EDR signals, decompose them into a series of sinusoidal oscillations with particular amplitudes and phases at every frequency [274]. The intensity of the coupling between these two signals, i.e., RR intervals and EDR signals, is associated with two major effects:

(1) The signals are coupled in the case that they incorporate reasonably large amplitudes at a given frequency. The cross spectral power can estimate this effect using the product of the powers of the signals at the given frequency.

(2) They are coupled if they attain uniform phase difference or synchronous oscillations at a given frequency. This effect can be quantified by measuring the coherence.

Thomas *et al*. used the product of the coherence and the cross spectral power to include these two effects in the evaluation of the cardiopulmonary coupling [274]. The sequential block diagram of measuring CPC is outlined in Figure 3.6. As shown, the beats or QRS complexes are first detected, then the RR intervals and EDR signals are measured and discrete Fourier transform (DFT) is calculated for both signals, as follows [274],

$$\widehat{\mathrm{RR}}_{\mathrm{n}} = \mathrm{A}_{\mathrm{n}}\mathrm{e}^{\mathrm{i}\Phi_{\mathrm{RR,n}}}\ ,\ \widehat{\mathrm{EDR}}_{\mathrm{n}} = \mathrm{B}_{\mathrm{n}}\mathrm{e}^{\mathrm{i}\Phi_{\mathrm{EDR,n}}} \tag{3.1}$$

where $\widehat{RR}_n$ and $\widehat{EDR}_n$ are the DFT of RR interval time series and EDR signal, A_n and B_n are the amplitudes and $\Phi_{RR,n}$ and $\Phi_{EDR,n}$ are the phases of the Fourier components of RR interval and EDR signals, respectively. The cross spectrum is calculated as follows,

$$\Gamma_n(RR, EDR) = \widehat{RR}_n \times \widehat{EDR}_n = A_n B_n e^{i[\Phi_{EDR,n} - \Phi_{RR,n}]} \tag{3.2}$$

where $\Gamma_n(RR, EDR)$ represents the cross spectrum of the two signals and $\times$ is elementwise multiplication. Thus, the amplitude of the cross-spectrum is the product of the corresponding Fourier transforms of each signal at a given frequency and their phase difference provides the phase of the cross-spectrum [274].

The coherence is a statistical measurement of the consistency of phase difference of the two signals at a given frequency of f_n and is described as the proportion of the squared average cross-spectrum and the product of the average spectral power of each signal, as shown below [274],

$$\Lambda_n = \frac{E(\Gamma_n(RR,EDR))^2}{E(\widehat{RR}_n^2)E(\widehat{EDR}_n^2)} \tag{3.3}$$

Where E( ) indicates averaging over frequencies of the spectrogram or averaging over multiple measurements at a frequency. It should be noted that the cross-spectral powers should be first normalised for coherence calculation; and it is important to compute a statistical average of the cross spectrum from multiple samples or frequencies [274]. If they are used without averaging, the coherence would be equal to 1, as the Fourier analysis considers the data as stationary and thus, the

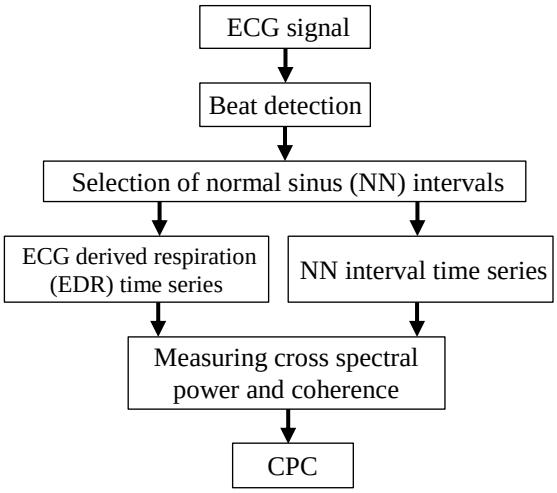

Figure 3.6. Sequential block diagram of deriving cardiopulmonary coupling (CPC) measures (Figure reproduced from Figure 3 in [274])

phase difference of the corresponding Fourier elements of two signals would be constant [274].

CPC of a single-lead ECG is derived by combining both cross spectral power and coherence as follows [274],

$$CPC(f_n) \equiv E(\Gamma_n(RR, EDR))^2 \Lambda_n \quad (3.4)$$

Through this combination, two significant elements are considered: first factor is the power at a given frequency f_n of both HRV and EDR, and the second element is the consistency of these signals in following one another, which is assessed by the coherence [274]. If the EDR signal is noisy, or the HRV response to respiration is enormously decreased due to different reasons, for instance, impaired autonomic function, the cardiopulmonary oscillations of either signal will still be derived by coherent cross power [274]. Thomas *et al.* assumed that the respiration cycle was sampled by R-wave amplitude variations for EDR signal [274]. According to the Nyquist theorem, the minimum sampling rate should be assumed twice the highest frequency component of the signal; for example, minimum two samples per cycle should present for every desired frequency component [274]. In a case that the sampling rate does not satisfy the above condition, aliasing occurs and the spectral component of the higher frequency would "wrap around" into the lower frequency components [274]. For instance, for a respiratory rate of 12 breaths per minute, the minimum required heart rate is 24 beats per minute [274].

In a study of OSA detection, Redmond and Heneghan in 2006 extracted cardiorespiratory features and measured RR-EDR cross-spectral features from ECG recordings of 37 subjects [264]. They computed VLF (0.01-0.05 Hz), LF (0.05-0.15 Hz) and HF (0.15-0.5 Hz) powers from cross spectrum of the RR-interval and EDR signals [264]. They used a quadratic discriminant classifier to detect sleep stages and the results showed that the method was not successful in distinguishing the sleep stages, thus the focus was given to OSA detection [104], [264]. A recent study by Zheng *et al.* in 2016 utilised a recursive least squares (RLS) adaptive filter to enhance EDR measurement for CPC analysis [275]. The study evaluated CPC using the nonlinear phase interactions between RR interval series and respiratory signals [275]. They concluded that adaptive filtering enhances the accuracy and robustness of CPC analysis [275]. It should be noted that the approach of Zheng *et al.* [275] for evaluating CPC is different from the approach of Thomas *et al.* [274] which included both amplitude and frequency coupling, that is incorporating both coherence and cross spectrum of RR interval and EDR signals [274], [275]. In fact, the study by Zheng *et al.* investigated CPC as the synchronisation between respiration and respiratory sinus arrhythmia (RSA) which is proportional to only the coherence in the frequency domain [275]. They stated that in order to evaluate their algorithm in sleep medicine, the information of amplitude coupling is required to be incorporated in CPC analysis [275]. In this thesis, the Thomas *et al.* approach was used including both the coherence and amplitude coupling according to the above equations and the algorithm of Figure 3.6. The combined features using CPC features and the results are demonstrated in section 5.2.3.

3.6.2. Power spectral density (PSD)

A major feature extracted from the ECG and EDR signals is the power spectral density. In general, PSD can be measured using two methods; non-parametric and parametric [110]. Non-parametric methods, which mostly use fast Fourier transform (FFT), have considerable advantages including, simple computation algorithm and the fast processing [110]. On the other hand, parametric methods involve simple post-processing of the spectrum and automatic measurement of low and high frequency power components and simple identification of the central frequency of each component and result in smoother spectral components [110]. Also parametric methods can measure PSD even on a few samples of the signal which maintain stationary [110]. It should be noted that ideally an infinite length of the signal is required in order to estimate PSD. In fact, estimating it on a longer length of the signal results in a higher frequency resolution but lower time resolution, that is, the product of the standard deviation in time and frequency is limited [276]–[278]. The main drawback of parametric methods is that they require evaluation and verification of the selected model parameters including the order and complexity [110]. Thus, a non-parametric method is suitable for faster automatic systems and was utilised in this thesis. The details of the PSD calculation in this thesis are provided in section 5.1.4. PSD features of RR-intervals, EDR signals from the ECG and RIP signals were estimated, with details described in section 5.2.

3.7. Machine learning algorithms

There are a number of machine learning algorithms used in the studies for detection of cardiorespiratory disorders, such as random forest, SVM [279],[280], binary decision tree (BDT) [9], KNN [240], autoregressive model [240], fuzzy logic C-means (FCM) [281]. Generally, the results using biomedical signals such as ECG show that using some of the simpler classifiers reduces the level of complexity and processing time significantly while maintaining acceptable performance [148], [241], [266], [282], [283]. In general, building a prediction model can be conducted using "supervised learning", i.e. the output variables are available as a training set to help the learning procedure, or conducted as "unsupervised learning", that is, only some features are present without any output measurements [284]. Least squares, linear regression, k-nearest neighbours, linear discriminant analysis are examples of supervised learning methods [284]. While neural networks are currently a popular approach of machine learning, I have not considered them in this thesis due to their long training time and acceptable performance of the simpler methods used in this thesis which has been reported by other studies.

One of the classifiers utilised in this project was extreme learning machine (ELM) which is a machine learning approach offering flexible, non-linear classification [285], [286]. The results of detecting cardiorespiratory disorders was compared to the classification performance of simpler classifiers such

as linear discriminant (LD) which has demonstrated adequate results in different studies [23], [71], [267], [279]. We will present the automated classifiers developed by the linear discriminant analysis (LDA), the support vector machine (SVM), and the extreme learning machine (ELM) training algorithms for diagnosis of cardiorespiratory disorders in the next chapter. We chose three different types of classifiers to cover a range of classifiers. We used LDA as a linear classifier, SVM as a standard approach and ELM as a flexible non-linear classifier, with the flexibility controlled through the number of hidden units. In the remainder of this chapter the principal theories behind these machine learning techniques are illustrated.

3.7.1. Linear discriminant analysis (LDA)

Linear discriminant analysis (LDA) is a simple and fast pattern recognition technique which maps the data into a low-dimensional space and labels the clusters and classifies with linear boundaries through a simple probabilistic decision making [284]. Figure 3.7 shows a sample dataset with three classes separable by linear decision boundaries which were accurately classified using LDA.

Suppose G(**x**) is our predictor to classify **x** into one of the *K* classes (*1, 2,…, K*) in the input space (**X**); The class posteriors Pr(G|X) for optimal classification using a simple application of Bayes' theorem, with $f_k(\mathbf{x})$ as class-conditional density of **X** in class $G = k$, and π_k as the prior probability of class *k*, where $\sum_{k=1}^{K} \pi_k = 1$, is formulated as follows [284],

$$\Pr(G = k|\mathbf{X} = \mathbf{x}) = \frac{f_k(\mathbf{x})\pi_k}{\sum_{l=1}^{K} f_l(\mathbf{x})\pi_l} \tag{3.5}$$

Some methods are based on models for class densities, such as linear discriminant analysis using Gaussian densities. Using flexible mixtures of Gaussians enables the nonlinear decision boundaries and nonparametric density estimates for any kind of class densities. It will provide the utmost plasticity [284]. LDA assumes every class density is a multivariate Gaussian with every class sharing

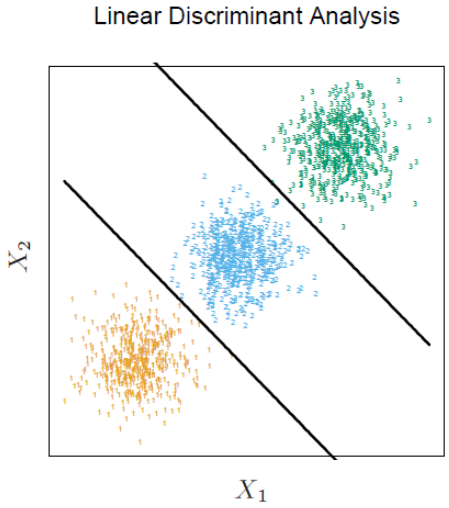

Figure 3.7. A sample dataset with three classes, simply separated by linear decision boundaries. The plot demonstrates the boundaries discovered using linear discriminant analysis (Figure adapted from Figure 4.2 in [284]).

a common covariance matrix Σ [284],

$$f_k(\mathbf{x}) = \frac{1}{(2\pi)^{p/2}|\Sigma_k|^{1/2}} e^{-\frac{1}{2}(\mathbf{x}-\mu_k)^T \Sigma_k^{-1}(\mathbf{x}-\mu_k)} \quad (3.6)$$

In the case of having two classes, *k* and *l*, the log-ratio of the class posteriors provides an equation which is linear in **x**, as shown below;

$$log\ \frac{\Pr(G=k|\mathbf{X}=\mathbf{x})}{\Pr(G=l|\mathbf{X}=\mathbf{x})} = log\frac{f_k(\mathbf{x})}{f_l(\mathbf{x})} + log\frac{\pi_k}{\pi_l} = log\frac{\pi_k}{\pi_l} - \frac{1}{2}(\mathbf{x}+\mu_k)^T\Sigma^{-1}(\mu_k-\mu_l) + \mathbf{x}^T\Sigma^{-1}(\mu_k-\mu_l) \quad (3.7)$$

This linear log-odds function shows that the decision boundary between classes *k* and *l* is linear in *x*, and provides a hyper-plane in *p* dimensions separating the classes, with *p* as the dimension of the feature space [284]. The training data is used to estimate the parameters of the Gaussian distributions [284]:

(1) $\hat{\pi}_k = N_k/N\ ,\ with\ N_k\ is\ the\ number\ of\ class\ k\ observations$

(2) $\hat{\mu}_{k=\sum_{g_i=k}\ \mathbf{x}_i/N_k}$,

(3) $\hat{\Sigma} = \sum_{k=1}^{K}\sum_{g_i=k}(\mathbf{x}_i-\hat{\mu}_k)(\mathbf{x}_i-\hat{\mu}_k)^T/(N-K)$.

The LDA rule results in classifying the data to class 2, in the case that [284];

$$\mathbf{x}^T\hat{\Sigma}^{-1}(\hat{\mu}_2-\hat{\mu}_1) > \frac{1}{2}\hat{\mu}_2^T\hat{\Sigma}^{-1}\hat{\mu}_2 - \frac{1}{2}\hat{\mu}_1^T\hat{\Sigma}^{-1}\hat{\mu}_1 + \log(N_1/N) - \log(N_2/N) \quad (3.8)$$

Otherwise, the output will be class 1 [284].

3.7.2. Support vector machine (SVM)

The SVM is a discriminative method, modelling the boundaries between classes linearly and providing a measurement of similarity using a kernel function [284], [287], [288]. SVM is an increasingly popular method due to many suitable characteristics compared to other classifiers, including, the ability to classify sparse data without over-training and maintain linear decision boundaries via kernel functions [330], [289]. When the two classes are linearly nonseparable and the classes overlap, SVM can still be used. It generates nonlinear boundaries by establishing a linear boundary in a new large and transformed feature space to linearly classify the data with reduced misclassification rate [284], [287], [290].

Given a training set (**x**) of k observations and their corresponding labels $\{(x_1,y_1),(x_2,y_2),\dots(x_k,y_k)\}$ which $y_i \in \{-1,1\}$, a hyper-plane is defined as follows [284], [287], [290],

$\{\mathbf{x}:\ f(x) = x^T\beta + \beta_0 = 0\}$,

where β is a unit vector, $\|\beta\| = 1$. A classification rule created by $f(\mathbf{x})$ is;

$$G(\mathbf{x}) = sign[\mathbf{x}^T\beta + \beta_0]. \quad (3.9)$$

Considering the classes are separable, a function $f(\mathbf{x})$ can be found with $\mathbf{y}_i f(\mathbf{x}_i) > 0, \forall i$ .Thus, a hyperplane can be found which produces the widest margin between the training samples for class 1 and -1, as shown in Figure 3.8. Then, the optimisation problem will be as follows [284], [287],

$$\max_{\beta,\beta_0,\|\beta\|=1} M$$

$$subject\ to\ \mathbf{y}_i(\mathbf{x}_i^T\beta + \beta_0) \geq M,\ i = 1, \dots, N. \tag{3.10}$$

As shown in Figure 3.8, the band is *M* units away from either side of the hyperplane and thus, *2M* units wide for so-called margin [284], [287]. The problem can be simplified by dropping the norm constraint;

$$\max_{\beta,\beta_0} \|\beta\|$$

$$subject\ to\ \mathbf{y}_i(\mathbf{x}_i^T\beta + \beta_0) \geq 1,\ i = 1, \dots, N. \tag{3.11}$$

In the case that the classes overlap in feature space, to solve the optimisation problem and maximise *M*, we can allow some error, i.e. some samples on the wrong side of the margin [284], [287] with a slack variable defined as $\xi = (\xi_1, \xi_2, \dots, \xi_N)$, as shown in the right panel of Figure 3.8. The limits of (3.11) will be reformed as below,

$$\begin{cases} \mathbf{y}_i(\mathbf{x}_i^T\beta + \beta_0) \geq M - \xi_i \quad , \\ \quad or \\ \mathbf{y}_i(\mathbf{x}_i^T\beta + \beta_0) \geq M(1 - \xi_i)\ , \end{cases} \qquad \forall i\ ,\ \xi_i \geq 0, \sum_{i=1}^{N} \xi_i \leq constant. \tag{3.12}$$

Where ξ_i determines the amount of error accepted for the prediction of $f(\mathbf{x}_i) = \mathbf{x}_i^T\beta + \beta_0$ to be on the wrong side of the margin, as displayed in the right panel of Figure 3.8 [284], [287]. In order to limit the training misclassifications which happen when $\xi_i > 1$, the $\sum \xi_i$ is bounded to a constant [284]. Assuming $= 1/\|\beta\|$, (3.11) can be written as;

$$\min\|\beta\|\ subject\ to \begin{cases} \mathbf{y}_i(\mathbf{x}_i^T\beta + \beta_0) \geq 1 - \xi_i \quad \forall i\ , \\ \xi_i \geq 0\ ,\ \Sigma\xi_i\ \leq constant. \end{cases} \tag{3.13}$$

In general, an SVM classifier for nonseparable classes is defined by this equation, with the overlapping case demonstrated in the right panel of Figure 3.8 [284]. The criterion of this equation, (3.13), reveals that the data samples which are placed well within the class boundary are not critical in forming the boundary, but those within the margin around the boundary are important [284]. This is the major factor which distinguishes SVM from LDA classifier where the decision boundary is formed by the covariance of the class distributions and the location of the class centroids [284]. Equation (3.13) can be written in another form,

$$\min_{\beta,\beta_0} \frac{1}{2}\|\beta\|^2 + C\sum_{i=1}^{N} \xi_i \qquad subject\ to\ \xi_i \geq 0\ ,\ \ \mathbf{y}_i(\mathbf{x}_i^T\beta + \beta_0) \geq 1 - \xi_i \quad \forall i\ , \tag{3.14}$$

where C is the cost function, substituting the constant of previous equation, with $C = \infty$ for separable classes [284]. The Lagrange (primal) function results in [284], [287], [290];

$$L_p = \frac{1}{2}\|\beta\|^2 + C\sum_{i=1}^{N}\xi_i - \sum_{i=1}^{N}\alpha_i[\mathbf{y}_i(\mathbf{x}_i^T\beta + \beta_0) - (1-\xi_i)] - \sum_{i=1}^{N}\mu_i\xi_i \ , \tag{3.15}$$

Minimising it with respect to β, β_0 and ξ_i by setting the derivatives to zero leads to;

$$\beta = \sum_{i=1}^{N}\alpha_i\mathbf{y_i}\mathbf{x}_i \quad , \quad 0 = \sum_{i=1}^{N}\alpha_i\mathbf{y}_i \quad , \quad \alpha_i = C - \mu_i \ , \forall i \ , \ and \ \alpha_i, \mu_i, \xi_i \geq 0 \ , \forall i \ . \tag{3.16}$$

By replacing (3.16) into (3.15), a Lagrangian dual objective function will be achieved [284],

$$L_p = \sum_{i=1}^{N}\alpha_i - \frac{1}{2}\sum_{i=1}^{N}\sum_{i=1}^{N}\alpha_i\alpha_{i'}\,\mathbf{y}_i\mathbf{y}_{i'}\mathbf{x}_i^T\mathbf{x}_{i'} \ , \tag{3.17}$$

In this equation L_p should be maximised subject to $0 \leq \alpha_i \leq C$ and $\sum_{i=1}^{N}\alpha_i y_i = 0$. The Karush-Kuhn-Tucker conditions are also included with the (3.16) conditions for $i = 1, 2, \dots, N$,

$$\alpha_i[\mathbf{y}_i(\mathbf{x}_i^T\beta + \beta_0) - (1-\xi_i)] = 0 \ , \ \mu_i\xi_i = 0 \ , \ \alpha_i[\mathbf{y}_i(\mathbf{x}_i^T\beta + \beta_0) - (1-\xi_i)] \geq 0 \ , \tag{3.18}$$

These equations (3.16) - (3.18) result in the solution for primal and dual problem [284]. The solution for β from (3.16) has the following form;

$$\hat{\beta} = \sum_{i=1}^{N}\hat{\alpha}_i\mathbf{y}_i\mathbf{x}_i \ , \tag{3.19}$$

with nonzero coefficients $\hat{\alpha}_i$ for the observations i, satisfying the conditions of (3.18) [284]. These observations are known as support vectors, as $\hat{\beta}$ is presented using these observations [284], with some support vectors placing on the margin, $\hat{\xi}_i = 0$, leading (3.16) and (3.18) to $0 < \hat{\alpha}_i < C$. By using the margin samples with $0 < \hat{\alpha}_i, \hat{\xi}_i = 0$, the equation will be solved for β_0. Given the solutions $\hat{\beta}_0$ and $\hat{\beta}$, the decision function can be reformed, with the cost function, *C*, as the adjusting parameter:

$$\hat{G}(\mathbf{x}) = sign[\hat{f}(\mathbf{x})] = sign\left[\mathbf{x}^T\hat{\beta} + \hat{\beta}_0\right]. \tag{3.20}$$

The support vector classifier can be extended from finding the linear boundaries and become more flexible by expanding the feature space using basis functions or kernels [284]. For datasets which are

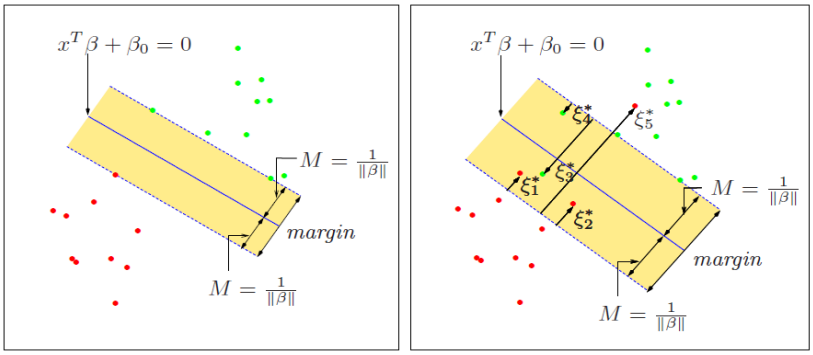

Figure 3.8. An illustration of a support vector machine. The left panel demonstrates the separable case, with solid line as decision boundary and dashed lines bounding the shaded maximal margin of width $2M = 2/\|\beta\|$. The right panel displays the nonseparable case with overlap. The samples labelled ξ_j^* placed on the wrong side of their margin by an amount of $\xi_j^* = M\xi_j$ and samples on the right side have $\xi_j^* = 0$. The margin is maximised subject to a total error of $\sum\xi_j \leq constant$. Thus, $\sum\xi_j^*$ is the total distance of the samples on the wrong side of their margin. (Figure adapted from Figure 12.1 in [284].)

not linearly separable, applying kernel functions to the original feature space of training set may generate better classification and separation with linear boundaries in the enlarged space, translated to nonlinear boundaries in the original feature space [284]. Thus, SVM can be formed using sums of a kernel function $K(.,.)$ [290];

$$D(\mathbf{x}) = \sum_k \alpha_k \mathbf{y}_k K(\mathbf{x}, \mathbf{x}_k) + b, \quad (3.21)$$

where the y_k are the ideal outputs, and b is a constant variable which is learnt,

$$\sum_k \alpha_k \mathbf{y}_k = 0 \text{ , and } \alpha i > 0. \quad (3.22)$$

Three examples of widely used kernels in the literature are [290]:

*d*th-degree polynomial: $K(\mathbf{x}, \mathbf{x}') = (1 + \langle \mathbf{x}, \mathbf{x}' \rangle)^d$,

Radial basis: $K(\mathbf{x}, \mathbf{x}') = \exp(-\gamma \|\mathbf{x} - \mathbf{x}'\|^2)$,

Neural network: $K(\mathbf{x}, \mathbf{x}') = \tanh(\kappa_1 \langle \mathbf{x}, \mathbf{x}' \rangle + \kappa_2)$

where $\langle \mathbf{x}, \mathbf{x}' \rangle$ respresents an inner product. To sum up, the support vectors x_i are obtained using the training set through an optimisation process, as described [289], [290]. The outputs ideally should take either 1 or -1, according to the class of the support vector, either class 1 or class 2 [290]. Assuming that the data can be linearly classified, the resulting decision function of an input vector x can be defined as follows,

$$D(\mathbf{x}) = \mathbf{w}.\mathbf{x} + b \quad , \; where\, w = \sum_k \alpha_k \mathbf{y}_k \mathbf{x}_k \quad (3.23)$$

In addition, the weight vector *w* is a linear combination of training data where most α_k are zero and include only values for the support vectors, $\mathbf{x}_k$ [290].

3.7.3. Extreme learning machine (ELM)

The extreme learning machine (ELM) is a feed forward neural network with a single hidden layer and randomly initialised input layer weights [285], [286].

Feed forward neural networks are used for their ability to approximate the complex nonlinear mappings directly from the inputs [285], [286]. In fact, they are capable of providing models for complex cases which are not easily classified by traditional parametric methods [285]. Researchers demonstrated that a single-hidden layer feedforward neural network (*SLFN*) with random input weights and biases for *N* hidden nodes and any desired nonlinear activation function has the ability to learn *N* distinct training samples [291]–[293]. In fact, unlike the traditional approach of adjusting the network parameters, it performs the learning algorithm without tuning the input weights and hidden layer biases [285]. The traditional approach of adjusting the network parameters results in a number of issues, such as dependency of the parameters of different layers and slow training procedure [285].

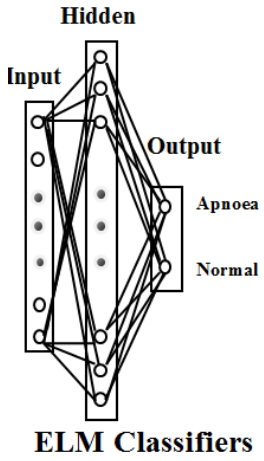

Figure 3.9. Schematic presentation of an extreme learning machine (ELM) classifier consisting of one hidden layer with a large number of non-linear hidden neurons in a feed-forward network.

Huang *et al*. in 2006 introduced ELM as a simple learning algorithm for SLFN that can be easily and quickly performed [285]. The method sets random values for input weights and hidden layer biases when adopting infinite differentiable activation functions for hidden neurons. Then, the network becomes a linear system (in its output) and the output weights can be determined using the pseudo inverse calculation in a single pass learning procedure, which is described in detail below [285], [294]. The tested results of this method on different applications and standard datasets have revealed strong generalisation performance and a fast learning procedure [285].

Figure 3.9 shows the structure of ELM classifier which is identical to a classic one-layer perceptron. ELM classifiers are generally characterised with "fan-out" number defined as the proportion of the number of hidden layer neurons to the input layer neurons [295].

An individual sample of data is assumed to be $\mathbf{x}_s \epsilon \mathbb{R}^{F\times 1}$ with s as the index of series or epochs and F as the number of input features. The forward propagation of the input signals through to the output of the classifier can be defined as [285]:

$$\mathbf{y}_{n,s} = \sum_{h=1}^{H} \mathbf{w}_{n,h}^{(2)}\, g\left(\sum_{f=1}^{F} \mathbf{w}_{h,f}^{(1)}\, \mathbf{x}_{f,s}\right) \tag{3.24}$$

where $\mathbf{y}_s \in R^{N\times 1}$ is the output vector, f and F correspond to the input features and the number of input features respectively and h and H correspond to hidden layer index and number of hidden neurons respectively. n and N are the output layer index and number of output neurons. $w^{(1)}$ and $w^{(2)}$ are the weights of input layer (input to hidden layer connections) and output layer (hidden to output layer connections), respectively. $g(\ )$ is the activation function of hidden layer which is a non-linear function [285].

As described above, $w^{(1)}$ are randomly set. $w^{(2)}$ are computed in a single propagation through to the output as below:

$$\mathbf{y}_{n,s} = \sum_{h=1}^{H} \mathbf{w}_{n,h}^{(2)} \mathbf{a}_{h,s} \quad where \quad \mathbf{a}_{h,s} = g\left(\sum_{f=1}^{F} \mathbf{w}_{h,f}^{(1)} \mathbf{x}_{f,s} \right) \tag{3.25}$$

The "fan-out" number which represented above as the number of hidden layer neurons, *H*, per input neuron, *F*, should be large enough to project the input to much higher dimension space in order to obtain better classification boundaries [285]. The output neurons are linear and the pseudo-inverse of hidden layer outputs and output targets resulted in output weights for each classifier. We can rewrite equation (2) as a matrix equation in which $\mathbf{W} \in \mathbb{R}^{N \times H}$ is the matrix with output layer weights $w_{n,h}^{(2)}$ as its elements, and $\mathbf{A} \in \mathbb{R}^{H \times S}$ is the matrix of hidden layer outputs through the entire epochs of the recording, **S** [285], [295]. The matrix of outputs $\mathbf{Y} \in \mathbb{R}^{N \times S}$ contains network outputs through the entire epochs of recordings as follows [285], [295]:

$$\mathbf{Y} = \mathbf{WA} \tag{3.26}$$

By replacing the target values as the desired outputs of the network in equation (4), we can set up an equation for determining the output weights. The target matrix can be defined as $\mathbf{T} \in \mathbb{R}^{N \times S}$ which is the outputs of the training set through the entire epochs of the recordings, substituting this into (4), we obtain:

$$\mathbf{T} = \mathbf{WA} \tag{3.27}$$

The optimisation procedure is to calculate the matrix *W*, which can be determined by calculating the Moore-Penrose pseudo-inverse $\mathbf{A}^{+} \in \mathbb{R}^{S \times H}$ of **A** [296]:

$$\mathbf{W} = \mathbf{T}\mathbf{A}^{+} \quad where \quad \mathbf{A}^{+} = \mathbf{A}^{T}(\mathbf{A}\mathbf{A}^{T})^{-1}. \tag{3.28}$$

By this method, the sum of square errors between outputs of the network *Y* and the target outputs *T* is minimised without the need for multiple iterations. The term "extreme" is due to the network's higher speed in learning, better generalisation and less training error [285]. This classifier was used for OSA detection in this thesis and the results were compared to the other two classifiers (LDA and SVM). In addition, the results of ELM classifier compared to LDA and SVM for OSA detection will be presented in section 5.2.

3.8. Performance measures

In diagnostic applications such as cariorespiratory detection, the outputs of the classifiers are the presence and absence of an apnoea episode or arrhythmia event. To measure the performance of the classifier, a count of the success in detecting the abnormal (apnoeic or arrhythmia) episodes and normal episodes is required. To do this, three measurements of accuracy, sensitivity and specificity were calculated to validate the system. They resulted from measuring True Positive (TP), True Negative (TN), False Positive (FP), and False Negative (FN), with the confusion matrix shown in Table 3.3 [16]. There are also two terms in classification known as positive for the occurence of the

Table 3.3. A confusion matrix for the performance assessment of a system discriminating between normal and apnoea events. "Actual" refers to the annotation labels provided by the expert and "Predicted" refers to the classification results obtained by the machine learning techniques.

		Actual	
		Normal	Apnoea
Predicted	Normal	TN	FN
	Apnoea	FP	TP

abnormality or the disorder including, the sleep apnoea or arrhthmia and negative for the occurrence of a normal epoch. Both can be classified correctly defined as "true" or incorrectly, defined as "false" [16]. Thus, TP corresponds to the epochs of data which were correctly classified as abnormal epochs matched with the disordered annotation. TN represents the correctly classified epochs which are classified as normal epochs. FP implies those epochs which are misclassified as abnormal or disordered epoch, but they are actually a normal one. FN respresents the misclassified epochs as normal epochs, although they are abnormal or disordered ones [16]. The basic measures of classifier performance used are accuracy, sensitivity or true positive rate (*TPR*) and specificity or true negative rate (*TNR*). They are defined as:

$$\text{Sensitivity} = \frac{\text{TP}}{\text{TP+FN}} \quad , \tag{3.29}$$

$$\text{Specificity} = \frac{\text{TN}}{\text{FP+TN}} \quad , \tag{3.30}$$

$$\text{Accuracy} = \frac{\text{TP+TN}}{\text{TP+FP+TN+FN}} \quad . \tag{3.31}$$

The receiver operating characteristic (ROC) curve, in some cases referred to as relative operating characteristic, plots the probability of true positives versus the probability of false positives or false

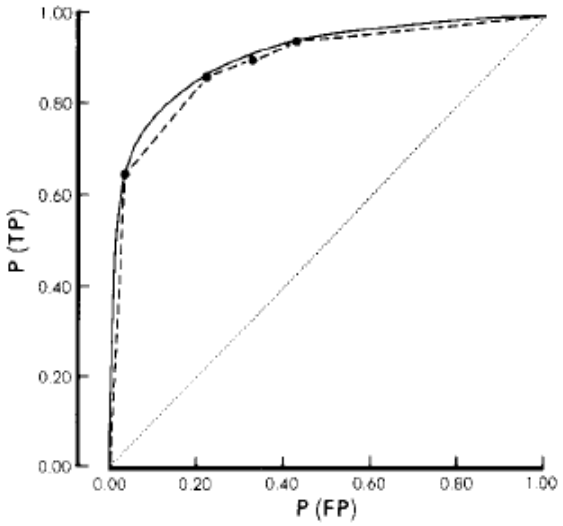

Figure 3.10. A sample ROC plot (the probability of TP (TPR) versus the probability of FP (FPR)). The dotted diagonal line shows no discrimination or the random predictions (AUC=0.5) and the solid line shows a smoothed Gaussian-based curve. (Figure adapted from Figure 1 [300])

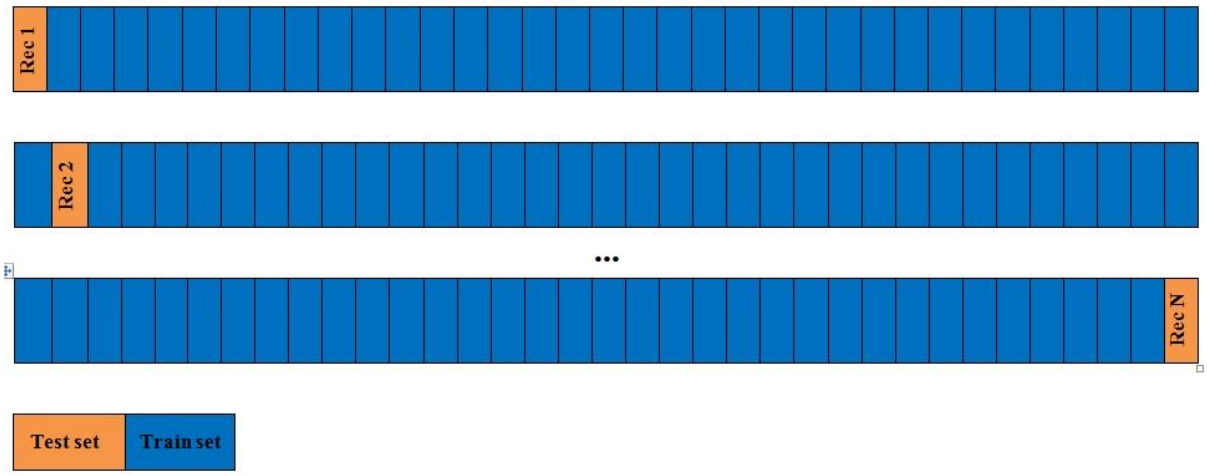

Figure 3.12. An illustration of leave-one-record-out cross validation for N recordings, with one record set to the test or validation set and the remaining recordings used as the training set in every iteration.

alarm rate [298]–[300]. The area under the ROC curve provides a measure of diagnostic ability of the classification features, as shown in Figure 3.10 [298]–[300]. The diagonal line indicates the outcome from random predictions which corresponds to an AUC of 0.5 and the degree of concavity determines the performance measure, with an AUC=1 corresponding to a perfect prediction [299].

The performance measures were calculated using leave-one-record-out cross-validation, which used one record as the validation set and the remaining records as the train set in every iteration, as shown in Figure 3.11. The results are shown in section 5.2. It should be noted that although cross-validation is known to present an unbiased estimate of the expected value of prediction error, which is the average performance over the test set, estimation of the variance of the cross-validation is a difficult task, as it generates dependent test errors [301], [302]. Bengio *et al.* showed that the cross-validation is unable to provide an unbiased estimate of the variance of model performance [302]. Thus, we used leave-one-record-out method to minimise the bias on the average performance but it introduces a bias on the variance of the system performance.

3.9. Summary

In this chapter, the methodology and algorithms used in the literature for automated diagnosis of cardiorespiratory disorders were surveyed. The chapter commenced with outlining the principal modules of an ideal automated arrhythmia detector and sleep disordered breathing recognition system. Also the proposed approaches for reducing the false arrhythmia alarms were surveyed. Then, the major blocks of an automated system for diagnosis of cardiorespiratory disorders and signal processing methods previously used in the published studies were described. First, different ECG preprocessing approaches and noise removal techniques were reviewed. Then, the QRS detection techniques and different algorithms for distinguishing the R peaks and correcting the missed or spurious QRS detections were illustrated in detail. I also listed two major biosignals captured from the ECG recordings: the RR-intervals and the EDR signals. It was followed by an outline of the features utilised for the diagnosis of cardiorespiratory disorders including the CPC features and PSD features. Finally, the algorithms and mathematics behind the machine learning approaches used in this thesis, linear discriminant analysis (LDA), support vector machine (SVM), and extreme learning machine (ELM) were explained. I also described the performance measures that were used to report the results and the performance of the algorithms presented in this research for both applications. In the following chapters, the developed algorithms of this thesis for both applications are illustrated.

Chapter 4

Application 1

4. Application 1: reducing false arrhythmia alarms in the ICU

In the previous chapter, an overview of the background signal processing techniques and the associated algorithms of automating the diagnosis of cardiorespiratory disorders was presented. In this chapter, the multimodal signal processing algorithms developed through this thesis for false arrhythmia alarm reduction are described.

In section 4.1, I commence by describing the database used, and the characteristics of the utilised multimodal recordings in section 4.1.1. This is followed by the ECG signal processing techniques which includes the algorithms developed for baseline wander noise removal, RR-interval or heart rate variability (HRV) calculation and segmentation (see sections 4.1.3 and 4.1.4). Then, the proposed approach for ECG signal quality index evaluation is described (see section 4.1.5). Following this, the pulsatile signal processing (ABP and PPG signals) and the applied methods are explained in section 4.1.6. Then, the alarm detection and multimodal signal processing scheme are outlined, followed by a detailed description of the arrhythmia alarm detection (section 4.1.9) in which the extracted features, combined feature set, the thresholds, alarm detection methods and signal fusion are described in detail. Finally, in section 4.2, the results obtained by the proposed algorithms are demonstrated and, in section 4.3, the results are discussed for every arrhythmia types.

4.1. Methodology of application 1

In the first application of this thesis, we developed a signal processing system for automatic detection of five life threatening arrhythmias. This study developed algorithms to reduce arrhythmia false alarms in the ICU by processing one or more of the multimodal signals: photoplethysmography (PPG), arterial blood pressure (ABP), Lead II and augmented right arm (aVr) ECG. The goal was to detect the five critical arrhythmias comprising asystole (ASY), extreme bradycardia (EBR), extreme tachycardia (ETC), ventricular tachycardia (VTA), and ventricular flutter or fibrillation (VFB). To train and test our system, we have used the signals of the *Computing in Cardiology Challenge 2015 Dataset* (section 4.1.1). The arrhythmia detections are then used to assess the validity of alarms generated by ICU equipment with the goal of identifying false alarms. The different characteristics of the arrhythmias suggested the application of individual signal processing techniques for each alarm and the combination of the algorithms to enhance false alarm detection. Thus, different features and signal processing techniques were used for each arrhythmia type (section 4.1.9). The ECG signals

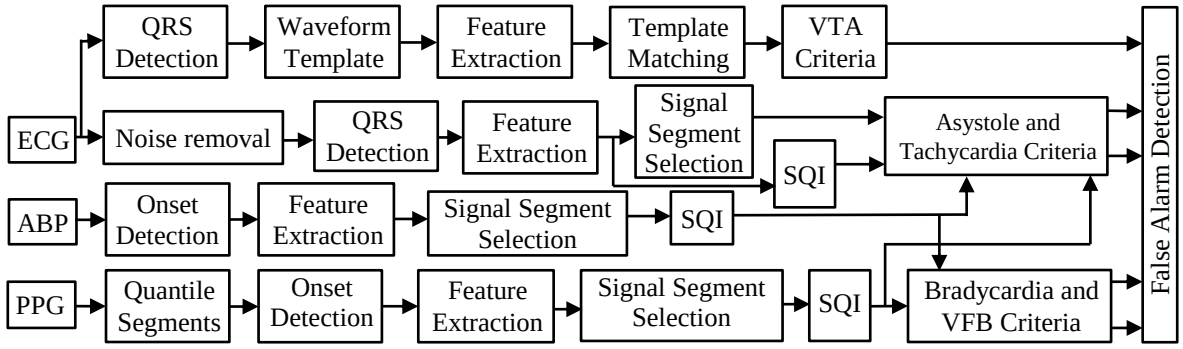

Figure 4.1. Block diagram of the proposed system for arrhythmia false alarm detection in the ICU.

Abbreviations: arterial blood pressure (ABP), electrocardiogram (ECG), photoplethysmogram (PPG), signal quality index (SQI), ventricular flutter or fibrillation (VFB), ventricular tachycardia (VTA)

were first processed to reduce signal interference, as described in section 4.1.3. Then, a Hilbert-transform based QRS detector algorithm was used to identify the QRS complexes, which were then processed to determine the instantaneous heart rate (section 4.1.4). The pulsatile signals (PPG and ABP) were processed to discover the pulse onset of beats which were then used to measure the heart rate (section 4.1.6). The signal quality index (SQI) of the signals was calculated to verify the integrity of the heart rate information (section 4.1.5). The signal processing algorithms I describe here were the basis of our entry in the *PhysioNet/Computing in Cardiology Challenge 2015*. An early description of these algorithms was published in *Computing in Cardiology Challenge 2015* [60].

The block diagram of the proposed system for false arrhythmia alarm detection is shown in Figure 4.1. A high level description of the system is provided here and more detail is given in the following sections. The top-down order of the signal blocks represents the priority for signal selection in the analysis process.

VTA detection relied solely on features extracted from the ECG signals which were processed without noise removal and using template matching. QRS detection was applied to the ECG signal for the identification of QRS complexes. A reference waveform template was generated from the first QRS and subsequent QRSs were compared to the reference to determine if they were irregular beats. If five or more beats were deemed irregular in the alarm segment then the VTA alarm confirmation was set to true, otherwise it was set to false.

The alarm confirmation procedure of asystole and tachycardia were similar. First, signal interference was removed from the ECG signals. QRS beats were detected from the clean ECG signals and discriminating features were extracted. A segment of the ECG signal containing the alarm was identified and SQI measurements were determined. A similar process was applied to the ABP and PPG signals resulting in SQI and feature values. Finally, for the alarm segment, the features of the ECG signals, the ECG SQI measures, the extracted features and SQI measures of the available pulsatile signals served as inputs to assess the validity of the tachycardia alarms. Processing

techniques for the asystole alarm evaluation were similar except that we did not use the SQI measures of the ECG signals for the asystole alarms.

The process of detecting bradycardia and VFB false alarms were identical. The pulsatile signals were used to diagnose these two arrhythmias. After distinguishing the onset beats of ABP signals, features were measured and the segment of the alarm was identified for criteria assessment and SQI evaluation. The available pulsatile signals, ABP and PPG, were processed similarly, with the exception of the PPG processing which included a quantile segmentation step prior to onset detection. This was followed by feature extraction and identifying the alarm segment and the features in that segment. Finally, the SQI of the alarm segment was measured and the features from available ABP and PPG with their SQI measures were used to confirm the bradycardia or VFB alarm status.

In the following sections, I first describe the database and signal processing methods for interference removal, heartbeat identification, SQI measurement and feature extraction for the ECG, PPG and ABP signals. I then describe the designed hierarchical processing of the ECG and pulsatile signals to determine the final alarm status.

4.1.1. Database

The input dataset was provided by the *PhysioNet/Computing in Cardiology Challenge 2015* [33]. The dataset incorporates 1250 arrhythmia alarms which were selected randomly from four hospitals in the USA and Europe. Less than three alarms from the five arrhythmia types were selected from an individual patient and were often more than five minutes apart. The dataset was divided into 750 open-access recordings used as a learning set and 500 recordings for test set which were hidden. Train and test set were comprised of signals recorded from different patients. Five hundred and ninety recordings in the training data included four signals comprising of two ECG signals (ECG leads II and aVr) and two pulsatile signals (the photoplethysmogram (PPG) and arterial blood pressure (ABP)). One hundred and sixty recordings in the training data comprised of three of the four signals listed above (i.e. two ECG and one pulsatile or one ECG and two pulsatile signals). Each patient had a maximum of two recordings of separate alarms in the dataset. The chosen recordings had been annotated by three or more experts and the alarm outcome was determined by agreement of at least two-thirds of the experts. Recordings that did not have a two-thirds agreement were excluded. Each alarm was annotated as “true”, “false”, or “impossible to tell”. The type of the arrhythmia alarm is also provided with the annotations. For example, record a64 has a label of asystole false alarm, as shown in Figure 4.2. Each record includes an alarm at the fifth minute from the start of the record and the corresponding arrhythmia event happens within ten seconds of the alarm (i.e., between 4:50 and 5:00 minutes). If further arrhythmias occurred before the fifth minute of a record, they were not annotated. The repeated alarms and information from alarms prior to the annotated one are not used to reduce the probability of transferring errors from one alarm to the next one. Resampling was applied

to the four sensor signals at the rate of 250 Hz, 16 bit. Band-pass filtering in the range of 0.05 to 40 Hz was implemented with an FIR filter. Also, common notch filters were utilised for noise removal of powerline noise. Pacemaker and other noise artefacts still existed in the ECG signals. In some cases, movement artefacts, failure in sensor connection, line flush, coagulation and other interferences also influenced the pulsatile signals.

4.1.2. ECG signals

In order to diagnose the high risk arrhythmias, the ECG signals are functional and informative. The recordings in the challenge dataset are comprised of lead II and/or lead aVr. The block diagram of the proposed system for the first application of this thesis to detect false arrhythmia alarms in the ICU using ECG signal processing is shown in Figure 4.1. The ECG signals are mostly corrupted by movement artefact, pacemaker, and fibrillator signals. A first step was to detect and remove these artefacts. A filter, as described below, was applied to the raw ECG signals to remove the unwanted interference. The filtered signals were then processed to find the QRS complexes. After calculation of RR-intervals from the QRS detection points and applying the above signal processing steps, there were still QRS complexes in some recordings that were not detected successfully. To attempt to recover these missed signal beats, we detected heart beats in the other sensor channels and then used the beat detections across all channels to obtain an enhanced recognition. The final step was feature extraction for arrhythmia detection (see section 4.1.9).

4.1.3. Baseline wander noise removal

Interference removal was performed by applying filters for noise reduction. The ECG signals of the database were distorted by baseline wander noise which originated from movement, respiration and perspiration affecting the electrode impedance [245]. Baseline wander noise affects the low frequency component of the ECG signals [246] and can influence the clinical interpretation of ECG signal. A first step in signal processing algorithm is to detect and remove these artefacts. The filtering process, described below, was applied to the raw ECG signals to remove the unwanted interference. In this study, baseline wander noise was removed by two median filters [71]. The first median filter with 200-ms width is applied to remove the QRS complexes and P waves. Then, the resulting PQRS-free signal is used to apply the second median filter. The width of the second median filter was 600-ms to eliminate T waves. Thus, the output of the second median filter did not include the information from the ECG waves and contained only the baseline wander. By subtracting the output of the second median filter from the raw input ECG signals, the resulting signal contained the P-QRS-T complexes minus baseline wander. This method was applied to leads II and aVr of each ECG recordings. Reliable identification of QRS complexes is difficult due to the changing nature of their morphology and the influence of unwanted interference on the ECG signal [303]. By removing the unwanted

interference from the ECG signals, we can improve the likelihood of successful arrhythmia detection. The other important factor is the changing morphology of the QRS complexes which were taken into account in the utilised QRS detection algorithm explained in the following section.

4.1.4. RR interval and signal segment selection

The first step toward feature extraction for arrhythmia recognition by ECG signal is QRS detection. There are various QRS detection algorithms but selecting a reliable method is highly significant for false arrhythmia alarm recognition. In this work, the QRS complexes were identified by a Hilbert transform based algorithm, which was described in section 3.4 [263]. Finally, the QRS detections were used for feature extraction. The RR-intervals were determined by calculating the time difference between two adjacent QRS detections. Then, the information closer to the alarm is utilised for false alarm identification. Thus, the segment comprising the alarm is selected for arrhythmia recognition. In this study, the alarm segment begins 16 seconds prior to the alarm and ends at the alarm point which occurs during the fifth minute of the signal.

4.1.5. ECG signal quality index (SQI)

Visual observation of QRS detection points and corresponding RR intervals revealed that some of the heart beats were missed or falsely detected. Missing value intervals and noisy alarm segments can produce issues during signal processing and suspect QRS detection beats. Also, ECG artefact was reported as a reason for false arrhythmia alarms [175]. Therefore, before further processing, the quality of the ECG signal was assessed.

In order to assess the quality of the ECG signal, the signal quality index (SQI) was exploited to determine if it possessed reliable information for false alarm detection. The signal evaluation index has been widely studied [304], [305]. Four tests were applied to determine the ECG SQI and if the alarm segment satisfied the tests, it was allowed to proceed for further processing. The first test determined if the segment was empty. No heart beat in the segment indicated a failure of the heart beat identification algorithms and was indicative of the presence of significant signal interference. In the second test, the number of the detected QRS detection complexes or the available beats of each ECG signal was measured in the segment. This test allowed recognition of the signals with a high proportion of missing heart beats and the inspection of the proportion of motion artefact, failure in sensor attachment and other noises in the segment. The minimum number of beats was set to ten beats. If an ECG signal segment contained less than this minimum, it was not considered further in arrhythmia detection. The third test was the maximum RR-interval or minimum heart rate. This test examines the physiological reliability of the heart rate and indicates the noisy alarm segments and missed QRS complexes. The maximum measure of the third test was set to six seconds. If all RR-

interval in a segment were less than six seconds, the test was passed. The fourth ECG SQI test was the standard deviation of the ECG in the segment containing the alarm. This test helps identify the segments with a high percentage of noise and artefact. The optimum standard deviation was adopted as 0.05 over the whole segment. We set these tests to address most of the observed corruptions on the ECG signals comprising the level of noise and the percentage of missed or spurious QRS detections in the segment. The output of the ECG SQI algorithm determines whether the ECG signal is satisfactory for next processing.

It should also be noted that for some arrhythmias, some of the SQI steps were skipped. Studies revealed that SQI evaluation diminished the diagnosis accuracy of particular categories of the arrhythmias due to their noisy manifestation [306]. Since the behaviour of specific classes of arrhythmias such as VTA is homogenous to noise structure, application of our ECG SQI tests reduced the performance of our developed algorithms for detection of arrhythmias and was removed from the false alarm detection of those types of arrhythmias.

It should be noted that we adopted these methods from the studies in order to provide simple tests for quality evaluation of the challenge database. Further work is required to optimise the methods and extend the tests for this application. Further details will be described in section 4.1.9.

4.1.6. Pulsatile signals

It is reported that implementation of pulsatile signals which contain cardiac cycles improves the diagnosis of false arrhythmia alarms when combined with cardiac cycle information from ECG signals [175]. In the *PhysioNet/CinC Challenge 2015* dataset, one or both arterial blood pressure (ABP) and photoplethysmogram (PPG) signals were available and we utilised them to reduce the false alarm rate. The signal processing algorithms of the sample submission provided by the *PhysioNet/CinC Challenge 2015* were utilised for determining the beat onset points from the pulsatile signals and arrhythmia identification in this study. We provide a short description of these algorithms in the following sections.

Arterial blood pressure (ABP) was another signal used to verify the false arrhythmia alarms. As it is recorded separately to the ECG leads, it rarely contains identical interference to the ECG signal [175]. Also, ABP is regarded as the pressure signal with the least noise and artefact [51]. There were three PhysioNet open-source algorithms used to process the ABP. In order to find the onset of the ABP pulses, the ‘wabp’ algorithm, which is an open-source ABP beat detector available on the PhysioNet, was executed on ABP signal [307]. The Length transform is used in this technique [308] and noise removal and feature enhancement was applied through the algorithm. The performance of this algorithm was examined in different studies and showed an acceptable performance level and hence we adopted it in this study [25], [212], [309], [310]. Following this, ABP features were calculated

with the ‘abpfeature’ algorithm. The features include systolic pressure, diastolic pressure, systolic area, and mean pressure on the onset beats of the ABP pulses. Next, ABP quality index (SQI) was estimated by the ‘jSQI’ algorithm at each ABP detected beats [311]. The ABP SQI algorithm explores if the features are physiologically plausible. The features that were not clinically reliable were eliminated. Lastly, the time between the pulse onsets in the ABP signal was measured to generate pulse intervals of ABP signal to be used for further signal processing.

The other pulsatile signal used for false alarm detection was the photoplethysmogram (PPG) which was available in many of the recordings in the learning set of PhysioNet/CinC Challenge 2015. The open-source PhysioNet algorithms were used to process the PPG signal. Firstly, the signal was divided into three partitions by the open-source ‘quantile’ algorithm. The three quantiles used were 5%, 50% and 95%. Next, the subtraction of third quantile and first quantile was measured and used to detect pulse onsets. The onset beats of the PPG waveform was verified with ‘wabp’ algorithm [307]. Then, the pulse intervals were measured by the difference of the adjacent onset beats and used to calculate the heart rate. Finally, the PPG signal quality was evaluated with ‘ppgSQI’ algorithm through a beat template correlation technique.

4.1.7. Alarm detection

The segment containing the alarm from the available signals of each recording was selected from the 16 seconds prior to the alarm ending. The heart rates and intervals corresponding to the alarm segment were used for further signal processing. This thesis aimed to recognise the false arrhythmia alarms in real-time and avoid using the data following the alarm occurrence. Our proposed algorithm can also be implemented in a retrospective manner which uses the information after the occurrence of the alarm. In the *PhysioNet/CinC Challenge 2015* dataset, the alarms were set to appear at five minutes after the beginning of the signal. To guarantee alarm inclusion in the segment, the segment started 16 seconds before the alarm time. Next, the beats in the alarm segment were identified for the available signals of each recording and the corresponding RR-intervals, pulse intervals and heart beats were chosen. Finally, the features were calculated from the heart rates, RR-intervals or pulse intervals of the pulsatile waveforms. It should be noted that signal processing for each arrhythmia alarm condition was separately executed with different models and features [306].

4.1.8. Multimodal signal processing

As it has been indicated in chapter 3, interference in the ECG signal can be a source of the false arrhythmia alarms. Using other leads of the ECG signal simultaneously with other signals to combine the information can improve the diagnosis [175]. Thus, exploiting information from multimodal signals enhances the arrhythmia detection.

In this thesis, the Hilbert QRS detector identified the QRS complexes with a decent accuracy [265], [268]. So the QRS detections of the ECG signals were reliable measures with which to proceed with signal processing and advance to the detection of pulse onsets of pulsatile signals provided by 'wabp' algorithm.

Considering the available signals in the majority of the training set and the quality of the available signals of the challenge dataset, the signals were prioritised from ECG signals to the pulsatile signals for feature extraction. However, unwanted interference can corrupt the signal properties which are significant measures for arrhythmia detection. As previously mentioned, the noisy signals are known as a major source of false arrhythmia alarms [175]. Thus, the SQI of the signals were evaluated to identify noisy signals. If the signal passed the SQI tests, then features of the signal were extracted. The signal SQI measures were processed in the following order of ECG II, ECG aVr, ABP and PPG. The SQI of the ECG signals was evaluated as explained in section 4.1.5. For every alarm with the exception of bradycardia and VFB, the result was decided based on the highest priority signal with the best quality of those considered and the alarm suppression or trigger was determined by that signal. For bradycardia and VFB, every considered signal satisfying the quality criteria were used in the decision-making process. The algorithm has been shown in the block diagram of the system in Figure 4.1.

Combining the features and information of multimodal signals and evaluating the signal quality addressed the intervals with missing values or noise such as failure in sensor attachment and motion artefact, as observed in the challenge training set. This approach with multimodal signals benefits false arrhythmia alarm assessment in dealing with signals recorded in a real environment. We analysed each arrhythmia through a different approach which are explained in the following section.

4.1.9. Arrhythmia alarm detection

For this application, different signal processing approaches were applied for individual arrhythmia types, commencing with asystole alarm detection. *Asystole (ASY)* was defined as an absence of a heart beat for at least four seconds [33]. Thus, the minimum threshold for asystole detection was set to four seconds with a tolerance of 0.5 second. Two sample ECG II signals with asystole alarm labels (true and false) from the challenge dataset are shown in Figure 4.2. The priorities of signals used for asystole detection were defined as ECG II, followed by ECG aVr followed by the available pulsatile signals. The criteria for using the ECG signals encompassed successful beat detection, a maximum RR-interval of less than the defined threshold for signal quality and a standard deviation (SD) within the defined threshold. This was less restrictive for use of the lower priority pulsatile signals where an availability of detected beats was sufficient. As is shown in the block diagram of the system in Figure 4.1, the ECG SQI measures were not used in asystole detection. This algorithm design decision was made as we found that implementing SQI measures tended to knock out heart beats, which increased

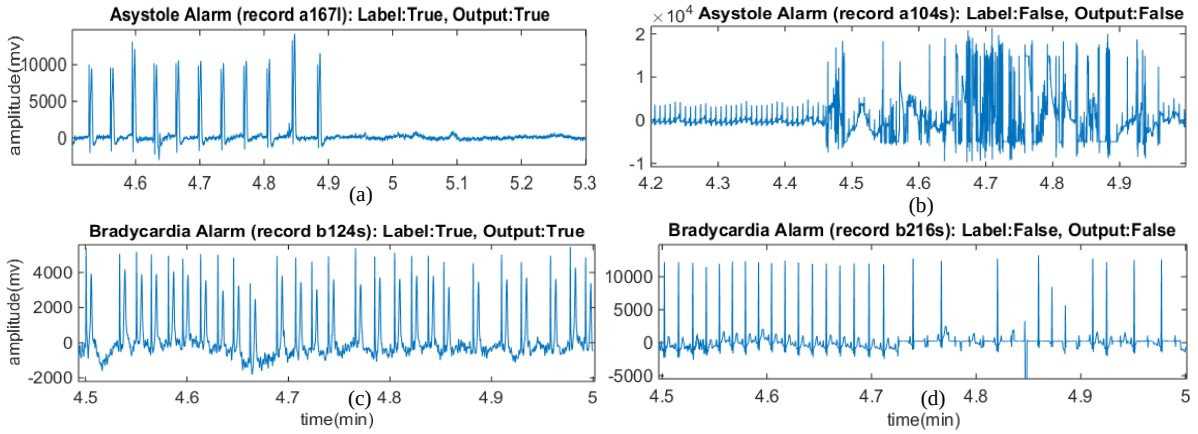

Figure 4.2. Sample ECG II signals from the Computing in Cardiology challenge dataset. Records with of arrhythmia alarms labels of (a) true asystole alarm label and predicted as true alarm by our algorithm, (b) false asystole alarm label and predicted as false alarm, (c) true bradycardia alarm label, predicted as true alarm, (d) false bradycardia label and predicted as false alarm.

the likelihood of false asystole alarm detections. The first signal to satisfy the aforementioned selection criteria was then used to determine the alarm result. The feature used for asystole was the maximum RR-interval of the segment which, if above the specified threshold and tolerance, triggered an alarm or otherwise, suppressed it. An alarm on the selected sensor resulted in the final decision being set to true alarm.

Extreme *bradycardia (EBR)* was defined as five continuous beat intervals greater than 1.5 seconds [33]. We detected extreme bradycardia by processing the estimated minimum heart beats and identifying five or more consecutive beats with intervals exceeding 1.5 seconds. Two sample ECG II signals with extreme bradycardia alarm labels (true and false) from the challenge dataset are shown in Figure 4.2. The pulsatile signals were exploited for EBR alarm recognition and the minimum heart rate of the available ABP and PPG signals were measured. Five or more consecutive beats with intervals exceeding 1.5 seconds were identified as the features called “Low HR”. Firstly, the SQI of the pulsatile signal was assessed. The SQI threshold for pulsatile signals set to 0.9. If the SQI of the signal satisfied the threshold, then the alarm segment was checked if it contained beats meeting the above criteria. If the feature was over the threshold with the tolerance for either pulsatile signals of ABP or PPG, the alarm was set to true. Otherwise, the alarm was assigned to false.

Extreme tachycardia (ETC) was defined as a heart rate elevation of more than 140 beats per minute for 17 consecutive beats [33]. Two sample ECG II signals with extreme tachycardia alarm labels (true and false) from the challenge dataset are shown in Figure 4.3. The algorithm begins with processing the ECG II signal, followed by ECG aVr and the pulsatile signals, in the same order as that for asystole detection. The last feature of the ECG SQI which was the standard deviation of the segment was omitted in the SQI evaluation for tachycardia alarm detection. Instead, a minimum number of beats defined for tachycardia served as an additional criterion for signal selection. This threshold was set to 11, which was chosen based on an iterative process, varying the threshold and adjusting according to the tachycardia detection performance on the training set. If ECG SQI reported a high

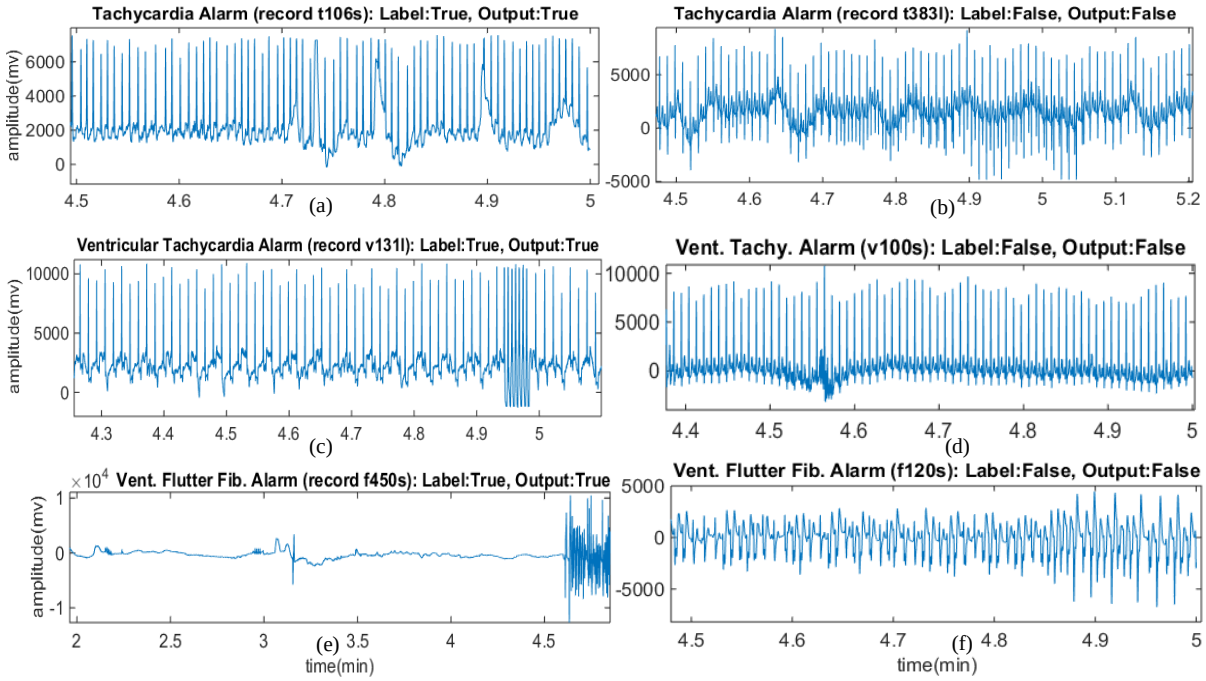

Figure 4.3. Sample ECG II signals from the Computing in Cardiology challenge dataset. Records with of arrhythmia alarms labels of (a) true tachycardia alarm label and predicted as true alarm by our algorithm, (b) false tachycardia alarm label and predicted as false alarm, (c) true ventricular tachycardia alarm label, predicted as true alarm, (d) false ventricular tachycardia label and predicted as false alarm, (e) true ventricular flutter fibrillation alarm label, predicted as true alarm, (f) false ventricular flutter fibrillation label and predicted as false alarm.

quality signal and there was a sufficient number of beats detected in the segment, the signal was utilised for the next phase of tachycardia detection. Tachycardia minimum threshold was set to 110 bpm with a tolerance of 10 bpm. For the ABP signal, the SQI was compared to the threshold of 0.9 and the number of identified beats in the alarm segment was compared to the minimum acceptable beats for tachycardia detection. The heart rates from the selected signal were then able to trigger an alarm in two ways; the first was if the number of beats exceeded 30 for the acquired segment or secondly, if the number of beats above the tachycardia threshold and tolerance exceeded the minimum acceptable beats. If neither of these criteria were fulfilled, the alarm was suppressed.

Ventricular tachycardia (VTA) was defined as five or more ventricular beats with heart rate higher than 100 beats per minute [33]. Two sample ECG II signals with ventricular tachycardia alarm labels (true and false) from the challenge dataset are shown in Figure 4.3. Diagnosis of VTA was obtained by a template subtraction process using the raw ECG signals only. We did not use the pulsatile signals for VTA. Also, by removing the ECG SQI measures used in the other alarms from the process, the performance of false alarm detection was enhanced as VTA signals generally had poor SQI.

The first QRS complex in the series was taken as the reference template against which the subsequent waveforms were compared. A beat-to-beat sliding window was applied to the alarm segment to detect each QRS complex. The standard deviation (SD) and mean value of each QRS waveform were subsequently calculated and compared with the peak of the waveform. The complexes with peaks that did not lie within one SD of the mean were chosen for evaluation. Then, the mean value of each

complex as well as the mean of the template waveform was removed. The waveforms with a SD that did not lie within 0.6 of the overall SD of the segment were labelled as 'irregular' waveforms. This feature was labelled the "filter vector". If there were four or more irregular waveforms in the alarm segment, that is, the minimum threshold of 5 beats for VTA with a tolerance of 1 beat, the VTA alarm was set to true. Otherwise, it was labelled as a false alarm.

Ventricular flutter or fibrillation (VFB) was assumed to be fibrillatory, flutter, or oscillatory waveform for at least four seconds [33]. Two sample ECG II signals with ventricular flutter or fibrillation alarm labels (true and false) from the challenge dataset are shown in Figure 4.3. It is recognised as a difficult condition to detect using ECG signal [179], [180]. The comparisons of the studies in the literature showed the importance of threshold tuning and choosing the appropriate criteria [178]–[181], [224]. To detect VFB in this study, the ABP SQI was evaluated and compared to the threshold of 0.9. If SQI was above threshold, then the maximum heart rate in the alarm segment was compared to the VF threshold. The VFB threshold was set to 250 bpm with a tolerance of 10 bpm. If the maximum heart rate of alarm segment was greater than the VFB threshold with the tolerance, the VFB alarm was set to true. A similar algorithm was repeated for PPG signal. Either of the pulsatile signals satisfying the criteria resulted in an alarm being triggered.

As a final comment, we describe one signal processing step we tried and abandoned as it did not result in improvement in the scores for either the training or test set. The signal processing step attempted to boost the heart rate identification by multimodal signal integration. The algorithm examined the detected beats of the ECG signals. In case of low quality ECG signals or missing beats, it switched to pulsatile signals. In order to match the R peaks of the ECG with the pulse onsets of pulsatile signals, the delay between R peaks of ECG signals and pulse onset of pulsatile signals was measured. We adapted a fusion method proposed in the *PhysioNet/Computing in Cardiology Challenge 2014* by Johnston *et al*. [149]. The peaks of the available ECG signals and pulsatile signals in the alarm segment were checked. In the case that more than 90% of the R peaks were followed by the pulse onsets of the pulsatile signal, the delays between the peaks were measured. The average of the delays in the alarm segment was set to the delay for the whole segment containing the alarm. A default delay value of 200 ms was used for the segments which did not satisfy the criteria. Then, the R peaks and the corresponding pulse onset beats of the pulsatile signal were compared in a one second window through the whole alarm segment. The percentage of the R peaks matching the pulsatile onset beats in an interval of the corresponding delay between them was calculated. If the matching rate was above 90% then the signal quality was deemed acceptable. As our algorithm was not successful, further work is needed to improve the integration technique. Finding an optimum matching rate and adjusting the delay for the available signals can enhance the performance of the algorithm.

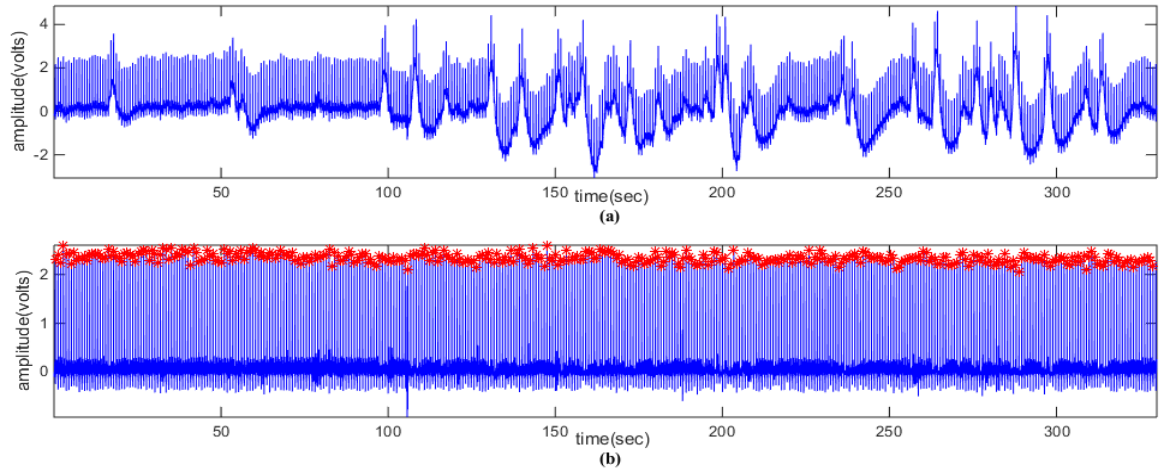

Figure 4.4. Sample result of applying interference removal to ECG signal (a64) and noise removal. (a) Raw ECG lead II with asystole as a false alarm. (b) The result of applying interference removal on the input ECG. Red stars are the R peaks detected by Hilbert QRS algorithm.

4.2. Results of application 1

The results of the algorithms developed for this application are demonstrated in this section. We commence by displaying the outcome of the artefact removal of the ECG recordings as well as the outcome of applying the Hilbert QRS detection algorithm. Then, the performance results of training set and test set from our final entry submission to the challenge are demonstrated. The performance measures reported for the training set include true positive (TP), false positive (FP), true negative (TN), false negative (FN), true positive rate (TPR), true negative rate (TNR) and score. The scoring was presented by the challenge organisers to calculate the percentage of alarms detected correctly. It weights the suppression of the true alarms five times higher than the acceptance of the false alarms. The score is measured as follows,

$$score = \frac{(TP + TN)}{[TP + TN + FP + (5 \times FN)]} \tag{4.1}$$

The performance measures of the hidden test set reported by the evaluation team of the challenge included three measures of TPR, TNR and score.

Table 4.1. The results of true positive rates, true negative rates, and scores of training set.

	TP	FP	FN	TN	TPR (%)	TNR(%)	Score(%)
Asystole:	0.164	0.057	0.016	0.762	91.11	93.04	87.11
Bradycardia:	0.517	0.247	0	0.236	100	48.86	75.3
Tachycardia:	0.936	0.043	0	0.021	100	32.81	95.7
VFB:	0.103	0.19	0	0.707	100	78.82	81.0
VTA:	0.246	0.361	0.015	0.378	94.25	51.15	58.87
Average:	0.393	0.18	0.006	0.421	98.50	70.05	79.49
Gross:	0.383	0.225	0.009	0.383	97.70	62.99	73.94

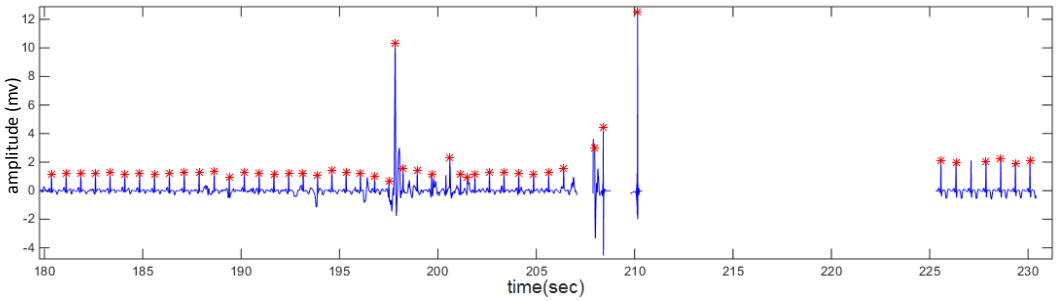

Figure 4.5. Result of the application of Hilbert QRS detector on the ECG lead-II signal after interference removal.

Next, the list of the extracted features from our algorithm incorporated in every arrhythmia alarm detection are demonstrated to identify which features were responsible in making the individual alarm detections. The final set of results reported in this section provides the proportion of each arrhythmia alarm detected by each signal of training data.

The first step was to detect and filter the artefacts from the raw ECG signals. The filtered signals were then processed to find the QRS complexes. The result of applying the interference removal algorithm on an ECG signal of the challenge training set is shown in Figure 4.4. The baseline wander noise is easily seen in Figure 4.4(a) of the raw ECG recording. The resulting signal after this interference removal is shown in Figure 4.4(b) which reveals that interference including the baseline wander was appropriately eliminated. By removing the unwanted interference from the ECG signals, we improved the likelihood of successful arrhythmia detection. Subsequent to interference removal and denoising the ECG signals, QRS detection was applied to the signals, the result of which is shown in Figure 4.4(b). It can be visually observed that the QRS detection algorithm is working well with a suitable outcome. It is important to note that a number of signals in the training set contained different artefacts as well as missing data. The missing data can distort the outcome of different QRS detection algorithms. An example of the outcome of the algorithms of this thesis on a noisy ECG signal with missed values from the training set is displayed in Figure 4.5. It shows that the QRS detection algorithm can identify the QRS complexes of a noisy signal with missed values. The outcome of the artefact removal and QRS detection algorithm was then utilised for arrhythmia alarm detection.

The results of train and test set are shown in Table 4.1 and Table 4.2 respectively. The results of the test set were reported by the challenge webpage [312] after applying our submitted entry to the hidden

Table 4.2. Results of final submission from test set.

	TPR	TNR	Score
Asystole	78%	93%	82.46%
Bradycardia	100%	52%	71.13%
Tachycardia	100%	80%	99.10%
VFB	100%	59%	65.52%
VTA	91%	55%	58.07%
Real-time	95%	65%	69.92%
Retrospective	98%	66%	74.03%

test set. We submitted six entries to the challenge with the results of our final submission shown in Table 4.1 and Table 4.2.

The highest scores of both training and test set obtained in tachycardia detection by our algorithm and were 96% for train and 99% for test set. It resulted in 100% TPR and 80% TNR for the hidden test set. It was followed by asystole which obtained a score of 87% for train set and a score of 82% for test set. For asystole, we obtained 78% of TPR and 93% of TNR. It can also be seen that our algorithm achieved 100% of TPR for three arrhythmias including bradycardia, tachycardia and VFB. The average score of train set was 79%. While for the test set, the real-time score achieved 69.9% and retrospective score reached 74% and placed among the top ten scores of the *PhysioNet/Computing in Cardiology Challenge 2015*. Our algorithm obtained 95% TPR for real-time and 98% TPR for retrospective schemes. It can also be observed that the performance results of our algorithm for train and test set are almost comparable, except for VFB detection which perhaps is due to the low number of the records with VFB alarms in the train set (less than 10 of the 750 recordings).

Table 4.3 shows a list of the features that contributed to individual arrhythmia alarm detection. It demonstrates which features were responsible in making the decision for individual arrhythmia alarm identification. The last feature of the table, 'Number over threshold', refers to the number of beats above the tachycardia threshold and tolerance which exceeded the minimum acceptable beats. The results of arrhythmia detection and their used features of Table 4.3 suggest that the drawback of the

Table 4.3. The features that were selected in the evaluation process for each alarm type.

Features[a]	Asystole	Bradycardia	Tachycardia	VFB	VTA
Number of ECGII beats	√		√		√
Max RR of ECGII	√		√		
ECGII SD	√				
Number of ECG aVr beats	√		√		√
Max RR of ECG aVr	√		√		
ECGaVr SD	√				
Number of ABP beats	√	√	√		
Max pulse intervals of ABP	√				
ABP SQI		√	√	√	
Low HR of ABP		√			
Max HR of ABP				√	
Number of PPG beats	√	√	√		
Max of RR PPG	√				
PPG SQI		√	√	√	
Low HR of PPG		√			
Max HR of PPG				√	
Length of filter vector					√
Number over threshold			√		

[a] The features were measured over the alarm segment and the detected beats and peaks in the segment.

Table 4.4. The use of each signal in the decision criteria for each arrhythmia in the training set.

Signals	Asystole	Bradycardia	Tachycardia	VFB	VTA
ECG II	75.4%	Not used	100%	Not used	88.6%
ECG aVr	1.6%	Not used	Not used	Not used	3.2%
ABP	3.4%	10.1%	Not used	22.4%	Not used
PPG	13.9%	13.5%	Not used	8.6%	Not used
Not suppressed[a]	5.7%	76.4%	0%	69.0%	8.2%

[a] Algorithm was not able to suppress the alarm using any of the four input signals.

proposed algorithm is the variety of features used. We obtained our best result with extreme tachycardia alarm detection which the results of this exploration at Table 4.3 showed to have the largest variety of features.

The contribution of each type of training data signal to arrhythmia alarm detection is shown in Table 4.4, which was identified after implementing and running the algorithm with the training set. It can be seen that multimodal signals benefit the arrhythmia recognition differently with various usage distributions. For instance, the table demonstrates that 75.4% of the asystole alarms were detected by ECG II signals and 13.9% of the asystole alarms were detected by PPG signals. Only 5.7% of the asystole alarms cannot be suppressed using any of the four input signals. Since we had a hierarchical or priority-based approach to selecting the signals to use (i.e., ECG was used firstly, then ABP followed by PPG), we did not necessarily use all of the signals to make the final decision. The results from investigating the usage of the signals supported the assumption of giving the highest priority to ECG signals for asystole detection. It revealed that only 5.7% of the asystole alarms were not suppressed, meaning that none of the four input signals can identify them. While 76.4% of the bradycardia alarms were not suppressed by input signals and none of the pulsatile signals which were used for bradycardia detection in the algorithm can diagnose it. Also, the ECG II distribution denotes that for only 11.4% of VTA recordings, QRS detection did not successfully identified the beats. We found that varying the threshold setting significantly affected false alarm detection. The results are further discussed in the following section.

4.3. Discussion

The final results obtained by our algorithm on the hidden test set was reported by the evaluation team of the *PhysioNet/Computing in Cardiology Challenge 2015* and contained the three measures of TPR, TNR and score (see section 4.2). Our result placed us among the top ten scores of the challenge. Our proposed system achieved the highest score in detecting tachycardia false alarms. Our best performing algorithm used multimodal signals, combined the information from ECG and pulsatile signals, extracted and evaluated a number of features of the signals for alarm identification. The results and the performance of the developed algorithms of this application are discussed in this section. Our

system detected false alarms in the following order: asystole, extreme bradycardia, extreme tachycardia, VTA and VFB.

4.3.1. Asystole

We first analysed the recordings that included the asystole alarms. For asystole detection, the ECG signals were investigated first and then the algorithm progressed to the pulsatile signals for processing (see Figure 4.1). The first signal to satisfy the selection criteria was used to determine the alarm result. The ECG SQI measures were not used in asystole detection, as the tests tended to knock out heart beats, which increased the likelihood of false asystole alarm detections. The results of the signal usage for the decision criteria (see Table 4.4) show that the asystole alarms were mainly detected by the ECG II signal (75.4% of the alarms for train set). It is also shown that by processing the four available signals for the asystole detection, 94.3% of the asystole alarms of the train set were suppressed (see Table 4.4). Thus, the distribution of the signal usage in Table 4.4 confirms the order of the selection criteria of our proposed algorithms (explained in section 4.1.9 and shown in Figure 4.1).

4.3.2. Extreme bradycardia

The ECG signals containing the bradycardia alarms were mostly noisy with a high rate of missed values (due to sensor disconnection and other artefacts). Thus, the QRS detection algorithm was unable to perform successfully on the bradycardia signals and distorted the corresponding features and worsened the alarm detection. Therefore, we removed the ECG signals from the signal processing implementation of bradycardia detection. The algorithm analysed the bradycardia records by processing the pulsatile signals (first ABP, followed by PPG signals).

4.3.3. Extreme tachycardia

Thirdly, the algorithm investigated the records containing the extreme tachycardia alarms. The algorithm followed the same order for using the signals as for asystole detection; it began with processing the ECG II signal, followed by ECG aVr and the pulsatile signals. For the ECG signal processing, both noise reduction and the signal quality index (SQI) evaluation were applied which improved the performance of the tachycardia detection. In addition, we refined the SQI tests for tachycardia records (see section 4.1.9). We removed the standard deviation test from the SQI evaluation and included another criterion for signal selection (a minimum number of beats defined for tachycardia). We chose the threshold for the selection criteria of the SQI evaluation of tachycardia signals based on an iterative process and adjusting the thresholds according to the tachycardia detection performance on the training set. This process further enhanced this alarm detection on the test set. Also, the algorithm processed the largest variety of features for tachycardia alarm detection

compared to the variety of features used for other alarms (see Table 4.3). Our proposed system achieved the highest score in detecting tachycardia false alarms on the test set with a score of 99.10%, a TPR of 100% and a TNR of 80%.

4.3.4. Ventricular tachycardia (VTA)

The VTA detection was carried out based on the features extracted from the raw ECG signals (ECG lead II, followed by ECG aVr), which were processed using template matching based on correct heart beat detection. The VTA signals exhibited behaviour similar to the noise, which our noise removal algorithms were designed to remove. Accordingly, we did not apply interference removal to the ECG signal for the VTA arrhythmia alarm detection. Also, by removing the ECG SQI measures used in the other alarms from the process, the performance of the false alarm detection was enhanced as VTA signals generally had poor SQI.

4.3.5. Ventricular flutter or fibrillation (VFB)

Finally, the VFB records were analysed for alarm detection using the pulsatile signals (ABP followed by the PPG signal). Similar to the bradycardia records, the QRS detection algorithm was unable to perform successfully on the ECG signals of the VFB records due to the noisy records, which distorted the QRS detections and the corresponding features. Thus, we removed the ECG signals from the processing algorithm and the extracted features from the pulsatile signals were evaluated for the alarm detection.

4.3.6. Overall system

The results (see Table 4.3) suggest that the drawback of the proposed algorithm for VFB and VTA is the low variety of features used, as opposed to the larger variety of features that was processed for extreme tachycardia alarm detection. As explained above, the noisy behaviour of these alarms on the ECG signals distorted the QRS detections and using the features extracted from the corrupted QRS detections reduced the performance. Thus, we removed the corresponding features from the processing. The use of more specialised noise removal, SQI evaluation and QRS detection algorithms could possibly help revising the QRS detection results and retrieving the ECG information for better feature extraction and thus enhancing the alarm detection. We note that the VTA alarm was reported as the most difficult alarm for detection among the entries at the *CinC Challenge 2015* [33].

We also found that varying the threshold setting of the SQI measures and tests for ECG signals and pulsatile signals significantly affected false alarm detection and further enhanced the tachycardia

alarm detection on the test set. We anticipate that model optimisation and further threshold tuning adapted to every arrhythmia alarm can enhance the scores.

We have obtained comparable results for arrhythmia alarm detection reported in the literature. A study by Clifford *et al.* in 2006 analysed the ABP and ECG signals to detect five life-threatening arrhythmia alarms (asystole, extreme bradycardia, extreme tachycardia, VTA and VFB) in the ICU [51]. They detected 25% false alarms from 89 arrhythmia alarms and reported low results for VTA and VFB false alarm detection. Their proposed method recognised a single VTA false alarm (6.25% false alarm rate) and no VFB/VTA false alarm detection [51]. In another study, Aboukhalil *et al.* used a single lead ECG signal simultaneously with ABP signals aiming to combine the information and improve the diagnosis [175]. Their false alarm (FA) suppression algorithm reported 59.7% of the false alarms. The FA reduction rate obtained by their algorithm for extreme tachycardia was 63.7%, for VFB/VTA it was 58.2% and for VTA it was 33.0%. It also obtained an FA reduction rate for asystole of 93.5% and for extreme bradycardia was an 81.0%. They achieved 0% true alarm (TA) reduction rates for every arrhythmia alarm, except for the ventricular tachycardia alarms, for which, the algorithm achieved 9.4% TA reduction rate.

Our best performing algorithm used multimodal signals, combining the information from ECG and pulsatile signals, and extracted and evaluated a number of features from these signals for alarm identification. Modification of the signal quality measures for different arrhythmias (rather than using a fixed SQI for every arrhythmia), by setting the threshold in an iterative performance evaluation, and considering various possible effects of each arrhythmia on the features from the signals enhanced the arrhythmia identification performance.

4.4. Summary

In this chapter, we described the algorithms developed in this thesis for the first application of reducing false arrhythmia alarms in the ICU. We first explained the details of the utilised database. Then, we proposed the signal processing methods applied to the ECG signals including baseline wander noise removal, RR-interval measurement, signal segmentation and ECG signal quality index. We then explained the signal processing approaches conducted for pulsatile signals (ABP and PPG signals). It was followed by describing the details of using the multimodal signal processing and the customised approaches for detecting the arrhythmia alarms. Ultimately, we demonstrated the results of the developed algorithms and the performance obtained by our presented system at the *CinC Challenge 2015*.

Our overall result on the hidden test set placed us among the top ten scores of the *PhysioNet/Computing in Cardiology Challenge 2015* with a retrospective score of 74.03%, a TPR of 98% and a TNR of 66% and a real-time score of 69.92%, a TPR of 95% and a TNR of 55%.

Our results showed that better detection was achieved for tachycardia and asystole, followed by bradycardia when more features were utilised for the algorithm. Our algorithm obtained the highest result for extreme tachycardia alarm detection in the *CinC Challenge 2015*.

Chapter 5

Application 2

5. Application 2: Sleep apnoea diagnosis

In the previous chapter, the developed algorithms for application 1 of this thesis were explained in detail and the results of applying the algorithms to the database were demonstrated and discussed. In this chapter, the algorithms developed as a part of the second application (sleep apnoea diagnosis) are illustrated. This application aims to provide automated screening of sleep apnoea (SA) with the main focus on the ECG signal processing and evaluate the results using the chest respiratory effort signals with the developed algorithms.

In the former chapters, the clinical and methodology background of sleep apnoea detection were explained including the aetiology factors involved in sleep apnoea and the corresponding characteristics as well as the diagnostic sensors, different feature extraction and machine learning methods. As described in chapter 3, a measure of the respiratory effort during a sleep study is an important contributor to the diagnosis of sleep apnoea. A common way of measuring respiratory effort is using bands with stretch sensors placed around the chest and/or abdomen, as explained in section 2.2.4. An alternative, and convenient method from the patient's perspective, is via the EDR signal (see section 3.5.2) which provides an estimate of the respiratory effort at each heartbeat using ECG sensors. As discussed in sections 2.2.1 and 2.3.2, using ECG as an SA diagnosis tool is attractive as it provides a low-cost system with minimal disturbance on sleep and the diagnostic test can be performed at home. In addition, using the ECG signals, both HRV and EDR features can be extracted which the combination of the features can boost the performance of sleep apnoea diagnosis. Thus, if the EDR approach works, both cardiovascular information and respiratory information are obtained from one sensor.

This chapter commences with an explanation of the recordings and characteristics of the two utilised databases (see section 5.1.1). The methods applied to the chest respiratory effort signal and the different resampling schemes are described in section 5.1.2. Following the chest respiratory signal, the system developed using ECG recordings is explained in section 5.1.3. I first illustrate the methods of estimating ECG derived respiration (EDR) including the QRS area method, standard principal component analysis (PCA) and kernel PCA. Then, I describe the issues involved in applying PCA method to the entire overnight ECG recordings, our solutions and novel techniques of segmented PCA and approximated PCA. It is followed by a description of the interval-based power spectral density (PSD) feature measurement adapted for this application. Ultimately, the results of the proposed algorithms are obtained in three phases and demonstrated for each phase separately in section 5.2. In

section 5.3, I evaluate the performance results and discuss the advantages and disadvantages of the proposed signal processing methods in three phases separately in sections 5.3.1, 5.3.2 and 5.3.3.

5.1. Methodology of application 2

In this chapter, the developed algorithms of this thesis for SA diagnosis are described, with the block diagram of the proposed system for this application displayed in Figure 5.1. It shows the main blocks of the system using ECG signals comprised of preprocessing (noise removal and QRS detection), biosignal measurement (EDR and HRV signals), feature extraction (PSD and CPC), epoch classification and AHI estimation. The block diagram also shows the modules for using respiratory inductance plethysmography (RIP) for apnoea classification in order to use for evaluating the respiratory information of ECG signals. As shown in the block diagram, the RIP signal is used in three schemes; the full signal and two resampled signals (HR and uniformly sampled). Then, the features are extracted from every signal and applied to classifiers for apnoea detection.

The results of these algorithms, reported in section 5.2, were obtained in three main phases with the outline displayed in Table 5.1.

- Phase I: EDR methods and proposed solutions for EDR estimation of overnight recordings using the PCA method,
- Phase II: EDR evaluation and selection of the highest performing EDR method and classifier; and
- Phase III: optimising sleep apnoea detection and combining the ECG-based features (phase III) (as shown in Table 5.1).

Phase I involves estimation of EDR signal using different methods. First, the EDR signal was extracted from an hour of ECG recording through different algorithms (QRS amplitude, the standard principal component analysis (PCA) and kernel PCA). The ELM classifier was utilised in this phase for apnoea detection and different hyperparameters were evaluated. PCA method obtained the highest

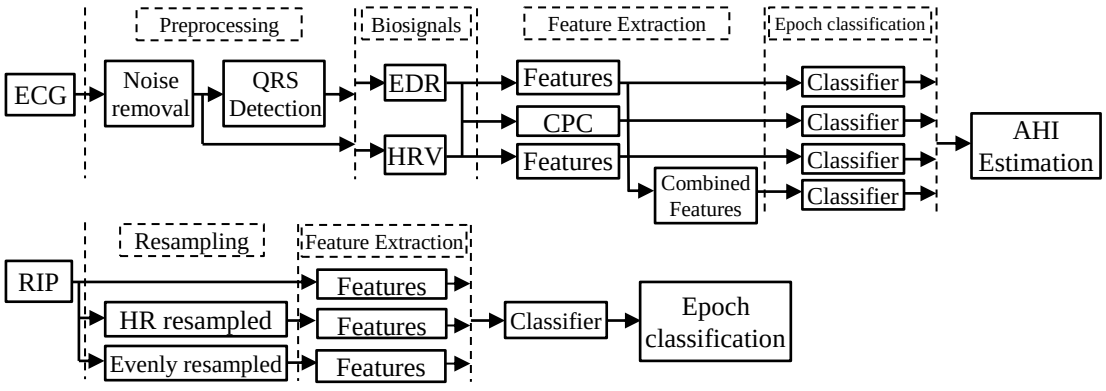

Figure 5.1. The block diagram of the proposed system for SDB diagnosis.

performance of apnoea detection, reported in section 5.2.1. Thus, we extended the work and presented two approaches to apply PCA method to overnight ECG recordings for EDR estimation in order to precisely evaluate the apnoea detection. The approaches run successfully on a standard PC and have low memory requirements. In the first approach, the overnight ECG signals were segmented and PCA applied to each 30 minutes segment. In the second approach, an approximation PCA method [300] was applied to the overnight signal, as described in detail in section 5.1.3 and the results are reported in section 5.2.

In phase II, the respiratory information of EDR signals are evaluated in comparison with chest respiratory effort signal in two ways (see section 5.2.2); first, the sample-based correlation of three automated algorithms measuring the EDR signal (QRS area, segmented PCA and approximated PCA) was measured against the chest respiratory effort signal. Second, a side-by-side comparison of the discrimination information was performed for identifying epochs of sleep apnoea contained in the chest respiratory effort signals and the EDR signals. That is, one-minute epochs were classified as being apneic or normal using three EDR and three chest respiratory effort signals (full signal, HR sampled and uniformly sampled respiratory signals) using identical respiratory-based features. The methods were evaluated on simultaneously recorded chest band respiratory effort signals and ECG signals extracted from overnight PSG data of two databases (*MIT PhysioNet Apnea-ECG* database and *St. Vincent's University Hospital* database) using three machine learning techniques (LDA, ELM and SVM). The highest performing EDR signal is chosen according to the results, reported in section 5.2.2. The performance was measured using leave-one-record-out cross-validation, meaning that, in every iteration, one record was set as the validation set and the remaining records were used as the train set, with an illustration shown in Figure 3.11, section 3.8, and the results shown in section 5.2.2.

Table 5.1. Outline of the steps and expected outcomes of the three phases of the proposed algorithms of application 2.

Phases		**Steps**	**Outcomes**
I	Extending EDR methods to overnight recordings	• 60 min data: QRS area, PCA and kernel PCA • Overnight recordings: seg. and appr. PCA • ELM classifier: fan-out (1-50)	Advantages and disadvantages of EDR methods and solutions, and evaluate the classifier hyperparameters
II	Choosing an EDR method and a classifier	• Sample-based correlation • Apnoea detection - On 2 databases - Using 3 EDR and 3 Resp. signals - On 3 classifiers (LDA, ELM, SVM)	Recommend the highest performing EDR estimation method and classifier
III	Combining EDR with other ECG based features	• apnoea detection: - HRV+EDR+CPC features - Optimisation techniques • AHI estimation and subject-based apnoea detection	Final system performance

Seg.: segmented, Appr.: approximated

In phase III (section 5.2.3), we applied different schemes to optimise the sleep apnoea detection. We took the highest performing EDR method from the previous phase and supplemented the feature set utilising heart rate variability (HRV) and cardiopulmonary-coupling (CPC) features. We applied temporal optimisation methods including overlapping one-minute segments by 30 seconds and averaging the features of adjacent epochs. Then, the performance of the developed algorithm was evaluated in three ways; one-minute epoch apnoea classification, AHI estimation and subject-based apnoea detection (see section 5.2.3). The final system performance including the combined features and applying optimisation methods is reported in section 5.2.3. We commence with explaining the details of the two utilised databases as follows.

5.1.1. Databases

The performance of our algorithms was evaluated on two open-access datasets which consist of signals extracted from the standard PSG from overnight sleep studies. The first dataset is the *MIT PhysioNet Apnea-ECG* dataset proposed for *Computing in Cardiology 2000 Challenge* which was captured from standard sleep laboratory signal recordings [191], [307]. While the full dataset contains 70 overnight ECG signals recorded using a modified lead V2 electrode setup, we used 35 recordings of the train set.

The signals of the 35 recordings were recorded from 32 subjects (25 male and 7 females) with an average age of 33 years (between 27 to 63 years of age, BMI between 20.3 and 42.1 with weights between 53 and 135 kg and AHI of 0 to 93.5). The length of each overnight recorded signal ranged between 455 and 529 minutes [301]. The digitised single channel of modified lead V2 ECG signals were recorded from healthy subjects and OSA patients with 16-bit resolution. Both ECG signals and chest respiratory effort signals were recorded at a sampling rate of 100 Hz. The training data of 35 ECG signals were utilised which were accompanied by QRS annotations and minute-by-minute apnoea annotations by respiratory experts with each epoch labeled as “apnoea” or “normal” produced by human experts using simultaneously recorded respiratory signals [191], [307]. The database also provides the QRS complexes onset beats which were identified using Englese and Zeelenberg algorithm [221], which was explained in section 3.4.

Eight recordings of the data contained chest and abdominal respiratory effort signals collected by inductance plethysmography and were acquired from 7 males and 1 female (aged 31-54, weight of 63 to 120 kg, AHI 0-77.9 events/hour).

The second database utilised in this thesis was the *St. Vincent’s University Hospital, University College Dublin Sleep Apnea* database collected from patients with suspected OSA, central sleep apnoea or snoring [265]. It provides 25 overnight PSGs containing ECG recordings (modified lead V2) and thoracic and abdominal respiratory effort signals (uncalibrated inductance plethysmography).

The signals were acquired from 21 males and 4 females (aged 28-68 years, AHI 1.7-90.9 events/hour, and BMI 25.1-42.5 kg/m^2). The ECG signals were sampled at 128 Hz, and the chest respiratory effort signals were sampled at 8 Hz. An expert annotated the onset times and durations of sleep-disordered breathing events including obstructive, central, and mixed sleep apnoea, as well as hypopnea and periodic breathing events. To be consistent with the *MIT PhysioNet Apnea-ECG* database, we converted the annotations to one-minute epochs labeled as apnoea and normal following the mapping method of [302]. We note that periodic breathing episodes were labeled as normal, since the aim of the study is to detect sleep apnoea including OSA and hypopnoea events.

5.1.2. Chest respiratory effort signal

An indirect method of monitoring respiration is using movement in thorax or abdomen by which the disturbance on sleep and normal breathing reduces, as discussed in section 2.2 [146]. Accordingly, chest respiratory effort signal recorded by inductance plethysmogram was used for the second phase of this study and provided a benchmark for the performance of EDR information for SA detection.

The respiratory signals of the datasets comprise of chest and abdominal respiratory signals. The chest respiratory signals were chosen in this thesis as they are most closely related to the modulated EDR signals recorded by ECG electrodes placed on the chest.

Due to the fact that the EDR signals are measured and sampled at the QRS detection beats (see section 3.5.2), an objective of this thesis was to measure the impact of different sampling schemes on the respiratory effort signal and develop a matching condition by resampling the chest respiratory effort signals. Thus, the chest respiratory effort signal from the two datasets was used for sleep apnoea classification in three schemes;

1. First, the full overnight chest respiratory effort signals of both datasets were used for feature extraction. The utilised chest respiratory effort signals of the *MIT PhysioNet Apnea-ECG* dataset were originally sampled at 100 Hz and the respiratory effort signals provided with the *St. Vincent's* dataset were sampled at 8 Hz. For this scheme, we used the recordings in their raw form (see section 5.2.2).
2. Second, the HR sampled respiratory signals were estimated, that is, the overnight respiratory effort signals were resampled at the heart rate using the QRS onset beats of the input ECG signals. By applying this resampling process, the respiratory effort signal and the EDR signals were sampled in the same way. For the *MIT PhysioNet Apnea-ECG* dataset, these QRS onset beats were provided by the dataset and for the *St. Vincent's* dataset, they were detected by applying Hilbert transform-based QRS detection algorithm, (see section 3.4). Through this approach, the sampling rate of the respiratory effort signals were reduced to the heart rate (HR), meaning that only those samples of respiratory signals containing information of the

heart rate variability were collected for apnoea recognition. Therefore, we expected that both respiratory reactions and heart rate variations resulting from apnoea events will be captured. This signal was used for analysis in phase II (see section 5.2.2).

3. Next, a uniform resampling scheme was applied to the respiratory signals with a frequency identical to the HR in each one-minute epoch (uniformly resampled respiratory signal). Meaning that, the HR for each one-minute epoch was measured using the number of QRS complexes in that one-minute epoch. Then, each one minute epoch of the chest respiratory effort signal was resampled with a sampling rate equal to the HR measured over that epoch with uniform intervals. Thus, the resulting samples are not placed on the QRS detection beats (in contrast to the previous resampling scheme). Therefore, comparing the results with the results of the previous scheme will explore the impact of sampling the respiratory signal at the average local heart rate but will ignore the uneven sampling caused by using instantaneous heart beat sampling (see section 5.2.2).

We aimed to evaluate the influence of heart rate sampling occurring in EDR signals by heart rate sampling of the chest respiratory effort signal. Also we aimed to answer the question that the different results of the EDR signals compared to the respiratory effort signal is caused by the unevenly sampling rate of the EDR signals or a result of the lower sampling rate of the EDR signals. These respiratory effort signals were used in phase II to evaluate the respiratory information of EDR signals in two ways; firstly, a sample-based correlation between respiratory signals and EDR methods assessed by Pearson linear correlation coefficient (CC) provided the sample-by-sample comparison. Secondly, sleep apnoea classification of the minute-by-minute segments of the ECG-based respiratory signals and the chest respiration based signals were performed. After segmenting the signals into one-minute epochs, identical features were extracted from each epoch and the matrix of features was given to the machine learning techniques. It is described in phase II, where the performance results of the EDR approaches for SA detection were evaluated (see section 5.2.2).

5.1.3. ECG system

In this section, we explain the signal processing methods applied to the ECG signals in order to capture the required respiratory information for SA detection, followed by comparing the respiratory information of the EDR with the chest respiratory signals and the process of optimising our developed SA detection system.

The EDR signals which are the main biosignals captured from ECG recordings for SA detection purposes, as defined in section 3.5.2, and the different algorithms for estimating the EDR signals are described. In section 5.2.3, we describe how to optimise the system and combine the EDR feature set with further biosignals and features (RR-intervals and CPC features).

As the first step toward extracting respiratory information from ECG signals, we explain our algorithms of ECG signal preprocessing including the artefact removal and QRS detection. Then, different methods used for EDR estimation are explained including QRS area, PCA, and kernel PCA. The issues involved in estimating the EDR signal of an overnight recording using the PCA method are described and our two developed algorithms to solve the issues are explained, including segmented PCA and approximated PCA.

EDR estimation

Before measuring the EDR signals through either method, two preprocessing steps were applied to the ECG signal to remove artefact interference and identify the QRS complexes.

First, interference removal was implemented to eliminate the baseline wander noise distorting the low frequency component of the ECG signals [246] which can affect and alter the features of ECG signal and their clinical translation useful for SA recognition. The baseline wander noise was removed by applying two median filters to the ECG signal [71]. The first median filter had a width of 200 ms which removed the QRS complexes and P waves from the signal. The second median filter had a width of 600 ms and was applied to the PQRS-free signal (output of the first stage) and removed the T waves. The output from this filter was a signal that contained the baseline wander only. Finally, the output of the second median filter was subtracted from the unfiltered ECG signal to obtain the baseline wander-free ECG signal. Then, the QRS complexes were identified as follows.

The *MIT PhysioNet Apnea-ECG* database provided the QRS onset points using the QRS-complex detection technique by Englese and Zeelenberg (see section 3.4) and we utilised these beats in our analysis. We required a reliable QRS detection algorithm for the *St. Vincent's Sleep Apnea* database, as such we used an algorithm based on the Hilbert transform [263] to identify the R peaks of the QRS complex; previous studies demonstrated a reliable method with good noise tolerance [264], [265], as described in section 3.4. The result of applying the Hilbert QRS detection algorithm on a sample recording is shown in section 5.2.2 (Figure 5.14). Following the preprocessing steps, the clean ECG signal and the QRS detection beats were used for EDR estimation.

A number of different strategies were used to capture EDR [157], [234], [236], [238]. Some of the early methods used amplitude modulation of ECG wave, such as R wave amplitude, RS amplitude, QRS complex area, and R wave area [234], [235]. The characteristics of ECG signal used for some of the EDR methods were demonstrated in Figure 3.4 , such as R wave amplitude (R_{ampl}), RR interval (R_{int}) and R wave area (the shaded area) [235]. Amplitude-based EDR methods were reported as competent tools for diagnosis of SDB [148], [266], [267]. Thus, a common approach of QRS area EDR was first used in this thesis as a benchmark, while a novel method of PCA application for EDR estimation was also investigated in this project. Two novel algorithms were proposed in this thesis to

resolve the computational limitations of PCA application on lengthy overnight ECG recordings for deriving EDR signal which are described in the remainder of this section.

As described in section 3.5.2, the temporal pattern of breathing can be extracted as a surrogate signal modulated on the ECG signal [70]. In this thesis, two main techniques were utilised to estimate the EDR signals. The first technique was the QRS complex area method [71], which as it had been previously used for apnoea detection from the ECG signal, was used as the reference method. Then, we estimated the EDR signal using the PCA method, as well as kernel PCA as a nonlinear approach in phase I. The objective of PCA is to reduce the signal dimensions. It is implemented based on the principal components, by computing eigenvectors of the variance of the features [313]. In this study, QRS complexes were chosen as the feature for PCA method; thus, the PCA algorithm was applied to QRS complexes in order to capture the temporal variation of breathing modulated on the ECG signal which causes alteration in the QRS complexes. After explaining the PCA method and kernel PCA for EDR measurement, we explain the computational issues involved with EDR estimation of overnight recordings using PCA method for this application. Then, we describe our two solutions for the issues by developing algorithms of segmented PCA and approximated PCA.

The results of the developed algorithms of the EDR methods as well as comparing the respiratory information of the EDR signals against the chest respiratory efforts signals are demonstrated in sections 5.2.1 and 5.2.2.

1) QRS area EDR

A common approach is to estimate the respiration from the ECG signal by calculating the area under each QRS complex, with the area varying in unison with the breathing cycle [157], [235]. The EDR signal can be estimated from the baseline free ECG signal by calculating the area under the QRS complex measured in a window of 100 ms, as shown in Figure 5.2 [71]. In fact, the window starts at the QRS onset point which might be different from the output of some QRS detection algorithms. For example, the QRS detection using the Englese and Zeelenberg algorithm applied on the *PhysioNet Apnea-ECG* database provides the QRS onset beats, thus, the window simply starts at the output of the QRS detection algorithm [148], [221], [233]. While, applying the Hilbert QRS detection to the *St. Vincent's University Hospital/University College Dublin Sleep Apnea* Database provides R-peaks, the window should be surrounding the output of the QRS detection algorithm [263], [264], [314], [269]. Ultimately, the area under each QRS complex was assigned to each QRS beat as the EDR signal for that beat (see Figure 5.2). This method was used in this thesis as the baseline EDR method and we compared the performance of the proposed PCA algorithms against this method. The results of the approach will be demonstrated in section 5.2.

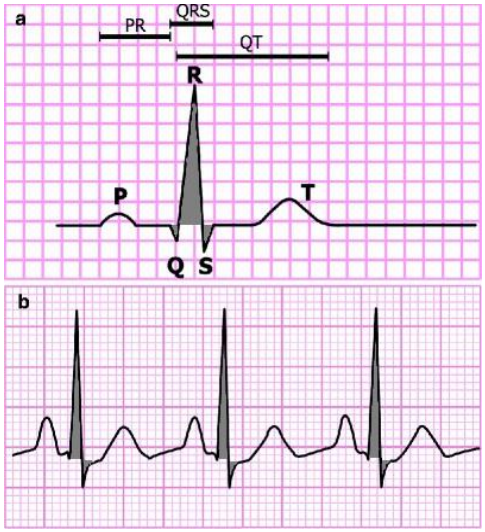

Figure 5.2. (a) Demonstration of a single PQRST ECG complex including the QRS interval. The shaded area displays the area under QRS complex used for measuring the QRS area EDR signal. (b) An excerpt of an ECG signal showing the normal sinus rhythm with rate of about 80 bpm. The shaded area under every QRS complex is assigned to the EDR signal for that beat. (modified on Figure 11 from [357])

2) Principal component analysis (PCA)

PCA is an orthogonal linear transformation of a multivariate signal that provides a useful tool for decreasing the dimensionality of data while retaining much of the signal variance. It finds the sequence of orthogonal directions in which the data has the highest variance (or spread). The direction values for the data are known as the principal components (PCs) [313]. It has been shown that PCA can represent beat-to-beat variations in ECG features including R-peaks and QRS amplitude [70]. Thus, by detecting variation of the correlation between the signal features, the EDR signal is recognised as a modulatory signal altering the ECG beats [70]. This algorithm can be applied to any ECG feature. In this thesis, the QRS complex was chosen in order to be consistent with other EDR measurement methods to enable a reliable comparison. The PCA algorithm is described in the following section with the block diagram of EDR estimation using PCA method shown in Figure 5.3.

First, a matrix of centred QRS complexes was built by applying a sliding window to the ECG signals in order to partition the signal into consecutive QRS complexes [70]. The length of the window was chosen in a way to cover the whole QRS complex. For the *MIT PhysioNet Apnea-ECG* database, the length of the window was set to 250 ms, m = 25 samples × 100 Hz. As the QRS onset beats were provided with this dataset, the window ran from the QRS onset -75 ms to QRS onset +175 ms. For the *St. Vincent's Sleep Apnea* database which the R peaks of the QRS complex were identified using Hilbert algorithm, a window of 120 ms, m = 15 samples × 128 Hz, was implemented around the R peak to extract QRS complexes. Therefore, if there are *n* QRS complexes, *n* windows covering each QRS complex will be applied.

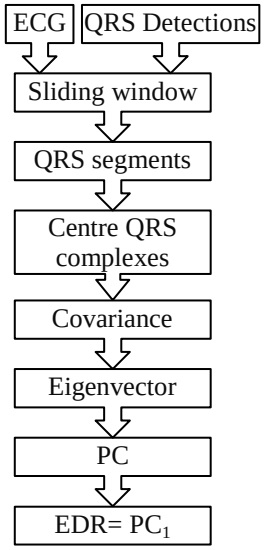

Figure 5.3. Block diagram of EDR estimation using PCA method.

Next, the mean of the QRS complexes was subtracted from each sample and the complexes were centred in a $m \times n$ matrix, as shown in Figure 5.5, where *m* is the length of the window to extract each QRS complex and *n* is the number of QRS complexes or heart rate over the ECG recording [73].

$$\mathbf{X} = [\mathbf{x}_1, \mathbf{x}_2, \dots, \mathbf{x}_n] = [(QRS_1 - mean(QRS_1)), (QRS_2 - mean(QRS_2)), \dots, (QRS_n - mean(QRS_n))]_{m \times n} \quad (5.1)$$

Then, the covariance of the centred matrix **X** was measured resulting in a $n \times n$ matrix:

$$\mathrm{C} = \frac{1}{\mathrm{m}-1}\sum_{\mathrm{i}=1}^{\mathrm{m}} \mathbf{x}_\mathrm{i}{}^{\mathrm{T}}\mathbf{x}_\mathrm{i} \quad (5.2)$$

Finally, the eigenvectors, α_j, and eigenvalues, λ_j, were computed using covariance, *C*, and principal components, *PC*, were obtained [70]:

$$\mathbf{C}\boldsymbol{\alpha}_\mathrm{j} = \lambda_\mathrm{j}\boldsymbol{\alpha}_\mathrm{j}\ , \quad j = 1,2,\dots,n \quad (5.3)$$

$$\mathbf{PC}_\mathrm{j} = \boldsymbol{\alpha}_\mathrm{j}\mathbf{x}\ , \quad j = 1,2,\dots,n \quad (5.4)$$

It should be noted that matrix **C** has *m* non-zero eigenvalues with the remaining eigenvalues equal to zero. The principal components are linearly transformed from the signal beats by transformation coefficients of eigenvectors which represent the EDR signal [70]. There is a significant correlation between the ECG signal beats and the large variation of the EDR signal, with the first principal component being the most sensitive to respiration. In fact, a "typical" beat morphology of the QRS complexes is obtained by using the first PC to reconstruct the signal. The scaling required of the typical beat to best match each beat is contained in the coefficients of the first principal component. Thus, the first PC was chosen as the EDR signal [70].

$$EDR = PC_C^1 \quad (5.5)$$

An example of a sequence of nine consecutive QRS complexes of a sample ECG recording from the PhysioNet database and the corresponding reconstructions using the first PC is demonstrated in Figure

5.4. As shown, the red curve shows the reconstruction of the QRS complex using PC^1, which represents the typical QRS complex with an unvarying morphology across the signal for all of the QRS complexes. What changes across different QRS complexes (Figure 5.4(a)-(i)) is the amplitude of this typical morphology, which represents the modulatory respiration or the EDR signal estimation. This figure confirms the choice of the first PC as the EDR signal.

By this approach, the covariance matrix resulted in a square matrix of $n \times n$ where n is the number of QRS complexes of the ECG recording [73]. The published studies of PCA methods show good results for estimating respiratory signals but, due to the need to store a large covariance matrix, the method is limited to processing signals of less than an hour using standard desktop PCs. For apnoea detection studies, we typically require analysis of overnight signals of about eight hours duration and hence published PCA methods are not suitable [70], [73]. We proposed two solutions for this problem which

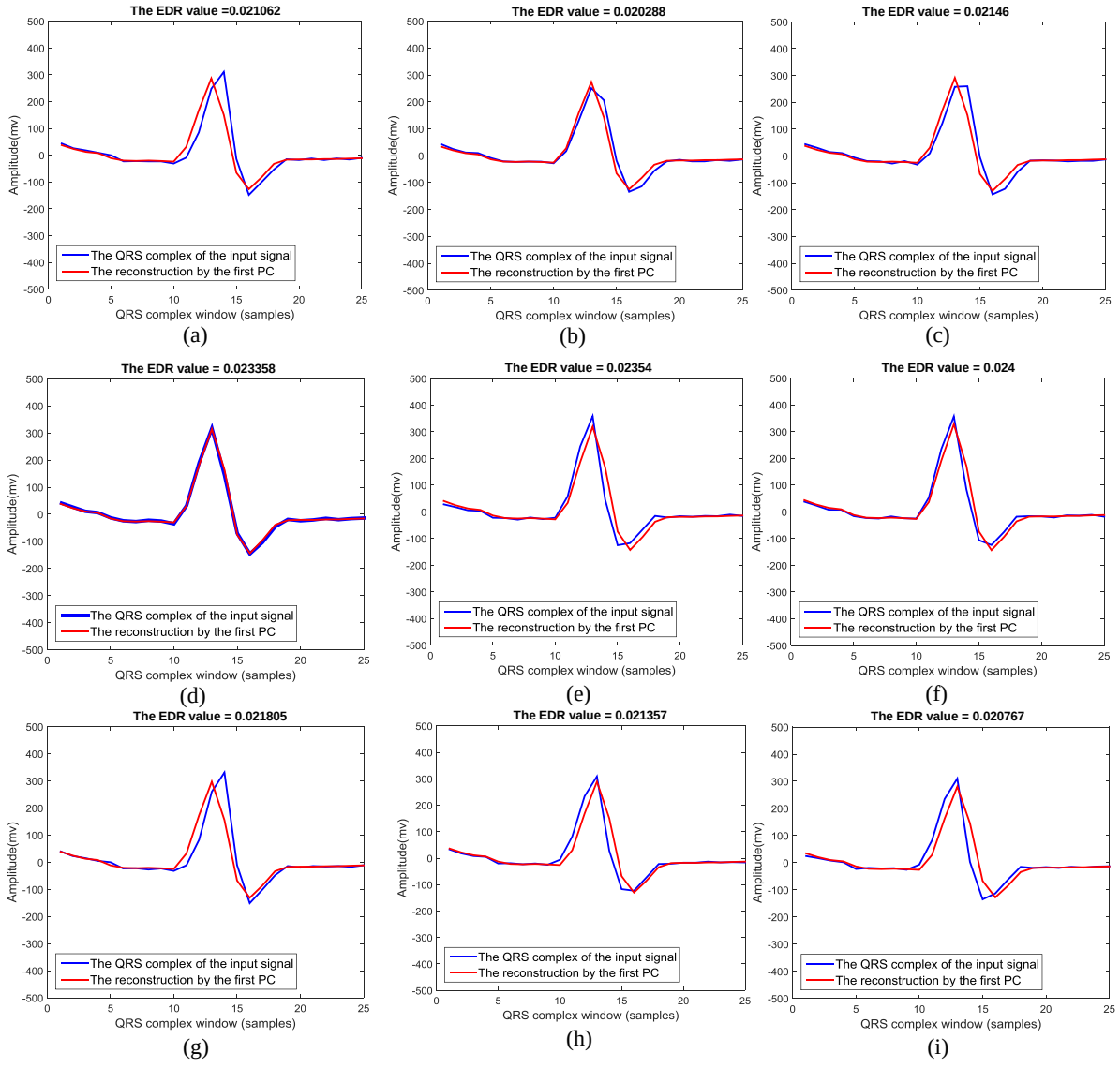

Figure 5.4. A series of nine consecutive QRS complexes and the reconstruction of the corresponding QRS complex using the first PC of a sample ECG recording from the PhysioNet dataset.

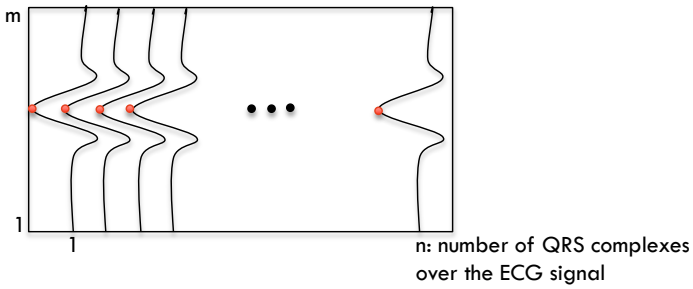

Figure 5.5. Centred QRS complexes used to develop the feature matrix (reproduced from[73]). m is the length of the window to extract each QRS complex and n is the number of QRS complexes or the heart rate over the ECG recording.

are described later in this section (following the kernel PCA method description).

3) Kernel PCA

In case of nonlinear patterns existing in the dataset, linear PCA may not recognise them and nonlinear kernel PCA can provide more information [315]. In kernel PCA, a nonlinear function, $\Phi(x_j)$, is applied to the dataset and PCA is applied to the mapped space, $\Phi(x_j)$. The covariance matrix becomes [313],

$$\bar{C} = \frac{1}{n}\sum_{j=1}^{n} \Phi(x_j)\Phi(x_j)^T \quad (5.6)$$

Then, the eigenvectors and eigenvalues are computed,

$$\lambda V = \bar{C}V \ , \qquad V = \sum_{i=1}^{n} \alpha_i \, \Phi(x_i) \quad (5.7)$$

In order to prevent mapping difficulties in high dimensional datasets and measuring the dot products of $\Phi(x_j)$, the nonlinear function is replaced by a Mercer kernel such as Gaussian kernels and polynomial kernels [315]. The Gaussian kernel was used in this thesis, which is a symmetric $n \times n$ kernel matrix, *K*,

$$K_{ij} = \left(\Phi(x_i).\Phi(x_j)\right) \quad (5.8)$$

$$K(x_i, x_j) = exp\left(-\frac{\|x_i - x_j\|^2}{2\sigma^2}\right) \quad (5.9)$$

The Gaussian kernel was chosen for the radial basis function (RBF) of this application as it has been shown to provide the suitable fitting for biological signals and produce the best result for EDR estimation [72], [73]. Using this kernel, both the linear and nonlinear interactions between respiration and the morphology of the QRS complexes are considered in the implementation [72].

Summarising the steps of applying kernel PCA [313];

1. First, the K_{ij} matrix was computed. The variance of the Gaussian kernel, σ^2, was chosen as $\sigma^2 = m.mean(var(X))$ [73], with m being the window length which extracted the QRS complexes and *X* being the matrix of centred QRS complexes.

2. Next, the eigenvalue problem was solved by diagonalising *K* [73],[313],

$$m\lambda K\alpha = K^2\alpha \quad , \quad m\lambda\alpha = K\alpha \tag{5.10}$$

3. Then, the eigenvalues of *K*, λ_i, were ordered in terms of the magnitude and the eigenvectors, α^i, were normalised which was satisfied by centring the QRS complexes.
4. The first principal component was assigned to the EDR signal.

This method was applied in the first attempt of phase I of this application to an hour of the data which the results are shown in section 5.2.1 and are compared to the other methods of EDR estimation.

The computation and storage of the covariance matrix during PCA grows with square of the length of the ECG recording. In the first step of this thesis which was published [63], we successfully applied PCA to an hour of the ECG signals. In order to precisely recognise sleep apnoea by EDR signals, we require applying PCA to overnight ECG recordings with average length of 8 hours. To apply the PCA to the entire ECG signal with average length of 8 hours at 60 beats per minute, storage of about 7GB is required for double precision which surpasses the standard memory of 8GB of PCs. This proved to be beyond the capabilities of a standard desktop PC and thus we extended the work and presented two solutions. In the first solution, the overnight ECG signals were segmented and PCA was applied to each segment. In the second solution, an approximation PCA method [316] was applied to the overnight signal. Both methods can run successfully on a standard PC. The methods are described in detail in the remainder of this section and the results are reported in section 5.2.

4) Segmented PCA EDR

The segmented PCA algorithm is outlined as follows. The inputs to the PCA algorithms are the entire overnight ECG signals which were first preprocessed. The input signals were partitioned into 30 minutes segments and the PCA algorithm described earlier in this section was applied to every 30

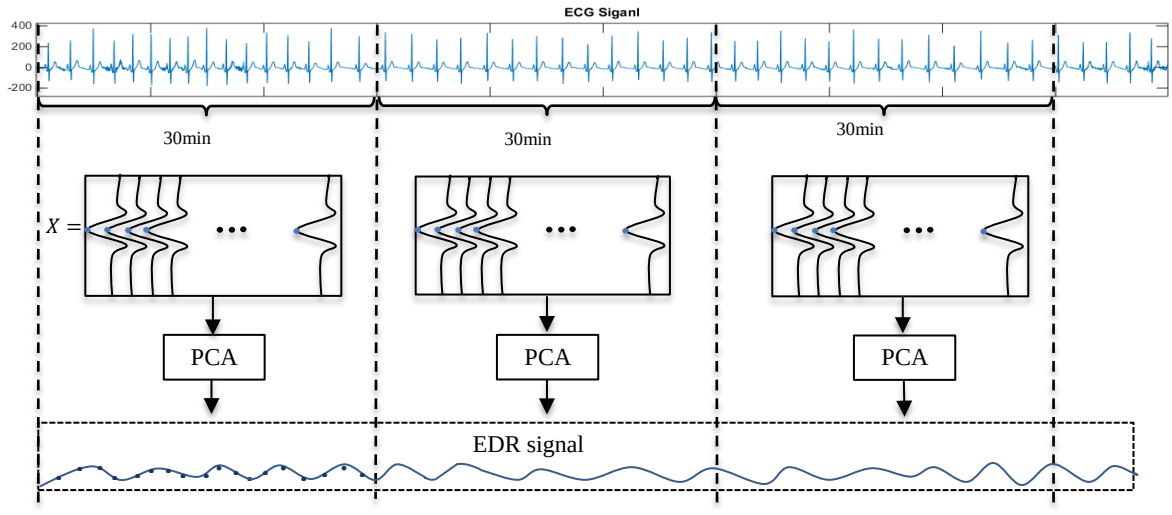

Figure 5.6. Schematic illustration of segmented PCA for estimation of EDR signal.

minutes segment of the data as the schematic is demonstrated in Figure 5.6.

The algorithm was repeated for each 30-minutes segment of ECG signals and the eigenvalue, eigenvectors and principal components were extracted. The first PC of every segment was joined to build the EDR signal for the entire recording, as shown in Figure 5.6.

Covariance (*C*) in equation (4.2) is a square matrix of size $n \times n$ where n is the number of QRS complexes in the recording. By partitioning the overnight recordings into 30 minutes segments, the length of n was reduced to about *1/16* of the original length (about 8 hours). This will lead to the required storage of about 30 MB for double precision which enormously reduced the memory requirement as well as the processing time. The results of applying this method to the datasets and comparing the results to the other EDR methods are widely demonstrated in section 5.2.

5) Approximated PCA

As the second solution for computational issue of PCA method for EDR estimation, we proposed an approximation method for PCA which was adapted from a speaker recognition study [316]. As demonstrated in the block diagram of Figure 5.8, many blocks of the approximated PCA algorithm are similar to the segmented PCA algorithm. The differences in the algorithms are summarised below.

1. The feature matrix of n centred QRS complexes for the entire recording ($[X_{QRS}(t)]_{m\times n}$), shown in Figure 5.5, was transposed and the PCA method was applied to $X_{approx} = X^T$.
2. The covariance matrix was measured over X^T resulting in a $m \times m$ matrix, where m is the number of the samples of the QRS window (for example 25 samples for a window of *250 ms* with *100 Hz* sampling rate of *MIT PhysioNet Apnea-ECG* database);

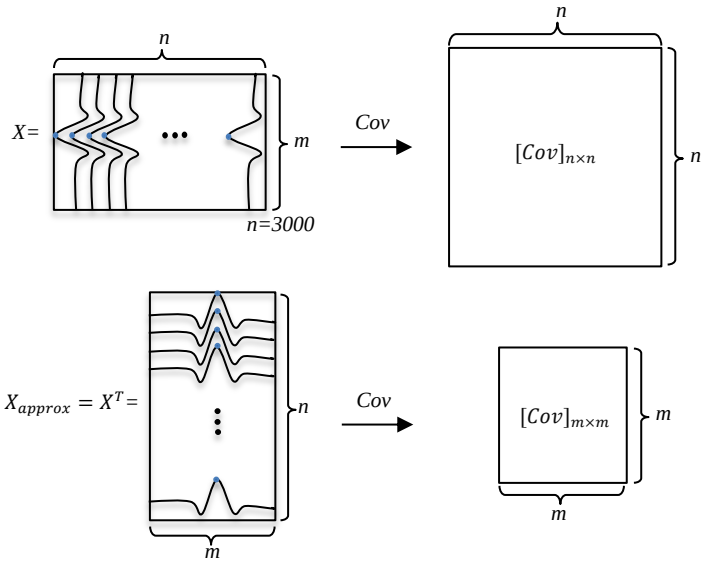

Figure 5.7. The dimensions of the covariance matrix of the standard PCA method against the approximated PCA method, *n*: the number of QRS complexes over the recordings, *m*: the length of the QRS complex window (*samples*).

$$C_{approx} = \frac{1}{m-1} XX^T \quad (5.11)$$

3. Then, the first PC of the approximated method (PC_{approx}) was measured by eigenvectors of the C_{approx} matrix.
4. Finally, the product of the generated PC and X_{approx} resulted in the EDR signal;

$$EDR = PC_C^1 = X^T PC_{C_{approx}}^1 \quad (5.12)$$

The demonstration of the enormous reduction in the dimension of covariance matrix using approximated PCA method compared to the standard PCA method is demonstrated in Figure 5.7. By processing X^T matrix rather than the X matrix, the dimension of the covariance matrix was reduced to $m \times m$ from $n \times n$, with m being the length of the QRS segmentation window, and n being the number of QRS complexes which for an ECG recording with an average length of 8 hours at 60 beats per minute is about 30,000. Thus, it results in a considerably reduced computational burden, memory requirement and processing time [65]. It leads to a lower dimension covariance matrix compared to the segmented PCA method [65]. The results of this approach on the two datasets and comparing their performance of SA detection as well as the processing time against the other EDR methods are demonstrated in section 5.2. Different implementation steps for three EDR measurement techniques of QRS area method compared to segmented PCA and approximated PCA used for developing the algorithms of this thesis are outlined in Table 5.2.

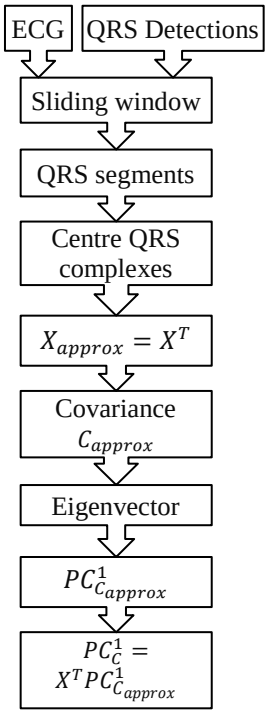

Figure 5.8. Block diagram of EDR estimation using approximated PCA method.

Table 5.2. Steps for the three methods of ECG derived respiration

Steps	QRS Area	Segmented PCA	Approximated PCA
1	Clean ECG	30 min segments	QRS windows
2	Detect QRS	QRS windows	Subtract mean
3	100-ms windows	Subtract mean	Centred QRSs= X
4	Area under QRSs	Center QRSs	$X_{approx} = X^T$
5	Join the areas	Covariance	Covariance
6		Eigenvectors	Eigenvectors
7		Join 1st PCs of 30 min segments	$X^T PC^1_{approx}$

5.1.4. PSD features

The main feature set captured from the biosignals in this project are PSD features, which is adapted from the interval-based PSD measurement [317]. The procedure of PSD calculation of this application can be summarised as follows.

In order to calculate the PSD features, we first zero-padded the particular signal segment in each epoch to reach length *L*. The value of *L* used for the signals is discussed below. The block diagram of computing PSD feature is demonstrated in Figure 5.9. As shown in Figure 5.9, the zero-padded signals in each epoch were subjected to standardisation by subtracting from each sample the epoch mean and dividing by the epoch standard deviation. The standardised signal was then transformed into the frequency domain by applying discrete Fourier transform (DFT). The PSD of the signal segments was computed by squaring the amplitude of the DFT coefficients. Due to symmetry, only the first half of the frequency spectrum was used for the feature calculation from this point onwards. Finally, four adjacent frequency bins of the PSD coefficients across the epoch were averaged in order to reduce the dimension of the feature-space. Due to the symmetric pattern, the first half of the 64-point averaged outputs was assigned as 32 PSD features, calculated over each epoch for all candidate signals.

For the application of this thesis, EDR signals, HRV and respiratory signal (which was sampled at three different rates), *L* was assumed to be equal to 256. This value was chosen as it was the first power of 2 exceeding the maximum number of hearts beats in an epoch (based on maximum physiologically plausible heart rate of 240 bpm). The length of DFT and zero padding for some examples of heart rates (*N*) are displayed in Table 5.3 for *MIT PhysioNet Apnea-ECG* dataset and in Table 5.4 for *St. Vincent's* dataset.

The frequency intervals Δf_{RR} resulting from the DFT of the EDR and HR sampled respiratory effort

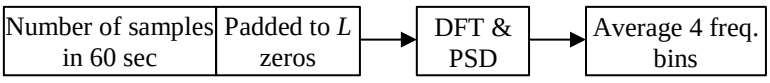

Figure 5.9. The block diagram of measuring PSD features.

Table 5.3. The zero padding and DFT lengths for some example heart rates for the chest respiratory effort signal of MIT PhysioNet Apnea-ECG dataset with F_s=*100H*

N	L	DFT length	Bins averaged
60	19600	25600	4
70	15943	21943	4
80	13200	19200	4
90	11067	17067	4
120	6800	12800	4
240	400	6400	4

N = heart rate, *L* = length of zero padding, F_s = 100Hz

signal segments in each epoch can be calculated as:

$$\Delta f_{RR} = \frac{1}{256/4}\left(\frac{cycles}{RR\ intervals}\right) = \frac{1}{256/4}\frac{cycles}{RR\ intervals}\frac{RR\ intervals}{sec} = \frac{N/60}{256/4}\frac{cycles}{sec}, \quad (5.13)$$

where *N* is the number of QRS complexes in each epoch of 60 seconds (i.e. the heart rate).

For the respiratory effort signal, *L* was calculated for each epoch so that the Δf_{Resp} was the same as the Δf_{RR} for the heart-beat sampled signals. We impose this condition so that the resulting features from the respiratory signal and the heart rate sampled respiratory signals contained the same frequency bins.

The calculation of *L* for respiratory signal proceeded as follows. Let F_s denote the sampling rate of the chest respiratory signal. The Δf_{Resp} on the zero-padded signal segment in each epoch, is given by:

$$\Delta f_{Resp} = \left(\frac{1}{\frac{60 \times F_s}{4}}\right)\left(\frac{1}{1/F_s}\right)\frac{cycles}{secs} = \frac{4F_s}{60F_s + L}\frac{cycles}{secs} \quad (5.14)$$

Equating the Δf_{RR} from (5.13) and Δf_{Resp} from (5.14) and solving for *L* results in the following equation for *L*.

$$\frac{N/60}{256/4} = \frac{4Fs}{60Fs + L} \qquad \Rightarrow \qquad L = \frac{Fs \times 256 \times 60}{N} - 60 \times Fs \quad (5.15)$$

For the first utilised dataset, *MIT PhysioNet Apnea-ECG* database [233], where F_s=100 Hz, the number of zeros needed for padding to measure the DFT for chest respiratory effort signals is;

$$L_{PhysioNet} = \frac{1536000}{N} - 6000 \quad (5.16)$$

The length of DFT and zero padding for some examples of heart rates (*N*) for the chest respiratory effort signals are displayed in Table 5.3 for *MIT PhysioNet Apnea-ECG* dataset. As listed in the table, 4 bins for averaging were assumed for every example.

For the second utilised dataset of this project, *St. Vincent's University Hospital, University College Dublin Sleep Apnea* database [314], *Fs*=8 Hz, *L* was measured as follows.

$$L_{St.Vincents} = \frac{122880}{N} - 480 \quad (5.17)$$

Table 5.4. The zero padding and DFT lengths for some example heart rates for the chest respiratory effort signal of St. Vincent's database with *Fs=8 Hz.*

N	L	DFT length	Bins averaged
60	1568	2048	4
70	1275	1755	4
80	1056	1536	4
90	885	1365	4
120	544	1024	4
240	32	512	4

N = heart rate, L = length of zero padding, F_s = 100 Hz

The calculated lengths of DFT and zero padding for some examples of heart rates (N) for the chest respiratory effort of the second database are shown in Table 5.4.

Using the PSD features, the matrices of features over one-minute epochs were extracted from each EDR signal and chest respiratory effort signal and were applied to the classifiers and the performance of every signal in apnoea detection was evaluated (see section 5.2.2). The performance of apnoea recognition was analysed through leave-one-out cross-validation. Reported performance factors were accuracy, sensitivity, specificity, and the area under curve of receiver operator characteristic (AUC-ROC), as described in section 3.8 [16]. The results of the developed algorithms of this application including the EDR estimation methods and PSD features are demonstrated in the following section.

5.2. Results of application 2

The results of application 2 were obtained in three phases, as outlined in section 5.1. This section commences with demonstrating the results of phase I, using different methods of EDR estimation for apnoea detection (see section 5.2.1). Three methods were implemented to measure EDR signals; QRS area method, standard PCA and kernel PCA. The EDR signals were first obtained for an hour of the recordings (the *MIT PhysioNet* database). In this phase, the ELM classifier was utilised for apnoea classification and the performance results of the classifier using different hyperparameters were evaluated. We then applied two PCA techniques (approximated PCA and segmented PCA) to estimate the EDR signals of the entire overnight ECG recordings. The two EDR signals using the developed algorithms were evaluated for apnoea detection using the ELM classifier. The classification results were obtained using a wider range of hyperparameters. The outcome of phase I was to illustrate the advantages and disadvantages of different EDR estimation methods as well as evaluate and choose the optimum hyperparameter of the ELM classifier.

In phase II, section 5.2.2, we compared the respiratory information of three automated algorithms measuring the EDR signals (QRS area method, segmented PCA and approximated PCA) against the chest respiratory effort signals in two steps; sample-based correlation and epoch-based apnoea classification.

In the first step of phase II, the respiratory information comparison is performed by measuring the sample-based correlation of the three EDR signals against the chest respiratory effort signals. First, the EDR signals were estimated through three methods (QRS area, segmented and approximated PCA) using the recordings of two databases (the *MIT PhysioNet* database and the *St. Vincent's* database). Then, the results of the correlation coefficient measurement of the three EDR signals against the corresponding chest respiratory signals for the two databases were obtained.

In the second step of phase II, the respiratory information of the EDR signals obtained from the full overnight ECG recordings was evaluated for one-minute epoch apnoea classification against the chest respiratory effort signals. The results of apnoea detection using three EDR signals (QRS area, segmented and approximated PCA) were compared to the results of apnoea detection using the chest respiratory effort signals. Three chest respiratory effort signals were utilised for this step including the full signal, HR sampled and the uniformly sampled signal. We utilised the three chest respiratory signals with different resampling schemes to evaluate the different characteristics of the EDR signals such as, sampling at the heart rate, lower sampling rate and their impact on the apnoea detection.

The six signals (EDR and respiratory signals) were obtained for both databases (the *MIT PhysioNet* database and the *St. Vincent's* database). Identical features were captured from every one minute epoch of every signal and applied to the classifiers for apnoea detection. Three automated machine learning techniques were used for classification including ELM, LDA and SVM classifiers. We compared the performance results of ELM classifier with the optimum hyperparameter (obtained from phase I) against the results of LDA and SVM classifiers for apnoea detection to evaluate the performance of different machine learning techniques for this application and choose the highest performing technique. We assessed the apnoea detection performance of three EDR estimation algorithms on different databases to choose the highest performing EDR signal to utilise in phase III for optimising the performance of the final system. Thus, the outcome of phase II is to choose the highest performing EDR method and machine learning technique.

Ultimately, phase III represents optimisation of the sleep apnoea detection through extracting HRV and CPC features and combining them with the feature set of the highest performing EDR signal which was chosen according to the results of phase II (see section 5.2.3). The results are evaluated in three ways; one-minute epoch apnoea classification, AHI estimation and subject based apnoea detection. The first performance measure (one-minute apnoea classification) was reported for every individual feature set including HRV, CPC, the highest performing EDR features and the combination of the feature sets using the highest performing classifier which chosen according to the results of phase II. Also two optimisation methods were applied including overlapping one-minute epochs by 30 seconds and averaging the features of every three adjacent epochs to boost the performance of the machine learning algorithm. We then estimated AHI of the recordings from the two databases using the results of one-minute epoch classification. Finally, we measured the subject-based sleep apnoea

detection using the AHI estimation results. We commence the remainder of this section with illustrating phase I and the performance results of the EDR estimation methods as follows.

5.2.1. Phase I: Extending EDR methods

Phase I of application 2 involved estimating EDR signals in order to use the respiratory information for apnoea detection. Prior to estimating EDR signals and feature extraction, the first step of ECG signal processing is interference removal, as discussed in sections 3.3 and 5.1.3. The result of applying the baseline wander noise removal algorithm is demonstrated in Figure 5.10(b) and the magnified demonstration of the result on an excerpt of the signal is shown in Figure 5.10(d). It shows an example of the effect of filtering on a sample ECG signal of the *MIT PhysioNet* dataset (Figure 5.10(a)), demonstrating the suitable performance of the baseline wander noise removal algorithm. Also the onset beats of the QRS complexes are shown in red stars in Figure 5.10(b), with the magnified results of an excerpt of the clean signal and the QRS onset beats in Figure 5.10(d).

The artefact removed ECG signals and the QRS detections were then used to estimate the EDR signals for the first phase of the application. First, data from the first 60 minutes of the 35 ECG recordings for the *MIT PhysioNet Apnea-ECG* database was used to capture EDR signal using three algorithms (QRS area, PCA and kernel PCA), as described in sections 3.5.2 and 5.1.3. We note that previous studies of PCA methods for EDR estimation utilised short ECG recordings of less than an hour and removed the ectopic beats [70], [73], thus, we first applied PCA method to an hour of data to investigate the performance of the method for apnoea detection. In the first step of the PCA application, we form a matrix of centred QRS complexes. Two examples of this input matrix used for the PCA application are shown in Figure 5.11, with an example of well-aligned complexes without ectopic beats (Figure 5.11(a)) and an example of a recording with ectopic beats (Figure 5.11(b)).

An example of an excerpt of the input ECG signal and the estimated EDR signals using three algorithms including QRS area method, PCA and kernel PCA method (using the Gaussian kernel) are illustrated in Figure 5.12. The visual observation of the EDR signals in Figure 5.12 reveals that the EDR signals estimated by QRS area method and PCA method follow a similar trend, as a modulatory signal on the ECG signal, while this behaviour is not observable for the EDR signal estimated by kernel PCA method.

Following estimating the EDR signals, they were partitioned into one minute segments. A matrix of 34 features for each segment was extracted from one minute epochs of every EDR signal and applied to an extreme learning machine (ELM) classifier (see section 3.7.3). The extracted features were average value, standard deviation, and 32 PSD of the EDR signals, as explained in section 5.1.4.

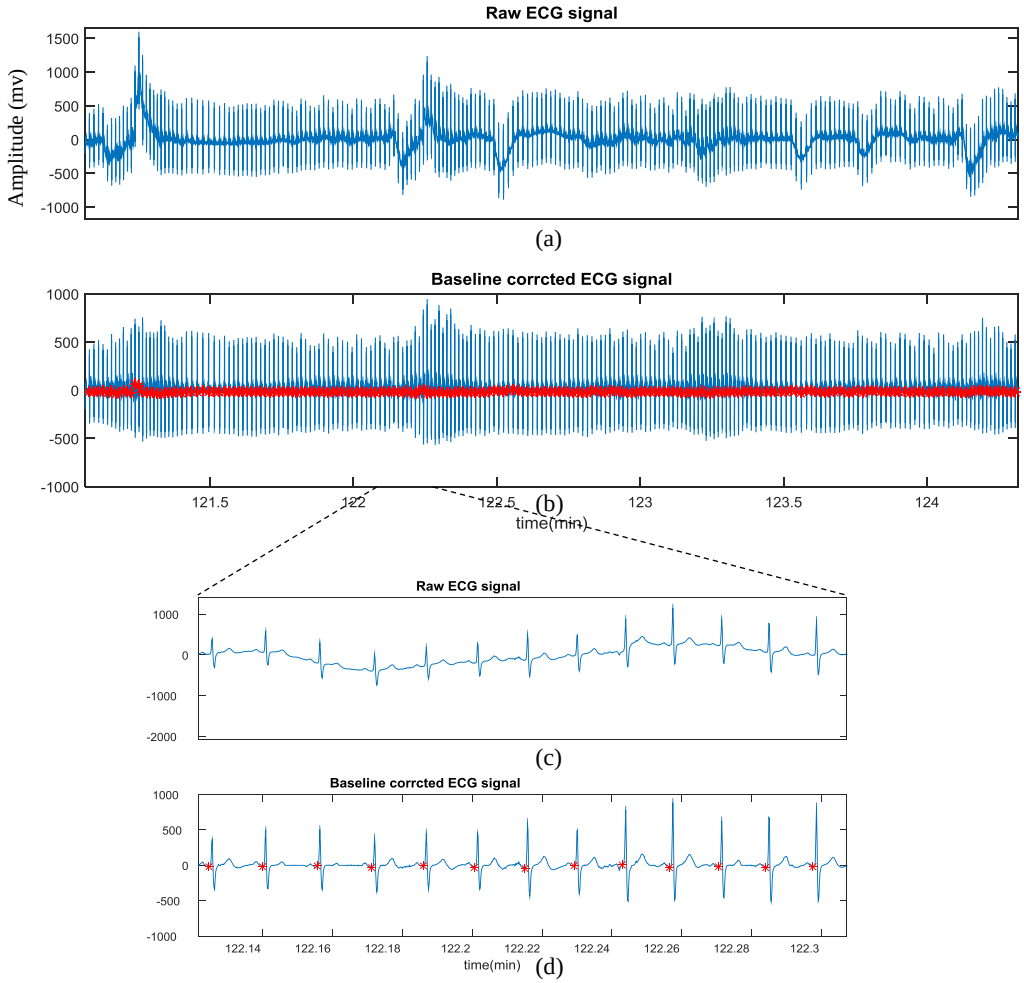

Figure 5.10. (a) A sample ECG signal from MIT PhysioNet database, (b) the result of applying baseline wander noise removal. The red stars are the QRS detection beats. (c) magnified demonstration of an excerpt of the ECG signal, (d) magnified demonstration of the baseline corrected signal and the QRS onset beats.

We also evaluated the impact of the hyperparameters of the ELM classifier. As described in section 3.7.3, ELM classifier is trained through a single iteration learning procedure using the pseudo-inverse to calculate the output weights. The weights of the input layer set to uniformly distributed random numbers between -1.5 to 1.5. *tanh* was set as the activation function. In this phase, we explored the impact of the different number of hidden layer neurons per input (fan-out) and examined the apnoea detection performance. Thus, the fan-out of the ELM classifier was varied between one and ten. The ELM classifier was trained by 35 training records of the dataset using the three different EDR signals separately.

The performance results of the training set are shown in Table 5.5, and the performance results obtained using the 35 test records evaluated by leave-one-out cross validation are indicated in Table 5.6. The highest accuracy for training set was 85.92% achieved by PCA EDR features at a fan-out of 5 with sensitivity of 61.4% and specificity of 92.58%. The highest performance during cross-validation was also obtained by PCA EDR features at a fan-out of 10 with an accuracy of 79.36%,

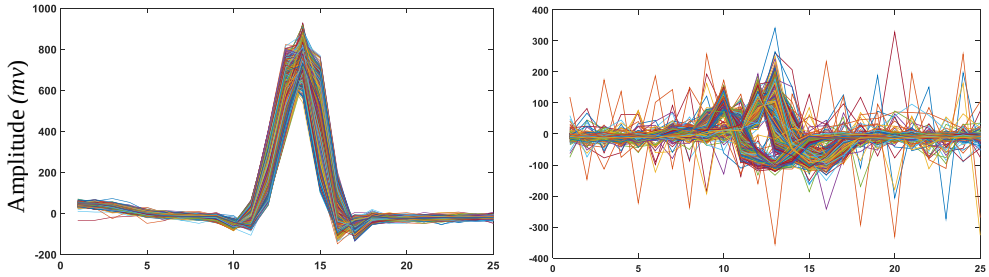

Figure 5.11. Examples of the centred QRS complexes used to develop the feature matrix of *X*. (a) a good example with well-aligned QRS complexes and (b) a representation of a feature matrix with ectopic beats

sensitivity of 48.76%, and a specificity of 87.68% [157]. Thus, at this stage, our maximum fan-out of 10 achieved the highest performance of sleep apnoea detection. Based on these outcome we explored using higher fanouts in a second series of experiments described below.

We applied kernel PCA in order to investigate identification of the nonlinear patterns of respiration and compare the performance with linear methods. The results of test set (Table 5.6) demonstrate that the highest performance of kernel PCA was obtained at a fan-out of 1 with an accuracy of 68.08%, sensitivity of 26.18% and specificity of 79.44%. It revealed that PCA method obtained higher accuracy and specificity and further higher sensitivity for apnoea detection. It confirms the result of the visual observation of the EDR signals in Figure 5.12 where kernel PCA did not demonstrate similar trend (of ECG modulation) as the EDR signals estimated by PCA and QRS area methods. We concluded that the low cross validation performance shows that the kernel PCA did not provide further information to enhance the apnoea detection. Thus, it was not utilised in the following phases of this application.

Table 5.5. Epoch-based apnoea classification results from training set of first 60 minutes of the data.

	Fan-out	Accuracy	Sensitivity	Specificity
QRS area	**1**	66.71	73.81	68.59
	2	70.58	67.72	71.36
	5	79.87	68.85	82.88
	10	84.95	76.29	87.31
PCA	**1**	75.80	52.60	82.10
	2	82.55	58.69	89.03
	5	85.92	61.40	92.58
	10	84.95	76.30	87.32
KPCA	**1**	71.88	29.80	83.29
	2	73.90	33.63	84.82
	5	77.71	39.95	87.94
	10	80.36	44.70	90.02

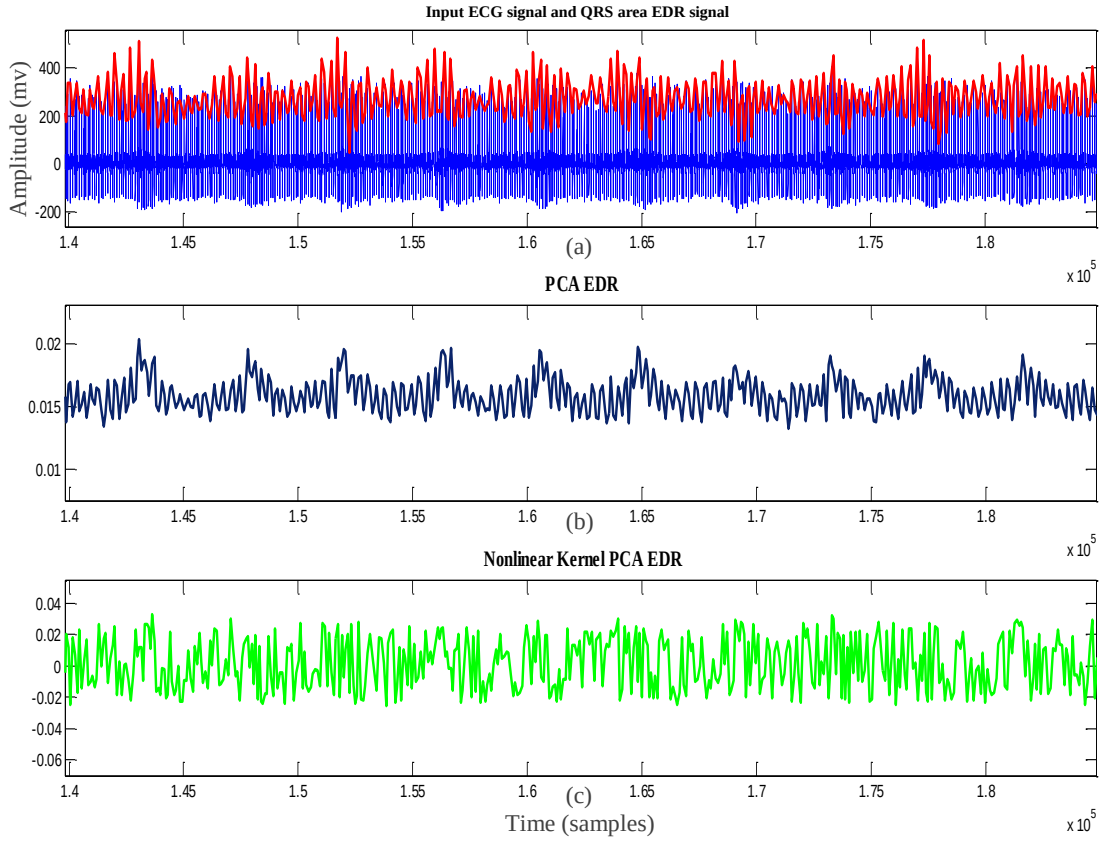

Figure 5.12. (a) Input ECG signal (in blue) and the QRS amplitude EDR (in red), (b) linear PCA, and (c) Nonlinear EDR for the first attempt of phase I (60 minutes of the data from MIT PhysioNet database).

As stated in section 5.1.3, the published studies of PCA methods were limited to processing signals of less than an hour in addition to removing the ectopic beats and choosing clean excerpts of data. For the application of this thesis, we require analysis of overnight signals with duration of about eight hours. As the EDR signal estimated by PCA method on an hour of the data resulted in the highest performance of apnoea detection (see Table 5.6), it was extended for estimating the EDR signal of the full overnight recordings. When we attempted to implement PCA and apply the algorithm to the full overnight ECG recordings, due to the need to store a large covariance matrix, our standard PC ran out

Table 5.6. Epoch-based apnoea classification results from cross validation (test-set) of first 60 minutes of the data.

	Fan-out	Accuracy	Sensitivity	Specificity
QRS area	**1**	71.49	53.72	76.31
	2	74.91	56.20	79.98
	5	75.30	48.75	82.49
	10	75.73	44.69	84.15
PCA	**1**	71.12	43.34	78.66
	2	77.24	48.98	84.92
	5	77.39	45.15	86.14
	10	79.36	48.76	87.68
KPCA	**1**	68.08	26.18	79.44
	2	67.31	25.51	78.64
	5	66.68	23.48	78.39
	10	65.82	24.61	76.99

of memory and hence the published PCA methods were not suitable. Thus, we proposed two algorithms to resolve the computational issues and memory requirement.

Following applying PCA to 60 minutes of the data, we applied an approximation method for PCA technique to the entire overnight ECG recordings to estimate the respiration (see section 5.1.3). We compared the results to a full PCA method which we presented as segmented PCA by applying PCA to 30 minutes segments of the ECG signal, with the algorithm explained in section 5.1.3. An example of the centred QRS complexes to form the matrix for applying PCA is shown in Figure 5.11. Similar to the previous attempt (using 60 minutes of the data), the recordings from *MIT PhysioNet Apnea-ECG* database were used. Also similarly, 34 features (average value, standard deviation, and 32 PSD of EDR signals) were calculated for every one-minute epoch of the EDR signals and ELM classifier (see section 3.7.3) was trained to detect OSA. According to the ELM classifier performance results of the previous experiment (Table 5.6), our best results occurred at our largest fan-out of 10, suggesting that further performance improvement may be possible. Hence, for future experiments, we evaluated higher values of the fan-out.

Extending the PCA EDR estimation

The cross-validation performance of the ELM classifier for fan-out of 1 to 50 (corresponding to varying the number of hidden units between 34 and 1700 as there were 34 features) for segmented PCA method and approximated PCA method are illustrated in Table 5.7 and Table 5.8. The results from ELM classifier demonstrated the highest performance of 75.9% at fan-out 10 for segmented PCA and 76.4% for approximated PCA method. The performance results of apnoea detection show that the EDR signal estimated by approximated PCA method achieves relatively higher performance measures compared to the segmented PCA method at every fan-out value.

Our results also indicate that increasing the fan-out and the number of hidden neurons per input elevated classifier performance reaching an optimal value at fan-out of 10. The standard deviation of accuracies across the recordings were measured and reported in the Table 5.7 and Table 5.8. The standard deviation was about 3% which was due to the inter-subject variability. In order to estimate this variability, we applied leave-one-out cross validation technique.

Table 5.7. Performance result from cross-validation by ELM classification of segmented PCA (*MIT PhysioNet* dataset).

Fan-out	Accuracy	Sensitivity	Specificity
1	72.86±2.78	75.85	71.01
2	74.53±2.53	77.98	72.39
5	74.83±2.66	75.72	74.27
10	75.91±2.61	74.34	76.88
20	75.30±2.52	71.73	77.52
50	74.25±2.42	70.06	76.86

Table 5.8. Performance result from cross-validation by ELM classification of approximated PCA (*MIT PhysioNet* dataset).

Fan-out	Accuracy	Sensitivity	Specificity
1	73.97±2.56	84.32	67.55
2	75.69±2.44	83.60	70.79
5	75.34±2.43	82.65	70.81
10	76.38±2.32	80.15	74.04
20	76.17±2.27	77.38	75.41
50	75.19±2.25	73.51	76.23

The processing time for EDR extraction of a sample recording using approximated PCA was 0.33 seconds and using segmented PCA was 4.32 seconds. Thus, both developed algorithms successfully performed and the approximated PCA method was approximately 13 times faster than the segmented PCA method. The processing time of measuring the EDR signal using the original PCA method for a sample overnight recording on a specialised desktop computer with 64GB of memory was over an hour and required a memory of about 9GB.

The accuracy of two PCA methods of EDR feature extraction for apnoea detection is demonstrated in Figure 5.13. The performance of ELM classifier for fan-out of 1 to 50 is shown. It revealed relatively better apnoea detection by approximated PCA method and the highest performance of ELM classification occurred for fan-out of 10 (340 hidden neurons). In the previous attempt of phase I, we measured the PCA method on an hour of the ECG recordings and obtained 79% of accuracy with 49% of sensitivity and 88% of specificity. The results from full overnight study is comparable and revealed better sensistivity and balanced performance. The approximated PCA method can be useful for other problems with high dimensional signal analysis.

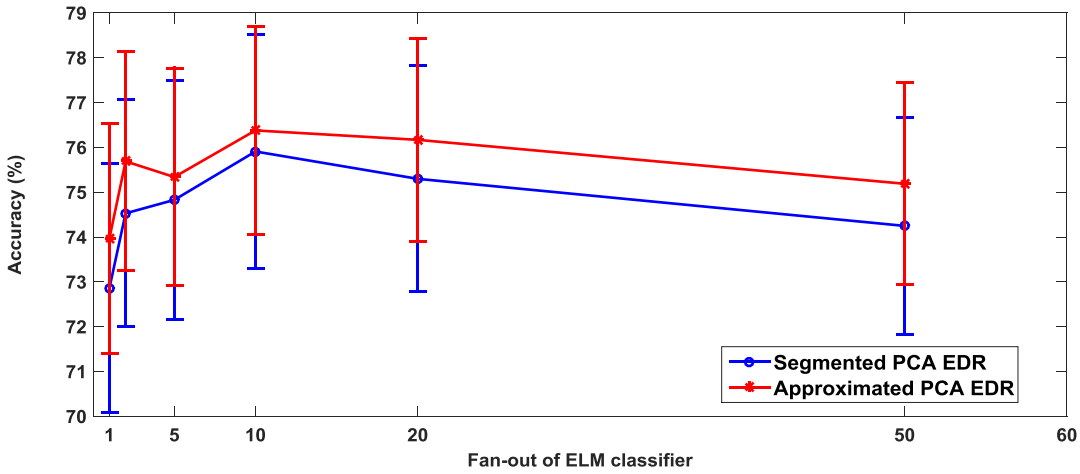

Figure 5.13. The performance of ELM classifier for OSA detection using the EDR features obtained by two proposed PCA methods (*MIT PhysioNet* dataset).

5.2.2. Phase II: respiratory information comparison

In the phase II, we evaluated the respiratory information captured by the EDR methods and performed a side-by-side comparison of the discrimination information for identifying sleep apnoea contained in the chest respiratory effort signal and three methods of the EDR signal estimation. Phase II is mainly carried out in two steps; in the first step, the sample-based correlation of the estimated EDR signals and the chest respiratory effort signal was evaluated. We measured the sample-based correlation of three EDR signals (QRS area, segmented PCA and approximated PCA methods) against the chest respiratory signals from two databases (*MIT PhysioNet Apnea-ECG* database and *St. Vincent's* database).

In the second step, apnoea classification of the chest respiratory effort signal and three methods of the EDR signal were assessed. We utilised the recordings of two databases, extracted identical features from one-minute epochs of every signal and applied the features to three machine learning techniques (ELM, LDA and SVM classifiers) to identify sleep apnoea. Three EDR signals (QRS area, segmented PCA and approximated PCA methods) and three chest respiratory effort signals were utilised. The respiratory effort signals included the full respiratory effort signal, the heart rate (HR) sampled and uniformly sampled respiratory signal. By comparing the performance results of the six signals for apnoea detection, the highest performing EDR estimation method and machine learning technique was chosen in order to use in phase III for optimisation of the final system.

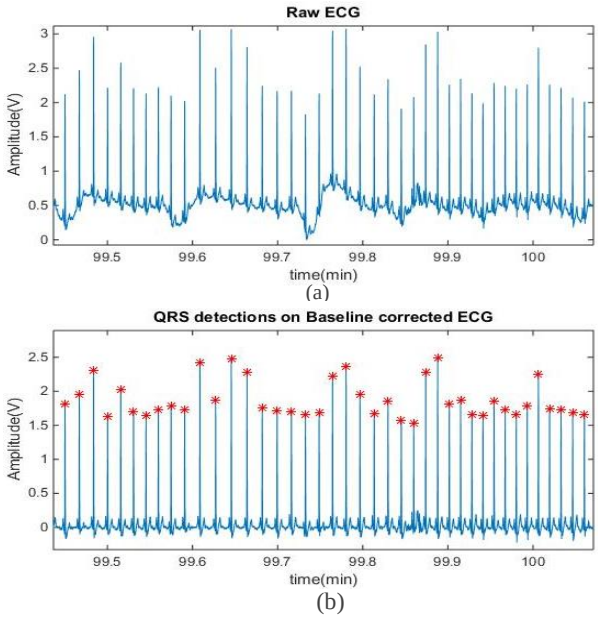

Figure 5.14. a) A sample ECG signal from St. Vincent's Dataset, and b) the result of applying baseline wander noise removal and Hilbert QRS detection.

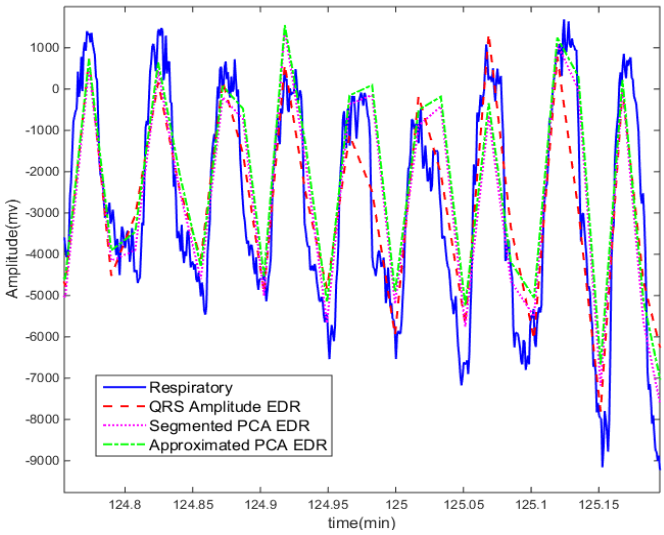

Figure 5.15. Illustration of the chest respiratory effort signal compared to three EDR signals including QRS area, approximated PCA, and segmented PCA. The EDR signals were time shifted and scaled to fit in the frame for demonstration.

Step 1: sample-based correlation

In the first step of phase II, the Pearson linear correlation coefficient (CC) was measured separately for three EDR signals (QRS area method, segmented and approximated PCA methods) against the chest respiratory signals.

The recordings of two databases were utilised for this phase. Simultaneously-recorded chest band and ECG recordings from eight overnight PSG data of the *MIT PhysioNet Apnea-ECG* database were used. The ECG signals and respiratory effort signals were both recorded at a sampling rate of 100 Hz. Also simultaneously recorded ECG signals and thoracic respiratory effort signals extracted from 25 overnight PSG data from the *St. Vincent's University Hospital, University College Dublin Sleep Apnea* database were utilised. The ECG signals were sampled at 128Hz and the thoracic respiratory effort signals were sampled at 8 Hz.

Prior to EDR estimation, the baseline wander noise was first removed from the ECG recordings and the Hilbert QRS detection algorithm was applied to the clean ECG signals (see sections 3.4 and 5.1.3). An example of the result of applying the baseline wander noise removal algorithm to an excerpt of the raw ECG signal from the *St. Vincent's* dataset is demonstrated in Figure 5.14(b). The results of the detected QRS complexes are shown with red stars in Figure 5.14(b). The visual

Table 5.9. The correlation coefficient of the respiratory effort signals and the EDR signals for MIT PhysioNet dataset.

Correlation Coefficients								
Respiratory	Rec.1	Rec.2	Rec.3	Rec.4	Rec.5	Rec.6	Rec.7	Rec.8
QRS area	0.34	0.02	0.05	0.21	0.01	0.15	0.03	0.15
Segment.PCA	0.14	0.06	-0.05	0.02	-0.01	0.18	0.06	0.04
Approx.PCA	0.18	0.12	0.06	0.06	0.01	0.42	0.03	0.15

observation of the baseline removed signal and the detected QRS beats showed a suitable performance of the algorithms.

The artefact removed ECG signals and the QRS detections were then used to estimate the EDR signals (QRS area method, segmented and approximated PCA methods) of the two databases, as explained in sections 3.5.2 and 5.1.3. The three estimated EDR signals in comparison with the chest respiratory effort signal for a sample recording of *MIT PhysioNet Apnea-ECG* database are displayed in Figure 5.15. It implies that the EDR signals follow the trend of the chest respiratory signal and display comparable behaviour. It should be noted that the temporal values were scaled and shifted to fit in the frame of Figure 5.15 for demonstration purpose.

In order to compare the the correlation between the estimated respiratory signals from ECG against the chest respiratory effort signal, Pearson linear correlation coefficient (*CC*) is measured by the ratio of the covariance of two signals normalised to the product of the variance of the signals [318], [319],

$$CC = \frac{C_{xy}}{\sigma_x \sigma_y} \quad . \tag{5.18}$$

The x and y represent the EDR signal and the chest respiratory effort signal, C_{xy} represents the covariance and σ represents the variance of the amplitude of the signals.

The correlation coefficient results of the chest respiratory effort signals and the three EDR signals are demonstrated in Table 5.9 and Table 5.11 for the two datasets. The correlation coefficient results of the QRS area EDR signals against the two PCA methods are shown in Table 5.10. The tables demonstrate the low correlation between respiratory signals and EDR methods indicating low similarity in sample by sample comparison. The negative correlation coefficient occurred in segmented PCA EDR method for some records may be caused by the random sign of eigenvalues which in some cases results in opposite behaviour of the signals. On the other hand, the correlation between different methods of EDR measurement, indicated in Table 5.10, revealed higher results and was reasonably appropriate.

Although, Figure 5.15 manifested a homogeneous trend of EDR signals and respiratory effort signal, the sample based correlation measurements between EDR signals and respiratory effort signals of Table 5.9 and Table 5.11 manifested low level of equivalence in terms of sample by sample analogy. In the following step, we investigated the performance of the ECG extracted respiratory signals in sleep apnoea detection and compared the performance against the chest respiratory effort signals in

Table 5.10. The correlation coefficient of the QRS area EDR signal and the PCA EDR signals for MIT PhysioNet dataset.

Correlation Coefficients								
QRS area	Rec.1	Rec.2	Rec.3	Rec.4	Rec.5	Rec.6	Rec.7	Rec.8
Segment.PCA	0.47	0.42	-0.16	0.31	-0.28	-0.12	0.27	0.22
Approx.PCA	0.62	0.51	0.51	0.67	0.88	0.54	0.38	0.81

Table 5.11. The correlation coefficients of the respiratory signals and the EDR signals for the St. Vincent's dataset.

Correlation Coefficient																									
	Records																								
Resp.	1	2	3	4	5	6	7	8	9	10	11	12	13	14	15	16	17	18	19	20	21	22	23	24	25
QRS.	.02	.02	.01	.02	.02	.01	.01	.03	.01	.02	.01	.01	.01	.03	.04	.03	.04	.03	.04	.05	.04	.01	.01	.03	.03
Seg.	.01	.01	.01	.02	.05	.01	.01	.01	.01	.01	.01	.01	.02	.03	.04	.01	.03	.03	.03	.02	.02	.01	.01	.02	.01
Appr.	.01	.01	.02	.03	.04	.01	.02	.01	.01	.01	.03	.01	.01	.03	.03	.01	.02	.02	.01	.03	.01	0.01	.01	.03	.02

Resp.: Respiratory effort signal, QRS: QRS area EDR signal
Seg.: Segmented PCA EDR signal, Appr.: Approximated PCA EDR signal

apnoea classification, described as follows. Our hypothesis was that, while the shape of the EDR did not correlate well with the respiratory signal and the sample-based correlation results were not satisfactory, the discriminative information based on respiration for sleep apnoea detection was preserved in the EDR.

Step 2: apnoea classification

In the second step of Phase II, the EDR signals and respiratory effort signals of both datasets were utilised for minute-by-minute apnoea recognition and the classification performance were compared using a leave-one-out cross validation method. Homogenous signal processing algorithms and machine learning techniques were applied to both datasets.

We note that each EDR technique provides one sample of the EDR per heartbeat. In order to investigate the impact of the heart rate sampling of EDR signals, we compared them against three

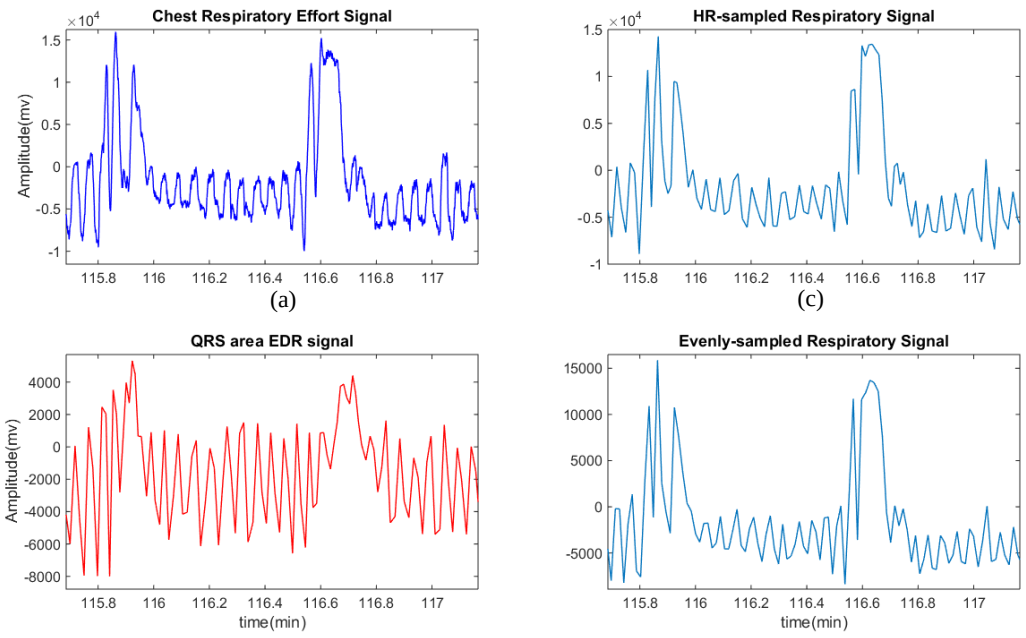

Figure 5.16. A sample recording from the MIT PhysioNet database, (a) the full respiratory signal, (b) the QRS area EDR signal, (c) the heartbeat sampled respiratory effort signal and (d) the evenly sampled respiratory effort signal. OSA events started at the 115.85 minutes (lasted for 10s) and 116.55 minutes (lasted for 12s).

forms of the chest respiratory effort signals; the full respiratory effort signal, the heart rate or QRS-sampled respiratory signal (HR sampled signal) and the uniformly sampled respiratory signal (see section 5.1.2). By including the uniformly sampled signal, we investigated whether the unevenly sampling rate of the EDR signals is affecting the results. Thus, six signals were evaluated in this step.

Figure 5.16 demonstrates a sample of an excerpt of the full chest respiratory signal compared to the HR sampled chest respiratory signal, uniformly sampled chest respiratory signal and QRS area EDR signal of the *MIT PhysioNet* dataset, displaying comparable behaviour.

In order to conduct a systematic comparison of one-minute epoch classification, each EDR and respiratory signals was segmented into one-minute epochs and 34 identical features (two time domain features including the average and standard deviation of the signal amplitude plus 32 interval-based PSD features of each epoch) were extracted.

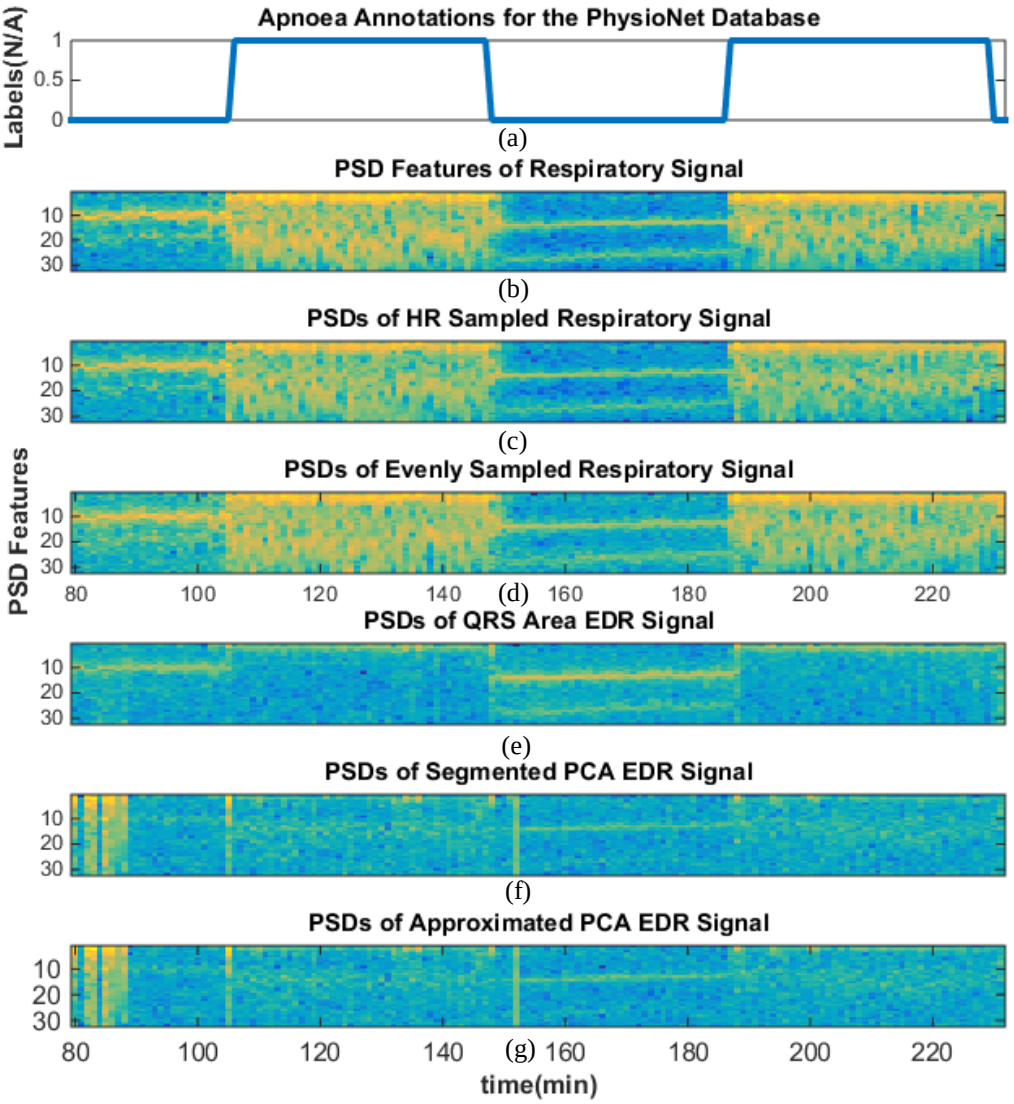

Figure 5.17. The PSD spectrograms of five respiratory effort signals of the MIT PhysioNet dataset. (a) Illustration of labels (apnoea=1, normal=0) from expert annotations, (b) PSD features of chest respiratory effort signal, (c) QRS (heart rate) sampled respiratory signal, (d) QRS area EDR, (e) segmented PCA EDR and (f) approximated PCA EDR signal.

Figure 5.17 shows an example of the PSD spectrograms derived from five respiratory signals with the frequency content of the signals illustrated in the lighter colour compared to the background. It also demonstrates the normal-apnoea labels per one-minute epochs from the provided annotations with the database. The PSD spectrograms of all of the respiratory signals have shown variations corresponding to the apnoea labels (shown in the top sub-figure, Figure 5.17(a)). The resemblance is quite prominent in the spectrograms from the respiratory signal, the HR sampled respiratory signal and the uniformly sampled respiratory signal compared to the EDR signals. The respiration model can be identified as the brighter colour which has a narrow and well-distinguished pattern for the intervals with normal labels and distorted pattern in apneic intervals. The QRS area EDR spectrogram appears to capture the steady breathing activity during normal breathing better than the PCA based EDRs.

We also aimed to investigate whether machine learning techniques other than ELM classifier (used in phase I) can enhance the apnoea detection. Thus, in this phase, classification of the minute-by-minute segments of the signals was evaluated using the machine learning techniques (ELM, LDA and SVM methods). The matrices of features were used to train the classifiers and each signal was evaluated individually through leave-one-record-out cross validation for each classifier. Every segment of every signal was classified into one of two classes: apnoea or non-apnoea.

We first utilised ELM classifier with the characteristics chosen in phase I (see section 5.2.1). The only

Table 5.12. The cross validation results of the MIT PhysioNet dataset with 34 features for apnoea detection.

Signals	**Accuracy (%)**	**Sensitivity (%)**	**Specificity (%)**	**AUC**
ELM classifier *(Fan-out=10)*				
Respiratory	77.3±1.8	91.0	67.9	0.88
HRSampl Resp.	78.5±1.5	89.6	70.9	0.88
UniformSamplResp	79.3±1.5	90.4	71.6	0.89
QRS Area	79.6±2.3	87.5	74.2	0.89
Approx. PCA	73.8±2.5	84.2	66.7	0.81
Segment. PCA	63.0±3.9	50.8	71.4	0.69
LDA classifier				
Respiratory	87.4±2.7	85.6	90.2	0.94
HRSampl Resp	86.4±3.2	83.4	90.7	0.94
UniformSamplResp	86.6±2.9	84.1	90.3	0.94
QRS Area	84.4±4.1	84.2	77.1	0.91
Approx. PCA	65.3±10.8	60.9	67.4	0.71
Segment. PCA	68.3±8.2	78.5	49.3	0.75
SVM classifier				
Respiratory	87.4	86.0	88.4	
HRSampl Resp	Not obtained			
UniformSamplResp	Not obtained			
QRS Area	80.9	70.8	87.7	
Approx. PCA	69.4	64.8	72.6	
Segment. PCA	66.4	49.5	78.1	

Resp = respiratory, HRSampl Resp = Heart rate (QRS) sampled respiratory, approx.= approximated, Segment = Segmented.

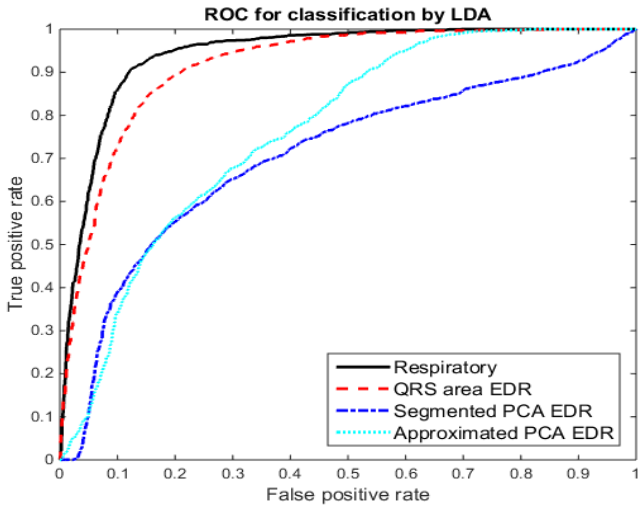

Figure 5.18. The receiver operator characteristic (ROC) of respiratory effort signal compared to three EDR methods of QRS area, segmented PCA and approximated PCA of PhysioNet dataset by LDA classifier.

difference was the fan-out which was set to 10, as this was previously found to give the optimal performance. We perfomed the training and testing of SVM classification using LibSVM [289].

The cross validation results of the signals for the two databases using three classifiers are shown in Table 5.12 and Table 5.13. The results revealed that the full chest respiratory effort signal obtained the highest performance of apnoea recognition using LDA classifier with an accuracy of 87%,

Table 5.13. The cross validation results of the St Vincent's dataset with 34 features for apnoea detection.

Signals	**Accuracy (%)**	**Sensitivity (%)**	**Specificity (%)**	**AUC**
ELM classifier*(Fan-out=10)*				
Respiratory	67.5±1.2	45.5	75.1	0.66
HRSampl Resp	61.8±1.0	44.7	68.0	0.61
UniformSamplResp	61.2±1.0	44.7	66.9	0.61
QRS Area	62.9±1.2	54.4	65.8	0.62
Approx PCA	61.5±1.3	53.8	64.2	0.62
Segment PCA	61.6±1.3	48.8	66.0	0.60
LDA classifier				
Respiratory	67.9±1.9	68.0	67.7	0.69
HRSampl Resp	61.5±2.1	60.7	63.6	0.62
UniformSamplResp	61.8±2.1	60.6	65.4	0.62
QRS Area	65.6±1.3	66.6	62.7	0.68
Approx PCA	65.6±1.7	67.4	60.5	0.70
Segment PCA	65.8±1.8	67.4	61.1	0.68
SVM Classifier				
Respiratory	67.7	68.5	67.1	
HRSampl Resp	Not obtained			
UniformSamplResp	Not obtained			
QRS Area	65.7	61.2	64.1	
Approx. PCA	65.5	62.5	63.4	
Segment. PCA	65.9	60.0	66.5	

Resp = respiratory, HRSampl Resp = Heart rate (QRS) sampled respiratory, approx. = approximated, Segment = Segmented.

sensitivity of 86%, specificity of 90%, and ROC AUC of 0.94 for the *MIT PhysioNet* dataset and an accuracy of 68%, sensitivity of 68%, specificity of 68%, and AUC of 0.65 for the *St. Vincent's* dataset. This result is not unexpected as the full respiratory signal carries the most detailed information about respiration and, presumably about sleep apnoea, compared to the other signals considered. However, for the *MIT PhysioNet* data, remarkably close performance was achieved using the heartbeat sampled respiratory signal – with an accuracy of 86.4%, sensitivity of 83.4% and specificity of 90.7%. This suggests that despite the sub-sampling process, which substantially reduced the number of samples from 100 Hz to approximately 1 Hz (considering average human heart rate), the information significant for sleep apnoea detection is still retained. The decrease of accuracy for sub-sampled respiratory signals of the *St. Vincent's* dataset might exist due to the extra sampling

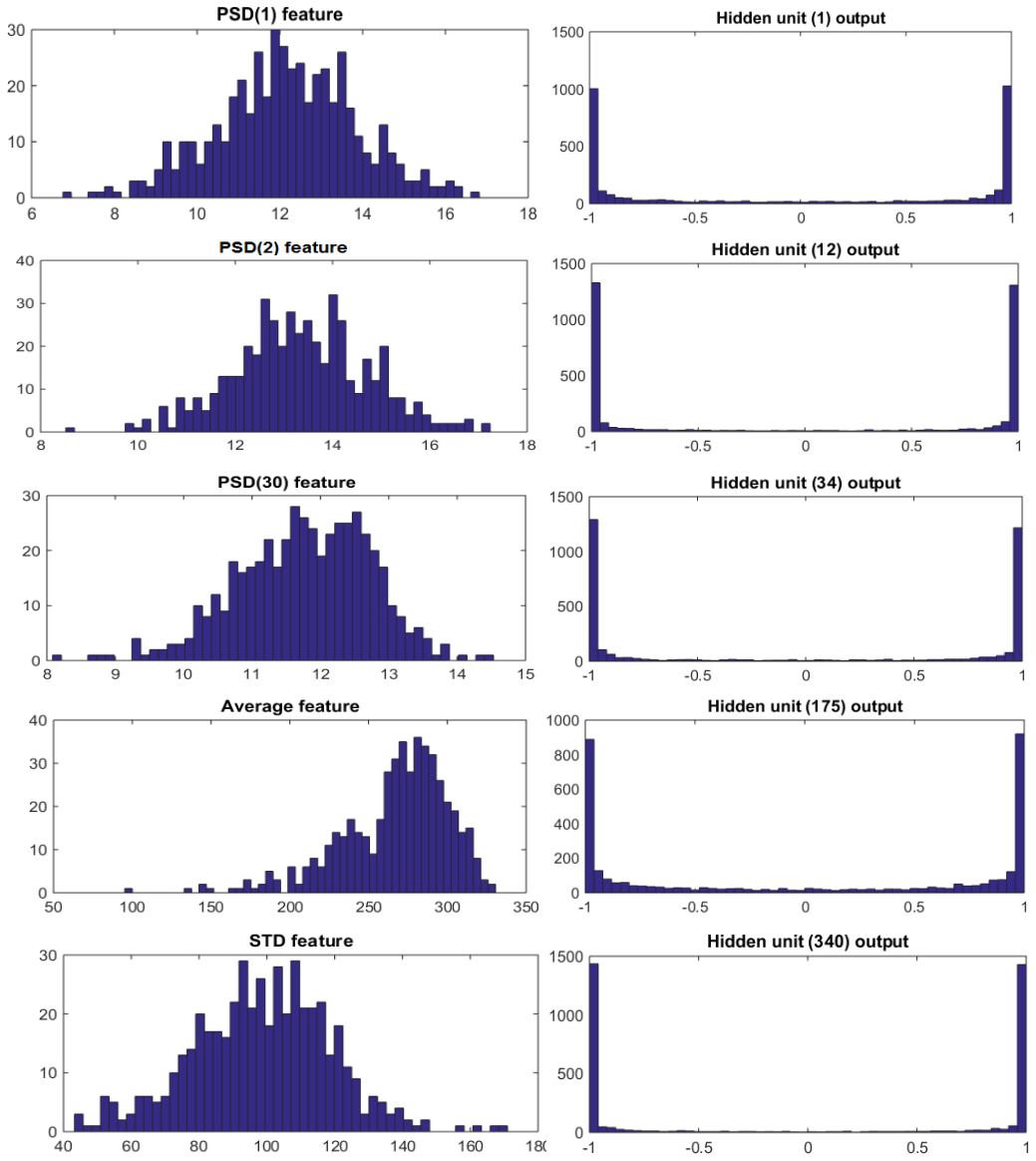

Figure 5.19. The histograms of five examples of the input features (three PSD features, the average and standard deviation feature) of the ELM classifier and the outputs of the hidden layer units for a sample PhysioNet data.

instant quantisation that was introduced by the 8 Hz sampling rate of the chest respiratory recordings.

The highest accuracy among the EDR methods was achieved by QRS area method using LDA classifier of 84% with sensitivity of 84%, specificity of 77% and ROC AUC of 0.91 for the *MIT PhysioNet* dataset and accuracy of 66%, sensitivity of 67% and specificity of 63% for the *St. Vincent's* dataset. Moreover, the processing time for the EDR estimation using the QRS area method for a sample overnight recording was 0.041 seconds, which is about eight times faster than that for the approximated PCA method. For the *St. Vincent's* dataset, the three EDR methods obtained comparable performance by both classifiers with relatively higher ROC AUC of 0.70 by approximated PCA EDR using LDA classifier.

For *MIT PhysioNet* data, the apnoea detection accuracy of the QRS-area EDR is 6.1% less than the result of the full chest respiratory effort signal. The sensitivity is almost identical to sensitivity of the respiratory effort signal while the specificity is 13% less. Comparing the three EDR methods reveals that the QRS area-EDR estimation has performed much better in apnoea detection than either PCA based EDR estimations in terms of the accuracy, sensitivity and specificity.

The standard deviation of the accuracies (using LDA classifier) across the recordings of the *St. Vincent's* dataset was around 2%, while it varied between 2% to 11% for the *MIT PhysioNet* dataset as a result of the intra-subject variability. The results of the *St. Vincent's* dataset are worse than the results of the *MIT PhysioNet* dataset. It can be due to the fact that the recordings of the *MIT PhysioNet* dataset contain only OSA events, while the recordings of the *St. Vincent's* dataset contain different types of the sleep apnoea (obstructive, central, mixed sleep apnoea and hypopnea).

The LDA classifier provided the highest performance of apnoea detection among the three utilised machine learning techniques. The histograms of some examples of the input features (three PSD features, average value and standard deviation) of the ELM classifier from a sample PhysioNet data and the histograms of five examples of the outputs of the hidden units are shown in Figure 5.19. The input features show Gaussian distributions and saturation can be observed in the output of the hidden layer after applying the random input weights and the non-linear function (tanh) to the input features. It will be further discussed in section 5.3.2. The performance results of the SVM classifier are almost equivalent to the performance results obtained by LDA classifier. Thus, based on the identical results, utilising LDA was preferred as a technique providing simpler and faster processing for the following optimisation phase of the final system.

The ROC of the respiratory effort signal is displayed in Figure 5.18 in comparison with ROC of three EDR methods for the *MIT PhysioNet* database. It shows that the QRS area EDR achieves the highest AUC which was almost equivalent to the respiratory effort signal. The PCA EDR signals resulted in relatively similar AUC, while approximated PCA EDR signal presented slightly higher AUC than the segmented PCA EDR signal.

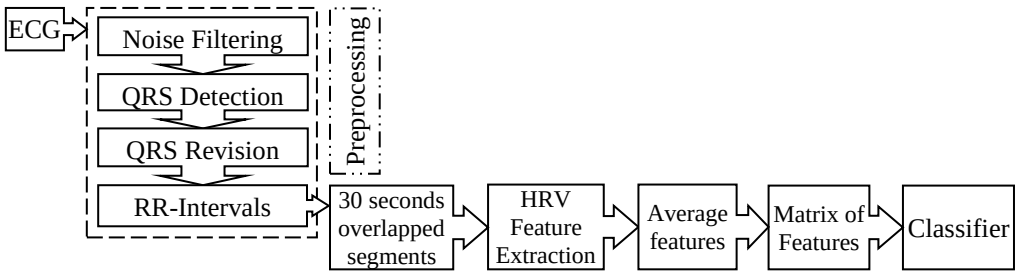

Figure 5.20. Schematic representation of the first step of phase III of our proposed ECG system for apnoea detection using HRV features.

5.2.3. Phase III: optimising apnoea detection

In phase III, we optimised the final system performance and boosted the results of the top performing EDR signal by deriving further features, combining the features and optimising the temporal information for the apnoea detection. The results of this phase are demonstrated in three measures; one-minute epoch apnoea classification, AHI estimation and subject-based apnoea detection.

First, we extracted the RR-interval (HRV) features, with the signal processing steps shown in the block diagram in Figure 5.20. In this approach, noise removal was applied to the ECG signals (see sections 3.3, 3.4 and 3.5.1). RR-intervals were computed using QRS complexes provided with the *MIT PhysioNet Apnea-ECG* database and using the output of the Hilbert QRS detection algorithm for *St. Vincent's* database, as discussed in section 3.4. In order to refine the performance of the QRS detector, a QRS revision algorithm was carried out and the sequence of improved RR-intervals were obtained (see section 3.4 [38]).

Two temporal optimisation methods were applied to every feature set measurement in this phase. According to the results of the studies by de Chazal *et al.*, a 30-second overlap applied to every one-minute epoch improves the results of apnoea detection [320]. Thus, the 34 features (the average and standard deviation of the signal amplitude plus 32 interval-based PSD features) were derived from 30 seconds overlapped one-minute epochs of the corrected RR-intervals (see sections 3.6.2 and 5.1.4). The authors also found that adjacent epochs are not independent in sleep apnoea classification and by averaging the features of every epoch with the features of the adjacent epochs, the relation of the surrounding epochs is taken into account and the classification performance can be further improved [69], [71]. According to the results of the study, we chose to average every seven adjacent segments, which was indicated to produce the maximum accuracy for classification [71]. Through this approach, the features of every one-minute epoch was replaced by the averaged features of the epoch with the three neighbour epochs on each side. It should be noted that the features of the first three and last three epochs were averaged with the available neighbours. Finally, the matrix of the averaged HRV features was applied to the classifier for apnoea detection

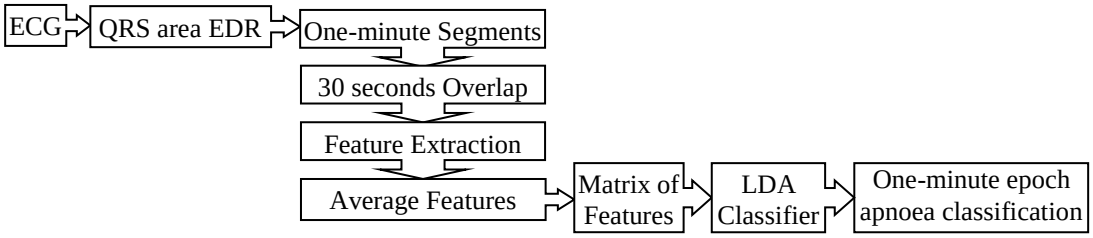

Figure 5.21. Schematic representation of the second step of phase III, optimising sleep apnoea detection, using two methods of 30 seconds overlaps of the epochs and averaging the features of every three epochs.

The other feature set extracted in this phase are cardiopulmonary coupling (CPC) features (see section 3.6.1 with the block diagram shown in Figure 3.6). To calculate the CPC features, the DFT was applied on 30 seconds overlapped one-minute epochs of both zero-mean RR-intervals and the highest performing EDR signal (QRS area method) which were zero padded to 256-points. Then, the pairwise multiplied DFT coefficient was used to measure the absolute value. Finally, every four adjacent bins were averaged and first half of the 64 points were used as 32 CPC features (*cycles/intervals*). Finally, the second temporal optimisation method, the seven epochs averaging of the features, was applied to the CPC feature set which was then used for sleep apnoea classification.

The other feature set was extracted from the highest performing EDR signal (QRS area method), with the block diagram shown in Figure 5.21. In this step, the EDR signals were first segmented into one-minute epochs. The features (32 PSD features, average and standard deviation) were produced for one-minute epochs overlapped by 30 seconds [320]. Then, the features of every seven epochs were averaged and the matrix of averaged features was applied to the classifier for sleep apnoea detection.

The LDA classifier was utilised for the optimisation phase as it showed the highest performance in the previous sections as well as it provides a simple and fast computational process. The LDA model was optimised using the maximum likelihood estimators for the mean and common covariance matrix and the class with the highest posterior probability estimate selected as the winning class.

In addition to apnoea classification using every individual features set, we used the late integration approach for apnoea detection using the combined features. The 34 EDR features, 34 HRV features and 32 CPC features measured over each one-minute epochs were used to form a combined feature set. Thus, it resulted in a matrix of 100 features for every minute of the ECG recording and was

Table 5.14. The cross-validation results of 35 recordings of PhysioNet dataset for averaged features of each three adjacent epochs.

Features	Accuracy (%)	Sensitivity (%)	Specificity (%)	AUC
		LDA classifier		
QRS EDR	84.6±3.5	81.6	87.7	0.92
RR	83.4±2.2	80.9	89.8	0.90
CPC	87.7±1.4	86.8	88.8	0.94
QRSEDR+RR+CPC	89.2±1.6	89.9	87.9	0.95

CPC = Cardiopulmonary Coupling, 34 EDR, 34 RR, 32 CPC

applied to the LDA classifier. The cross validation results of apnoea identification by three feature sets and the combined features for the two databases are demonstrated in Table 5.14 and Table 5.15.

As revealed for the 35 recordings of the *MIT PhysioNet* dataset, the highest performance of apnoea recognition among the individual features corresponds to the CPC signals with accuracy of 88%, sensitivity of 87%, specificity of 89%, and ROC AUC of 0.94, followed by the EDR features with accuracy of 85%, sensitivity of 82%, specificity of 88% and ROC AUC of 0.92. The combined features obtained the highest apnoea classification with an accuracy of 89%, sensitivity of 90% and specificity of 88%, and AUC of 0.94.

The results of the 25 recordings of the *St. Vincent's* dataset (Table 5.15) revealed that among the individual features, CPC achieved the highest accuracy of 70% and ROC AUC of 0.74, while among all, the combined features obtained the highest accuracy of 71% and ROC AUC of 0.75.

In the second step of phase III, after obtaining one minute epoch classification, the AHI was estimated by measuring the number of one-minute epochs labelled as an apnoea class over the total length of the recording (in minutes). The predicted apnoea index versus the true apnoea index provided with the datasets is presented for both datasets in Figure 5.22. The *MIT PhysioNet* data contains recordings in three classes including, apnoea class, borderline, and normal or control class. The apnoea class includes recordings with more than an hour with apnoea index of over 10 which also should include more than 100 minutes of apnoea epochs (20 records). The borderline class comprises of the recordings with minimum an hour of apnoea index of 5 or more which also should include 5 to 99 minutes of apnoea epochs (5 records). The third class is the normal class which corresponds to the recordings with less than 5 minutes of apnoea epochs (10 records). For the *St. Vincent's* dataset, apnoea class was defined as the records with AHI over 10 while the normal class corresponds to the records with AHI below 10. The results of AHI estimation for *MIT PhysioNet* dataset (Figure 5.22(a)) shows that all of the records with apnoea labels and normal labels were classified correctly. The results of AHI for the *St. Vincent's* database shows that only two records with an apnoea label and two records with normal labels were classified incorrectly.

The confusion matrices for two databases are shown in Table 5.16 and Table 5.17. With the labelling scheme of the *MIT PhysioNet* database, explained above, the data between AHI of 5 and 10 is labelled

Table 5.15. The cross-validation results of recordings of St. Vincent's dataset for averaged features of each three adjacent epochs.

Features	**Accuracy (%)**	**Sensitivity (%)**	**Specificity (%)**	**AUC**
		LDA classifier		
QRS EDR	67.8±1.4	70.0	61.5	0.64
RR	67.5±2.2	67.9	66.5	0.68
CPC	69.6±2.0	70.9	64.9	0.74
QRSEDR+RR+CPC	70.6±1.9	72.8	69.9	0.75

CPC = Cardiopulmonary Coupling, 34 EDR, 34 RR, 32 CPC features

Table 5.16. The confusion matrix for MIT PhysioNet database.

		Actual		
		Normal	Borderline	Apnoea
Predicted	Normal	8	0	0
	Borderline	2	1	0
	Apnoea	0	4	20

as borderline. Accordingly, two of the normal records are classified as borderline, four records from borderline class are classified as apnoea and one borderline data is classified as the borderline. All of the records from apnoea class (AHI over 10) were classified correctly (*TP = 20*). The confusion matrix of St. Vincent's database shows the two classes of normal (AHI less than 10) and apnoea class (AHI over 10).

Finally, we measured the subject-based sleep apnoea detection. Using the AHI measures, the record-based apnoea detection was achieved by labelling the records with AHI of over 10 as sleep apnoea patient and the subjects or records with AHI of less than 10 as normal subject. It revealed that our algorithm discriminates normal from apnoea records for *MIT PhysioNet* database with an accuracy of 100% and for *St. Vincent's* database with an accuracy of 84%. The performance difference of the two databases probably relates to the heterogeneity of the *St. Vincent's* database containing recordings from control subjects and patients with obstructive, mixed and central sleep apnoea events; while, the *MIT PhysioNet* recordings are obtained from control subjects and obstructive sleep apnoea patients. The results will be further discussed in the following section.

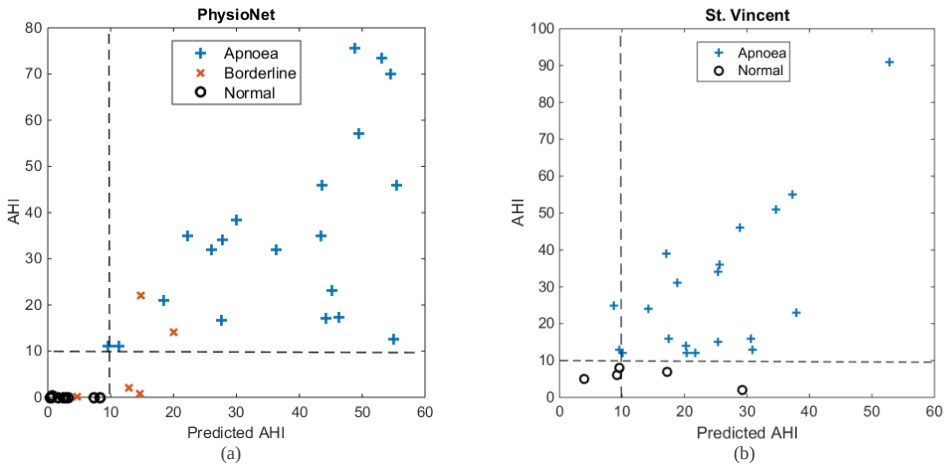

Figure 5.22. Predicted AHI by LDA classifier versus target AHI for; a) PhysioNet dataset which the records with AHI over 10 are classified as apnoea and the other records with AHI of less than 10 were categorized as normal or control. The dataset also contains records annotated as borderline which were classified in either of two classes. b) St. Vincent dataset that the records with AHI over 10 classified as apnoea and those with AHI less than 10 labelled as normal.

Table 5.17. The confusion matrix for the St. Vincent's database.

		Actual	
		Normal	Apnoea
Predicted	Normal	3	2
	Apnoea	2	18

5.3. Discussion

The results of the developed algorithms were examined in three main phases and the same order of the phases is followed in this section for discussing the results.

5.3.1. Phase I

We proposed two algorithms based on the PCA method to enable EDR estimation from lengthy recordings such as ECG signals. For apnoea detection studies, PCA analysis of overnight recordings is required and the need to store a large covariance matrix leads to a standard PC running out of memory. For the PCA algorithm, the dominant computation is the calculation of the eigenvalues and eigenvectors, which grows with the cube of the length of the recording [321]–[323], which places a limit on the length of the ECG recording that can practically be processed. The size of the covariance matrix for the PCA based method calculated over each full recording (with an average length of 8 hours at 100 Hz sampling rate) was approximately 30,000 × 30,000. Thus, the memory required for the PCA method to be applied to an average full recording was over 8 GB which was not plausible with a standard PC (Core i7 processor and 8GB RAM).

We developed two methods (segmented and approximated PCA) to resolve the computational issues of this PCA application on lengthy recordings. The approximation method is computationally fast and has low memory requirements compared to the full PCA method. The average memory required for the EDR estimation of the overnight recordings using approximated PCA method is 1 GB and the computation grows linearly with the length of the recording. The memory required for the segmented PCA method is approximately 3 GB and the computation again scales with the length of the recording. Compared to the memory required for applying the full PCA method to an overnight recording which is about 9 GB, our developed methods save memory space. Our presented methods performed well on overnight ECG recordings and can also process even longer signals if required.

The other important factor in processing the ECG, besides the performance measures and memory requirement is the processing time. The two proposed PCA based techniques reduced the computation time for EDR estimation. As reported in section 5.2.3, the processing time of EDR measurement of a

sample overnight ECG recording for the segmented PCA method was about 4.3 seconds, and the approximated PCA required about 0.3 seconds on a standard PC with Core i7 processor. When we estimated EDR using the original PCA method on a sample overnight ECG recording on a specialised desktop computer with 64GB of memory, the processing time was over an hour. We also note that the processing time for the EDR estimation of a sample recording using the QRS area method was 0.041 seconds.

Overall, the innovation of the proposed algorithms was rectifying the high memory requirement of the full PCA method for processing lengthy recordings. More importantly, the computation and processing time scaled with the length of the recording rather than the cube of the length of the recording required by the full PCA method without compromising the accuracy.

The computational limitations, mentioned in previous studies of PCA methods for EDR estimation, have restricted the implementations to use a selection of recordings of less than an hour [70], [72], [73]. For instance, Widjaja *et al.* in 2012 manually selected 5 minutes of the total recording per subject and applied the PCA method [73]. Another study on PhysioNet dataset by Varon *et al*. in 2015 using PCA method for EDR estimation selected 6000 ECG segments for the training set (324 minutes from 34 recordings in total), reporting an accuracy of 84.74%, a sensitivity of 84.71%, a specificty of 84.69% and a AUC of 88.07% for their optimised system [72]. In contrast, we utilised 35 full recordings (35×500 segments) and applied the developed algorithm to the full recordings with comparable results to Varon *et al*.

To our knowledge, we are the only team that has applied PCA to estimating the EDR on full overnight ECG recordings. The approximated and segmented PCA methods can be useful for other problems with high dimensional signal analysis.

It should be noted that multiple iteration comparison and the hyperparameter searching to optimise the machine learning techniques can introduce a bias to the model. It is increasingly recognised in multilayer neural networks that the hyperparameter searching, whether explicitly performed or implicitly, by the usual human-in-the-loop search for optimal network structures and parameters, represents a type of overfitting [324]–[328]. The overfitting occurs due to the fact that it feeds back and corrects the error on the test data set, rather than the training dataset.

5.3.2. Phase II

In phase II of this analysis, we answered the question that appears to be unanswered in the literature thus far; "in comparison to the actual respiratory effort signals, how well does the EDR capture breathing information relevant for sleep apnoea detection?". Remarkably close performance on the *MIT PhysioNet* database was achieved from the LDA classifier for the full respiratory signal and the HR-resampled respiratory signal (see Table 5.12 and Table 5.13). The sensitivity and specificity of

HR-resampled respiratory signal were also comparable with results from the full respiratory effort signal.

The highest performance in sleep apnoea detection using the EDR signals was achieved by the QRS-area method using the LDA classifier. Moreover, exploring the ROC of the respiratory effort signal in comparison with the QRS-area EDR signal provided further evidence of their comparable performance in the apnoea detection. This suggests that despite the sub-sampling process, which substantially reduced the number of samples from 100 Hz to approximately 1 Hz (considering average human heart rate), the information significant for sleep apnoea detection is still retained by these sub-sampled signals. While, there is some degradation of the discriminative information in the EDR signal relative to the respiratory effort signal, there still seems to be sufficient information for the EDR signal to be of use for accurate apnoea classification.

When we compared the performance results of the EDR methods (QRS-area, segmented PCA and approximated PCA), the QRS area method surpassed the PCA techniques and was closer to the result of the respiratory effort signal. Moreover, the processing time for estimating the EDR signal using the QRS area method for a sample overnight recording was about eight times faster than that for the approximated PCA method. A visual comparison of the PSD spectrograms (see Figure 5.17) revealed that the respiratory patterns and the variations corresponding to the apnoea labels are distinguishable in every respiratory signal and EDR signal. The resemblance is quite apparent in the spectrograms of the respiratory signal and the HR sampled respiratory signal compared to the EDR signals. In fact, the QRS area EDR spectrogram appears to capture the steady breathing activity during normal breathing better than the PCA based EDRs. A reason behind this can be the fact that we did not detect and eliminate the ectopic beats and they may have affected the PCA-based measurement, while they may have less impact on the linear QRS area method. The ROC comparison also confirmed that the QRS area EDR leads to the highest AUC among the EDR methods, which is almost equivalent to the AUC of the respiratory effort signal. Thus, the QRS area method was chosen as the highest performing EDR signal for apnoea detection for optimising the final system (for phase III).

We note that the trends of the performance results of the *St. Vincent's* database for the respiratory signals are different from the results of the *MIT PhysioNet* database (see Table 5.12 and Table 5.13). The respiratory effort signal obtained an accuracy of 68% and the HR-resampled respiratory signal achieved an accuracy of 62%, all three EDR methods obtained an accuracy of 66% for the *St. Vincent's* database. We hypothesise that the difference in the trends is due to the 8 Hz sampling rate of the respiratory effort signals of the *St. Vincent's* database. When the respiratory signal was resampled at the heart beats, extra quantisation noise was introduced into the system as each heart beat was quantised to the nearest $1/8^{th}$ second. This potentially degraded the performance results of

the HR resampling respiratory signals. An obvious area of future work is to compare the methods on other databases where the respiratory signals are acquired at a higher sampling rate.

We also examined the performance of three automated machine learning algorithms (see Table 5.12 and Table 5.13). The highest performing approach was the LDA with almost equivalent performance results obtained by the SVM. Thus, based on the similar results of LDA and SVM, utilising LDA was preferred as it provided simpler and much faster processing. We found that the performance of the ELM classifier was notably worse than the other two methods. It can been observed from the histograms of the input features and hidden units outputs of the ELM classifier, shown in Figure 5.19, that the ELM interferes with the Gaussian distribution of the input data. By randomly combining the input data and applying a non-linear transformation, the distribution of the resulting data was highly non-Gaussian, which we hypothesised caused the poor performance of the ELM classifier. To explore this further a linear regression classifier, which is equivalent to an ELM classifier with no hidden layer, was used to process the data. The results of the linear regression classifier showed better performance (an accuracy of 87% for the respiratory signal and 84% for the QRS area EDR signal of the PhysioNet dataset) compared to the ELM classification results. This confirmed that in our application, there was no benefit from the non-linearity and randomly combining features and projecting the features to a higher space using the ELM classifier.

Interestingly, both QRS EDR method and the LDA classifier that were chosen as the highest performing technique and they both involve the simplest implementation and the least computational effort.

Overall, the reduction in apnoea detection introduced by the EDR process does not appear to be related to the heartbeat sampling process, but is likely due to fact that the EDR only detects the chest wall movement at one site. Nevertheless, given the reduced invasiveness to the patient by the ECG sensor compared to the chest band, we believe that the results demonstrate that the EDR does capture worthwhile breathing effort information for sleep apnoea detection. We also note that the HRV information from the ECG is independently useful for the identification of sleep apnoea events and further boosts the performance of an ECG based apnoea detection system. Thus, we added the HRV and CPC information for optimising the performance of the final system in phase III.

5.3.3. Phase III

In phase III, we combined the features of the highest performing EDR method (QRS-area) with HRV and CPC features and applied two temporal based optimisation methods. Our best results using the individual HRV features (accuracy 84%, sensitivity 81%, specificity 90% and AUC 0.90) are comparable with and even outperforms the results obtained by other researchers [190], [267], [329]. Mietus *et al.* in 2000 obtained a minute by minute accuracy of 82.1% and subject-based accuracy of

86.6% on the same *PhysioNet* database [178]. Isa *et al.* in 2010 obtained a minute by minute classification with an AUC of 0.85 with their highest performing model and a subject based classifictaion accuracy of 74% on the *PhysioNet* database [329]. Comparatively, our optimised system obtained 100% subject-specific classification accuracy.

Our apnoea classification results using the QRS area EDR features (accuracy 85%, sensitivity 82%, specificity 88% and AUC 0.92) are also comparable to the results of the previous studies [71], [235]. A study by Correa *et al.* in 2009 compared the apnoea detection of three methods of EDR estimation (R wave area, HRV and R peak amplitude) on eight recordings of the *PhysioNet* database. Their highest performing EDR method obtained both sensitivity and specificity of 88% [235]. In a study by de Chazal *et al.* in 2003, the highest performing model using the EDR features obtained an accuracy of 86%, a sensitivity of 80% and a specificity of 90% [71].

By implementing the CPC features for apnoea recognition, the results surpassed the performance of the EDR and HRV features, presumably as it incorporates the information of both signals. For the final optimisation, we combined the features of the EDR signal with HRV and CPC features after applying the temporal optimisation techniques. The balanced performance measures are evidence of a well-balanced system for apnoea recognition.

The apnoea detection performance results of the *St. Vincent's* database are 16% lower than the results of the *MIT PhysioNet* database and the ROC AUC is 0.18 lower. While there are differences in the results, the trends on the two databases are similar. The performance difference on the two databases probably relates to the selection of the recordings. The *St. Vincent's* database represents a set of recordings from sequentially-admitted patients assessed for suspected sleep apnoea. It contains control subjects and patients with obstructive, mixed and central sleep apnoea events. The *MIT PhysioNet* database was a more homogeneous database as it contains control subjects and patients with primarily obstructive sleep apnoea and who demonstrated bradycardia/tachycardia responses to obstructive events. Given the increased heterogeneity of the *St. Vincent's* database, perhaps it is not surprising our results were not as good as compared to the *MIT PhysioNet* database.

The outcomes of the final system were comparable to the best outputs of the algorithms presented in the literature [38], [71], [72], [63], [241]. A study by Schrader *et al*. in 2000 on the PhysioNet database reported an accuracy of 87.6% [188]. Mendez in 2007 used an autoregressive model on the *PhysioNet* database and reported an accuracy of 86% [240]. A research by Xie *et al*. in 2012 utilised combined classifiers including, AdaBoost, Decision Stump, Bagging and SVM and feature selection from ECG and SPO_2 , which showed the highest accuracy of 84.4% and a specificity of 85.9% [241]. A study by de Chazal *et al.* in 2003 obtained the highest results using the RR-interval features and the EDR features with the LDA classifier with an accuracy of 90.0%, a sensitivity of 86.4% and a specificity of 92.3% [71].

An objective of this study was to extend the work by de Chazal *et al.* in 2003 [71]. To achieve this, we undertook a comprehensive evaluation of the system by comparing the performance of different classifiers and EDR estimation methods, as well as an additional novel feature extraction for sleep apnoea detection. In this thesis, we implemented different EDR methods (QRS area, segmented PCA, approximated PCA and kernel PCA) and extracted CPC features. We compared the respiratory information of the EDR methods with the chest respiratory effort (RIP) signals. We also evaluated the performance results using three different machine learning techniques (LDA, ELM and SVM classifier). Moreover, we assessed the performance of the algorithms on two databases when comparing the methods. Interestingly, our results show that the highest performing methods are similar to the approaches used in the work by de Chazal *et al.* in 2003 [71].

Another noteworthy achievement was that our final ECG based classification system outperformed (with an accuracy of 89% and an AUC of 0.95) the performance results of the RIP respiratory signals (with an accuracy of 87% and an AUC of 0.94 for the *MIT PhysioNet* database). Similar behaviour was seen for the *St. Vincent's* database, where the results for the ECG outperformed the RIP respiratory signals. The advantage is that the respiratory information is captured from the ECG recordings without the need of a sensor on the torso. Overall, the automatic apnoea recognition results of the final phase by optimising the final system were comparable to the best results reported in the literature.

To recapitulate, the main results of this application are as follows:

1) We proposed two algorithms for PCA calculation, which enabled the EDR to be estimated from lengthy ECG recordings. Our algorithms required much less memory than the published PCA methods. The computational requirements increased linearly with the length of the recording rather than the cube of the length of the recording which was the case for the existing methods. With this innovation, we were able to apply this method to overnight ECG recordings, which has not been feasible in the literature thus far.
2) We answered the question that appears to be unanswered in the literature; "in comparison to the respiratory effort signals, how well does the EDR capture relevant breathing information for sleep apnoea detection". Our research indicates that the heart rate sampling inherent in the EDR process does not have a large impact on the discriminative information required for sleep apnoea classification. While, there is some degradation of the discriminative information in the EDR relative to the respiratory effort signal, there still seems to be sufficient information for the EDR to be of use for accurate apnoea classification.
3) Three different EDR measurement methods were evaluated and the highest performing EDR signal for apnoea detection was the QRS area method.

4) Three automated machine learning algorithms were compared for the sleep apnoea classification and the highest performing approach was the LDA classifier followed closely by the SVM. We found that the performance of the ELM classifier was notably worse than the other two methods.
5) We combined the features of the EDR signal with HRV and CPC features. When we applied temporal optimisation techniques (overlapped epochs and averaging the features of every seven epochs) to this system, we obtained comparable classification performance to the best results of the literature.
6) Our final system using only discriminative information from the ECG signals outperformed the system based on the RIP sensors. As the ECG system is a more tolerable to a patient than the RIP sensors, we have developed a more convenient and better performing system from the patient's perspective.

5.4. Summary

In this chapter, we described the algorithms developed in this thesis for the automated diagnosis of sleep apnoea. For this application, we commenced with explaining the characteristics of the recordings of the two utilised databases. We then described the methods applied to the chest respiratory effort signals. It was followed by explaining the signal processing algorithms applied to the ECG system and estimating the EDR signals including, the QRS area method, the standard PCA and kernel PCA. Then, we illustrated the two developed algorithms extending the EDR estimation using PCA method for the overnight recordings (the segmented PCA and approximated PCA). We also explained the interval based PSD feature measurement for this application.

Finally, we presented the results obtained for the second application in three phases. In phase I, we demonstrated the results of the EDR estimation methods (QRS area, standard PCA and kernel PCA) and extending the PCA method for measuring the EDR signal of the overnight recordings (segmented PCA and approximated PCA). We also showed the results for different hyperparameters of the ELM classifier and chose the highest performing hyperparameter. In phase II, we showed the results of respiratory information comparison of the EDR signals against the chest respiratory effort signals in two ways: sample based correlation and apnoea classification. We compared three methods of EDR estimation (QRS area, segmented and approximated PCA) with three respiratory effort signals (full signal, HR-sampled and uniformly sampled signal). We also compared the performance of three automated machine learning algorithms (LDA, ELM and SVM) for apnoea classification. The outcome of this phase was choosing the highest performing EDR signal and classifier for the next phase. In phase III, the features extracted from the highest performing EDR signal (QRS area method) was combined with HRV and CPC features and applied to the highest performing classifier (LDA classifier). Two optimisation methods (30 seconds overlapped epochs and seven epochs feature averaging) were also applied. The results of apnoea classification with every individual feature set were compared to the combined features. Ultimately, we demonstrated the results of AHI estimation and subject based apnoea detection for both databases.

In the final section, the results of this application and the advantages and disadvantages of the developed algorithms were discussed in detail.

In the following chapter, we propose the concluding remarks and the future directions of the two applications of this thesis.

Chapter 6

Conclusion and future work

6. Conclusion and future work

In the previous chapters, the developed algorithms of this thesis for both applications were described and the performance results were discussed. The advantages and disadvantages of the proposed algorithms and the main outcomes were highlighted. In this chapter, the concluding remarks and the future directions are proposed for both applications addressed in this thesis.

In this thesis, two categories of cardiorespiratory disorders were addressed, including critical arrhythmias and sleep disordered breathing. For the first application, we aimed to reduce the false arrhythmia alarms in the ICU and for the second application, we aimed to reduce the number of diagnostic sensors for automated sleep apnoea detection. We were successful in achieving these goals and were able to improve the performance of the current automated diagnostic systems. Although, we optimised our proposed algorithms and improved the performance results of our automated diagnostic systems to be comparable to the best results in the literature within the timeframe of this study, further work may enhance the results and extend the developed algorithms. In this chapter, I highlight the concluding remarks of both applications and list different strategies that can possibly enhance the performance results.

6.1. Application 1

In the first application, we developed algorithms to detect five critical arrhythmias and reduced the false arrhythmia alarms in the ICU and submitted a successful entry to the *PhysioNet/Computing in Cardiology Challenge 2015*. Customised signal processing approaches were used for individual arrhythmia alarm detection. The records were processed in the following order for arrhythmia detection; asystole, extreme bradycardia, extreme tachycardia, followed by ventricular fibrillation/ flutter (VFB) and ventricular tachycardia (VTA). We developed a hierarchical approach for processing four multimodal signals (Lead II and augmented right arm ECG signals, ABP and PPG).

The algorithm first analysed the asystole alarms. Features were extracted from the four available signals. The ECG signals were first processed without SQI evaluation, and then the pulsatile signals (ABP and PPG) were analysed. The algorithm obtained a TPR of 78%, a TNR of 93% and a score of 82.46% for asystole alarms.

Then, the bradycardia alarms were detected by processing the pulsatile signals (first ABP, followed by PPG signals) which resulted in a TPR of 100%, TNR of 52% and a score of 71.13% on the test set.

Next, the tachycardia alarms were detected using the same order of signal processing as for the asystole detection; the ECG II signal, followed by ECG aVr and the pulsatile signals (ABP and PPG).

The noise reduction was applied to the ECG signals and the ECG SQI evaluation tests and the thresholds of the SQI criteria were adapted for tachycardia records. Our proposed system achieved the highest score of the entries at the *Computing in Cardiology Challenge 2015* in detecting tachycardia false alarms on the test set with a score of 99.10%, TPR of 100% and TNR of 80%.

The VTA detection was conducted based on the raw ECG signal processing (ECG lead II, followed by ECG aVr) using template matching without noise removal and SQI evaluation. It resulted in a TPR of 91%, TNR of 55% and score of 58.07% for VTA detection on the test set.

Finally, the VFB alarms were detected using the pulsatile signals (ABP followed by PPG signal) and achieved a TPR of 100%, a TNR of 59% and a score of 65.52%.

The overall result obtained by our algorithms was a score of 74.03% with 98% TPR and 66% TNR for retrospective and a score of 69.92% with 95% TPR and 65% TNR for real-time analysis. Our result placed us among the top ten scores of the *PhysioNet/Computing in Cardiology Challenge 2015*.

Our best performing algorithm used multimodal signals, combining the information from ECG and pulsatile signals, and we extracted and evaluated a number of features from the signals for alarm identification. Modification of the signal quality measures for different arrhythmias (rather than using a fixed SQI measure for every arrhythmia), setting the quality threshold in an iterative performance evaluation, and considering various possible effects of each arrhythmia on the features of the signals enhanced the arrhythmia identification performance.

The developed algorithm for this application could still benefit from improvements on detecting VTA and VFB. An analysis of the algorithms of the top scored entries to the *Computing in Cardiology Challenge 2015* revealed that better VTA and VFB alarm detection was achieved through algorithms that included phase wrapping [177], adaptive frequency tracking and adaptive mathematical morphology approach [222], descriptive statistics and hand-selected transform and QRS detection by amplitude envelopes using Fourier and Hilbert transform [176]. In our approach, the ECG signals were not utilised for the VFB and extreme bradycardia detection algorithms due to the noisy signals and the low performance of the QRS detection algorithm. Thus, using the above methods could enhance the extracted features and the QRS detections. Hence, incorporating the ECG information and further features can improve the false alarm detection of these arrhythmias.

We applied a multimodal fusion algorithm which we trialled and abandoned as it did not result in improvement in the performance outcomes. It aimed to boost the heart rate identification by multimodal signal integration and examining the detected QRS complexes of the ECG signals and the detected pulse onset beats of the pulsatile signals. We adapted the fusion method proposed in the *PhysioNet/Computing in Cardiology Challenge 2014* by Johnston *et al.* [149]. Further work could improve the integration technique by finding an optimum matching rate and adjusting the delay for the available signals. Using an optimised signal fusion technique and correcting the QRS detections

and the pulse onset beats by switching between the signals with the highest quality could enhance the overall performance results of the multimodal signal processing system.

We also found that varying the threshold setting of the SQI measures significantly affected false alarm detection. Thus, implementation of parameter optimisation methods such as SVM (support vector machine) as a threshold tuning and model selection algorithm could improve the performance results.

An interference removal algorithm was not applied to the ECG signal for the VTA arrhythmias in our system. In fact, our noise removal algorithms were designed to remove the noise to which the VTA signals exhibited similar behaviour. For further improvement, a redesign of our noise removal algorithms so they did not knock out the VTA signal could possibly enhance the results.

Also some of the other teams at the *CinC Challenge 2015* used machine learning techniques for feature selection and arrhythmia detection, which reduced the false alarms [32], [330], [331]. We have not applied feature selection. Thus, applying machine learning techniques for arrhythmia classification and comparing the performance of different approaches to find the optimum technique for this application can further reduce the false alarms.

In summary, for future false alarm management systems, a modified noise removal algorithm, adaptive SQI measurements for each arrhythmia, using machine learning techniques for detection, multimodal signal integration with optimum matching rate and adjusted delay could improve the performance.

6.2. Application 2

The second application of this thesis provided automated signal processing algorithms for the diagnosis of sleep apnoea with the main focus on the ECG signal processing. The evaluation of the results was carried out by comparing the performance against the use of the chest RIP signals, which was performed in three phases.

In phase I, we proposed two algorithms for PCA based EDR estimation of long duration signals such as the overnight ECG recordings. The approaches incorporated a segmented PCA method executed on 30 minutes segments over the entire overnight ECG recordings and a fast approximation PCA technique. The computation and processing time of the proposed PCA algorithms were scaled with the length of the recording rather than the cube of the length of the recording required by the full PCA method. Thus, our presented methods are computationally fast with low memory requirements and resolved the computational issues of the PCA application on the lengthy recordings, which had limited the EDR estimation of the previously published studies to use a selection of short data.

In the first step of the PCA method application, we formed a matrix of the centred QRS complexes. The results showed that the QRS complexes are well centred for most of the recordings. However, we

observed some recordings with ectopic beats that required better alignment of the QRS complexes. For future work, developing an automated algorithm which could detect the ectopic beats could help further improvements. By automated classification of the beats into normal and abnormal beats and the removal of the ectopic beats, the EDR signals could be measured for the normal beats and could form better-centred matrix of features to improve the performance.

We were also unable to confirm the benefits of the kernel PCA method that were presented in the literature. For future development, we could perform kernel PCA on other databases and also automatically detect and exclude the ectopic beats in order to improve the performance of the kernel PCA algorithm.

In phase II, we evaluated the respiratory information using three methods of EDR estimation (QRS area, segmented PCA and approximated PCA method). We compared their performance in the diagnosis of sleep apnoea against the chest respiratory effort signal. We also evaluated the performance of three automated machine learning algorithms (ELM, LDA and SVM) for sleep apnoea detection. The highest performance in sleep apnoea detection was obtained using the LDA classifier using the full respiratory signal with an accuracy of 87.4%, a sensitivity of 85.6%, a specificity of 90.2% and a ROC AUC of 0.94 for the *MIT PhysioNet* database. The performance results of the full respiratory signal from the *St. Vincent's* database obtained an accuracy of 67.9%, a sensitivity of 68%, a specificity of 67.7% and a ROC AUC of 0.65. However, remarkably close performance was achieved using the heartbeat resampled respiratory signal with comparable sensitivity and specificity-the accuracy being 86.4%, sensitivity of 83.4%, specificity of 90.7% and AUC of 0.94 for the *MIT PhysioNet* database. The highest performing EDR method was based on the QRS area method and the result was closer to the respiratory effort signal performance – an accuracy of 81.3% with a sensitivity of 84.2%, specificity of 77.1% and a ROC AUC of 0.91 for the *MIT PhysioNet* database and accuracy of 65.6% with a sensitivity of 66.6%, specificity of 62.7% and ROC AUC of 0.59 for the *St. Vincent's* database. The QRS area-EDR method and LDA classifier performed the best in this analysis and therefore, were chosen for the optimisation of the final apnoea detection system. Overall, we found that while the sample-based correlation of the EDR signals and the chest respiratory effort signals showed low results and there is some information loss in the EDR estimation process, the EDR signal contains the hidden information of respiratory patterns which is functional in sleep apnoea diagnosis and provides a convenient approach. For future work, the EDR and respiratory signals can be divided into shorter segments for better correlation coefficient measurements. In fact, a study by Widjaja *et al.* in 2014, which measured the correlation between the EDR signal and respiratory signal, used only 5 minutes of the entire dataset [332].

A future area of study is to understand why the QRS area based EDR method outperformed the PCA based methods. The reduction in apnoea detection introduced by the EDR process compared to the respiratory effort signal recorded using RIP sensors does not appear to be related to the heartbeat

sampling process, but is likely due to fact that the EDR only detects the chest wall movement at one site. An area of further work is to look at multisite EDR and see if this improves the detection accuracy.

One of the utilised machine learning techniques in this thesis was the ELM classifier. It has been introduced in the literature as a suitable classifier for biological signal processing applications. In this application, it did not perform as well as the other techniques (the LDA and the SVM classifier). In order to investigate the reason of the low performance of the ELM classifier, I evaluated the histograms of the input features and the hidden units outputs and performed a linear regression classifier. They revealed that the non-linearity and random projection to higher space of the ELM classifier disturbed the Gaussian distribution of the input features. It may benefit from further optimisation and the use of other non-linear functions for hidden layer units and application of regularisation techniques to enhance the results.

In phase III, we optimised the apnoea detection performance of the final system by extracting HRV and CPC features from the ECG signal and combining them with the highest performing EDR features (the QRS area method). We also performed temporal optimisation methods by implementing overlapped one minute epochs and averaging the features of every seven adjacent epochs. We compared the apnoea classification results of the individual feature sets with the combined feature set using the late integration approach. The highest apnoea recognition results among the individual features were obtained by the CPC features with an accuracy of 88%, a sensitivity of 87%, a specificity of 89% and a ROC AUC of 0.94, followed by the EDR features with an accuracy of approximately 85%, a sensitivity of 82%, a specificity of 88% and ROC AUC of 0.92 for the *MIT PhysioNet* dataset. The combined features achieved the highest apnoea classification with an accuracy of 89%, a sensitivity of 90% and a specificity of 88%, and the AUC of 0.95. The AHI estimation and the record-based apnoea classification demonstrated that our algorithm discriminates normal records from apnoea records with an accuracy of 100% for the *MIT PhysioNet* database and an accuracy of 84% for the *St. Vincent's* database. The performance difference of the two databases probably results from the heterogeneity of the *St. Vincent's* database containing recordings from control subjects and patients with obstructive, mixed and central sleep apnoea events; while, the *MIT PhysioNet* database was recorded from control subjects and obstructive sleep apnoea patients.

Overall, applying the temporal optimisation techniques and combining the CPC features with HRV and EDR features boosted the performance of sleep apnoea diagnosis using the ECG signals and outperformed the results of the RIP respiratory signals. Thus, we successfully developed an automated apnoea detection system performing on overnight ECG signals which obtained comparable performance to the best results in the literature. The advantage of the proposed algorithm is that the respiratory information is captured from ECG recordings without the need of a sensor on the torso which reduces the disturbance to the patients.

Future work could also consider processing the HRV, EDR and CPC signals with separate classifiers and then combining the outputs with a majority vote technique. This would offer the advantage that if a feature group is corrupted by an artefact, it may be compensated by the other feature groups (if they are not affected).

It should be noted that the common methods used in both applications of this thesis, including the baseline wander noise removal algorithm, the Hilbert QRS detector and the HRV feature extraction such as the PSD features, performed well for both applications and improved the results. On the other hand, evaluating the SQI, which was used in the first application for arrhythmia detection in the ICU, could also be used for the second application to further improve the performance results of sleep apnoea detection. Similarly, identifying the arrhythmias in the sleep apnoea recordings may help in obtaining more information about the sleep disordered breathing and also identifying possible comorbidities. This could provide a more comprehensive evaluation in the future.

7. References

[1] American Academy of Sleep Medicine, “AASM - Manual for the Scoring of Sleep and Associted Events,” *AASM*, pp. 3–59, 2007.

[2] American Academy of Sleep Medicine, “Obstructive Sleep Apnea,” *AASM*, 2008.

[3] C. N. Joseph, C. Porta, G. Casucci, N. Casiraghi, M. Maffeis, M. Rossi, and L. Bernardi, “Slow breathing improves arterial baroreflex sensitivity and decreases blood pressure in essential hypertension.,” *Hypertension*, vol. 46, no. 4, pp. 714–8, Oct. 2005.

[4] G. Thomas and V. Duffin-Jones, “Monitoring arterial blood pressure,” *Anaesth. Intensive Care Med.*, vol. 16, no. 3, pp. 124–127, 2015.

[5] B. H. McGhee and E. J. Bridges, “Monitoring arterial blood pressure—what you may not know,” *Crit Care Nurse*, vol. 22, no. 2, 2002.

[6] A. O. Donnell, “The autonomic nervous system,” *New Zeal. Med. Student J.*, vol. 13, pp. 11–13, 2012.

[7] M. J. Parkes, “Evaluating the importance of the carotid chemoreceptors in controlling breathing during exercise in man.,” *Biomed Res. Int.*, vol. 2013, pp. 1–18, Jan. 2013.

[8] C. Sullivan, M. Berthon-Jones, F. Issa, and L. Eves, “Reversal of obstructive sleep apnoea by continuous positive airway pressure applied through the nares,” *Lancet*, vol. 317, no. 8225, pp. 862–865, Apr. 1981.

[9] M. Bsoul, H. Minn, M. Nourani, G. Gupta, and L. Tamil, “Real-time sleep quality assessment using single-lead ECG and multi-stage SVM classifier.,” *Proc. Annu. Int. Conf. IEEE Eng. Med. Biol. Soc.*, vol. 2010, pp. 1178–81, Jan. 2010.

[10] J. M. Mangrum and J. P. DiMarco, “The evaluation and management of bradycardia.,” *N. Engl. J. Med.*, vol. 342, no. 10, pp. 703–709, 2000.

[11] D. Durham and L. I. G. Worthley, “Cardiac arrhythmias: diagnosis and management. The tachycardias,” *Crit Care Resusc*, vol. 4, no. 1, pp. 35–53, 2002.

[12] J. Achten and A. Jeukendrup, “Heart rate monitoring: applications and limitations.,” *Sport. Med.*, vol. 33, no. 7, pp. 517–38, 2003.

[13] N. Netzer, A. H. Eliasson, C. Netzer, and D. A. Kristo, “Overnight pulse oximetry for sleep-disordered breathing in adults: a review,” *Chest*, vol. 120, no. 2, pp. 625–33, Aug. 2001.

[14] M. J. Morrell, P. Palange, P. Levy, and W. De Backer, “Neuroanatomy and neurobiology of sleep,” *ERS Handb. Respir. Sleep Med.*, pp. 1–5, 2008.

[15] M. Tripuraneni, S. Paruthi, E. S. Armbrecht, and R. B. Mitchell, “Obstructive sleep apnea in children.,” *Laryngoscope*, vol. 123, no. 5, pp. 1289–93, May 2013.

[16] American Thoracic Society, “Obstructive Sleep Apnea In Children; Patient Information Series,” *Am. J. Respir. Crit. Care Med.*, vol. 180, pp. 5–5, 2009.

[17] D. A. K. Nicolaus Netzar, Arn H Eliasson, Cordua Netzar, “Overnight Pulse Oximetry for Sleep- Disordered Breathing in Adults,” *CHEST J.*, vol. 120, no. 2, pp. 625–633, 2001.

[18] L. M. Nilsson, “Respiration signals from photoplethysmography,” *Anesth. Analg.*, vol. 117, no. 4, pp. 859–865, 2013.

[19] J. G. Park, K. Ramar, and E. J. Olson, “Updates on definition, consequences, and management of obstructive sleep apnea.,” *Mayo Clin. Proc.*, vol. 86, no. 6, pp. 549–54, 2011.

[20] R. K. A. Allen, “Home sleep studies,” *Aust. Prescr.*, vol. 35, no. 2, pp. 62–4, 2012.

[21] I. Silva, B. Moody, J. Behar, A. Johnson, J. Oster, G. D. Clifford, and G. B. Moody, “Robust detection of heart beats in multimodal data.,” *Physiol. Meas.*, vol. 36, no. 8, pp. 1629–44, 2015.

[22] G. G. Mazeika and R. Swanson, “Respiratory Inductance Plethysmography: An Introduction,” *Pro-Tech Serv.*, vol. 98275, no. 425, p. 13, 2007.

[23] P. de Chazal, C. Heneghan, and C. Chua, “Home-Based Assessment of Sleep Apnoea using Simultaneous Electrocardiogram and Oximetry Signals,” *Prog. Sleep Apnea Res. Chapter 4, Nov. Sceince Publ.*, pp. 115–139, 2007.

[24] P. Openshaw, “Breathing and control of heart rate,” *Br. Med. J.*, vol. 1, no. 6157, p. 199, 1972.

[25] Q. Li and G. D. Clifford, “Signal quality and data fusion for false alarm reduction in the intensive care unit.,” *J. Electrocardiol.*, vol. 45, no. 6, pp. 596–603, 2012.

[26] C. Guilleminault and V. C. Abad, “Obstructive sleep apnea syndromes,” *Med. Clin. North Am.*, vol. 88, no. 3, pp. 611–630, 2004.

[27] M. Pallin, E. O’Hare, A. Zaffaroni, P. Boyle, C. Fagan, B. Kent, C. Heneghan, P. de Chazal, and W. T. McNicholas, “Comparison of a novel non-contact biomotion sensor with wrist actigraphy in estimating sleep quality in patients with obstructive sleep apnoea.,” *J. Sleep Res.*, vol. 23, no. 4, pp. 475–84, Aug. 2014.

[28] M. A. Carskadon and W. C. Dement, “Chapter 2 – Normal Human Sleep : An Overview,” in *Monitoring and staging human sleep, Principles and practice of sleep medicine, 5th edition*, 2011, pp. 16–26.

[29] D. Alvarez, R. Hornero, J. Victor Marcos, F. Del Campo, C. Zamarron, and M. Lopez, “Applying time, frequency and nonlinear features from nocturnal oximetry to OSA diagnosis.,” *Conf. Proc. IEEE Eng. Med. Biol. Soc.*, vol. 2008, pp. 3872–5, 2008.

[30] A. Ravelo-García, J. Kraemer, J. Navarro-Mesa, E. Hernández-Pérez, J. Navarro-Esteva, G. Juliá-Serdá, T. Penzel, and N. Wessel, “Oxygen Saturation and RR Intervals Feature Selection for Sleep Apnea Detection,” *Entropy*, vol. 17, no. 5, pp. 2932–2957, 2015.

[31] U. R. Abeyratne, V. Swarnkar, C. Hukins, and B. Duce, “Interhemispheric asynchrony correlates with severity of respiratory disturbance index in patients with sleep apnea.,” *IEEE Trans. Biomed. Eng.*, vol. 57, no. 12, pp. 2947–55, Dec. 2010.

[32] C. Daluwatte, L. Johannesen, J. Vicente, C. G. Scully, L. Galeotti, D. G. Strauss, and S. Spring, "Heartbeat Fusion Algorithm to Reduce False Alarms for Arrhythmias," *Comput Cardiol*, vol. 42, pp. 745–748, 2015.

[33] G. D. Clifford, I. Silva, B. Moody, Q. Li, D. Kella, A. Shahin, T. Kooistra, D. Perry, and R. G. Mark, "The PhysioNet/Computing in Cardiology Challenge 2015 : Reducing False Arrhythmia Alarms in the ICU," *Comput Cardiol*, vol. 42, pp. 273–276, 2015.

[34] A. Baldzizhar, E. Manuylova, R. Marchenko, Y. Kryvalap, and M. G. Carey, "Ventricular Tachycardias: Characteristics and Management," *Crit. Care Nurs. Clin. North Am.*, vol. 28, no. 3, pp. 317–329, 2016.

[35] S. W. Porges, J. A. Doussard-Roosevelt, and A. K. Maiti, "Vagal Tone and the Physiological Regulation of Emotion," *Wiley Soc. Res. Child Dev.*, vol. 59, no. 2/3, pp. 167–186, 1994.

[36] M. Vadivelan, "Invasive Monitoring in the Intensive Care Unit," *Crit. Care*, vol. 24, no. 5, pp. 430–435, 2013.

[37] A. M. Patel, P. K. Gakare, and A. N. Cheeran, "Real Time ECG Feature Extraction and Arrhythmia Detection on a Mobile Platform," *Int. J. Comput. Appl.*, vol. 44, no. 23, pp. 40–45, 2012.

[38] Y. Donchin and F. J. Seagull, "The hostile environment of the intensive care unit.," *Curr. Opin. Crit. Care*, vol. 8, no. 4, pp. 316–320, 2002.

[39] M. Imhoff, S. Kuhls, U. Gather, and R. Fried, "Smart alarms from medical devices in the OR and ICU," *Best Pract. Res. Clin. Anaesthesiol.*, vol. 23, no. 1, pp. 39–50, 2009.

[40] J. H. Kerr and B. Hayes, "An 'Alarming' situation in the intensive therapy unit," *Intensive Care Med.*, vol. 9, no. 3, pp. 103–104, 1983.

[41] S. Lawless, "Crying wolf: False alarms in a pediatric intensive care unit," *Crit Care Med*, vol. 22, pp. 981–985, 1994.

[42] M. C. Chambrin, "Alarms in the intensive care unit: how can the number of false alarms be reduced?," *Crit. Care*, vol. 5, no. 4, pp. 184–188, 2001.

[43] S. Sendelbach, "Alarm Fatigue," *Nurs. Clin. North Am.*, vol. 47, no. 3, pp. 375–382, 2012.

[44] C. F. Baker, "Discomfort to environmental noise: heart rate responses of SICU patients.," *Critical Care Nursing Quarterly*, vol. 15, no. 2. pp. 75–90, 1992.

[45] S. Bentley, F. Murphy, and H. Dudley, "Perceived noise in surgical wards and an intensive care area: An objective analysis," *Bmj*, vol. 2, no. 6101, pp. 1503–1506, 1977.

[46] S. A. Falk and N. F. Woods, "Hospital Noise — Levels and Potential Health Hazards," *N. Engl. J. Med.*, vol. 272, pp. 489–98, 1973.

[47] B. a Hilton, "Quantity and quality of patients' sleep and sleep-disturbing factors in a respiratory intensive care unit," *J Adv Nurs*, vol. 1, no. 6, pp. 453–468, 1976.

[48] M. A. Pisani, R. S. Friese, B. K. Gehlbach, R. J. Schwab, G. L. Weinhouse, and S. F. Jones, "Sleep in the intensive care unit," *Am. J. Respir. Crit. Care Med.*, vol. 191, no. 7, pp. 731–738, 2015.

[49] S. Parthasarathy and M. J. Tobin, "Sleep in the intensive care unit.," *Intensive Care Med.*, vol. 30, no. 2, pp. 197–206, Feb. 2004.

[50] M. a Novaes, a Aronovich, M. B. Ferraz, and E. Knobel, "Stressors in ICU: patients' evaluation.," *Intensive Care Med.*, vol. 23, no. 12, pp. 1282–1285, 1997.

[51] G. D. Clifford, A. Aboukhalil, J. X. Sun, W. Zong, B. a. Janz, G. B. Moody, and R. G. Mark, "Using the blood pressure waveform to reduce critical false ECG alarms," *Comput. Cardiol.*, vol. 33, pp. 829–832, 2006.

[52] B. Chaska, J. P. Kiley, R. P. Millman, B. A. Phillips, S. D. Rogus, K. P. Strohl, P. J. Strollo, P. M. Suratt, J. K. Walsh, J. W. Weiss, D. White, and B. Zepf, "Sleep apnea: is your patient at risk? National Heart, Lung, and Blood Institute Working Group on Sleep Apnea.," *Am. Fam. Physician*, vol. 53, no. 1, pp. 247–253, 1996.

[53] American Academy of Sleep Medicine Task Force, "Sleep – Related Breathing Disorders in Adults : Recommendations for Syndrome Definition and Measurement Techniques in Clinical Research," *Sleep*, vol. 22, no. 5, pp. 667–689, 1999.

[54] T. Young, P. E. Peppard, and D. J. Gottlieb, "Epidemiology of Obstructive Sleep Apnea," *Am. J. Respir. Crit. Care Med.*, vol. 165, no. 9, pp. 1217–1239, May 2002.

[55] D. Leger, "The cost of sleep-related accidents: A report for the National Commission on Sleep Disorders Research.," *Sleep*, vol. 17, no. 1, pp. 84–93, 1994.

[56] J. A. L. Chesson, R. A. Ferber, J. M. Fry, M. Grigg-Damberger, K. M. Hartse, T. D. Hurwitz, S. Johnson, G. a Kader, M. Littner, G. Rosen, R. B. Sangal, W. Schmidt-Nowara, and A. Sher, "The indications for polysomnography and related procedures," *Sleep*, vol. 20, no. 6, pp. 423–87, 1997.

[57] American Sleep Disorders Association Standards of Practice, "Practice parameters for the indications for polysomnography and related procedures," *Sleep*, vol. 20, no. 6, pp. 406–422, 1997.

[58] N. a Collop, W. M. Anderson, B. Boehlecke, D. Claman, R. Goldberg, D. J. Gottlieb, D. Hudgel, M. Sateia, and R. Schwab, "Clinical Guidelines for the Use of Unattended Portable Monitors in the Diagnosis of Obstructive Sleep Apnea in Adult Patients," *J. Clin. sleep Med. JCSM Off. Publ. Am. Acad. Sleep Med.*, vol. 3, no. 7, pp. 737–747, 2007.

[59] N. a Collop, S. L. Tracy, V. Kapur, R. Mehra, D. Kuhlmann, S. a Fleishman, and J. M. Ojile, "Obstructive sleep apnea devices for out-of-center (OOC) testing: technology evaluation.," *J. Clin. Sleep Med.*, vol. 7, no. 5, pp. 531–48, Oct. 2011.

[60] N. Sadr, J. Huvanandana, D. T. Nguyen, C. Kalra, A. McEwan, and P. de Chazal, "Reducing false arrhythmia alarms in the ICU using multimodal signals and robust QRS detection," *Physiol. Meas.*, vol. 37, no. 8, pp. 1340–1354, 2016.

[61] N. Sadr, J. Huvanandana, D. T. Nguyen, C. Kalra, A. McEwan, and P. de Chazal, "Reducing False Arrhythmia Alarms in the ICU by Hilbert QRS Detection," *Comput. Cardiol. 2015*, vol. 42, pp. 1173–76, 2015.

[62] N. Sadr and P. de Chazal, "Automated Detection of Obstructive Sleep Apnoea by Single-lead ECG through ELM Classification," *Comput Cardiol*, vol. 41, pp. 909–912, 2014.

[63] N. Sadr and P. de Chazal, "A Comparison of Obstructive Sleep Apnoea Detection using Three Different ECG Derived Respiration Algorithms," *Comput Cardiol*, vol. 42, pp. 301–304, 2015.

[64] N. Sadr, P. de Chazal, A. van Schaik, and P. Breen, "Sleep apnoea episodes recognition by a committee of ELM classifiers from ECG signal," *Proc. Annu. Int. Conf. IEEE Eng. Med. Biol. Soc. EMBS*, vol. 2015-Novem, pp. 7675–7678, 2015.

[65] N. Sadr and P. de Chazal, "A Fast Approximation Method for Principal Component Analysis Applied to ECG Derived Respiration for OSA detection," in *38th Annu. Int. Conf. IEEE Eng. Med. Biol. Soc.*, 2016, pp. 6198–6201.

[66] N. Sadr and P. de Chazal, "Comparing ECG Derived Respiratory Signals and Chest Respiratory Signal for the Detection of Obstructive Sleep Apnoea," *Comput Cardiol*, vol. 43, pp. 1029–32, 2016.

[67] H. Nosrati, N. Sadr, and P. de Chazal, "Apnoea-hypopnoea index estimation using craniofacial photographic measurements," *Comput Cardiol*, vol. 43, pp. 1033–1036, 2016.

[68] P. de Chazal, N. Sadr, and M. Jayawardhana, "An ECG oximetry system for identifying obstructive and central apnoea events," *Proc. Annu. Int. Conf. IEEE Eng. Med. Biol. Soc. EMBS*, vol. 2015-Novem, pp. 7671–7674, 2015.

[69] P. de Chazal and N. Sadr, "Sleep apnoea classification using heartrate variability, ECG derived respiration and cardiopulmonary coupling parameters," *38th Annu. Int. Conf. IEEE Eng. Med. Biol. Soc.*, pp. 3203–3206, 2016.

[70] P. Langley, E. J. Bowers, and A. Murray, "Principal component analysis as a tool for analyzing beat-to-beat changes in ECG features: Application to ECG-derived respiration," *IEEE Trans. Biomed. Eng.*, vol. 57, no. 4, pp. 821–829, 2010.

[71] P. de Chazal, C. Heneghan, E. Sheridan, R. Reilly, P. Nolan, and M. O'Malley, "Automated processing of the single-lead electrocardiogram for the detection of obstructive sleep apnoea.," *IEEE Trans. Biomed. Eng.*, vol. 50, no. 6, pp. 686–96, Jun. 2003.

[72] C. Varon, A. Caicedo, D. Testelmans, B. Buyse, and S. Van Huffel, "A Novel Algorithm for the Automatic Detection of Sleep Apnea From Single-Lead ECG.," *IEEE Trans. Biomed. Eng.*, vol. 62, no. 9, pp. 2269–2278, 2015.

[73] D. Widjaja, C. Varon, A. Dorado, J. A. K. Suykens, and S. Van Huffel, "Application of Kernel Principal Component Analysis for Single-Lead-ECG-Derived Respiration," *IEEE Trans. Biomed. Eng.*, vol. 59, no. 4, pp. 1169–1176, 2012.

[74] G. V Chow, "Epidemiology of Arrhythmias and Conduction Disorder in Older Adults," *Clin Geriatr Med*, vol. 28, no. 4, pp. 539–553, 2012.

[75] J. Andrade, P. Khairy, D. Dobrev, and S. Nattel, “The clinical profile and pathophysiology of atrial fibrillation: Relationships among clinical features, epidemiology, and mechanisms,” *Circ. Res.*, vol. 114, no. 9, pp. 1453–1468, 2014.

[76] A. B. de Luna, “Basic Electrocardiography Normal And Abnormal ECG Patterns , Blackwell Publishers,” *Blackwell Publ.*, 2007.

[77] J. Malmivuo and R. Ponsey, “Bioelectromagnetism: Principles and Applications of Bioelectric and Biomagnetic Fields,” *New York Oxford Univ. Press*, 1995.

[78] J. M. Clarke, J. R. Shelton, J. Hamer, S. Taylor, and G. R. Venning, “The rhythm of the normal human heart,” *Lancet*, vol. 2, pp. 508–512, 1976.

[79] J. M. Mangrum and J. DiMarco, “The Evaluation and Management of Bradycardia,” *N. Engl. J. Med.*, vol. 342, no. 10, pp. 703–709, 2000.

[80] W. T. Force, “Classification of cardiac arrhythmias and conduction disturbances,” *Am. Heart J.*, vol. 98, no. 2, pp. 263–267, 1979.

[81] L. Schamroth, “How to approach an arrhythmia.,” *Circulation*, vol. 47, no. 2, pp. 420–6, 1973.

[82] D. F. Dickinson and O. Scott, “Ambulatory electrocardiographic monitoring in 100 healthy teenage boys,” *Br. Heart J.*, vol. 51, no. 2, pp. 179–183, 1984.

[83] P. F. Cranefield, “Ventricular Fibrillation,” *N. Engl. J. Med.*, vol. 289, no. 14, pp. 732–736, 1973.

[84] WHO/ISC Task Force, “Definition of terms related to cardiac rhythm,” *Am. Hear.*, vol. 95, no. 6, pp. 796–806, 1978.

[85] R. I. Birchfield, E. E. Menefee, and G. D. N. Bryant, “Disease of the Sinoatrial Node Associated with Bradycardia, Asystole, Syncope, and Paroxysmal Atrial Fibrillation,” *Circulation*, vol. 16, no. 1, pp. 20–26, 1957.

[86] C. Guilleminault, S. J. Connolly, and R. A. Winkle, “Cardiac arrhythmia and conduction disturbances during sleep in 400 patients with sleep apnea syndrome,” *Am. J. Cardiol.*, vol. 52, no. 5, pp. 490–494, 1983.

[87] F. Roche, A. N. T. Xuong, I. Court-Fortune, F. Costes, V. Pichot, D. Duverney, J. M. Vergnon, J. M. Gaspoz, and J. C. Barthélémy, “Relationship among the severity of sleep apnea syndrome, cardiac arrhythmias, and autonomic imbalance,” *PACE - Pacing Clin. Electrophysiol.*, vol. 26, no. 3, pp. 669–677, 2003.

[88] J. L. Hossain and Colin M. Shapiro, “The Prevalence , Cost Implications , and Management of Sleep Disorders : An Overview,” *Sleep Breath.*, vol. 6, no. 2, pp. 85–102, 2002.

[89] P. C. Deegan and W. T. McNicholas, “Pathophysiology of obstructive sleep apnoea,” *Eur. Respir. J.*, vol. 8, no. 7, pp. 1161–1178, Jul. 1995.

[90] R. Alvarez-Sala, F. García-Río, F. Del Campo, C. Zamarrón, and N. C. Netzer, “Sleep apnea and cardiovascular diseases.,” *Pulm. Med.*, vol. 2014, pp. 1–2, Jan. 2014.

[91] C. Gulleminault, a T. Lehrman, L. Forno, and W. C. Dement, “Sleep apnoea syndrome: states of sleep and autonomic dysfunction.,” *J. Neurol. Neurosurg. Psychiatry*, vol. 40, no. 7, pp. 718–25, Jul. 1977.

[92] R. B. Berry, R. Budhiraja, D. J. Gottlieb, D. Gozal, C. Iber, V. K. Kapur, C. L. Marcus, R. Mehra, S. Parthasarathy, S. F. Quan, S. Redline, K. P. Strohl, S. L. D. Ward, and M. M. Tangredi, “Rules for scoring respiratory events in sleep: Update of the 2007 AASM manual for the scoring of sleep and associated events,” *J. Clin. Sleep Med.*, vol. 8, no. 5, pp. 597–619, 2012.

[93] L. A. Block, A. J; Boysen, P. G; Wynne, J. W; Hint, “Sleep Apnea, Hypopnea and Oxygen Desaturation in Normal Subjects: A Strong Male Predominance,” *Surv. Anesthesiol.*, vol. 24, no. 3, p. 147, 1980.

[94] C. Guilleminault and S. Chowdhuri, “Upper airway resistance syndrome is a distinct syndrome,” *American Journal of Respiratory and Critical Care Medicine*, vol. 161, no. 5, pp. 1412–1413, 2000.

[95] A. R. Gold, C. L. Marcus, F. Dipalo, and M. S. Gold, “Upper Airway Collapsibility During Sleep in Upper Airway Resistance Syndrome,” *CHEST J.*, vol. 12, no. 5, pp. 1531–1540, 2002.

[96] Q. S. Iber C, Ancoli-Israel S, Chesson AL Jr, “The AASM manual for the scoring of sleep and associated events: rules, terminology and technical specifications,” *Am. Acad. SleepMedicine*, 2007.

[97] G. Pillar and P. Lavie, “Obstructive sleep apnea: diagnosis, risk factors, and pathophysiology.,” *Handb. Clin. Neurol. Chapter 25*, vol. 98, pp. 383–99, Jan. 2011.

[98] D. J. Eckert and A. Malhotra, “Pathophysiology of adult obstructive sleep apnea.,” *Proc. Am. Thorac. Soc.*, vol. 5, no. 2, pp. 144–53, Feb. 2008.

[99] C. Dickens, “The Posthumous Papers of the Pickwick Club,” *London Chapman Hall*, 1836.

[100] W. Dement, “History of sleep physiology and medicine.,” *Princ. Pr. sleep Med. 3rd Ed. Philadelphia WB Saunders*, pp. 1–14, 2000.

[101] M. Thorpy, “Historical perspective on sleep and man,” in *Culebras A, editor. Sleep disorders and neurological disease, New York: Marcel Dekker*, 2000, pp. 1–36.

[102] W. a Whitelaw and K. R. Burgess, “Diagnosis of sleep apnoea: some critical issues.,” *Indian J. Med. Res.*, vol. 131, no. February, pp. 217–29, Feb. 2010.

[103] S. Ancoli-Israel, D. F. Kripke, M. R. Klauber, W. J. Mason, F. R, and O. Kaplan, “Sleep-disordered breathing in community-dwelling elderly.,” *Sleep*, vol. 14, no. 6, pp. 486–495., 1991.

[104] A. Roebuck, V. Monasterio, E. Gederi, M. Osipov, J. Behar, A. Malhotra, T. Penzel, and G. D. Clifford, “A review of signals used in sleep analysis.,” *Physiol. Meas.*, vol. 35, no. 1, pp. R1–57, Jan. 2014.

[105] H. Bearpark, L. Elliott, R. Grunstein, S. Cullen, H. Schneider, W. Althaus, and C. Sullivan, “Snoring and sleep apnea: A population study in Australian men,” *Am. J. Respir. Crit. Care Med.*, vol. 151, no. 5, pp. 1459–1465, 1995.

[106] Z. F. Udwadia, A. V. Doshi, S. G. Lonkar, and C. I. Singh, "Prevalence of Sleep-disordered Breathing and Sleep Apnea in Middle-aged Urban Indian Men," *Am. J. Respir. Crit. Care Med.*, vol. 169, no. 2, pp. 168–173, 2004.

[107] A. Hansford, "Thirty years of CPAP A brief history of OSA," *ResMedica Clin. Newsl.*, no. 14, pp. 1–16, 2011.

[108] I. Ayappa and D. M. Rapoport, "The upper airway in sleep: physiology of the pharynx," *Sleep Med. Rev.*, vol. 7, no. 1, pp. 9–33, Feb. 2003.

[109] V. K. Somers, M. E. Dyken, M. P. Clary, and F. M. Abboud, "Sympathetic neural mechanisms in obstructive sleep apnea.," *J. Clin. Invest.*, vol. 96, no. 4, pp. 1897–904, Oct. 1995.

[110] European Society of Cardiology and the North American Society of Pacing and Electrophysiology, "Guidelines Heart rate variability," *Eur. Heart J.*, vol. 17, pp. 354–381, 1996.

[111] I. C. Gleadhill, A. R. Schwartz, N. Schubert, R. a. Wise, S. Permutt, and P. L. Smith, "Upper Airway Collapsibility in Snorers and in Patients with Obstructive Hypopnea and Apnea," *Am. Rev. Respir. Dis.*, vol. 143, no. 6, pp. 1300–1303, 1991.

[112] R. L. Horner, R. H. Mohiaddin, D. G. Lowell, S. a. Shea, E. D. Burman, D. B. Longmore, and a. Guz, "Sites and sizes of fat deposits around the pharynx in obese patients with obstructive sleep apnoea and weight matched controls.," *Eur. Respir. J. Off. J. Eur. Soc. Clin. Respir. Physiol.*, vol. 2, no. 7, pp. 613–622, 1989.

[113] O. P. Mathew, Y. K. Abu-Osba, and B. T. Thach, "Influence of upper airway pressure changes on respiratory frequency," *Respir. Physiol.*, vol. 49, no. 2, pp. 223–233, 1982.

[114] W. S. Mezzanotte, D. J. Tangel, and D. P. White, "Waking genioglossal electromyogram in sleep apnea patients versus normal controls (a neuromuscular compensatory mechanism).," *J. Clin. Invest.*, vol. 89, no. 5, pp. 1571–9, May 1992.

[115] M. Dematteis, P. Lévy, and J.-L. Pépin, "A simple procedure for measuring pharyngeal sensitivity: a contribution to the diagnosis of sleep apnoea.," *Thorax*, vol. 60, no. 5, pp. 418–26, May 2005.

[116] X. Tang, A. R. Chander, L. P. Schramm, and P. Lawrence, "Sympathetic activity and the underlying action potentials in sympathetic nerves : a simulation," vol. 21205, pp. 1504–1513, 2003.

[117] A. S. Jordan, A. Wellman, R. C. Heinzer, Y.-L. Lo, K. Schory, L. Dover, S. Gautam, A. Malhotra, and D. P. White, "Mechanisms used to restore ventilation after partial upper airway collapse during sleep in humans.," *Thorax*, vol. 62, no. 10, pp. 861–7, Oct. 2007.

[118] R. Horner, J. Innes, K. Murphy, and A. Guz, "Evidence for reflex upper airway dilator muscle activation by sudden negative airway pressure in man," *J Physiol*, vol. 436, pp. 15–29, 1991.

[119] W. S. Mezzanotte, D. J. Tangel, and D. P. White, "Influence of sleep onset on upper-airway muscle activity in apnea patients versus normal controls.," *Am. J. Respir. Crit. Care Med.*, vol. 153, no. 6 Pt 1, pp. 1880–7, 1996.

[120] J. a Jo, A. Blasi, E. Valladares, R. Juarez, A. Baydur, and M. C. K. Khoo, "Model-based assessment of autonomic control in obstructive sleep apnea syndrome during sleep.," *Am. J. Respir. Crit. Care Med.*, vol. 167, no. 2, pp. 128–36, Jan. 2003.

[121] U. Wiklund, B. Olofsson, K. Franklin, H. Blom, P. Bjerle, and U. Niklasson, "Autonomic cardiovascular regulation in patients with obstructive sleep apnoea: a study based on spectral analysis of heart rate variability," *Clin. Physiol.*, vol. 20, no. 3, pp. 234–241, May 2000.

[122] M. C. K. Khoo, T. S. Kim, and R. B. Berry, "Spectral Indices of Cardiac Autonomic Function in Obstructive Sleep Apnea," *Sleep*, vol. 22, no. 4, pp. 443–51, 1999.

[123] M. Carrera, F. Barbé, J. Sauleda, M. Tomás, and C. Gómez, "Patients with Obstructive Sleep Apnea Exhibit Genioglossus Dysfunction that Is Normalized after Treatment with Continuous Positive Airway Pressure," *Am. J. Respir. Crit. Care Med.*, vol. 159, pp. 1960–1966, 1999.

[124] M. Gugger, S. Bögershausen, and L. Schäffler, "Arousal responses to added inspiratory resistance during REM and non-REM sleep in normal subjects.," *Thorax*, vol. 48, no. 2, pp. 125–129, 1993.

[125] E. K. Sauerland and R. M. Harper, "The human tongue during sleep: Electromyographic activity of the genioglossus muscle," *Exp. Neurol.*, vol. 51, no. 1, pp. 160–170, 1976.

[126] F. G. Issa and C. E. Sullivan, "Arousal and breathing responses to airway occlusion in healthy sleeping adults," *J. Appl. Physiol.*, vol. 55, no. 4, pp. 1113–1119, 1983.

[127] S. a. Shea, J. K. Edwards, and D. P. White, "Effect of wake-sleep transitions and rapid eye movement sleep on pharyngeal muscle response to negative pressure in humans," *J. Physiol.*, vol. 520, no. 3, pp. 897–908, 1999.

[128] F. G. Issa, P. Edwards, E. Szeto, D. Lauff, and C. Sullivan, "Genioglossus and breathing responses to airway occlusion: effect of sleep and route of occlusion.," *J. Appl. Physiol.*, vol. 64, no. 2, pp. 543–9, 1988.

[129] L. Wiegand, C. W. Zwillich, D. Wiegand, and D. P. White, "Changes in upper airway muscle activation and ventilation during phasic REM sleep in normal men.," *J. Appl. Physiol.*, vol. 71, no. 3, pp. 488–97, 1991.

[130] C. M. Schröder and R. O'Hara, "Depression and Obstructive Sleep Apnea (OSA).," *Ann. Gen. Psychiatry*, vol. 4, p. 13, 2005.

[131] P. M. Macey, R. Kumar, M. A. Woo, E. M. Valladares, F. L. Yan-go, and R. M. Harper, "Brain Structural Changes in Obstructive Sleep Apnea," *Sleep*, vol. 31, no. 7, pp. 967–977, 2008.

[132] D. W. Beebe, L. Groesz, C. Wells, a Nichols, and K. McGee, "The neuropsychological effects of obstructive sleep apnea: a meta-analysis of norm-referenced and case-controlled data," *Sleep*, vol. 26, no. 3, pp. 298–307, 2003.

[133] C. W. Davies, J. H. Crosby, R. L. Mullins, Z. C. Traill, P. Anslow, R. J. Davies, and J. R. Stradling, "Case control study of cerebrovascular damage defined by magnetic resonance imaging in patients with OSA and normal matched control subjects.," *Sleep*, vol. 24, no. 6, pp. 715–720, 2001.

[134] N. Canessa, V. Castronovo, S. F. Cappa, M. S. Aloia, S. Marelli, A. Falini, F. Alemanno, and L. Ferini-Strambi, "Obstructive sleep apnea: brain structural changes and neurocognitive function before and after treatment.," *Am. J. Respir. Crit. Care Med.*, vol. 183, no. 10, pp. 1419–26, May 2011.

[135] D. Baltzis, J. P. Bakker, S. R. Patel, and A. Veves, "Obstructive Sleep Apnea and Vascular Diseases," *Compr. Physiol.*, vol. 6, no. 3, pp. 1519–1528, 2016.

[136] L. R. Young, Z. H. Taxin, R. G. Norman, J. a Walsleben, D. M. Rapoport, and I. Ayappa, "Response to CPAP withdrawal in patients with mild versus severe obstructive sleep apnea/hypopnea syndrome.," *Sleep*, vol. 36, pp. 405–12, 2013.

[137] J. Haba-Rubio, E. Sforza, T. Weiss, C. Schröder, and J. Krieger, "Effect of CPAP treatment on inspiratory arousal threshold during NREM sleep in OSAS," *Sleep Breath.*, vol. 9, no. 1, pp. 12–19, 2005.

[138] T. Kirby, "Colin Sullivan: inventive pioneer of sleep medicine.," *Lancet*, vol. 377, no. 9776, p. 1485, Apr. 2011.

[139] S. Randerath WJ, Sanner BM, Somers VK (eds), Yim, A. Jordan, and A. Malhutra, "Obstructive sleep apnea: Clinical presentation, diagnosis and treatment," *Sleep Apnea, Prog Respir Res. Basel, Karger*, vol. 35, pp. 118–136, 2006.

[140] E. Balk, D. Moorthy, and N. Obadan, "Diagnosis and Treatment of Obstructive Sleep Apnea in Adults," *Comp. Eff. Rev. Adency Healthc. Res. Qual.*, no. 32, pp. 1–213, 2011.

[141] A. M. Esquinas and P. Cistulli, "Is prediction of cpap adherence in obstructive sleep apnea in the perioperative setting feasible?," *Journal of Clinical Sleep Medicine*, vol. 9, no. 7. p. 731, 2013.

[142] A. Oksenberg, E. Arons, and P. Froom, "Does the severity of obstructive sleep apnea predict patients requiring high continuous positive airway pressure?," *Laryngoscope*, vol. 116, no. 6, pp. 951–955, 2006.

[143] S. I. Lasserson and M. Haniffa, "Interventions to improve use of continuous positive airway pressure for obstructive sleep apnoea (Review)," *Wiley*, no. 4, pp. 1–81, 2009.

[144] M. P. Mansukhani, B. P. Kolla, E. J. Olson, K. Ramar, and T. I. Morgenthaler, "Bilevel positive airway pressure for obstructive sleep apnea.," *Expert Rev. Med. Devices*, vol. 11, no. 3, pp. 283–294, 2014.

[145] M. K. Reeves-Hoché, D. W. Hudgel, R. Meck, R. Witteman, A. Ross, and C. W. Zwillich, "Continuous versus bilevel positive airway pressure for obstructive sleep apnea," *Am. J. Respir. Crit. Care Med.*, vol. 151, pp. 443–449, 1995.

[146] A. Oliven, R. P. Schnall, G. Pillar, N. Gavriely, and M. Odeh, "Sublingual electrical stimulation of the tongue during wakefulness and sleep," *Respir. Physiol.*, vol. 127, pp. 217–226, 2001.

[147] A. Oliven, D. J. O'Hearn, A. Boudewyns, M. Odeh, W. De Backer, P. van de Heyning, P. L. Smith, D. W. Eisele, L. Allan, H. Schneider, R. Testerman, and A. R. Schwartz, "Upper airway response to electrical stimulation of the genioglossus in obstructive sleep apnea.," *J Appl Physiol*, vol. 95, no. 5, pp. 2023–29, 2003.

[148] T. Penzel, J. McNames, A. Murray, P. de Chazal, G. Moody, and B. Raymond, "Systematic comparison of different algorithms for apnoea detection based on electrocardiogram recordings.," *Med. Biol. Eng. Comput.*, vol. 40, no. 4, pp. 402–7, Jul. 2002.

[149] A. E. W. Johnson, J. Behar, F. Andreotti, G. D. Clifford, and J. Oster, "Multimodal heart beat detection using signal quality indices," *Physiol. Meas.*, vol. 36, no. 8, pp. 1665–1677, 2015.

[150] G. Moody, B. Moody, and I. Silva, "Robust detection of heart beats in multimodal data: The PhysioNet/Computing in Cardiology Challenge 2014," *Comput. Cardiol. Conf. (CinC), 2014*, pp. 549–552, 2014.

[151] W. T. McNicholas, "Diagnosis of obstructive sleep apnea in adults.," *Proc. Am. Thorac. Soc.*, vol. 5, no. 2, pp. 154–60, Feb. 2008.

[152] L. P. Pillar G, Peled N, Katz N, "Predictive value of specific risk factors, symptoms and signs, in diagnosing obstructive sleep apnoea and its severity," *J Sleep Res*, vol. 3, no. 4, pp. 241–244, 1992.

[153] T. Young, L. Evans, L. Finn, and M. Palta, "Estimation of the clinically diagnosed proportion of sleep apnea syndrome in middle-aged men and women.," *Sleep*, vol. 20, no. 9, pp. 705–6, Sep. 1997.

[154] M. S. M. Ip, B. Lam, I. J. Lauder, K. W. T. Tsang, K. F. Chung, Y. W. Mok, and W. K. Lam, "A community study of sleep-disordered breathing in middle-aged Chinese men in Hong Kong," *Chest*, vol. 119, no. 1, pp. 62–69, 2001.

[155] M. R. Shepertycky, K. Banno, and M. H. Kryger, "Differences between men and women in the clinical presentation of patients diagnosed with obstructive sleep apnea syndrome.," *Sleep*, vol. 28, no. 3, pp. 309–14, Mar. 2005.

[156] V. Hoffstein and J. P. Pzalai, "Predictive Value of Clinical Features in Diagnosing Obstructive Sleep Apnea," *Sleep*, vol. 16, no. 2, pp. 118–122, 1993.

[157] C. O'Brien and C. Heneghan, "A comparison of algorithms for estimation of a respiratory signal from the surface electrocardiogram.," *Comput. Biol. Med.*, vol. 37, no. 3, pp. 305–14, Mar. 2007.

[158] G. B. Moody and R. G. Mark, "Derivation of respiratory signals from multi-lead ECGs," *Comput. Cardiol.*, vol. 12, no. August, pp. 113–116, 1985.

[159] R. J. Kimoff, "Physiology of the upper airways and upper airway obstruction in disease," *Physiol. basis Respir. Dis. , Chapter 50, BC Decker Inc Hamilt.*, pp. 581–596, 2005.

[160] J. L. Pépin, P. Lévy, B. Lepaulle, C. Brambilla, and C. Guilleminault, "Does Oximetry Contribute of Apneic Events ?," *CHEST J.*, vol. 99, no. 5, pp. 1151–7, 1991.

[161] P. Y. Carry, P. Baconnier, A. Eberhard, P. Cotte, and G. Benchetrit, "Evaluation of respiratory inductive plethysmography: Accuracy for analysis of respiratory waveforms," *Chest*, vol. 111, no. 4, pp. 910–915, 1997.

[162] S. J. Redmond, P. de Chazal, C. O'Brien, S. Ryan, W. T. McNicholas, and C. Heneghan, "Sleep staging using cardiorespiratory signals," *Somnologie - Schlafforsch. und Schlafmedizin*, vol. 11, no. 4, pp. 245–256, Oct. 2007.

[163] T. Morgenthaler, C. Alessi, L. Friedman, J. Owens, V. Kapur, B. Boehlecke, T. Brown, A. Chesson, J. Coleman, T. Lee-Chiong, J. Pancer, and T. J. Swick, “Practice parameters for the use of actigraphy in the assessment of sleep and sleep disorders: an update for 2007.,” *Sleep*, vol. 30, no. 4, pp. 519–529, 2007.

[164] L. de Souza, A. A. Benedito-Silva, M. L. N. Pires, D. Poyares, S. Tufik, and H. M. Calil, “Further validation of actigraphy for sleep studies.,” *Sleep*, vol. 26, no. 1, pp. 81–85, 2003.

[165] B. Sivertsen, S. Omvik, O. E. Havik, S. Pallesen, B. Bjorvatn, G. H. Nielsen, S. Straume, and I. H. Nordhus, “A comparison of actigraphy and polysomnography in older adults treated for chronic primary insomnia.,” *Sleep*, vol. 29, no. 10, pp. 1353–1358, 2006.

[166] J. Hedner, G. Pillar, S. D. Pittman, D. Zou, L. Grote, and D. P. White, “A novel adaptive wrist actigraphy algorithm for sleep-wake assessment in sleep apnea patients.,” *Sleep*, vol. 27, no. 8, pp. 1560–1566, 2004.

[167] P. de Chazal, N. Fox, E. O’Hare, C. Heneghan, A. Zaffaroni, P. Boyle, S. Smith, C. O’Connell, and W. T. McNicholas, “Sleep/wake measurement using a non-contact biomotion sensor.,” *J. Sleep Res.*, vol. 20, no. 2, pp. 356–66, Jun. 2011.

[168] A. Zaffaroni, B. Kent, E. O’Hare, C. Heneghan, P. Boyle, G. O’Connell, M. Pallin, P. de Chazal, and W. T. McNicholas, “Assessment of sleep-disordered breathing using a non-contact bio-motion sensor.,” *J. Sleep Res.*, vol. 22, no. 2, pp. 231–6, Apr. 2013.

[169] C. Heneghan, “Wireless Sleep Measurement: Sensing sleep and breathing patterns using radio-frequency sensors.,” *IEEE Pulse*, vol. 5, no. 5, pp. 22–25, Sep. 2014.

[170] T. Ballal, C. Heneghan, A. Zaffaroni, P. Boyle, P. de Chazal, R. Shouldice, W. T. McNicholas, and S. C. Donnelly, “A pilot study of the nocturnal respiration rates in COPD patients in the home environment using a non-contact biomotion sensor.,” *Physiol. Meas.*, vol. 35, no. 12, pp. 2513–27, Dec. 2014.

[171] R. B. Shouldice, C. Heneghan, G. Petres, P. Boyle, W. Mcnicholas, P. de Chazal, and A. Overview, “Real Time Breathing Rate Estimation from a Non Contact Biosensor,” *Proc. Annu. Int. Conf. IEEE Eng. Med. Biol. Soc.*, pp. 630–633, 2010.

[172] E. O’Hare, D. Flanagan, T. Penzel, C. Garcia, D. Frohberg, and C. Heneghan, “A comparison of radio-frequency biomotion sensors and actigraphy versus polysomnography for the assessment of sleep in normal subjects,” *Sleep Breath.*, vol. 19, no. 1, pp. 91–98, Mar. 2014.

[173] a. Mäkivirta, E. Koski, a. Kari, and T. Sukuvaara, “The median filter as a preprocessor for a patient monitor limit alarm system in intensive care,” *Comput. Methods Programs Biomed.*, vol. 34, no. 2–3, pp. 139–144, Feb. 1991.

[174] D. F. Sittig and M. Factor, “Physiologic trend detection and artifact rejection: a parallel implementation of a multi-state Kalman filtering algorithm,” *Comput. Methods Programs Biomed.*, vol. 31, no. 1, pp. 1–10, 1990.

[175] A. Aboukhalil, L. Nielsen, M. Saeed, R. G. Mark, and G. D. Clifford, “Reducing false alarm rates for critical arrhythmias using the arterial blood pressure waveform,” *J. Biomed. Inform.*, vol. 41, no. 3, pp. 442–451, 2008.

[176] F. Plesinger, P. Klimes, J. Halamek, and P. Jurak, “False Alarms in Intensive Care Unit Monitors : Detection of Life-threatening Arrhythmias using Elementary Algebra , Descriptive Statistics and Fuzzy Logic,” *Comput Cardiol*, vol. 42, pp. 281–284, 2015.

[177] S. Ansari, A. Belle, and K. Najarian, “Multi-modal integrated approach towards reducing false arrhythmia alarms during continuous patient monitoring: The Physionet Challenge 2015,” *Comput Cardiol*, vol. 42, pp. 1177–1180, 2015.

[178] X. S. Zhang, Y. S. Zhu, N. V. Thakor, and Z. Z. Wang, “Detecting ventricular tachycardia and fibrillation by complexity measure,” *IEEE Trans. Biomed. Eng.*, vol. 46, no. 5, pp. 548–555, 1999.

[179] I. Jekova, “Comparison of five algorithms for the detection of ventricular fibrillation from the surface ECG,” *Physiol. Meas.*, vol. 21, pp. 429–439, 2000.

[180] R. H. Clayton, a Murray, and R. W. F. Campbell, “Comparison of 4 Techniques for Recognition of Ventricular-Fibrillation from the Surface Ecg,” *Med. Biol. Eng. Comput.*, vol. 31, no. 2, pp. 111–117, 1993.

[181] S. Chen, N. V Thakor, and M. M. Mower, “Ventricular fibrillation detection by a regression test on the autocorrelation function,” *Med. Biol. Eng. Comput.*, vol. 25, pp. 241–249, 1987.

[182] C. Guilleminault, S. Connolly, R. Winkle, K. Melvin, and A. Tilkian, “Cyclical variation of the heart rate in sleep apnoea syndrome. Mechanisms, and usefulness of 24 h electrocardiography as a screening technique.,” *Lancet*, vol. 1, no. 8369, pp. 126–31, Jan. 1984.

[183] J. Gubbi, A. Khandoker, and M. Palaniswami, “Classification of Obstructive and Central Sleep Apnea Using Wavelet Packet Analysis of ECG Signals,” *Comput Cardiol*, vol. 36, pp. 733–736, 2009.

[184] P. de Chazal, C. Heneghan, E. Sheridan, R. Reilly, P. Nolan, and M. O’Malley, “Automatic classification of sleep apnea epochs using the\nelectrocardiogram,” *Comput. Cardiol.*, vol. 27, pp. 745–748, 2000.

[185] M. Jarvis and P. Mitra, “Apnea Patients Characterized by 0.02 Hz Peak in the Multipaper Spectrogram of Electrocardiogram Signals,” *Comput. Cardiol.*, vol. 27, pp. 769–772, 2000.

[186] J. McNames and A. Fraser, “Obstructive sleep apnea classification based on spectrogram patterns in the electrocardiogram,” *Comput. Cardiol.*, vol. 27, pp. 749–752, 2000.

[187] Z. Shinar, A. Baharav, and S. Akselrod, “Obstructive sleep apnea detection based on electrocardiogram\nanalysis,” *Comput. Cardiol.*, vol. 27, pp. 757–760, 2000.

[188] M. Schrader, C. Zywietz, V. Von Einem, B. Widiger, and G. Joseph, “Detection of sleep apnea in single channel ECGs from the PhysioNet\ndata base,” *Comput. Cardiol.*, vol. 27, pp. 263–266, 2000.

[189] M. J. Drinnan, A. Murray, C. J. Griffiths, and G. J. Gibson, “Interobserver variability in recognizing arousal in respiratory sleep disorders,” *Am. J. Respir. Crit. Care Med.*, vol. 158, no. 2, pp. 358–362, 1998.

[190] J. Mietus, C. K. Peng, P. C. Ivanov, and A. Goldberger, "Detection of Obstructive Sleep Apnea from Cardiac Interbeat Interval Time Series," *Comput. Cardiol.*, vol. 27, pp. 753–756, 2000.

[191] G. B. Moody, R. G. Mark, A. L. Goldberger, and T. Penzel, "Stimulating Rapid Research Advances Via Focused Competition : The Computers in Cardiology Challenge 2000," *Comput. Cardiol.*, vol. 27, pp. 207–210, 2000.

[192] Raymond Ben, Cayton RM, Bates RA, and Chappel MJ, "Screening for Obstructive Sleep Apnoea Based on the Electrocardiogram - Computers in Cardiology Challenge," *Comput. Cardiol. 2000*, vol. 27, pp. 267–270, 2000.

[193] A. Hertzman and C. Spealman, "Observations on the finger volume pulse recorded photo-electrically," *Am J Physiol*, vol. 119, pp. 334–5, 1937.

[194] J. R. Squire, "Instrument for measuring quantity of blood and its degree of oxygenation in web of the hand.," *Am. Heart J.*, vol. 4, pp. 331–339, 1940.

[195] F. Sériès, Y. Cormier, and J. La Forge, "Role of lung volumes in sleep apnoea-related oxygen desaturation," *Eur. Respir. J.*, vol. 2, pp. 26–30, 1989.

[196] R. Golpe, A. Jiménez, R. Carpizo, and J. M. Cifrian, "Utility of Home Oximetry as a Screening Test for Patients with Moderate to Severe Symptoms of Obstructive Sleep Apnea," *Sleep*, vol. 22, no. 7, pp. 932–937, 1999.

[197] F. Sériès, I. Marc, Y. Cormier, and J. La Forge, "Utility of Nocturnal Home Oximetry for Case Finding in Patients with Suspected Sleep Apnea Hypopnea Syndrome," *Ann Intern Med.*, vol. 119, no. 6, pp. 449–453, 1993.

[198] W. a Whitelaw, R. F. Brant, and W. W. Flemons, "Clinical usefulness of home oximetry compared with polysomnography for assessment of sleep apnea.," *Am. J. Respir. Crit. Care Med.*, vol. 171, no. 2, pp. 188–93, Jan. 2005.

[199] C. Heneghan, C. Chua, J. F. Garvey, P. de Chazal, R. Shouldice, P. Boyle, and T. Walter, "Sleep Apnea Assessment A Portable Automated Assessment Tool for Sleep Apnea Using a Combined Holter-oximeter," *Sleep*, vol. 31, no. 10, pp. 1432–1439, 2008.

[200] Z. Zhang, J. Zheng, H. Wu, W. Wang, B. Wang, and H. Liu, "Development of a respiratory inductive plethysmography module supporting multiple sensors for wearable systems.," *Sensors*, vol. 12, no. 10, pp. 13167–84, Jan. 2012.

[201] C. M. Vaughn and P. Clemmons, "Piezoelectric Belts as a Method for Measuring Chest and Abdominal Movement for Obstructive Sleep Apnea Diagnosis," *Neurodiagn J.*, vol. 52, pp. 275–280, 2012.

[202] Y. Yasuda, A. Umezu, S. Horihata, K. Yamamoto, R. Miki, and S. Koike, "Modified thoracic impedance plethysmography to monitor sleep apnea syndromes.," *Sleep Med.*, vol. 6, no. 3, pp. 215–24, May 2005.

[203] M. N. Fiamma, Z. Samara, P. Baconnier, T. Similowski, and C. Straus, "Respiratory inductive plethysmography to assess respiratory variability and complexity in humans," *Respir. Physiol. Neurobiol.*, vol. 156, no. 2, pp. 234–239, 2007.

[204] J. M. Bradley, L. Kent, B. O'Neill, A. Nevill, L. Boyle, and J. S. Elborn, "Cardiorespiratory measurements during field tests in CF: Use of an ambulatory monitoring system," *Pediatr. Pulmonol.*, vol. 46, no. 3, pp. 253–260, 2011.

[205] C. Iber, S. Ancoli-Israel, A. Chesson, and S. Quan, "The AASM Manual for the Scoring of Sleep and Associated Events: Rules, Terminology and Technical Specifications," *Am. Acad. Sleep Med.*, 2007.

[206] M. A. Cohn, A. S. V Rao, M. Broudy, S. Birch, H. Watson, N. Atkins, B. Davis, F. D. Stott, and M. A. Sackner, "The respiratory inductive plethysmograph: A new non-invasive monitor of respiration," *Bull. Eur. Physiopathol. Respir.*, vol. 18, pp. 643–658, 1982.

[207] L. Kent, B. O'Neill, G. Davison, A. Nevill, J. Stuart Elborn, and J. M. Bradley, "Validity and reliability of cardiorespiratory measurements recorded by the LifeShirt during exercise tests," *Respir. Physiol. Neurobiol.*, vol. 167, no. 2, pp. 162–167, 2009.

[208] C. F. Clarenbach, O. Senn, T. Brack, M. Kohler, and K. E. Bloch, "Monitoring of ventilation during exercise by a portable respiratory inductive plethysmograph," *Chest*, vol. 128, no. 3, pp. 1282–1290, 2005.

[209] M. A. Ritter, D. G. Nabavi, and R. E. Bernard, "Measurement of Arterial Pressure," *Dtsch Arztebl*, vol. 104, no. 20, pp. 1406–10, 2007.

[210] H. K. Kain, a T. Hinman, and M. Sokolow, "Arterial Blood Pressure Measurements With a Portable Recorder in Hypertensive Patients. I. Variability and Correlation With 'Casual' Pressures.," *Circulation*, vol. 30, no. December 1964, pp. 882–92, 1964.

[211] C. N. Joseph, C. Porta, G. Casucci, N. Casiraghi, M. Maffeis, M. Rossi, and L. Bernardi, "Slow breathing improves arterial baroreflex sensitivity and decreases blood pressure in essential hypertension.," *Hypertension*, vol. 46, no. 4, pp. 714–8, Oct. 2005.

[212] Q. Li and G. D. Clifford, "Suppress false arrhythmia alarms of ICU monitors using heart rate estimation based on combined arterial blood pressure and ECG analysis," *2nd Int. Conf. Bioinforma. Biomed. Eng. iCBBE 2008*, no. 6914565, pp. 2185–2187, 2008.

[213] F. Schmid, M. S. Goepfert, and D. A. Reuter, "Patient monitoring alarms in the ICU and in the operating room," *Crit. Care*, 2013.

[214] M. Imhoff and S. Kuhls, "Alarm algorithms in critical monitoring," *Anesth. Analg.*, vol. 102, no. 5, pp. 1525–1537, 2006.

[215] Q. Li and G. D. Clifford, "Dynamic time warping and machine learning for signal quality assessment of pulsatile signals," *Physiol. Meas.*, vol. 33, no. 9, pp. 1491–1501, 2012.

[216] W. Zong, G. B. Moody, and R. G. Mark, "Reduction of false arterial blood pressure alarms using signal quality assessment and relationships between the electrocardiogram and arterial blood pressure," *Med. Biol. Eng. Comput.*, vol. 42, pp. 698–706, 2004.

[217] G. D. Clifford, D. Lopez, Q. Li, and I. Rezek, "Signal quality indices and data fusion for determining acceptability of electrocardiograms collected in noisy ambulatory environments," *Comput Cardiol*, vol. 33, pp. 1419–33, 2012.

[218] C. Orphanidou, T. Bonnici, P. Charlton, D. Clifton, D. Vallance, and L. Tarassenko, “Signal-quality indices for the electrocardiogram and photoplethysmogram: Derivation and applications to wireless monitoring,” *IEEE J. Biomed. Heal. Informatics*, vol. 19, no. 3, pp. 832–838, 2015.

[219] M. T. Bianchi, T. Lipoma, C. Darling, Y. Alameddine, and M. B. Westover, “Automated sleep apnea quantification based on respiratory movement,” *Int. J. Med. Sci.*, vol. 11, no. 8, pp. 796–802, 2014.

[220] A. L. Chesson, R. B. Berry, and A. Pack, “Practice parameters for the use of portable monitoring devices in the investigation of suspected obstructive sleep apnea in adults.,” *Sleep*, vol. 26, no. 7, pp. 907–913, 2003.

[221] W. A. H. Englese and C. Zeelenberg, “Single scan algorithm for QRS detection and feature extraction,” *Comput. Cardiol.*, pp. 37–42, 1979.

[222] S. Fallet, S. Yazdani, and J. M. Vesin, “A multimodal approach to reduce false arrhythmia alarms in the intensive care unit,” *Comput Cardiol*, vol. 42, pp. 277–280, 2016.

[223] A. E. W. Johnson, J. Behar, F. Andreotti, G. D. Clifford, and J. Oster, “R-peak estimation using multimodal lead switching,” *Comput Cardiol*, vol. 41, pp. 281–284, 2014.

[224] N. V. Thakor, Y. S. Zhu, and K. Y. Pan, “Ventricular tachycardia and fibrillation detection by a sequential hypothesis testing algorithm,” *IEEE Trans. Biomed. Eng.*, vol. 37, no. 9, pp. 837–843, 1990.

[225] L. Chen, X. Zhang, and C. Song, “An Automatic Screening Approach for Obstructive Sleep Apnea Diagnosis Based on Single-Lead Electrocardiogram,” *IEEE Trans. Autom. Sci. Eng.*, vol. 12, no. 1, pp. 106–115, 2015.

[226] M. O. Mendez, A. M. Bianchi, M. Matteucci, S. Cerutti, and T. Penzel, “Sleep apnea screening by autoregressive models from a single ECG lead.,” *IEEE Trans. Biomed. Eng.*, vol. 56, no. 12, pp. 2838–50, Dec. 2009.

[227] C. A. Nigro, E. Dibur, and E. Rhodius, “Pulse oximetry for the detection of obstructive sleep apnea syndrome: can the memory capacity of oxygen saturation influence their diagnostic accuracy?,” *Sleep Disord.*, vol. 2011, pp. 1–9, Jan. 2011.

[228] W. W. Flemons, M. R. Littner, J. a Rowley, P. Gay, W. M. Anderson, D. W. Hudgel, R. D. McEvoy, and D. I. Loube, “Home Diagnosis of Sleep Apnea: A Systematic Review of the Literature,” *Chest*, vol. 124, no. 4, pp. 1543–1579, 2003.

[229] G. D’Addio, M. Cesarelli, M. Romano, A. De Felice, S. M. Foundation, T. Terme, B. Dpt, and F. Ii, “OSAS Severity is Associated with Decreased Heart Rate Turbulence Slope Methods Polysomnographic monitoring Statistical analysis,” *Comput. Cardiol. 2013*, vol. 40, pp. 1007–1010, 2013.

[230] R. Pallás-Areny, J. Colominas-Balagué, and F. J. Rosell, “The effect of respiration-induced heart movements on the ECG,” *IEEE Trans. Biomed. Eng.*, vol. 36, no. 6, pp. 585–90, 1989.

[231] G. Hahn, I. Šipinková, F. Baisch, G. Hellige, I. Sipinková, F. Baisch, and G. Hellige, “Changes in the thoracic impedance distribution under different ventilatory conditions,” *Physiol Meas*, vol. 16, pp. A161–A173, 1995.

[232] D. L. Eckberg, “The human respiratory gate,” *J. Physiol.*, vol. 548, no. 2, pp. 339–352, 2003.

[233] J. T Penzel, GB Moody, RG Mark, AL Goldberges and Peter, “The Apnea-ECG Database,” *Comput. Cardiol.*, vol. 27, pp. 255–258, 2000.

[234] G. Dorfman Furman, Z. Shinar, A. Baharav, and S. Akselrod, “Electrocardiogram derived respiration during sleep,” *Comput. Cardiol. 2005*, vol. 32, pp. 351–354, 2005.

[235] L. S. Correa, E. Laciar, V. Mut, A. Torres, and R. Jané, “Sleep apnea detection based on spectral analysis of three ECG - Derived respiratory signals,” *Proc. 31st Annu. Int. Conf. IEEE Eng. Med. Biol. Soc.*, pp. 4723–4726, 2009.

[236] D. Labate, F. La Foresta, G. Occhiuto, F. C. Morabito, A. Lay-Ekuakille, and P. Vergallo, “Empirical mode decomposition vs. wavelet decomposition for the extraction of respiratory signal from single-channel ECG: A comparison,” *IEEE Sens. J.*, vol. 13, no. 7, pp. 2666–2674, 2013.

[237] M. Campolo, D. Labate, F. La Foresta, F. C. Morabito, A. Lay-Ekuakille, and P. Vergallo, “ECG-derived respiratory signal using Empirical Mode Decomposition,” *Proc. IEEE Int. Symp. Med. Meas. Appl.*, no. 1, pp. 399–403, 2011.

[238] W. J. Yi and K. S. Park, “Derivation of respiration from ECG measured without subject’s awareness using wavelet transform,” *Proc. 24th Annu. Conf. aof Eng. Med. Biol.*, pp. 183–184, 2002.

[239] D. Widjaja, C. Varon, D. Testelmans, B. Buyse, L. Faes, and S. Van Huffel, “Separating respiratory influences from the tachogram : methods and their sensitivity to the type of respiratory signal,” *Comput. Cardiol. 2014*, vol. 41, pp. 609–612, 2014.

[240] M. O. Mendez, D. D. Ruini, O. P. Villantieri, M. Matteucci, T. Penzel, S. Cerutti, and A. M. Bianchi, “Detection of sleep apnea from surface ECG based on features extracted by an autoregressive model.,” *IEEE Eng. Med. Biol. Soc. Conf.*, vol. 2007, pp. 6106–9, Jan. 2007.

[241] B. Xie and H. Minn, “Real-time sleep apnea detection by classifier combination.,” *IEEE Trans. Inf. Technol. Biomed.*, vol. 16, no. 3, pp. 469–77, May 2012.

[242] Victor Barbero Romero, “ECG baseline wander removal and noise suppression analysis in an embedded platform,” *Univ. Complutence Madrid, Thesis*, pp. 1–67, 2009.

[243] M. Kaur, B. Singh, and Seema, “Comparisons of Different Approaches for Removal of Baseline Wander from ECG Signal,” *Proc. Int. J. Comput. Appl.*, pp. 30–36, 2011.

[244] M. S. Chavan, R. Aggarwala, and M. Uplane, “Suppression Of Baseline Wander And Power Line Interference in ECG Using Digital IIR Filter,” *Int. J. Circuits, Syst. Signal Process.*, vol. 2, no. 2, pp. 356–65, 2008.

[245] M. A. Tinati and B. Mozaffary, “A wavelet packets approach to electrocardiograph baseline drift cancellation,” *Int. J. Biomed. Imaging*, vol. 2006, pp. 1–9, 2006.

[246] N. Jain and D. K. Shakya, “Denoising Baseline Wander Noise from Electrocardiogram Signal using Fast ICA with Multiple Adjustments,” *Int. J. Comput. Appl.*, vol. 99, no. 2, pp. 34–39, 2014.

[247] B. Knight, F. Pelosi, G. Michaud, S. Strickberger, and F. Morady, “Clinical consequences of electrocardiographic artefact mimicking ventricular tachycardia,” *N. Engl. J. Med.*, vol. 341, no. 17, pp. 1270–1274, 1999.

[248] S. Gurumurthy, “System Design for Baseline Wander Removal of ECG Signals with Empirical Mode Decomposition Using Matlab,” *Int. J. Soft Comput. Eng.*, vol. 3, no. 3, pp. 85–92, 2013.

[249] R. Jane, P. Laguna, N. V. Thakor, and P. Caminal, “Adaptive baseline wander removal in the ECG: Comparative analysis,” *Proc. Comput. Cardiol.*, pp. 143–146, 1992.

[250] D. Zhang, “Wavelet Approach for ECG Baseline Wander Correction and Noise Reduction.,” *Conf. Proc. IEEE Eng. Med. Biol. Soc.*, vol. 2, no. 1, pp. 1212–1215, 2005.

[251] F. A. Orakzai, Q. Avenue, and W. Cantt, “Baseline Wandering Removal from Human Electrocardiogram Signal using Projection Pursuit Gradient Ascent Algorithm,” *Int. J. Electr. Comput. Sci.*, vol. 9, no. 10, pp. 9–11, 2009.

[252] S. P. Arunachalam and L. F. Brown, “Real-time estimation of the ECG-Derived Respiration (EDR) signal using a new algorithm for baseline wander noise removal,” *Proc. 31st Annu. Int. Conf. IEEE Eng. Med. Biol. Soc. Eng. Futur. Biomed. EMBC 2009*, vol. 1, no. 1, pp. 5681–5684, 2009.

[253] M. Elgendi, B. Eskofier, S. Dokos, and D. Abbott, “Revisiting QRS detection methodologies for portable, wearable, battery-operated, and wireless ECG systems,” *PLoS One*, vol. 9, no. 1, 2014.

[254] P. de Chazal, “Detection of supraventricular and ventricular ectopic beats using a single lead ECG,” *Proc. Annu. Int. Conf. IEEE Eng. Med. Biol. Soc. EMBS*, pp. 45–48, 2013.

[255] V. Krasteva and I. Jekova, “QRS template matching for recognition of ventricular ectopic beats,” *Ann. Biomed. Eng.*, vol. 35, no. 12, pp. 2065–2076, 2007.

[256] R. J. Thomas, J. E. Mietus, C.-K. Peng, G. Gilmartin, R. W. Daly, A. L. Goldberger, and D. J. Gottlieb, “Differentiating obstructive from central and complex sleep apnea using an automated electrocardiogram-based method.,” *Sleep*, vol. 30, no. 12, pp. 1756–69, Dec. 2007.

[257] J. N. McNames and A. M. Fraser, “Obstructive sleep apnea classification based on spectrogram patterns in the electrocardiogram,” *Comput. Cardiol.*, vol. 27, pp. 749–752, 2000.

[258] R. J. Oweis and B. O. Al-Tabbaa, “QRS Detection and Heart Rate Variability Analysis: A Survey,” *Biomed. Sci. Eng.*, vol. 2, no. 1, pp. 13–34, 2014.

[259] S. S. Kohli, N. Makwana, N. Mishra, and B. Sagar, “Hilbert transform based adaptive ECG R-Peak detection technique,” *Int. J. Electr. Comput. Eng.*, vol. 2, no. 5, pp. 639–643, 2012.

[260] S. T. Prasad and S. Varadarajan, “Heart Rate Detection Using Hilbert Transform,” *Int. J. Res. Eng. Technol.*, vol. 02, no. 08, pp. 508–513, 2013.

[261] U. D. Ulusar, R. B. Govindan, J. D. Wilson, C. L. Lowery, H. Preissl, and H. Eswaran, “Adaptive rule based fetal QRS complex detection using Hilbert transform.,” *Conf. Proc. IEEE Eng. Med. Biol. Soc.*, vol. 2009, pp. 4666–9, 2009.

[262] J. Pan and W. J. Tompkins, "A Real-Time QRS Detection Algorithm," *IEEE Trans. Biomed. Eng.*, vol. BME-32, no. 3, pp. 230–236, 1985.

[263] D. Benitez, P. a. Gaydecki, a. Zaidi, and a. P. Fitzpatrick, "The use of the Hilbert transform in ECG signal analysis," *Comput. Biol. Med.*, vol. 31, no. 5, pp. 399–406, 2001.

[264] S. J. Redmond and C. Heneghan, "Cardiorespiratory-based sleep staging in subjects with obstructive sleep apnea," *IEEE Trans. Biomed. Eng.*, vol. 53, no. 3, pp. 485–496, 2006.

[265] R. B. Shouldice, L. M. O'Brien, C. O'Brien, P. de Chazal, D. Gozal, and C. Heneghan, "Detection of obstructive sleep apnea in pediatric subjects using surface lead electrocardiogram features.," *Sleep*, vol. 27, no. 4, pp. 784–792, 2004.

[266] P. de Chazal, C. Heneghan, E. Sheridan, R. Reilly, P. Nolan, and M. O'Malley, "Automatic classification of sleep apnea epochs using the electrocardiogram," *Comput. Cardiol.*, vol. 27, pp. 745–748, 2000.

[267] P. de Chazal, R. Reilly, and C. Heneghan, "Automatic sleep apnoea detection using measures of amplitude and heart rate variability from the electrocardiogram," *Proc. 16th Int. Conf. Pattern Recognit.*, vol. 1, pp. 4–7, 2002.

[268] B. Hickey, C. Heneghan, and P. de Chazal, "Non-episode-dependent assessment of paroxysmal Atrial Fibrillation through measurement of RR interval dynamics and atrial premature contractions," *Ann. Biomed. Eng.*, vol. 32, no. 5, pp. 677–687, 2004.

[269] P. de Chazal, C. Heneghan, C.-P. Chua, R. Shouldice, L. Doherty, S. Ryan, and W. T. McNicholas, "Home-Based Assessment of Sleep Apnoea using Simultaneous Electrocardiogram and Oximetry Signals," *Prog. Sleep Apnea Res. Chapter 4, Nov. Sceince Publ.*, pp. 115–139, 2007.

[270] G. D. Clifford, F. Azuaje, and P. E. McSharry, "Advanced Methods and Tools for ECG Data Analysis," *Artech House*, 2006.

[271] M. C. Teich, S. B. Lowen, B. M. Jost, K. Vibe-Rheymer, and C. Heneghan, "Heart Rate Variability: Measures and Models," *Nonlinear Biomed. Signal Process. Dyn. Anal. Model. IEEE Press*, vol. II, pp. 1–86, 2001.

[272] G. B. Moody, R. G. Mark, M. A. Bump, J. S. Weinstein, D. Berman, J. E. Mietus, and A. L. Goldberger, "Clinical Validation of the ECG-Derived Respiration (EDR) Technique," *Comput. Cardiol.*, 1986.

[273] G. D. Clifford, L. F. Zapanta, B. a. Janz, J. E. Mietus, C. Y. Youn, and R. G. Mark, "Segmentation of 24-hour cardiovascular activity using ECG-based sleep/sedation and noise metrics," *Comput. Cardiol.*, vol. 32, pp. 595–598, 2005.

[274] R. J. Thomas, J. E. Mietus, C.-K. Peng, and A. L. Goldberger, "An electrocardiogram-based technique to assess cardiopulmonary coupling during sleep.," *Sleep*, vol. 28, no. 9, pp. 1151–1161, 2005.

[275] J. Zheng, W. Wang, Z. Zhang, D. Wu, H. Wu, and C. K. Peng, "A robust approach for ECG-based analysis of cardiopulmonary coupling," *Med. Eng. Phys.*, vol. 38, no. 7, pp. 671–678, 2016.

[276] E. Jacobsen and R. Lyons, “The sliding DFT,” *IEEE Signal Processing Magazine*, vol. 20, no. 2. pp. 74–80, 2003.

[277] J. B. Allen, “Short Term Spectral Analysis, Synthesis, and Modification by Discrete Fourier Transform,” *IEEE Transactions on Acoustics, Speech, and Signal Processing*, vol. 25, no. 3. pp. 235–238, 1977.

[278] E. Sejdić, I. Djurović, and J. Jiang, “Time-frequency feature representation using energy concentration: An overview of recent advances,” *Digit. Signal Process. A Rev. J.*, vol. 19, no. 1, pp. 153–183, 2009.

[279] Y. Bülent, M. H. Asyal, E. Ar, S. Yetkin, and F. Özgen, “Sleep stage and obstructive apneaic epoch classification using single-lead ECG,” *Biomed. Eng. Online*, vol. 9, no. 39, pp. 1–14, 2010.

[280] A. H. Khandoker, C. K. Karmakar, and M. Palaniswami, “Screening Obstructive Sleep Apnoea Syndrome from Electrocardiogram Recordings Using Support Vector Machines,” *Comput Cardiol*, vol. 34, pp. 485–488, 2007.

[281] A. Lewicke, E. Sazonov, M. J. Corwin, M. Neuman, and S. Schuckers, “Sleep versus wake classification from heart rate variability using computational intelligence: consideration of rejection in classification models.,” *IEEE Trans. Biomed. Eng.*, vol. 55, no. 1, pp. 108–18, Jan. 2008.

[282] P. de Chazal, T. Penzel, and C. Heneghan, “Automated detection of obstructive sleep apnoea at different time scales using the electrocardiogram.,” *Physiol. Meas.*, vol. 25, no. 4, pp. 967–983, 2004.

[283] W. Zhao, R. Chellappa, and N. Nandhakumar, “Empirical performance analysis of linear discriminant classifiers,” *Proc. IEEE Comput. Soc. Conf. Comput. Vis. Pattern Recognit.*, 1998.

[284] T. Hastie, R. J. Tibshirani, and J. Friedman, “The Elements of Statistical Learning, Data Mining, Inference, and Prediction,” *Springer , Second ed.*, vol. 27, no. 2, pp. 1–745, 2009.

[285] G.-B. Huang, Q.-Y. Zhu, and C.-K. Siew, “Extreme learning machine: Theory and applications,” *Neurocomputing*, vol. 70, no. 1–3, pp. 489–501, Dec. 2006.

[286] J. Tapson, G. Cohen, and A. van Schaik, “ELM solutions for event-based systems,” *Neurocomputing*, vol. 149, pp. 435–442, Feb. 2015.

[287] V. N. Vapnik, “An overview of statistical learning theory.,” *IEEE Trans. Neural Netw.*, vol. 10, no. 5, pp. 988–999, 1999.

[288] A. J. Smola and B. Schölkopf, “A tutorial on support vector regression,” *Stat. Comput.*, vol. 14, pp. 199–222, 2004.

[289] C. Chang and C. Lin, “LIBSVM : A Library for Support Vector Machines,” *ACM Trans. Intell. Syst. Technol.*, vol. 2, no. 27, pp. 1–39, 2011.

[290] V. Vapnik, “The Nature of Statistical Learning Theory,” *Springer Sci. Bus. Media*, pp. 1–188, 2013.

[291] G. Bin Huang and H. A. Babri, “Upper bounds on the number of hidden neurons in feedforward networks with arbitrary bounded nonlinear activation functions,” *IEEE Trans. Neural Networks*, vol. 9, no. 1, pp. 224–229, 1998.

[292] S. Tamura and M. Tateishi, “Capabilities of a four-layered feedforward neural network: Four layers versus three,” *IEEE Trans. Neural Networks*, vol. 8, no. 2, pp. 251–255, 1997.

[293] G. Bin Huang, “Learning capability and storage capacity of two-hidden-layer feedforward networks,” *IEEE Trans. Neural Networks*, vol. 14, no. 2, pp. 274–281, 2003.

[294] G. Bin Huang, Q. Y. Zhu, and C. K. Siew, “Real-time learning capability of neural networks,” *Tech. Rep. ICIS/45/2003*, 2003.

[295] J. Tapson and A. van Schaik, “Learning the pseudoinverse solution to network weights,” *Neural Networks*, vol. 45, pp. 94–100, 2013.

[296] R. Penrose and J. a. Todd, “On best approximate solutions of linear matrix equations,” *Math. Proc. Cambridge Philos. Soc.*, vol. 52, no. 01, p. 17, Oct. 2008.

[297] H. B. Wong and G. H. Lim, “Measures of Diagnostic Accuracy : Sensitivity , Specificity , PPV and NPV,” *Proc. Singapore Healthc.*, vol. 20, no. 4, pp. 316–318, 2011.

[298] M. Coffin and S. Sukhatme, “Receiver operating characteristic studies and measurement errors.,” *Biometrics*, vol. 53, no. 3, pp. 823–837, 1997.

[299] C. Marzban, “The ROC Curve and the Area under It as Performance Measures,” *Weather Forecast.*, vol. 19, no. 6, pp. 1106–1114, 2004.

[300] J. a Hanley and B. J. McNeil, “The Meaning and Use of the Area under a Receiver Operating (ROC) Curvel Characteristic,” *Radiology*, vol. 143, no. 1, pp. 29–36, 1982.

[301] L. Breiman, “Heuristics of instability and stabilisation in model selection,” *Ann. Stat.*, vol. 24, no. January 1995, pp. 2350–2383, 1996.

[302] Y. Bengio and Y. Grandvalet, “No unbiased estimator of the variancee of k-fold cross-valudation,” *J Mach Learn Res*, vol. 5, pp. 1089–1105, 2004.

[303] N. V. Thakor, J. G. Webster, and W. J. Tompkins, “Estimation of QRS Complex Power Spectra for Design of a QRS Filter,” *IEEE Trans. Biomed. Eng.*, no. 11, pp. 702–706, 1984.

[304] I. Silva, G. B. Moody, and L. Celi, “Improving the quality of ECGs collected using mobile phones: The PhysioNet/Computing in Cardiology Challenge 2011,” *Comput Cardiol*, pp. 273–276, 2011.

[305] G. D. Clifford and G. B. Moody, “Signal quality in cardiorespiratory monitoring,” *Physiol. Meas.*, vol. 33, no. 9, p. Editorial, 2012.

[306] J. Behar, J. Oster, Q. Li, G. D. Clifford, and S. Member, “ECG Signal Quality During Arrhythmia and Its Application to False Alarm Reduction,” *IEEE Trans. Biomed. Eng.*, vol. 60, no. 6, pp. 1660–1666, 2013.

[307] A. L. Goldberger, L. A. N. Amaral, L. Glass, J. M. Hausdorff, P. C. Ivanov, R. G. Mark, J. E. Mietus, G. B. Moody, C.-K. Peng, and H. E. Stanley, “PhysioBank, PhysioToolkit, and

PhysioNet : Components of a New Research Resource for Complex Physiologic Signals," *Circulation*, vol. 101, no. 23, pp. e215–e220, 2000.

[308] W. Zong, T. Heldt, G. B. Moody, and R. G. Mark, "An open-source algorithm to detect onset of arterial blood pressure pulses," *Comput. Cardiol. 2003*, pp. 259–262, 2003.

[309] A. E. W. Johnson, J. Behar, G. D. Clifford, and J. Oster, "Multimodal heart beat detection using signal quality indices," *Physiol. Meas.*, vol. 1665, pp. 1–15.

[310] Q. Li, R. G. Mark, and G. D. Clifford, "Artificial arterial blood pressure artifact models and an evaluation of a robust blood pressure and heart rate estimator.," *Biomed. Eng. Online*, vol. 8, p. 13, 2009.

[311] J. X. Sun, a. T. Reisner, R. G. G. Mark, W. Zong, G. B. Moody, and R. G. G. Mark, "A signal abnormality index for arterial blood pressure waveforms," *Med. Biol. Eng. Comput.*, vol. 42, no. 5, pp. 698–706, 2004.

[312] "Reducing False Arrhythmia Alarms in the ICU: the PhysioNet/Computing in Cardiology Challenge 2015, last accessed on 30/11/2015." [Online]. Available: https://physionet.org/challenge/2015/sources/.

[313] B. Schölkopf, A. Smola, and K.-R. Müller, "Nonlinear Component Analysis as a Kernel Eigenvalue Problem," *Neural Comput.*, vol. 10, no. 44, pp. 1299–1319, 1998.

[314] "St. Vincent's University Hospital/University College Dublin Sleep Apnea Database," *physionet*, 2008. [Online]. Available: http://physionet.org/physiobank/database/ucddb/.

[315] S. Mika, B. Schölkopf, A. Smola, K. Müller, M. Scholz, and G. Rätsch, "Kernel PCA and De-Noising in Feature Spaces," *Analysis*, vol. 11, no. i, pp. 536–542, 1999.

[316] L. Burget, P. Matějka, P. Schwarz, O. Glembek, and J. H. Černocký, "Analysis of feature extraction and channel compensation in a GMM speaker recognition system," *IEEE Trans. Audio, Speech Lang. Process.*, vol. 15, no. 7, pp. 1979–1986, 2007.

[317] R. W. DeBoer, J. M. Karemaker, and J. Strackee, "Comparing Spectra of a Series of Point Events Particularly for Heart Rate Variability Data," *IEEE Trans. Biomed. Eng.*, vol. BME-31, no. 4, pp. 384–387, 1984.

[318] G. Hall, "Pearson's correlation coefficient," 2015. [Online]. Available: http://www.hep.ph.ic.ac.uk/~hallg/UG_2015/Pearsons.pdf.

[319] G. Bohm and G. Zech, "Introduction to Statistics and Data Analysis for Physicists," *Desy*, pp. 1–398, 2010.

[320] P. de Chazal, C. Heneghan, R. Shouldice, and C.-P. Chua, "Automated screening for sleep apnoea in home environment," *Prog. Sleep Apnea Res. ed. R. Ferber, Publ. Novascience*, vol. 1, pp. 1–14, 2007.

[321] E. Kostina, M. a Saunders, and I. Schierle, "Computation of Covariance Matrices for Constrained Parameter Estimation Problems using LSQR," *Tech. Rep. SOL 2009-1, IWR, Uni Heidelberg, Im Neuenheimer 368, D-69120*, pp. 1–11, 2009.

[322] S. Béchu, M. Richard-Plouet, V. Fernandez, J. Walton, and N. Fairley, "Numerical Methods for Determining Principal Component Analysis Abstract Factors," *Surf. Interface Anal.*, vol. 48, no. 5, pp. 301–309, 2016.

[323] L. David, A. Galperin, O. Green, and Y. Birk, "Efficient parallel computation of the estimated covariance matrix," *Proc. IEEE 26th Conv. Electr. Electron. Eng.*, pp. 1–10, 2010.

[324] S. Geman, E. Bienenstock, and R. Doursat, "Neural Networks and the Bias/Variance Dilemma," *Neural Comput.*, vol. 4, no. 1, pp. 1–58, 1992.

[325] D. J. C. MacKay, "Bayesian Interpolation," *Neural Comput.*, vol. 4, no. 3, pp. 415–447, 1992.

[326] A. Krogh, A. Krogh, J. Vedelsby, and J. Vedelsby, "Neural Network Ensembles, Cross Validation, and Active Learning," *Nips*, pp. 231–238, 1995.

[327] K. Hornik, "Some new results on neural network approximation," *Neural Networks*, vol. 6, no. 8, pp. 1069–1072, 1993.

[328] S. Lawrence, A. C. Tsoi, and A. D. Back, "Function Approximation with Neural Networks and Local Methods : Bias , Variance and Smoothness," *Aust. Conf. Neural Networks*, pp. 16–21, 1996.

[329] S. M. Isa, M. I. Fanany, W. Jatmiko, and A. Murni, "Feature and Model Selection on Automatic Sleep Apnea Detection using ECG," *ICACSIS*, pp. 357–362, 2010.

[330] L. M. Eerik, J. Vanschoren, M. J. Rooijakkers, R. Vullings, and R. M. Aarts, "Decreasing the False Alarm Rate of Arrhythmias in Intensive Care Using a Machine Learning Approach," pp. 293–296, 2015.

[331] C. H. Antink and S. Leonhardt, "Reducing False Arrhythmia Alarms Using Robust Interval Estimation and Machine Learning," no. 5, pp. 285–288, 2015.

[332] D. Widjaja, C. Varon, D. Testelmans, B. Buyse, L. Faes, and S. Van Huffel, "Separating respiratory influences from the tachogram : methods and their sensitivity to the type of respiratory signal," *Comput. Cardiol. 2014*, vol. 41, pp. 609–612, 2014.

[333] American Thoracic Society, "What Is Obstructive Sleep Apnea In Adults; Patient Information Series," *Am. J. Respir. Crit. Care Med.*, vol. 179, pp. 5–6, 2009.

[334] E. O. Bixler, A. N. Vgontzas, H.-M. Lin, T. Ten Have, J. Rein, A. Vela-Bueno, and A. Kales, "Prevalence of Sleep-disordered Breathing in Women," *Am. J. Respir. Crit. Care Med.*, vol. 163, no. 3, pp. 608–613, 2001.

[335] M. S. M. Ip, B. Lam, L. C. H. Tang, I. J. Lauder, T. Y. Ip, and W. K. Lam, "A Community Study of Sleep-Disordered Breathing in Middle-Aged Chinese Women in Hong Kong: Prevalence and Gender Differences," *Chest*, vol. 125, no. 1, pp. 127–134, 2004.

[336] J. Kim, K. In, J. Kim, S. You, K. Kang, J. Shim, S. Lee, J. Lee, S. Lee, C. Park, and C. Shin, "Prevalence of sleep-disordered breathing in middle-aged Korean men and women," *Am. J. Respir. Crit. Care Med.*, vol. 170, no. 10, pp. 1108–1113, 2004.

[337] B. Lam, D. C. L. Lam, and M. S. M. Ip, "Obstructive sleep apnoea in Asia.," *Int. J. Tuberc. lung Dis.*, vol. 11, no. 1, pp. 2–11, 2007.

[338] T. Young, M. Palta, J. Dempsey, J. Skatrud, S. Weber, and S. Badr, "The occurrence of sleep-disordered breathing among middle-aged adults.," *N. Engl. J. Med.*, vol. 328, no. 17, pp. 1230–1235, 1993.

[339] L. Almazaydeh, K. Elleithy, and M. Faezipour, "Detection of Obstructive Sleep Apnea Through ECG Signal Features," *Crown*, 2012.

[340] J.-U. Park, H.-K. Lee, J. Lee, E. Urtnasan, H. Kim, and K.-J. Lee, "Automatic classification of apnea/hypopnea events through sleep/wake states and severity of SDB from a pulse oximeter," *Physiol. Meas.*, vol. 36, no. 9, pp. 2009–2025, 2015.

[341] T. Penzel, K. Kesper, I. Pinnow, H. F. Becker, and C. Vogelmeier, "Peripheral arterial tonometry, oximetry and actigraphy for ambulatory recording of sleep apnea," *Physiol. Meas.*, vol. 25, no. 4, pp. 1025–1036, Aug. 2004.

[342] M. J. Moron, E. Casilari, R. Luque, and J. a. Gázquez, "A wireless monitoring system for pulse-oximetry sensors," *Proc. Syst. Commun. ICW*, vol. 05, pp. 79–84, 2005.

[343] D. Alvarez-Estevez and V. Moret-bonillo, "Computer-Assisted Diagnosis of the Sleep Apnea-Hypopnea Syndrome : A Review," *Sleep Disord.*, vol. 2015, pp. 1–33, 2015.

[344] K. V. Madhav, M. Raghuram, E. H. Krishna, N. R. Komalla, and K. A. Reddy, "Extraction of respiratory activity from ECG and PPG signals using vector autoregressive model," *Proceeding IEEE Int. Symp. Med. Meas. Appl.*, pp. 1–4, 2012.

[345] B. Prathyusha, T. S. Rao, and D. Asha, "Extraction of Respiratory Rate From PPG Signals Using PCA and EMD," *Int. J. Res. Eng. Technol.*, vol. 1, no. 2, pp. 164–184, 2012.

[346] C. Karmakar, A. Khandoker, T. Penzel, C. Schobel, and M. Palaniswami, "Detection of respiratory arousals using photoplethysmography (PPG) signal in sleep apnea patients," *IEEE J. Biomed. Heal. Informatics*, vol. 18, no. 3, pp. 1065–1073, 2014.

[347] A. V. Deshmane, "False arrhythmia alarm suppression using ECG, ABP, and photoplethysmogram," *MIT*, pp. 1–93, 2009.

[348] A. Aboukhalil, L. Nielsen, M. Saeed, R. G. Mark, and D. Gari, "Reducing false alarm rates for critical arrhythmias using the arterial blood pressure waveform," *J Biomed Inform.*, vol. 41, no. 3, pp. 442–451, 2009.

[349] P. Couto, R. Ramalho, and R. Rodrigues, "Suppression of False Arrhythmia Alarms Using ECG and Pulsatile Waveforms," *Comput Cardiol*, vol. 42, pp. 749–752, 2015.

[350] S. Review, "Home Sleep Testing comparison guide," 2013. [Online]. Available: Sleepreviewingmag.com.

[351] P. K. Stein, S. P. Duntley, P. P. Domitrovich, P. Nishith, and R. M. Carney, "A simple method to identify sleep apnea using Holter recordings.," *J. Cardiovasc. Electrophysiol.*, vol. 14, no. 5, pp. 467–73, May 2003.

[352] R. Millis, O. Kocak, T. Bayrak, and A. Erdamar, "Automated Detection and Classification of Sleep Apnea Types Using Electrocardiogram (ECG) and Electroencephalogram (EEG) Features," *Adv. Electrocardiograms-clinical Appl. Publ. InTech*, pp. 211–331, 2012.

[353] Y. M. Chi and G. Cauwenberghs, “Wireless Non-contact EEG/ECG Electrodes for Body Sensor Networks,” *Proceeding Int. Conf. Body Sens. Networks*, pp. 297–301, Jun. 2010.

[354] I. Fietze, T. Penzel, M. Partinen, J. Sauter, G. Küchler, A. Suvoro, and H. Hein, “Actigraphy combined with EEG compared to polysomnography in sleep apnea patients.,” *Physiol. Meas.*, vol. 36, no. 3, pp. 385–396, Feb. 2015.

[355] M. Younes, “Role of arousals in the pathogenesis of obstructive sleep apnea.,” *Am. J. Respir. Crit. Care Med.*, vol. 169, no. 9, pp. 623–633, 2004.

[356] J. J. Hosselet, R. G. Norman, I. Ayappa, and D. M. Rapoport, “Detection of flow limitation with a nasal cannula/pressure transducer system.,” *Am. J. Respir. Crit. Care Med.*, vol. 157, pp. 1461–7, May 1998.

[357] R. Plonsey and R. C. Barr, “Cardiac Electrophysiology,” *Bioelectr. A Quant. Approach*, pp. 19–42, 2007.